

Innate Immunity in Brain Development and Adult Homeostasis

Kristine Elaine Zengeler
Charlottesville, VA

Bachelor of Science, Bates College, 2019

A Dissertation presented to the Graduate Faculty of the University of Virginia
in Candidacy for the
Degree of Doctor of Philosophy

Department of Neuroscience

University of Virginia
May, 2023

Abstract

The human brain is an astoundingly complicated organ. Containing a number of neurons and glial cells that add up to about half of the number of stars in the Milky Way galaxy, the brain is well-equipped to tackle the ambitious job of governing organismal function. It is estimated that the human brain may contain up to 100 trillion connections between neurons, summing up to an outstanding computational capacity of this organ. It is no wonder that we are just beginning to delve into the underpinnings of brain architecture and function. Our own brains cannot quite grasp their own complexity.

The immune system constitutes a rival for brain intricacy. This system has evolved to respond to environmental stimuli and generate appropriate responses; a similar task to which the nervous system is charged. Indeed, there is extensive overlap between brain and immune communication. Until recently, it was thought that the brain was an immune-privileged organ that functioned largely independent of the immune system during periods of health. It is now recognized that this concept is incredibly misconstrued. There is remarkable overlap in the evolutionary origins, organism development, and lifelong functioning of the immune and nervous systems.

The studies presented in this dissertation emphasize this critical interplay between immunity and brain function. The fledgling neuroimmunology field has begun to uncover homeostatic roles for immune molecules in the nervous system. Moreover, studies of neurologic diseases aimed at developing treatments have identified both beneficial and damaging roles for immune cells and signal molecules in terms of pathology and outcomes. This dissertation melds smoothly into such concepts, as the studies presented herein illustrate harmful impacts of immune activation on brain development but also reveal a necessity for immune signaling for proper brain function.

Perturbation to a mother's immune system, including infection, stress, metabolic disease, and autoimmunity, have been linked to altered offspring neurodevelopment. We found that activation of the immune system during pregnancy led to robust immune signaling in maternal-fetal-interface tissue, and that this changed the trajectory of offspring neurodevelopment and behavior. Pharmacologic medication further transformed the immune signaling landscape of the maternal-fetal-interface and developing offspring brains exposed to maternal inflammation. These findings highlight the critical importance of taking the entire maternal environment into account—and in particular the immune landscape—when striving to understand offspring brain development.

Recent studies have led to the appreciation that molecules originally characterized in the immune system are also used by nervous system cells for classically non-immune functions. We found that the immune-based inflammasome complex was activated throughout the adult brain in the absence of known immune triggers. The assembly of this complex was modulated by experience and age. A homeostatic role for the inflammasome is highlighted in this work by our findings that blockade of inflammasome activation notably influenced astrocyte-neuron communication, hippocampal physiology, and memory function. These data indicate a novel role for the inflammasome in the maintenance of healthy brain function.

In summary, this dissertation stresses the critical interaction between the immune and nervous systems for proper brain development and lifelong function. Our work contributes to an improved understanding of how perturbations to the immune system can influence the brain. This body of work emphasizes that a delicate balance of immune signaling must exist to provide necessary healthy support of brain development and function without straying into pathogenic overactivation and harmful consequences.

Acknowledgements

It has been the greatest pleasure and opportunity of a lifetime to be a part of the Neuroscience Graduate Program (NGP) at the University of Virginia (UVA). I believe that neuroscience research, which is inherently interdisciplinary, is best conducted as a team. Upon joining the NGP, I found a world-class group of graduate school teammates and have been blown away by the high quality of research and mentorship provided at UVA. I owe a huge thank you to my amazing committee, including its fearless leader Dr. Barry Condron and dedicated members Dr. Anna Cliffe, Dr. Christopher Deppmann, Dr. Ukpong Eyo, and Dr. Tajie Harris. The advice and direction provided by you has been critical to the success of my scientific training, research output, and future career direction.

Being a part of the highly interactive community of neuroscientists and immunologists that is the Brain Immunology and Glia (BIG) center has been a cornerstone of my training as a neuroimmunologist. The BIG center has cultivated enthusiasm and fostered collaboration for my research and others; building a strikingly supportive and unique training environment for which I am so grateful. My BIG center colleagues have not only been incredibly helpful research collaborators but have become cheerleaders for my success and often close friends outside of the lab.

I owe a special and notable thank you to my incredible mentor, Dr. John Lukens, who has never stopped encouraging me to conduct the research that most inspires me. John, you have always provided me with the support, tools, and resources necessary to accomplish all my goals inside and outside of the lab. I have grown tremendously in technical and conceptual aspects of research, and I have also discovered my enthusiasm for scientific writing, a piece of my training that you continue to impassion. You are an absolute expert at highlighting the strengths of your trainees while also encouraging aspects of improvement, which together allow for constant growth. You have skillfully crafted the lab environment of trainees who are driven, inspiring, and collaborative, and I am so grateful for that.

I am constantly inspired by my fellow trainees in the NGP, BIG center, and Lukens lab. It can be rare in life to meet such talented, down-to-earth, and truly supportive people as has become the standard for my colleagues at UVA.

My fellow Lukens lab trainees have been an incredibly special part of my graduate school experience and perhaps the sole reason for my continued happiness at the bench. From Lukens lab Gen 1: Dr. Elizabeth Frost, Dr. Catherine Lammert, Dr. Ashley Bolte, and Dr. Hannah Ennerfelt – you have all been tremendous supporters of mine from the very beginning and have each become a very dear friend to me. Elizabeth and Cat, you have provided phenomenal advice for navigating graduate school, and I thank you for enjoying Charlottesville's finest bike rides and your tasty eats with me. I have been so lucky to have the all-around superstar Ashley – aka Dr. Bolte (in the lab) aka Ash (on the slopes) – as a friend for which to enjoy mountain adventures by ski, hiking boot, and trail running shoe. Your constantly positive attitude, insane work ethic, passion for medicine and science, and enthusiasm for life is really an inspiration to us all.

From Lukens lab Gen 2: my fellow grad buddies Jess, Aman, Ana, Addie, Nick, Josh, Lexi, star undergrads Ava and Coco, and phenomenal techs Kate, Eric, and Maddi – thank you for the daily smiles. Aman and Jess, thank you for always being down for a drinksie and for seeing me through turmoil re: experiments, relationships, and beyond. You are both incredibly intelligent scientists, hilarious individuals, and such supportive friends. Ava and Coco, I wish I was as talented, brilliant, driven, and real as you two when I was in college! Ava, thank you for your priceless help in lab, non-stop goofiness, wild tales, and R. Pat propaganda. Coco, thank you for bringing my coolness factor up just a tinge through your friendship and for being down for literally anything, even eating unknown fruits in an international botanic garden.

To my phenomenal NGP cohort-mates! Thank you for doing this insane PhD journey along with me. David Tyus, Ryan Brown, Kendra Liu, Katriel Cho, and Jenny Fu, you have all been there since day one and have been particularly instrumental in helping me cross the dissertation finish line. Katriel, our take-out movie nights always re-center me. Your astounding artistic talent and perseverance through difficulties make you a remarkable

person. Kendra, I have been lucky to have you as a regular traveling on the struggle bus with me and so appreciate your dedication to your work, your friends, your cats, and your Pokémon Go.

My Milkshake Musketeers, my Hash Slinging Flashers, my Homies – Ryan and David – I am at a loss for words to describe how much your friendship has been instrumental to my happiness in grad school. From first year introductions to climbing, Wayside Fried Chicken, and tour de C’ville’s best milkshakes; to half marathons, tacos, and snake wrangling; and countless adventures in between, I have had a blast during every minute. David, I have never known a more patient person and cherish every joke, word of advice, and piece of encouragement that you never cease to provide. Ryan, I know I can always count on you for a listening ear over an IPA or a long scenic bike ride to pedal out any stress. The stunning and sometimes perilous adventures with you and Lindsey have been some of my greatest memories from the past few years.

Thank you to my college friends who continue to support my science and running endeavors that were sparked during our time together in Maine. My fellow Batesies – Caroline Gettens, Anna Setzer, Hannah Austin, Haoyu Sun, Alex Howard, and Hannah Smith – your continued friendship through catch-up sessions and new adventures has meant the world to me.

My dearest babes in apartment 2304B!! Anna Sviripa, Anukriti Shrestha, and Simona Bajgai – thank you for listening to my rants, feeding into my baking and plant addictions, and truly being the dream team of roommates to come home to every day. You’ve seen me through every good day, bad day, stress clean day, pastry baking day, binge-watch trashy tv show day, plant propagation day, and countless others.

Bret Greene, thank you for seeing me through “the last 1%” of grad school (your words!) – the most important part. It still baffles me that you actively chose to steal the heart of someone finishing their PhD, but I am so very thankful for it. It brings me endless joy that I can share my morning coffee, my afternoon run/climb, my evening Roots bowl with extra avocado, my every baked good, and countless adventures to come with you. I have never finished the last 50 meters of a race so strong, and I owe that all to your kind heart and unwavering support.

Dr. Hannah Ennerfelt – aka my work wife, Lentil, Public Enemy #1, Verified Elite Adventure Partner, my dearest friend – “thank you” just does not even come close. I am constantly inspired by your brilliant science, your tenacity in achieving your goals, your generalist knowledge ranging from birds to books to plants to baking (and now, Harry Potter), and your willingness to sign up for even the craziest adventures. Being trauma bonded to you is one of the greatest souvenirs I will take from my time here. I could not imagine lab, grad school, or life without your patient ear, fun spirit, expert morale boosting abilities, and words of confidence. You are the bestest Best Friend that a girl could ever hope for!

My Z squad sibs – Robert, Lauren, and Andrew Zengeler – you keep me humble. Robert, your thoughtfulness and gentle heart have always inspired me to be a better human. Lauren, my girl. My first and forever bestie. You are one of my greatest sources of emotional support, wisdom, advice, and are a truly genuine individual. I can only hope that one day I will grow up to be as strong, brilliant, funny, and caring as you, my lil sis. Andrew, your infectious charisma and exceptional taste in music have generated much awesomeness and will continue to do so for many more Years of Awesome ahead. Of course, I would not be where I am today (on this planet, or in this stage of life) without my parents, April Neumann and Tom Zengeler. Thank you for your never-ending support of my scholastic endeavors, countless sport ventures, escapades, and anything else life throws my way.

Love you all long time.

♡ KZ (soon-to-be Dr. Nugget)

Table of Contents

Chapter 1: Introduction	8
1.1 Abstract	8
1.2 List of abbreviations	8
1.3 Preface	8
1.4 A crash course in neurodevelopment	9
1.4.1 <i>Neural induction and cell genesis</i>	9
1.4.2 <i>Migration and elaboration</i>	10
1.4.3 <i>Refinement</i>	11
1.5 Microglia in the developing brain	12
1.5.1 <i>Identified roles of microglia in neurodevelopment</i>	12
1.5.2 <i>Microglial dysfunction and neurodevelopmental disorders</i>	14
1.5.3 <i>Sex differences and microglia</i>	15
1.6 Homeostatic functions of innate immune signaling in the developing CNS	16
1.6.1 <i>Complement</i>	16
1.6.2 <i>Toll-like receptors</i>	19
1.6.3 <i>Cytokines</i>	23
1.6.4 <i>Chemokines</i>	24
1.6.5 <i>Inflammasomes</i>	25
1.7 Maternal immune activation	27
1.7.1 <i>Autism spectrum disorder</i>	27
1.7.2 <i>Schizophrenia</i>	29
1.7.3 <i>Microglia: A common thread</i>	30
1.8 Conclusion	31
Chapter 2: SSRI treatment modifies the effects of maternal inflammation on <i>in utero</i> physiology and offspring neurobiology	32
2.1 Abstract	32
2.2 List of abbreviations	32
2.3 Introduction	32
2.4 Results	34
2.5.1 <i>MIA triggers a robust immune response acutely at the maternal-immune interface</i>	34
2.5.2 <i>The pro-inflammatory response to polyI:C is distinct at the placenta and the decidua</i>	37
2.5.3 <i>The MFI immune response to MIA is largely absent by E14</i>	39
2.5.4 <i>Baseline sex differences in the MFI transcriptome are dampened subacutely by MIA</i>	40
2.5.5 <i>MIA leads to sex-biased behavioral changes without an accompanying transcriptional shift in microglia</i>	43
2.5.6 <i>SSRI exposure reshapes the MFI response to MIA</i>	51
2.5.7 <i>SSRI exposure potentiates the offspring brain response to MIA</i>	54
2.5 Discussion	55
2.6 Conclusions	58
2.7 Methods	58
2.7.1 <i>Mice</i>	59
2.7.2 <i>SSRI treatment and maternal immune activation</i>	59
2.7.3 <i>Tissue collection</i>	59
2.7.4 <i>Sex genotyping</i>	59
2.7.5 <i>RNA extraction</i>	59

2.7.6. Magnetic-activated cell sorting	60
2.7.7. Flow cytometry	60
2.7.8. RNA-sequencing procedure and data analysis	60
2.7.9. cDNA synthesis and qPCR.....	61
2.7.10. Serotonin ELISA	61
2.7.11. Multiplex cytokine assay.....	61
2.7.12. Behavior	62
2.7.13. Statistics	62

Chapter 3: Astrocyte inflammasome signaling mediates neuronal physiology and memory 64

3.1 Abstract.....	64
3.2 List of abbreviations	64
3.3 Introduction	64
3.4 Results	66
3.4.1. The inflammasome is physiologically activated in the healthy adult brain.....	66
3.4.2. Blocking inflammasome function improves synaptic plasticity	70
3.4.3. Inflammasome activity in astrocytes regulates synaptic plasticity and memory function	73
3.4.4. Astrocyte inflammasomes regulate neuronal plasticity through IL-33 and perineuronal nets	82
3.5 Discussion	88
3.6 Methods	89
3.6.1. Mice	89
3.6.2. Caspase-1 inhibitor treatment	90
3.6.3. Environmental enrichment.....	90
3.6.4. Social isolation.....	90
3.6.5. Behavior	90
3.6.6. Tissue collection	92
3.6.7. Brain sample preparation	93
3.6.8. Magnetic-activated cell sorting	93
3.6.9. Immunofluorescence	93
3.6.10. RNA isolation, cDNA synthesis, qPCR.....	94
3.6.11. Western blotting.....	94
3.6.12. Statistics	95

Chapter 4: Discussion and future directions..... 96

4.1 Dissertation discussion.....	96
4.2.1. The maternal-fetal interface response to environmental changes.....	96
4.2.2. Inflammasome signal cascades in homeostatic brain states.....	97
4.2 Future directions.....	98
4.2.1. Homeostatic Neuronal Inflammasome Activation.....	98
4.2.2. The Relative Contribution of IL-33 to Inflammasome-Mediated Control of Neuronal Plasticity.....	99
4.2.3. Inflammasome Function Within the Hippocampus	99
4.2.4. Inflammasomes in Seizure Propagation.....	103
4.2.5. Inflammasomes in Alzheimer's Disease.....	111
4.3 Concluding remarks	112

Literature cited 113

List of Figures

Figure 1.1. Microglia influence a number of neurodevelopmental processes.....	13
Figure 1.2. Phagocytic signaling underlies synaptic pruning.....	19
Figure 1.3. AIM2 inflammasome signalling contributes to CNS cell dieback.....	26
Figure 1.4. Maternal immune activation promotes abnormal brain development and autism-like behaviors.....	29
Figure 2.1. PolyI:C-induced MIA does not appreciably impact maternal weight or litter size.....	34
Figure 2.2. The maternal-fetal interface undergoes a robust immune response acutely after polyI:C exposure.....	35
Figure 2.3. The E12 MFI response to polyI:C is similar between sexes.....	36
Figure 2.4. Expression of angiogenesis-related genes in the placenta 3 hours-post MIA.....	37
Figure 2.5. The effects of polyI:C in the decidua compared to the placenta.....	38
Figure 2.6. The MFI immune response is largely complete by 48 hpi.....	39
Figure 2.7. Baseline sex differences in the MFI transcriptome are dampened by MIA.....	41
Figure 2.8. The developmental trajectory of the MFI transcriptome.....	42
Figure 2.9. Maternal immune activation elicits sex-biased behavioral alterations in offspring but does not impact microglia on the transcriptional level.....	44
Figure 2.10. Microglia are effectively purified by CD11b+ MACS.....	45
Figure 2.11. Microglia transcriptional maturation.....	46
Figure 2.12. Microglia are not transcriptionally impacted by MIA.....	46
Figure 2.13. Lack of major transcriptional sex differences in microglia at baseline.....	47
Figure 2.14. Lack of major transcriptional sex differences in MIA microglia.....	48
Figure 2.15. The microglial transcriptional development program.....	49
Figure 2.16. scRNA-seq clustering and cluster expression of cell-type-specific markers for selection of microglia.....	50
Figure 2.17. Fluoxetine exposure reshapes the MFI response to MIA.....	51
Figure 2.18. MIA impacts fluoxetine pregnancy progression.....	52
Figure 2.19. Fluoxetine and MIA do not largely impact maternal cytokine levels but elicit combinatorial effects on MFI serotonin signaling.....	53
Figure 2.20. Fluoxetine exposure potentiates the embryonic brain response to MIA.....	54
Figure 3.1. Inflammasome activation is dynamically regulated by experience.....	66
Figure 3.2. The different morphological states of brain ASC specks.....	67
Figure 3.3. Environmental changes dampen inflammasome activation across hippocampal subregions, dampen expression of inflammasome components, and diminish hippocampal gliosis.....	68
Figure 3.4. Increased ASC speck formation activation and gliosis in the aged ASC ^{Citrine} brain.....	69
Figure 3.5. Spatial memory recall dampens inflammasome activation in the hippocampus but not the cerebellum.....	70
Figure 3.6. Caspase-1 inhibition improves long-term memory and hippocampal synapse formation.....	71
Figure 3.7. Caspase-1 inhibition contributes to moderate weight gain, but does not impact general locomotion, exploratory behavior, anxiety-like behavior, or spatial learning in mice.....	72
Figure 3.8. Caspase-1 inhibition shifts spine morphology.....	73
Figure 3.9. Astrocyte inflammasome activity regulates neuronal synapses.....	74
Figure 3.10. ASC specks can be found within astrocytes and neurons in the hippocampus.....	75
Figure 3.11. ASC specks are found in Purkinje cells in the cerebellum.....	76
Figure 3.12. Astrocytes harboring inflammasomes are not differentially activated, but GFAP and ASC speck levels are correlated.....	77
Figure 3.13. Loss of Casp1 expression specifically in astrocytes in Casp1 ^{ΔAst} mice.....	77
Figure 3.14. Astrocyte Caspase-1 ablation does not impact baseline locomotion, motor learning, spatial working memory, or associative fear memory, but improves long-term spatial memory flexibility.....	78
Figure 3.15. The acute loss of Caspase-1 function promotes reactivity but does not affect astrocyte numbers.....	79

Figure 3.16. Prolonged loss of astrocyte inflammasome function is detrimental to memory retention and synaptic health.	80
Figure 3.17. Astrocyte Caspase-1 modulates IL-33 production, perineural net coverage, and neuronal plasticity.	83
Figure 3.18. Astrocyte Caspase-1 regulates cellular IL-33 levels but does not impact neuron numbers or ability to respond to stimuli.....	84
Figure 3.19. Astrocyte Caspase-1 acutely limits perineuronal net coverage through a mechanism independent of microglial engulfment.	86
Figure 3.20. The loss of Caspase-1 in astrocytes does not overtly impact microglia.	87
Figure 4.1. Verification of AAV targeting specificity in the hippocampus.	100
Figure 4.2. Behavioral and hippocampal cytokine analyses of Casp1 ^{AAV-ΔAst} mice.	101
Figure 4.3. Behavioral analysis of Casp1 ^{AAV-ΔNeur} mice.	102
Figure 4.4. Long-term AAV presence in the hippocampus of Casp1 ^{AAV-ΔAst} and Casp1 ^{AAV-ΔNeur} mice. ...	103
Figure 4.5. Inflammasome activation propagates seizure progression.....	105
Figure 4.6. The inflammasome and neuronal activity are bidirectionally modulated.....	106
Figure 4.7. Cell-type-specific inflammasome activation contributes to seizure severity.	107
Figure 4.8. ASC ^{Citrine} mice exhibit mild protection from seizures.	109
Figure 4.9. NLRP1 contributes to seizure severity in a sex-specific manner.	110

Chapter 1: Introduction

1.1 Abstract

The immune and nervous systems have unique developmental trajectories that individually build intricate networks of cells with highly specialized functions. These two systems have extensive mechanistic overlap and frequently coordinate to accomplish the proper growth and maturation of an organism. The brain's resident innate immune cells, microglia, are pivotal sculptors of neural circuitry and coordinate copious and diverse neurodevelopmental processes. Moreover, many immune cells and immunity-related signaling molecules are found in the developing nervous system and contribute to healthy neurodevelopment. In particular, many innate immune mediators such as complement proteins, Toll-like receptors, and cytokines are critical contributors to healthy brain development. Further exemplifying the importance of innate immune processes in nervous system formation, dysfunction in innate immune signaling has been functionally linked to many neurodevelopmental disorders. This review will discuss the essential roles of microglia and innate immune signaling in the assembly and maintenance of a properly functioning nervous system.

1.2 List of abbreviations

ASD, autism spectrum disorder; BBB, blood-brain barrier; CNS, central nervous system; CSF, cerebrospinal fluid; DAMP, damage-associated molecular pattern; DRG, dorsal root ganglion; EE, environmental enrichment; EGL, external granule layer; EMP, erythromyeloid progenitor; GPC, granule precursor cell; IFN, interferon; IGL, internal granule layer; IL, interleukin; IL-1RAP, interleukin-1 receptor accessory protein; IRAK, interleukin-1 receptor associated kinase; LGN, lateral geniculate nucleus; LPS, lipopolysaccharide; MIA, maternal immune activation; mPOA, medial preoptic area; NPC, neural progenitor cell; OPC, oligodendrocyte progenitor cell; PAMP, pathogen-associated molecular pattern; pMN, pre-motor neuron; polyI:C, polyinosinic:polycytidylic acid; PRR, pattern recognition receptor; PS, phosphatidylserine; RGC, retinal ganglion cell; S1DZ, primary somatosensory cortex dysgranular zone; SFB, segmented filamentous bacteria; TF, transcription factor; TGF- β , transforming growth factor beta; TIR, Toll/interleukin-1 receptor; TLR, Toll-like receptor; TNF, tumor necrosis factor; VZ, ventricular zone; YS, yolk sac

1.3 Preface

The classic assertion that the brain is an immune privileged organ has undergone a paradigm shift and is now understood to be inaccurate. In recent years, the interplay between the immune and nervous systems has been well described in a wide array of pathological cases: from autoimmune diseases such as multiple sclerosis to more classical cognitive conditions of dysfunction like Alzheimer's disease. Beyond this, immune cells also actively contribute to homeostatic processes in the nervous system.^{1,2} For instance, meningeal $\gamma\delta$ T cells produce IL-17 that promotes glial production of BDNF to regulate synaptic plasticity and short-term memory.³ The resident macrophages of the central nervous system (CNS), microglia, have also been freshly upgraded from a janitorial role to one of sculpting and maintaining proper circuit function, among other essential responsibilities.^{4,5} More recently, it has been recognized that signaling components commonplace in the immune system are also expressed by nervous system cells and underlie important neurological processes.^{6,7,8}

The activation of immune signaling pathways is most frequently associated with the detection of danger or other threats to the body. However, recent studies demonstrate that classic immunity-related mechanisms underlie many critical everyday processes in the brain. Signaling pathways that have been characterized in immune cells in response to pathogens are also utilized by neurons and glia to maintain CNS homeostasis and contribute to proper functioning of the brain. The traditional role of microglia, bearing the diminutive name meaning "small glue", has been one of phagocytosing debris. It is now recognized that microglia are critical for the proper formation of neuronal circuits and are key regulators of neuronal communication.^{7,8} Furthermore, there is

increasing evidence that perturbations to the immune system during neurodevelopment can have catastrophic repercussions and lead to severe lifelong impacts on CNS function.^{9,10}

This review will focus specifically on the role of innate immunity in the developing CNS. It will first give a brief overview of the major processes in neurodevelopment. A few of the roles of the innate immune cells of the CNS, microglia, in sculpting nervous system assembly will then be introduced. The center point of this review will cover the functions of innate immune signaling molecules in setting up a properly functioning CNS. This discussion will include the complement proteins, Toll-like receptors, cytokines, chemokines, and inflammasomes. Finally, immune activation during gestation and the subsequent innate immune-driven consequences on neurodevelopment will be discussed.

1.4 A crash course in neurodevelopment

The human brain contains approximately 86 billion neurons and a comparable number of non-neuronal cells, known as glia,^{11,12} and these numbers do not even take into account the spinal cord or peripheral nervous system. The cells of the nervous system are exquisitely interconnected and function cooperatively to receive inputs from the body periphery and determine an appropriate output. Precise wiring and exact timing of neuronal activity are critical for proper neurologic function. The means through which the nervous system is assembled and maintained throughout the lifetime of the organism is a remarkable feat. The complexity of the nervous system will likely never be entirely comprehended, but recent scientific advances have markedly improved our understanding of the specialized cells that, arguably, define an individual. The construction of the nervous system involves a complex collection of exceptionally organized and highly dynamic processes of which the neurobiological underpinnings are beginning to be delineated.

1.4.1 Neural induction and cell genesis

Nervous system development begins soon after conception and continues into early adulthood. During the process of gastrulation, epiblast cells differentiate to an epidermal or neural fate, forming an epidermal-neural boundary.^{13,14} BMP4 signaling promotes an epidermal fate to cells, while inhibition of BMP4 (via factors such as noggin, chordin, and follistatin) allows for a neural fate.¹⁵ As an epidermal fate requires the presence of a positive epidermal signal and neural tissues form in the absence of additional signals, a neural fate is considered to be the default state.¹⁶ This process of neuralization generates neural stem cells which are capable of producing all of the types of cells in the nervous system.¹³

The first distinct neural structure that is formed is the neural tube, which is generated through the process of neurulation beginning during the third week of gestation in humans.¹³ This produces a hollow tube structure, that eventually forms brain ventricles and the central canal of the spinal cord, and is lined adjacently with neural progenitor cells (NPCs).¹³ Exposure to local environmental signals progressively restricts the fate of a given cell and initiates transcriptional programs specific to given differentiated lineages.¹⁷ For example, secreted Sonic hedgehog and transforming growth factor (TGF)- β from the neural tube floor plate and roof plate, respectively, generate opposing gradients from which combinatorial signals relay dorsal-ventral positional information to the cells.^{18,19} Secreted neural patterning signals like these create gradients from which combinatorial signals dictate the expression of transcription factors (TFs). A patterned TF code covering early neural tissue through development thus governs cell fate across distinct zones.^{13,17,20} Convergent signals and gradient changes through time integrate to generate the diversity of cell types that compose the nervous system.^{18,19}

The generation of neurons commences mid-first trimester in humans in ventricular zones (VZ) whence these cells migrate to their final destinations.¹³ Neural progenitors cells divide symmetrically to produce additional progenitors and asymmetrically to generate differentiated neurons.^{13,21} A pool of progenitors is retained that will later generate glia, thus, a balance between the production of neurons and the preservation of progenitors must be maintained. The switch from the genesis of neurons to that of oligodendrocytes and astrocytes (referred to here using the catch-all term “gliogenesis”) occurs as a result of altered TF expression patterns. Taking the pMN (pre-motor neuron) domain for example, a combinatorial code of secreted factors early on induces the expression

of the TFs *Nkx6.1*, *Pax6*, *Olig2*, *Ngn1*, and *Ngn2* which promotes a motor neuron fate.¹⁸ Over time, alterations to the gradient of secreted factors leads to downregulation of *Pax6*, *Ngn1*, and *Ngn2* and upregulation of *Nkx2.2* and *Sox10* which halts the production of neurons and instead promotes the production of oligodendrocytes.¹⁸ A similar switch occurs in the p2 domain whereby early signaling dictates pyramidal neuron fate and later signaling stimulates a switch to the production of astrocytes.¹⁹

The CNS parenchyma is made up of neural cells, vascular cells, and glia. The neural cells derive from the previously described phase of neurogenesis during development, and the switch to gliogenesis produces astrocytes and oligodendrocytes.¹⁹ The final major type of glial cell in the CNS are the microglia, which derive not from neural progenitors but instead hail from hematopoietic lineage.²² Hematopoietic precursors give rise to tissue resident macrophages through three waves of hematopoiesis, in which the first wave occurs in the yolk sac (YS) and the second two waves generate precursors that migrate first to the fetal liver and then to resident tissues.^{23,24} Microglia are tissue resident macrophages that derive from early erythromyeloid precursors (EMPs) in the YS and colonize the CNS parenchyma prior to blood-brain barrier (BBB) closure at E13.5.^{22,25,26} Lineage tracing studies have convincingly demonstrated that the majority of adult microglia derive from YS precursors,²⁷ though recent evidence suggests that a subset of adult microglia also derive from second-wave EMPs.²⁸ Canonical YS progenitors migrate to the brain and seed the CNS parenchyma beginning at E8.5.^{27,29} The population of microglia in the brain is maintained largely through self-renewal.³⁰ Under certain conditions, infiltrating peripheral monocytes derived from the bone marrow may also give rise to brain-resident macrophages that can resemble microglia in form and some functions, while also possessing unique transcriptional and functional features.^{24,31}

CSF1 signaling is necessary for microglial survival and fate specification during development and in the adult CNS.^{25,27} Expression of CSF1 promotes microglial maturation intrinsically and local environmental signals, such as TGF- β , additionally contribute.^{23,25,26,32} Immature microglia entering the CNS parenchyma display an amoeboid morphology until transitioning into a more ramified state around E14.^{25,26} These changes in morphology are also accompanied by altered epigenetic and transcriptional states in maturing microglia.^{24,33–35} Regional signals derived from neurons and other CNS cell types contribute to a heterogenic distribution and phenotype of microglia throughout the brain.^{36,37} Microglia appear to be particularly sensitive to additional cues such as hormones and microbiota-derived signals, which further impact their developmental trajectory.^{33,35,37–39}

1.4.2 Migration and elaboration

Neurons are produced in distinct proliferative zones and must migrate to their final destinations where these cells will remain for the lifetime of the organism. Here, the formation of the cortex will be taken as an example. Cortical excitatory neurons are generated in the VZ and migrate into the developing cortex via a process known as somal translocation or by climbing up nearby radial glia cells.^{13,40} These neurons move outward until reaching Cajal-Retzius cells at the most peripheral edge of the developing brain, a pattern that defines an “inside-out” mode of cortical development.^{13,40} In contrast, many inhibitory interneurons are generated in the ganglionic eminence and must migrate tangentially throughout the cortex.^{13,40} These processes of migration occur throughout the first and second trimesters of pregnancy in humans.⁹

A defining feature of the nervous system is the connectivity between cells that underlies circuit function and information processing capabilities. Neurons must undergo significant elaboration of processes during development to form these connections, and furthermore, the synapses that form must be productive and appropriate. A dense arbor of dendrites must be created onto which axon terminals from communicating cells form synapses. Any outgrowth from a neuron is known as a neurite, and the neurite that will become the axon of the neuron is known as a growth cone. The growth cone must navigate through a complex environment to find its target, which in many cases is far from the cell body. Attractive and repulsive guidance cues signal to the growth cone as it extends outward until the target cell is reached.^{13,41} These guidance cues are typically chemotropic molecules which can be secreted from neurons and glial cells to provide positional information.^{41,42}

Once the growth cone arrives at its target, morphological alterations are made to form a synapse onto a dendritic spine of the target neuron.^{13,41} Synaptogenesis involves the formation and strengthening of synaptic connections

between neurons and is a process that begins during development but is continued throughout the lifetime of an organism. Astrocytes are key mediators of synapse formation wherein astrocyte-derived signals both drive neurons to make synapses as well as mature synapses already formed.^{43,44} Astrocytes and microglia can also positively and negatively regulate synapse formation to ensure the proper balance of synaptic connections.⁴³⁻⁴⁵ The level of activity of a given synapse as well as local signals contribute to the strength and durability of that connection. Adhesion molecules on the growth cone and dendrite are also involved in mediating target recognition and initial synapse formation.⁴⁶ Synapse assembly requires the formation of pre- and post-synaptic densities. Pre-synaptically, synaptic vesicle precursors accumulate and also promote the delivery of vesicle docking and fusion proteins to the plasma membrane.⁴⁶ Post-synaptically, scaffolding proteins such as PSD-95, Homer 1c, and Shank2/3 begin to accumulate and neurotransmitter receptors are inserted into the membrane and begin to cluster.⁴⁶ Immature synapses are long, thin, and have a short half-life, whereas mature synapses are much more stable.⁴⁶ Mature spines fall into four recognized categories, including mushroom, branched, thin, or stubby.⁴⁶

1.4.3 Refinement

One of the common themes of neurodevelopment is overproduction followed by pruning. First, CNS resident cells are overproduced during development following which many undergo cell death to achieve the quantity of cells present in the mature CNS.⁴⁷ An incorrect number of neurons or synapses in any given region of the CNS can dramatically alter the proper formation of circuitry. Indeed, the overproduction of cortical neurons can alter the balance of excitatory to inhibitory neurons, and this is thought to underlie some of the network dysfunction and abnormal behaviors characteristic of neurodevelopmental disorders like autism spectrum disorder (ASD).^{48,49} This process of cell dieback during development is tightly regulated and controlled by a variety of mechanisms. One possible means for controlling the number of neurons in a given region is the amount of neurotrophic factor available, whereby the level of neurotrophic factor dictates the number of surviving neurons such that neurons must compete locally to avoid death.⁵⁰ Neurons uptake trophic factors into their terminals at target zones, and those that fail to receive trophic support undergo programmed cell death, ensuring that each target region contains an appropriate number of cells.⁵¹ A bidirectional interaction between neurons and glia co-regulates survival and death. For instance, microglia can influence neuron and astrocyte proliferation by secreting regulatory factors (both pro-survival and pro-apoptotic) and microglia can phagocytose intermediate precursor cells.^{42,43} Similarly, neurons require trophic support from nearby astrocytes for survival.⁴² Moreover, programmed cell death of neurons has been shown to influence the infiltration of microglia into the brain parenchyma during development.⁵²

Most cell death that occurs during healthy neurodevelopment is programmed, and apoptosis is believed to execute most of this neural dieback.⁴⁷ A critical role for apoptosis as a major cell death mechanism in the nervous system has been demonstrated using cell death pathway knockout mice.⁵³⁻⁵⁵ Work in recent years has uncovered other novel forms of cell death beyond the well-characterized apoptosis and necrosis. Interestingly, our studies demonstrate that pyroptosis, a gasdermin D-mediated form of cell death, also contributes to proper brain maturation.⁵⁶ Pyroptosis provides an alternative route of cell death for neural cells that harbor high levels of DNA damage, and elimination of the capability to accomplish pyroptosis contributes to brain and behavioral abnormalities.⁵⁶

Like neuronal cells, synapses are also overproduced and must go through a period of refinement. Though neuronal activity is not required for synaptogenesis during neurodevelopment, a lack of synaptic activity can be associated with synaptic elimination.⁴⁶ Indeed, the initial number of synapses formed in the developing brain is far greater than the number of synapses present in the mature brain; furthermore, synaptic pruning is crucial for the proper formation and function of many circuits. A paradigmatic example of this is the necessity of pruning retinogeniculate synapses for proper eye-specific segregation.⁵⁷ Retinal ganglion cells (RGCs) from the retina project to the lateral geniculate nucleus (LGN) of the thalamus and form an abundance of synapses with thalamic relay neurons during early development.⁵⁷ The synaptic connections in the LGN have several distinct features, one of which is a precise eye-specific segregation whereby projections from each eye form distinct, non-overlapping territories.⁵⁷ In order for this segregation to occur, inappropriate synapses are eliminated and failure

to achieve proper synapse numbers contributes to circuit dysfunction.^{57,58} Less active synapses are actively eliminated whereas more active synapses are spared and become strengthened.⁵⁸

Though most of the heavy lifting of neurodevelopment is accomplished prior to birth, several key processes continue postnatally. The innate immune system continues to be a pivotal regulator of these postnatal developmental processes. Specifically, the previously described dieback mechanisms of cell death and synaptic pruning persist until early adulthood.⁹ Innate immune molecules such as the complement proteins contribute to synaptic pruning as will be covered in more detail later.^{58,59} Synaptogenesis also continues postnatally and is especially influenced by astrocyte-secreted factors in the postnatal brain.^{42,44} Myelination, which begins toward the end of embryonic development and persists until adolescence,⁹ is a well-known mechanism for augmentation of neuronal action potential conduction.¹³ These oligodendrocyte-neuron connections also provide a key mechanism by which oligodendrocytes can relay trophic factors and metabolic products to support axonal health, as well as present a way for oligodendrocytes to clear K^+ and facilitate neuronal membrane repolarization.⁴³ Finally, neurogenesis and gliogenesis continue to occur throughout life to a limited degree in specialized regions of the brain.¹³ Proliferation in the olfactory bulb and hippocampus contribute to a small but important subset of newly generated neurons.¹³ Innate immune system processes including cytokine production and the complement cascade have been shown to regulate adult hippocampal neurogenesis.⁶⁰⁻⁶³ Glia also continue to proliferate in the adult brain; notably, oligodendrocyte progenitor cells (OPCs) persist and microglia continue to turnover throughout adulthood.¹³

1.5 Microglia in the developing brain

Only recently has a true appreciation been gleaned for immune cell function during homeostasis in the CNS. As the primary resident immune cells of the brain, microglia have been the innate immune cells most extensively characterized in the context of neurodevelopment. Few studies to date have investigated other populations of immune cells in the brain during development. Indeed, a limited amount of immune cells infiltrate into the adult brain parenchyma under non-inflammatory conditions, though many leukocytes and dendritic cells can be found at boundary regions.⁶⁴ One report found $CD11c^+$ cells (identified as dendritic cells) surrounding ventricles at E16 and P2,⁶⁵ while another search for lymphocytes during neurodevelopment found few $CD4^+$ and $CD8^+$ T cells but a small population of B-1 cells which were reported to promote OPC proliferation.⁶⁶ Mast cells are known to reside in the adult and developing brain parenchyma and are implicated in many behaviors.⁶⁷ Mast cells in the maturing brain contribute to masculinization and programming of adult sexual behavior.⁶⁸ Beyond this, whether other immune cells are present in the CNS during development and if such cells contribute to neurodevelopment remains to be discovered. In contrast, microglia have begun to be quite extensively studied in the context of nervous system development and it has become increasingly clear that these cells contribute to nearly every aspect of CNS formation. The many important functions that microglia have during neurodevelopment have been extensively covered in other reviews and is beyond the scope of the current discussion.^{1,25,37,42,43,69-72} This section will thus provide only a topical overview of certain roles that microglia play during neurodevelopment which have been characterized thus far, examples of neurodevelopmental dysfunction that can result when microglia function is impaired, and recent work concerning sex biases in microglia during development.

1.5.1 Identified roles of microglia in neurodevelopment

The immune functions of microglia are well known but these innate immune cells have essential jobs beyond the stereotypical roles as inflammatory mediators. It is becoming increasingly clear that microglia are key contributors to CNS development and that disruption of these innate immune cells can contribute to neurodevelopmental pathology. Microglia begin to colonize the brain at E8.5 and proliferate in the parenchyma then undergo a dieback phase until adult numbers of these brain resident macrophages are reached.⁶⁹ During this time, microglia contribute to diverse and important neurodevelopmental processes (Figure 1).⁶⁹ Evidence suggests that microglia in the developing brain are morphologically and functionally distinct from those in the adult brain.^{25,69} Immature microglia are more amoeboid (a typical characteristic of activated microglia) and have unique transcriptional profiles, though are not necessarily classically activated as a less ramified morphology might imply.^{25,69} Microglia follow a stepwise developmental program that has been demonstrated to be highly

sensitive to environmental perturbations.^{33,73} Local or systematic changes in the signaling milieu may contribute to altered microglia development and promote neurodevelopmental pathology.³³ For example, lipopolysaccharide (LPS) treatment has been shown to accelerate male microglia development.³⁵

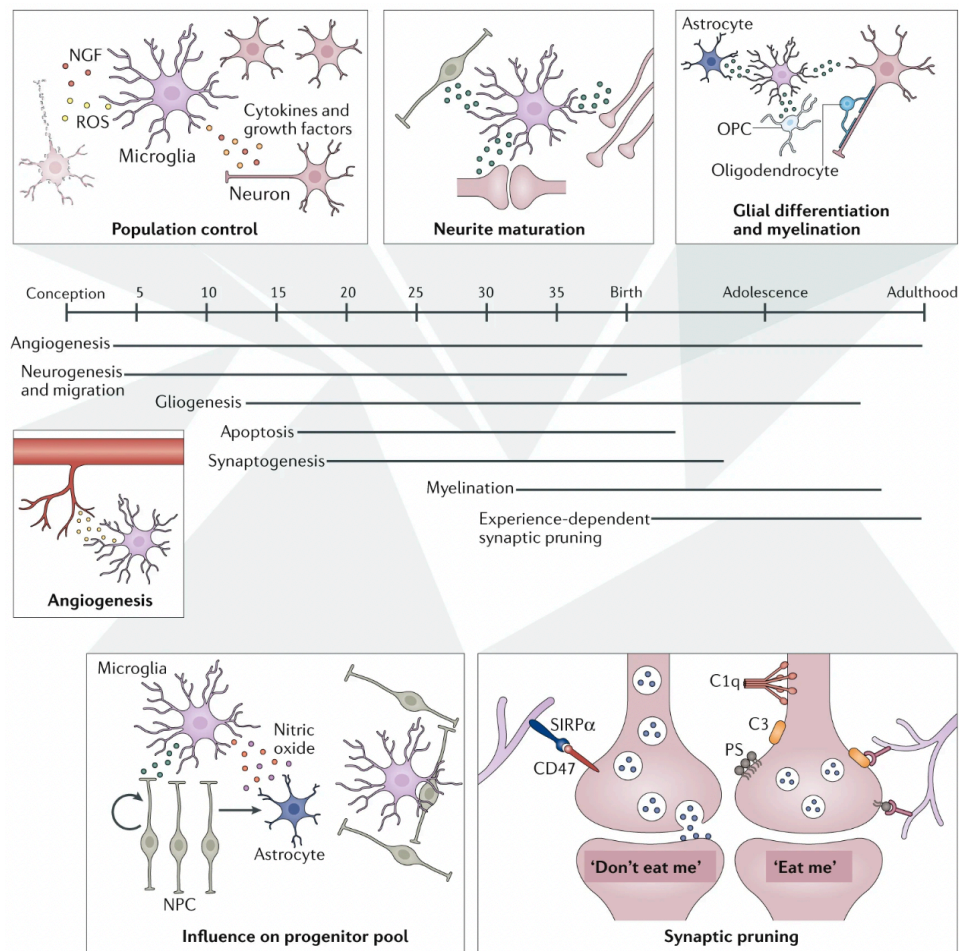


Figure 1.1. Microglia influence a number of neurodevelopmental processes.

Population control: microglia phagocytose immature neurons in proliferative regions, directly promote cell death (via the release of reactive oxygen species (ROS) and nerve growth factor (NGF)), and support cell survival (via the secretion of pro-survival molecules such as growth factors and cytokines). Neurite maturation: microglia promote synaptogenesis, influence neurite outgrowth and regulate axon tract fasciculation through secreted factors. Glial differentiation and myelination: microglial-derived factors support oligodendrocyte and astrocyte differentiation, and microglia can influence myelination. Angiogenesis: microglia associate with vasculature and influence angiogenesis via yet to be determined secreted factors. Influence on neural progenitor cell (NPC) pool: microglia influence the size of the NPC pool by secreting factors that promote their proliferation and by directly phagocytosing NPCs and oligodendrocyte precursor cells (OPCs). Nitric oxide-releasing microglia can promote the switch from neurogenesis to astroglialogenesis, thereby influencing the ratio of neurons to glia. Synaptic pruning: microglia eliminate inactive synapses. Phosphatidylserine (PS) and complement components (C1q and C3) tag unnecessary synapses and act as 'eat me' signals when recognized by microglia phagocytic receptors. Active synapses are protected by CD47 which, when recognized by SIRP α on microglia, acts as a 'don't eat me' signal.

Microglia are not distributed uniformly in the developing brain but associate more densely with zones that, presumably, require microglia support. For instance, microglia are found near blood vessels in the developing brain and it has been demonstrated that microglia contribute to angiogenesis during neurodevelopment (Figure 1). Secreted factors released from microglia have the ability to stimulate sprout formation and branching of vasculature.^{74,75} Microglia are found in the VZ where they have been shown to regulate cell genesis (Figure 1). The title of professional phagocytes is merited for microglia, as these cells engulf a broad array of substances during development including live cells, apoptotic cells, debris, and synapses.^{25,42,58,76} Microglia are commonly found nearby dead cells whereby microglia-mediated clearance of apoptotic bodies is crucial for modulating the environment.^{25,42,76} Microglia actively phagocytose NPCs during developmental and adult neurogenesis to control the size of the progenitor pool (Figure 1).⁷⁷ Microglia can also directly induce cell death independent of phagocytosis via secretion of noxious factors such as reactive oxygen species (Figure 1).^{78,79} In contrast to these negative functions for controlling cell numbers, microglia can also actively promote neuron survival by secreting

trophic factors and cytokines (Figure 1).^{80,81} Microglia also support astrocyte and oligodendrocyte differentiation and can stimulate myelination (Figure 1).^{82,83}

The frequent association of microglia with immature axons and spines supports the function of these cells in neurite growth, guidance, and pruning. Microglia are involved in modulating axon outgrowth and axon tract fasciculation, demonstrating an important role for these cells in neurite development (Figure 1).^{84,85} Preliminary evidence suggests that microglia may also be able to directly promote synaptogenesis as well as remodel presynaptic features to alter synapse function (Figure 1).⁸⁶⁻⁹⁰ It has now become well documented that microglia are key mediators of circuit wiring and plasticity on account of actively contributing to synaptic pruning (Figure 1).⁹¹⁻⁹³ Microglia engulf dendritic spines and axon terminals via recognition of “eat me” signals expressed by weak or otherwise unnecessary processes.^{91,93-97} This functional role for microglia in synaptic refinement and plasticity demonstrates a crucial ability for these cells to sculpt neuronal circuitry and therefore to modulate network function.^{71,72,98} These roles for microglia are by no means a comprehensive list, moreover, undiscovered functions of microglia in shaping neurodevelopment certainly remain.

1.5.2 Microglial dysfunction and neurodevelopmental disorders

As microglia contribute to such a broad spectrum of neurodevelopmental processes, it does not come as a surprise that proper microglial function is necessary for brain development and that abnormalities in developmental microglia programs can contribute to neuropathology. Mounting evidence suggests that microglia abnormalities exist in ASD and might act as a driving force or precipitating factor for this neurodevelopmental disorder.⁹⁹ A meta-analysis of transcriptomic datasets across psychiatric conditions identified enrichment for microglia and pruning-related modules in patients with ASD.¹⁰⁰ Microglia in the brains of autistic individuals show evidence of residing in a more activated state, characterized by an amoeboid morphology and excessive cytokine production.¹⁰¹⁻¹⁰⁵ Interestingly, similar microglia dysfunction has also been observed post-mortem in the brains of individuals with schizophrenia.^{106,107} Various behavioral abnormalities, such as autistic-like obsessive-compulsive behaviors and social impairments, have been attributed to neurodevelopmental microglial dysfunction.¹⁰⁸⁻¹¹¹

Immune activation during neurodevelopment has been increasingly linked to various cases of neurologic dysfunction. For example, maternal immune activation (MIA) has been shown to alter offspring microglial development and contribute to behavioral abnormalities.^{112,113} The nervous system is highly vulnerable to environmental perturbations during development and heightened inflammatory conditions may contribute to the pathology of certain neurodevelopmental disorders. Pre- and postnatal environmental stressors can induce altered microglia morphology which is associated with various aberrant behaviors.¹¹²⁻¹¹⁶ Abnormal immune activity during development has been shown to be a contributing factor for an altered trajectory of microglia development,³⁵ which in turn might disrupt microglia-mediated neurodevelopmental processes. This will be covered in greater detail later in this review.

It is conceivable that any neurodevelopmental process to which microglia contribute may be impaired in cases of abnormal microglia development. One major contributing factor to cultivation of neurodevelopmental disorders might be impaired synaptic pruning by microglia during development. A transient reduction in microglia during the synaptic pruning phase of postnatal development is associated with impaired neurotransmission, circuit connectivity, and autistic-like behaviors.¹⁰⁸ Furthermore, microglia-like cells derived from individuals with schizophrenia have a higher rate of synaptic phagocytosis, suggesting that abnormal synaptic pruning by microglia might also contribute to the pathology of schizophrenia.¹¹⁷ Beyond this, faulty microglia may underlie persistent neuropathology whereby homeostatic processes in the brain controlled by microglia are disturbed as a result of impaired microglia development. Moreover, immune-induced developmental microglia alterations might act as a primer whereby immune challenge later in life acts as a second hit to precipitate adult microglial dysfunction and promote neurologic disease. Altogether, these studies provide evidence for a causal link between microglia dysfunction and neurodevelopmental disease but mechanistic work investigating the particular circumstances in which this occurs as well as the specific neurobiological underpinnings is needed for a more complete understanding.

1.5.3 Sex differences and microglia

Sexual dimorphism exists in both the immune system and the nervous system. In general, the female immune response is stronger than the male response. For example, females typically display faster pathogen clearance but increased susceptibility to autoimmune disease.¹¹⁸ Sex differences in the brain are abundant, ranging from differences in cell number in certain brain regions to alternate use of signal transduction pathways.¹¹⁹ As illustrated by this review, the nervous and immune systems are intimately connected and the neuroimmune environment during development has its own sex-specific features. Indeed, microglia display their own stark sex differences both during neurodevelopment as well as in the adult brain.^{120–122} Understanding sex differences in microglia may contribute to an improved understanding of sex-biased neurodevelopmental disorders.

The process of sexual differentiation begins during embryonic development and is characterized in male offspring by a surge in male hormone production which abrogates feminization.¹¹⁹ Hormones contribute to differential developmental trajectories between the sexes, functioning primarily by binding cognate receptors to regulate gene transcription.¹¹⁹ Chromosome complement is also an augmenting factor for sexual differentiation, whereby females lack Y chromosome genes and also may express different levels of X chromosome genes compared to their male counterparts.¹¹⁹ Immunocompetent cells in the brain respond to sex hormones and many display sex differences. Here, a few of such sex-specific features in relation to microglia will be discussed. Two recent reviews cover sex differences in microglia during brain development in greater depth.^{121,122}

Microglial cells have sex-specific features and also directly contribute to the wiring of sex-specific neural circuitry in response to sex hormones. Sex influences the developmental trajectory of microglia which contributes to dimorphic functions.³⁵ Males and females differ in terms of microglia number, distribution, maturation, morphology, reactivity, and transcriptional state throughout development and into adulthood.^{35,123–125} Baseline sex differences in immune signaling has also been reported at different developmental timepoints in certain brain regions, such as disparities in the expression levels of cytokines, chemokines, and other inflammatory mediators.¹²⁶ These differences in signaling molecules could stem from the aforementioned variations in microglia number and reactivity, and might also be a contributing factor to these differences. Either way, such sex-specific features of innate immunity in the brain exist during neurodevelopment and these contribute to dimorphic behaviors.

Microglia contribute to sex-specific circuit wiring to organize dimorphic behaviors. In one classic example of this, microglia in the medial preoptic area (mPOA) are essential contributors to spine patterning that underlies the generation of male-specific behaviors.¹¹⁹ The male mPOA has a greater density of microglia that are more activated, which produce heightened levels of prostaglandin E₂.¹²⁷ The male mPOA also has a greater density of mast cells, which secrete histamine that promotes microglial production of prostaglandins.⁶⁸ The prostaglandin E₂ promotes dendritic spine formation, such that a greater spine density in the mPOA programs male-specific sexual behaviors.¹²⁷ Correspondingly, the loss of microglial function during this developmental stage abrogates the development of male copulatory behaviors.^{110,127} Brief temporary depletion of microglia during this critical postnatal period also contributes to sex-specific changes in stress response.¹²⁸ A similar process underlies the wiring of sex-specific social behavior, whereby complement-mediated microglial pruning of dopamine receptors in the nucleus accumbens shapes male-specific changes in behavior.¹²⁹

Many neurologic disorders have apparent sex bias in prevalence, severity, disease progression, and outcome, and this is no different for neurodevelopmental disorders. The sex differences observed during development in microglia might be critical for understanding such disparities in disease between the sexes. For instance, ASD is four times more prevalent in males than in females,¹³⁰ and it stands to reason that sex-specific features in microglia might partially explain this disparity. Indeed, ASD risk genes are not necessarily expressed at different levels in male compared to female brains, but microglia markers are significantly enriched among genes over-represented only in the male autistic brain.¹³¹ Mounting evidence suggests that environmental stressors are precipitating factors for developing ASD and that microglia are particularly vulnerable to such influences;^{132,133} therefore, sex-specific microglial responses to early life insults may contribute to sex bias in neurodevelopmental disorders. Emerging evidence suggests that environmental insults and subsequent neuroinflammation during early development can contribute to neurologic dysfunction, and microglia may be one contributing link. For

instance, prenatal exposure to diesel exhaust has been shown to predispose offspring to weight gain and increase susceptibility to cognitive dysfunction^{134,135} and is also associated with altered microglia development and long-term function in a sex-specific manner.¹¹⁵ Another example of differential sex responses of microglia to environmental perturbations was recently demonstrated wherein the absence of maternal microbiota lead to sex-specific changes in microglia development, including transcription profile and colonization dynamics.³⁹ In summary, microglia display overt baseline sex differences and respond differently to environmental perturbations during development, which might provide an understanding for sex bias in certain neurodevelopmental disorders.

1.6 Homeostatic functions of innate immune signaling in the developing CNS

The previous discussion highlighted that immune cells are present in the CNS during early development and are critical regulators of proper nervous system formation and function. Beyond immune cells, molecules used for innate immune signaling are also present in the developing and mature CNS and are expressed by all brain resident cells. These proteins were first characterized in the immune system but have recently been shown to play integral functional roles during CNS development. Innate immune molecules contribute to diverse neurodevelopmental processes including neurogenesis and gliogenesis, cell migration, regulation of cell proliferation and survival, neurite outgrowth, synaptogenesis, synapse elimination, and more. Many of these molecules are found to be dysregulated in neurodevelopmental disorders, emphasizing the functional importance of innate immune signaling for proper nervous system formation and homeostatic operation.

1.6.1 Complement

The complement system, comprised of an intricate web of pathways, has been extensively characterized as a key platform for host defense against invading organisms. The primary roles of complement in host protection are opsonization, recruitment of leukocytes, initiation of inflammation, and direct lysis of foreign microbes; thus, complement acts as a first line of defense as well as a bridge between innate and adaptive immunity.¹³⁶ Complement further underlies many diverse immunological processes on its own, including the clearance of immune complexes and debris, discrimination between healthy and apoptotic or foreign cells, angiogenesis, mobilization of hematopoietic cells, regenerative processes, and more.^{136,137} Complement proteins can be membrane-bound or circulate throughout the body as inactive zymogens. Binding of inactive complement proteins to surface structural motifs triggers proteolytic cleavage and the activation of downstream signaling events.¹³⁸

Box 1: Complement. In the periphery, complement can be activated along three arms, the alternative, lectin, and classical pathways, all of which generate a C3 convertase. The alternative pathway is constitutively active at low levels through constant spontaneous hydrolysis of soluble C3. This leads to downstream cleavage events which ultimately produces a membrane-bound C3 convertase made up of C3b and Bb proteins.¹³⁹ The lectin pathway is activated by mannose-binding lectin binding to foreign carbohydrate motifs, which stimulates the cleavage of MASP1 and MASP2.¹⁴⁰ The classical pathway requires antibody production and is initiated by antibody-antigen interaction triggering C1q-mediated cleavage of C1r and C1s.¹³⁸ The initiation of the lectin and classical pathways triggers the cleavage of C2 and C4 into C2a/C2b and C4a/C4b, respectively, of which C2a and C4b together form another form of a membrane-bound C3 convertase. All of the pathways converge at the formation of a C3 convertase, which cleaves C3 into C3a and C3b, of which C3a acts as an anaphylatoxin to promote inflammation and C3b can act as an opsonin. Binding of C3b to the C3 convertase generates a C5 convertase, which cleaves C5 into the anaphylatoxin C5a and C5b. C5b can initiate the formation of the membrane attack complex, comprised of C6, C7, C8, and C9, which is responsible for direct lysis of the target cell.¹³⁶ CNS resident cells express all of the complement components C1-C5 and low levels of components of the membrane attack complex (namely, C6-C9).¹⁴¹ Evidence that each of these three of these complement arms are active, at least in part, in the CNS will be discussed below.

Beyond peripheral inflammation, complement has also been implicated in many different states of brain dysfunction with inflammatory pathology, including but not limited to meningitis, traumatic brain injury, stroke, and neurodegenerative diseases such as Huntington's disease, Alzheimer's disease, and Parkinson's disease.^{139,140} The majority of complement proteins are produced by the liver.¹⁴¹ The brain is protected by the BBB, the arachnoid barrier, and the blood-CSF (cerebrospinal fluid) barrier at the choroid plexus which altogether limit immune cell infiltration and plasma protein influx under homeostatic conditions.¹⁴² Inflammatory conditions in the brain are associated with barrier leakage which might account for the roles of complement in diseases characterized by such immune infiltration; however, two decades ago complement proteins were identified in the

brain even under healthy conditions.^{143,144} It is now known that CNS-resident cells are capable of synthesizing select complement proteins and receptors with varying levels across developmental ages and often diminishing levels through maturation, and more recent work has shown that complement plays a role in the brain during homeostasis.^{139,140,145,146,58,147} Microglia and cultured astrocytes are high expressors of complement, with astrocytes expressing all of the complement components C1-C9 and microglia expressing C1-C4.¹⁴⁸ Microglia and astrocytes also both express the complement receptors CR2, C3aR, and C5aR, and microglia are the sole CNS resident cells expressing CR3.¹⁴⁸ Oligodendrocytes and neurons are also capable of expressing all of the complement components C1-C9, though to a lesser extent than that of astrocytes and microglia.¹⁴⁸ In peripheral tissues, inhibitors of complement (such as factor I, factor H, CD46, and CD55) are essential to protect against unwanted damage to healthy tissue.^{136,138} Surprisingly, most CNS neurons express very low levels of complement inhibitors, which would appear to make these cells vulnerable to complement-mediated destruction.^{149,150} This neuronal sensitivity to complement highlights the importance of characterizing the time and location in which complement proteins are synthesized in the brain during development, as well as which cells express complement receptors.

Neurogenesis

It is known that complement plays a role in cell proliferation and regeneration in various tissues,¹⁴⁰ and it has since been demonstrated that complement also functions in neurodevelopmental neurogenesis as well as during the production of new neurons in adult neurogenesis. For instance, signaling through C3aR mediates adult neurogenesis in the dentate gyrus and olfactory bulb.¹⁵¹ Further, C3d signaling through CR2 has been shown to inhibit NPC proliferation in the adult hippocampus, and this was not dependent on C5aR.^{60,152} These findings prompt the question of larger role for complement signaling during developmental neurogenesis. One developmental study found that inducing C3aR and C5aR signaling with respective agonists promotes granule neuron proliferation in the cerebellum.¹⁵³ Interestingly, the induction of C5aR signaling induces caspase-3 activation in developing Bergmann glia, which has been reported to promote differentiation rather than conventional apoptosis in these cells.^{153,154}

Beyond a putative role in neurogenesis, there have been preliminary reports describing a role for complement proteins in neuroprotective processes. The application of C1q, but not of C3a or C5a, to cultured primary cortical neurons was found to modulate various signaling pathways which ultimately promoted neuronal survival.¹⁵⁵ Furthermore in cultured granule neurons, C5aR agonism was found to inhibit caspase-3 activation during serum deprivation.¹⁵⁶ These protective mechanisms warrant further investigation as such signaling might promote the preservation of some cells during the neurodevelopmental cell pruning phase.

Migration

The successful migration of a neuron to its final destination is essential for proper circuit formation. Conventional teaching states that this process is largely guided by chemotrophic factors. In a non-canonical mechanism of migration, the lectin arm of the complement pathway has the ability to mediate neuronal migration in the developing cortex.¹⁵⁷ The proper migration of immature neurons from the VZ to the cortical plate is dependent on C3, MASP1, and MASP2.¹⁵⁷ Furthermore, the anaphylatoxin receptors C3aR and C5aR may also be involved in this process, as pharmacological activation of either of these receptors was sufficient to rescue migration deficits induced by the downregulation of C3 or MASP1/2.¹⁵⁷ Interestingly, C3aR agonism on its own has been demonstrated to enhance cell motility.¹⁵³ However, the loss of either C3aR or C5aR did not result in obvious migratory deficits in cerebellar granule cells as measured in one study.¹⁵³ This suggests that these anaphylatoxin receptors are not essential for guiding neuronal migration, but possess the ability to do so, perhaps under conditions of inflammation. The endogenous ligands capable of driving this process have yet to be identified.

Collective migration is an important mechanism by which a group of cells moves from its birth site to its target zone together during neurodevelopment. It has been demonstrated that neural crest cells co-express C3a and its receptor C3aR, and that this interaction underlies co-attraction of neural crest cells to promote collective migration.¹⁵⁸ C3a has also been shown to modulate SDF-1a-induced NPC migration *in vitro*, although it is not solely responsible for promoting migration in this setting.¹⁵⁹ This study also presented preliminary evidence that C3a modulates the fate decision of NPCs wherein C3a on its own promotes NPC differentiation into neurons.¹⁵⁹

Furthermore, C3a was not sufficient to induce any changes in proliferation or survival of the NPCs, suggesting that it does not operate as a growth factor.¹⁵⁹

Synaptic pruning

A landmark study over a decade ago was the first to demonstrate the role of complement in the pruning of unwanted synapses during development.¹⁶⁰ C1q localizes to RGC synapses *in vivo* in the LGN which tags these synapses for elimination (Figure 2). Microglia engulf C3-tagged synapses in a manner dependent on neuronal activity and microglial expression of CR3 (Figure 2).⁹¹ Developing astrocytes produce the cytokine IL-33 which recruits microglia to synapses that must be eliminated and promotes engulfment (Figure 2).¹⁶¹ Mice deficient in C1q, C3, or C3R fail to undergo proper circuit refinement that is necessary for eye-specific segregation.^{91,94,160} Indeed, microglial phagocytosis of unwanted synapses is crucial for proper circuit formation in the developing postnatal brain.^{91,92} For instance, recordings in young mice with microglia that cannot properly communicate with neurons (*Cx3cr1*^{-/-}) illustrated immature synaptic connections and a delay in the maturation of synaptic plasticity.⁹²

Early work demonstrated that the presence of astrocytes induces the upregulation of C1q in neurons.¹⁶⁰ A follow up report showed that astrocytic release of TGF- β was necessary and sufficient to induce RGC C1q expression, and that blocking TGF- β signaling abolished microglia-mediated synaptic pruning in the LGN and impaired proper eye-specific segregation.⁹⁴ Astrocytes are also able to directly engulf C1q-tagged synapses via MEGF10, a known C1q receptor, and MERTK, which is known to function in the phagocytic clearance of dead cells via recognition of extracellular phosphatidylserine (PS) (Figure 2).^{162,163} The finding that these phagocytic receptors typically utilized for the clearance of dead cells raises the possibility that synapses might use “eat me” signals similar to that of dead cells in order to recruit and promote glial phagocytosis.

It is indeed likely that local apoptotic-like mechanisms regulate the removal of complement-tagged synapses, as C1q-labeled synaptosomes are associated with caspase-3 and annexin V (Figure 2).¹⁶⁴ Diminished neuronal activity leads to higher levels of synaptic C1q and elevated caspase-3 cleavage, suggesting that neuronal apoptotic-like signaling aids microglial-mediated process removal of complement-tagged synapses.¹⁶⁴ The caspase-mediated apoptotic cascade results in the transfer of PS from the inner to the outer leaflet of the plasma membrane (Figure 2).^{165,166} Intriguingly, newly published work and pre-print articles demonstrate that neuronal synapses to be pruned expose PS which acts as an “eat-me” signal for microglial phagocytosis.^{95,97,167} Pushing the system by forcing continuous PS exposure on neurons leads to specific elimination of inhibitory post-synaptic terminals.⁹⁷ Neuronal PS can be recognized by microglia via both the phagocytic receptor TREM2 and an alternatively spliced isoform of the adhesion G-protein coupled receptor GPR56 (Figure 2).^{95,167} Interestingly, the loss of C1q leads to an increase in synaptic PS but a decrease in microglia-mediated synaptic pruning during development,⁹⁵ suggesting that PS acts as a common signal in microglial phagocytosis of synapses along multiple pathways. An explanation for how the decrease in one “eat-me” signal leads to the elevation of another is lacking, as the precise link between these two pathways has yet to be worked out.

Beyond its role in the developing LGN, complement-mediated synaptic pruning has also been implicated in the proper elimination of excitatory synapses in the neocortex during development.¹⁶⁸ Pyramidal neurons in mice deficient in C1q have more excitatory inputs, and this is associated with the generation of spontaneous and evoked epileptiform activity which underlies absence seizures in C1q-deficient mice.¹⁶⁸ It is likely that complement-mediated synaptic pruning plays distinct roles in different brain regions across development, but thorough studies have yet to be conducted. Though baseline levels of complement proteins are much lower in the adult brain,¹⁶⁰ complement has also been shown to be involved in the reorganization of synapses even in the mature brain, truly exemplifying the versatility of the system.^{169,170} Moreover, hyperactivation of the complement system has been linked to many neurodegenerative disorders, as heightened microglial phagocytosis of complement-tagged synapses might account for aberrant synapse elimination associated with disease progression.⁵⁸

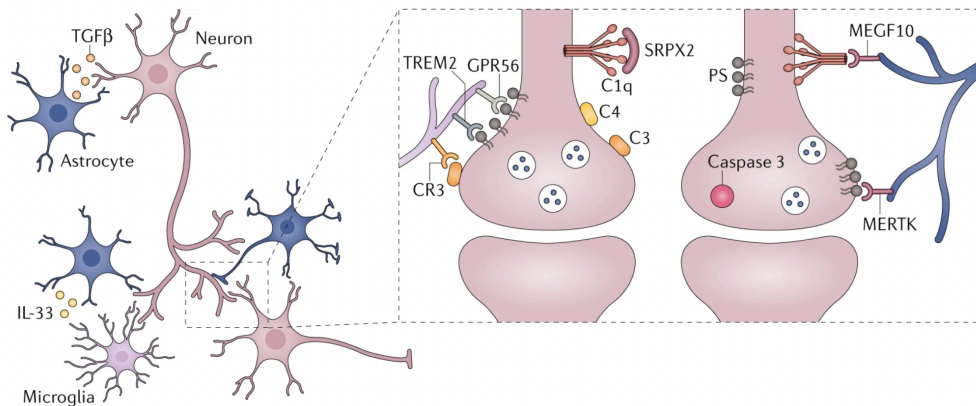


Figure 1.2. Phagocytic signaling underlies synaptic pruning

IL-33–ST2 signaling promotes synapse engulfment in the spinal cord and thalamus. Complement proteins (C1q, C4 and C3) are thought to mark synapses for elimination in the lateral geniculate nucleus. Astrocytes can release TGFβ to upregulate C1q on neurons. The recognition of C1q by MEGF10 is associated with astrocyte-mediated synapse elimination while CR3 recognition of C3 is associated with microglia-coordinated synapse phagocytosis. Complement-mediated synapse elimination can be limited by sushi repeat-containing protein SRPX2 binding of C1q. C1q-tagged synapses are also associated with caspase-3 and increased extracellular phosphatidylserine (PS). The phagocytic receptors GPR56, MERTK and triggering receptor expressed on myeloid cells 2 (TREM2) are thought to recognize extracellular PS and promote synapse elimination.

Another well-characterized mechanism that plays a role in limiting microglia-mediated synapse phagocytosis consists of signaling through the receptor CD47 and its ligand SIRPα.¹⁷¹ Neuronal CD47 acts as a “don’t eat me” signal recognized by microglial SIRPα and is specifically upregulated on more active synapses during development (Figure 1). The removal of CD47 from less active synapses serves as an additional signal for pruning. Synaptic pruning is an essential process for sculpting a properly functioning nervous system and has been extensively studied, though delineation of the details remains to be accomplished. Notably, glia play a critical role in this process by utilizing these complement-related mechanisms, among many others. These topics have been reviewed extensively elsewhere,^{172,173} thus, the discussion of synaptic pruning here will be limited simply to the role of the complement system. Finally, recent studies have demonstrated that homeostatic CNS complement activation is also intertwined with other innate immune signaling pathways including neuronal pentraxins and major histocompatibility complex molecules.

The importance of proper complement-mediated synapse control is highlighted by the association between disturbances in complement and neurodevelopmental disorders. A risk for schizophrenia is associated with certain C4 risk alleles which tend to produce heightened levels of C4.¹⁷⁴ Deposition of C4 may promote increased synapse elimination by microglia and promote neuropathology of schizophrenia.^{117,174} Certain alleles of complement control-related genes have also been identified as risk factors for schizophrenia.¹⁷⁵ Evidence for complement-mediated pathogenesis is also found in ASD. Elevated serum C1q levels have been reported in children with ASD,^{176,177} and C4 risk alleles as well as decreased plasma C4B levels have been associated with ASD.^{178–180} These links suggest that complement dysfunction may contribute to neurodevelopmental disorder pathology, presumably through dysregulated complement-mediated synapse elimination.

1.6.2. Toll-like receptors

Toll-like receptors (TLRs) are a class of receptors that recognize structural motifs common to invading pathogens and initiate signaling cascades that promote pathogen eradication.^{181–183} Work over the past two decades has revealed unconventional roles for TLRs in the development of the nervous system.^{184–188} It is known that TLRs are expressed by microglia and NPCs during neurodevelopment,¹⁸⁹ and by microglia, astrocytes, oligodendrocytes, and neurons in the adult CNS.^{190,191} TLR1-9 are expressed in the developing brain in temporally and spatially distinct patterns.¹⁸⁹ Microglia express a full repertoire of TLRs and utilize such PRR-mediated signaling to respond to pathogenic and other damaging insults to the CNS.^{184,192} Meanwhile, other CNS cell types only express select TLRs with differing levels throughout development and into adulthood.¹⁸⁴ It is now well accepted that non-immune cell types participate in immune responses to pathogens, and various instances of neuronal TLR function in response to CNS infection or injury have been uncovered.^{193–200} The

function of glial TLRs in health and disease have been reviewed elsewhere,^{187,201–205} as well as the function of neuronal TLRs in pathogenic conditions.^{187,201,205} Here, the focus will be on physiological functions of TLR signaling in neurons during CNS development. The functions of neuronal TLRs are beginning to be elucidated, and surprisingly, many roles for TLR signaling unrelated to PAMP/DAMP signaling have been uncovered.

Box 2: Toll-like receptors. Due to their ability to respond to such molecular patterns, TLRs are considered to be pattern recognition receptors (PRRs), a broader class of sensors that recognize pathogen-associated molecular patterns (PAMPs) and damage-associated molecular patterns (DAMPs).¹⁸⁵ PAMPs are pathogen-specific molecular signatures; for instance, bacterial LPS, dsRNA, unmethylated CpG DNA, flagellin, and peptidoglycans are all classified as PAMPs.¹⁸⁷ DAMPs are molecules associated with danger/damage which typically derive from the host; for instance, ATP, cytosolic DNA, and hyaluronan are all considered to be DAMPs.¹⁸⁸ There have been 10 human (TLR1-TLR10) and 12 mouse (TLR1-9, TLR11-13) TLRs identified to date which recognize intracellular or extracellular PAMPs and DAMPs as homo- or heterodimers along with co-receptors or accessory molecules.¹⁸⁵ Extracellular TLRs (TLR1, TLR2, TLR4-6, and TLR10) localized to the cell surface primarily recognize motifs common to the outside of a pathogen, whereas intracellular TLRs (TLR3, TLR7-9, and TLR11-13) localized to internal compartments of cells typically recognize nucleic acids.¹⁸⁵ TLRs signal with the aid of an adaptor molecule containing a TIR (Toll/IL-1 receptor) domain, such as MyD88 which is used by nearly all TLRs.¹⁸⁴ Association of MyD88 with a TLR recruits a kinase of the IRAK (interleukin-1 receptor-associated kinase) family, which then activates TRAF6 and downstream signaling that ultimately initiates the activation of transcription factors.¹⁸⁴ Such transcription factors include AP-1 and NFκB, which initiate the transcription of pro-inflammatory genes such as inflammatory cytokines and type I interferon (IFN) signaling components.^{184,185} MyD88-independent signaling can also occur in the case of TLR3 and TLR4, which utilize TRIF and ultimately can activate AP-1 and NFκB, in addition to the transcription factor IRF3, to transcribe pro-inflammatory genes.^{184,185}

Neurogenesis

TLRs classically recognize patterns associated with pathogen infection; however, it remains possible that novel endogenous ligands could activate these receptors during nervous system development. Extracellular TLR2 can be activated by multiple different PAMPs and DAMPs, mostly derived from bacteria, as a homodimer or as heterodimers with either TLR1 or TLR6.^{206,207} Intracellular TLR3 is activated by dsRNA, for instance, derived from viruses.^{206,207} It has been demonstrated that TLR2 and TLR3 are expressed in highly proliferative regions of the developing cortex and act to negatively regulate NPC proliferation in these zones.^{208,209} Activation of TLR2 signaling by injecting embryonic brains with TLR2 agonists arrests NPCs in M phase and significantly reduces the number of actively dividing cells.²⁰⁸ Though this data might suggest a mechanism by which brain growth could be stunted during embryonic infection, it has been shown that *Tlr3*^{-/-} mice have a significantly greater number of progenitors expressing markers of active division, indicating that TLR3 might possess roles in homeostatic brain development in the absence of a pathogen.²⁰⁹ These studies provide evidence that at least TLR3 has important homeostatic roles to limit NPC proliferation; nevertheless, ligands able to drive these effects have yet to be identified. Interestingly, soluble CD14, a well-characterized co-receptor for TLR2 and TLR4,²¹⁰ has been identified as a TLR2 ligand in the CNS,²¹¹ raising the possibility that it could function as an endogenous ligand during CNS development.

TLR4 has been shown to act in a similar manner in restricting RPC proliferation in the developing retina.²¹² Extracellular TLR4 classically recognizes bacterial LPS,^{206,207} but during development TLR4 deficiency increases RPC proliferation while TLR4 overexpression inhibits some RPCs from dividing.²¹² TLR4 appears to tune the responsiveness of RPCs to growth factor-induced proliferation, as deficiency in TLR4 enhances the number of RPCs induced to divide following growth factor administration *in vitro*.²¹² It has been suggested that TLRs act to regulate fate decisions of dividing progenitors in the developing brain, and therefore help dictate the balance of cell types in the adult brain. For instance, it has been shown that a deficiency in TLR4 fails to restrict RPC proliferation which ultimately leads to a greater number mature neurons, independent of changes in apoptosis.²¹² Again, the endogenous ligands mediating these effects have yet to be identified, but certain candidates exist. For example, gangliosides and heat shock proteins have both been demonstrated to act as TLR4 ligands in the CNS.^{213,214}

The exact mechanisms underlying the ability of TLRs to limit progenitor proliferation in the developing brain are still poorly described. However, studies in the adult brain have shed light on what the neurodevelopmental process might entail. One study found that MyD88-dependent PKCα/β activation of NFκB signaling regulated TLR2- and TLR4-mediated NPC proliferation and differentiation during hippocampal neurogenesis.²¹⁵ Furthermore, the TLR4 pathway was able to operate in a manner independent of MyD88 via IKK phosphorylation and activation of the transcriptional factor IRF3.²¹⁵ This is consistent with the operation of these signaling pathways in immune cells in response to PAMPs.

Cell dieback

Various intracellular TLRs have been implicated in the regulation of neuronal death,^{216–219} an important process for the proper sculpting of neuronal circuits during development. TLR8 is expressed in the developing brain and localizes specifically to neurites and axons.²¹⁶ Stimulation of TLR8 in primary cortical neurons can promote apoptosis via a mechanism that is independent of the canonical MyD88-MAPK-NFκB signaling cascade utilized by immune cells. Instead, the mechanism might involve the downregulation of IκBα and IRAK4.²¹⁶ In another possible signaling pathway, dual activation of endosomal TLR7 and TLR9 recruits the TLR adaptor SARM1 to mitochondria, which promotes the accumulation of damaged mitochondria in neurites and ultimately apoptosis.²²⁰ Beyond this, TLR7 can be activated by the neuronally-produced miRNA *Let7b*, which leads to cell death dependent on MyD88 signaling.²²¹ This process was shown to occur in the adult brain to cause neurodegeneration,²²¹ but it demonstrates the principle that endogenous RNAs could activate TLR signaling during healthy neurodevelopment.

Another mechanism that might utilize the TLR signaling cascade to regulate neuronal survival involves the MyD88 family protein, MyD88-5, which is expressed primarily in neurons of the developing brain and not in immune cells.²²² MyD88-5 associates with mitochondria and recruits JNK3 to the mitochondrial compartment in response to hypoxia and glucose deprivation.²²² JNK3 has previously been characterized to promote apoptosis by inhibiting anti-apoptotic proteins and promoting pro-apoptotic protein effector functions.^{223–227} As both TLR8 and MyD88-5 are expressed in healthy developing brains, it raises the possibility that these two proteins have the capability to promote the survival of developing neurons along separate pathways; however, functional *in vivo* studies to demonstrate this have not been conducted to date.

Neuronal morphology

Physiological roles for TLRs that recognize patterns specific to pathogens may be difficult to ascertain; however, some TLRs recognize patterns associated with host cells in addition to pathogens. For instance, TLR7- and TLR8-mediated recognition of ssRNA can act to alert host cells of danger but might also provide a mechanism that could be co-opted for homeostatic reasons. TLR8 has been shown to localize to axons and neurites of immature neurons,^{216,228} placing it in an appropriate position to potentially regulate the dynamics of these structures during the critical neurodevelopmental phases of target selection and synaptic formation. Indeed, activation of TLR8 *in vitro* leads to a reduction in neurite outgrowth that would typically be observed in freshly cultured neurons, along with an increase in spine density, while axonal growth is not impacted.^{216,228} Hippocampal neurons of *Tlr7*^{-/-} mice have more complex dendritic architecture compared to TLR7-sufficient mice,²²⁹ suggesting that TLR7 is necessary for achieving proper dendritic pruning in some neurons during CNS development. Interestingly, this effect was observed at P7 in the hippocampus, but not in the cortex at any time points evaluated nor at P21 in the hippocampus.²²⁹ These results suggest that TLR7-mediated neuronal morphology control is region- and time-dependent and that other mechanisms may compensate at later time points for the loss of this process.

It has been shown that TLR7 and TLR8 are able to recognize host-derived ssRNAs. These TLRs are able to activate in response to endogenous miRNAs in various processes that contribute to diverse aspects of neuronal function.^{221,229–232} miRNAs exert their effects by restricting the translation of their target mRNAs, which can occur cell non-autonomously via exosome release or cell-autonomously.^{233,234} In the cell non-autonomous case, neighboring cells may take up released exosomes, allowing miRNAs to inhibit target translation via cellular transfer.²³⁴ Multiple miRNAs, such as *MiR21*, *MiR29*, and members of the *Let7* family, have been shown to be recognized by neuronal TLRs and regulate various neuronal functions such as the induction of cell death or production of action potentials.^{221,229,231,232} The ssRNA-sensing, neuronally-expressed TLR7 is activated by the endogenous miRNAs *Let7c* and *MiR21* during postnatal periods of circuit sculpting.^{229,235} This activation results in a restriction of dendritic outgrowth via a classic immune system MyD88-cFos-IL-6 signaling pathway.²³⁵ TLR-mediated activation of MyD88 can lead to the expression of the immediate early gene, *cFos*, and cytokines like *IL6* as a result of the activation of transcription factors such as NFκB and AP-1.²³⁶ The data presented in this study suggest that IL-6 can act in both an autocrine and paracrine manner to regulate neuronal morphology. Furthermore, the miRNAs *Let7c* and *MiR21*, expressed by neurons, could function in both cell-autonomous and cell-non-autonomous manners. In a cell autonomous case, a single neuron could release the miRNA which would be taken up by that same neuron to elicit its effect. In contrast, a non-cell-autonomous pathway would

function by exosome release of the miRNA to neighboring neurons, which then restricts dendritic growth in neurons that uptake those exosomes. The precise mechanism underlying this has yet to be fully elucidated.

Though it remains unknown whether TLR3 recognizes endogenous dsRNA (such as motifs of secondary RNA intra-molecular interactions), activation of TLR3 has been shown to correlate with the collapse of growth cones in developing dorsal root ganglion (DRG) sensory neurons.²¹⁷ TLR3 localizes to endosomes in growth cones of DRG neurons and its activation inhibits neurite outgrowth in a mechanism independent from the canonical MyD88-NF κ B signaling axis.²¹⁷ Interestingly, the mechanisms controlling axon and dendrite outgrowth might be separate as TLR3 activation in cultured neurons inhibits dendritic growth in a mechanism dependent on MyD88 signaling. In this case, MyD88-driven signaling was found to induce the expression of *Disc1*, a component necessary for the change in dendritic growth.²³⁷ Notably, both of these studies directly activated TLR3 using the viral dsRNA mimetic polyinosinic:polycytidylic acid (polyI:C); thus, it still remains unclear whether TLR3 acts to control neurite outgrowth via endogenous ligands in a healthy developing nervous system.

Overall, intracellular TLRs recognizing endogenous RNAs act to restrict dendritic growth, yet the precise effects and downstream signaling mechanisms differ. All three of these intracellular TLRs (i.e. TLR3, TLR7, and TLR8) can use the canonical MyD88-dependent signaling pathway to mediate these changes in neuronal morphology; however, the transcriptional effects are quite diverse.²²⁸ TLR3 and TLR7 activation tends to induce transcriptional programs characteristic of innate immune responses, while TLR8 activation does not lead to robust changes in similar programs.²²⁸ TLR3 activation also leads to the downregulation of transcriptional programs related to cell adhesion, while TLR8 activation downregulates the expression of immediate early genes such as *Arc* and *Egr1*.²²⁸ The effectors driving these changes are just as diverse; for instance, TLR7 requires the involvement of IL-6 function while TLR8 and TLR3 are able to function independently of cytokine signaling.^{228,235,238} It is also highly likely that these different TLR-mediated morphology programs are utilized in spatially and temporally distinct manners, and even more, that the programs themselves differ in the same aspects.

The TLR adaptor molecule SARM1 is also independently able to regulate neuronal morphology via interaction with Syndecan-2, which is known to promote spine formation during neurodevelopment.²³⁸ SARM1 promotes dendritic arborization and contributes to spine formation during development in conjunction with Syndecan-2, via a pathway that utilizes JNK signaling.²³⁸ SARM1 has also been shown to be protective against Wallerian degeneration,²³⁹ a process of axon dieback that occurs as a result of traumatic severing,²⁴⁰ suggesting that this adaptor could also potentially function to regulate axonal growth during development.

Behavior

Studies of the adult brain act to demonstrate the functional importance of TLRs in contributing to proper neurodevelopment, as the loss of particular TLRs has been shown to contribute to various behavioral abnormalities. *Tlr2*^{-/-} mice exhibit hyperlocomotion, reduced anxiety, impaired sociability, aggression, and cognitive defects.²⁴¹ *Tlr2*^{-/-} mice reconstituted with wild type bone marrow are also highly susceptible to high fat diet-induced obesity, suggesting a non-hematopoietic-related involvement of TLR2 in metabolic regulation.²⁴² Indeed in one study TLR2 was shown to act as a metabolic regulator on hypothalamic neurons to modulate feeding behavior.²⁴² *Tlr3*^{-/-} mice have lowered anxiety and enhanced hippocampus-dependent memory.²⁴³ These abnormalities might be driven by an increase in hippocampal neurogenesis in these mice, which correlates with an increase in CA1 and dentate gyrus volumes,²⁴³ or as a result of altered neuronal excitability and synaptic transmission, which has been observed following the activation of TLR3 in neurons.²⁴⁴ Similar memory and anxiety changes are seen in *Tlr4*^{-/-} mice, in addition to disturbances in drug reward behavior.^{245,246} *Tlr7*^{-/-} mice have reduced exploratory behaviors, lowered anxiety, reduced aggression, sharpened olfaction, and impaired contextual fear memory.^{235,247} Furthermore, *Tlr9*^{-/-} mice have been reported to have hyper-responsive sensory and motor phenotypes, with no alteration in learning and memory.²⁴⁸ Finally, the TLR adaptor SARM1 is also critical for proper brain development, as *Sarm1*^{-/-} mice have impairments in associative fear memory, cognitive flexibility, and sociability.²⁴⁹

Aberrant TLR activation during development is also a significant risk factor for neurodevelopmental disorders. Neuronal TLR3 activation inhibits dendrite outgrowth and activation during postnatal development contributes to altered synaptogenesis.²³⁷ Prenatal activation of TLR7 leads to diverse behavioral deficits alongside altered

microglia colonization and morphology.²⁵⁰ Interestingly, altered gene expression profiles resulting from prenatal TLR7 activation were highly sex-dependent.²⁵⁰ Moreover, the most commonly used model of MIA utilizes the TLR3 agonist polyI:C which faithfully recapitulates many of the core phenotypes of ASD in offspring.^{251,252} The contribution of gestational inflammation to neurodevelopmental dysfunction will be discussed in greater depth in later sections. Altogether, these behavioral studies point toward important functional consequences of TLR action in the developing brain, and further suggest that different TLRs play both separate and overlapping roles during neurodevelopment.

In summary, multiple TLRs are implicated in the processes of neurogenesis, cell dieback, and in shaping neuronal morphology during development of the nervous system. In many cases, the activating ligands have yet to be identified and the downstream effectors remain under-characterized. It has been posited that the overarching function of TLRs during CNS development is to guide the positioning of neurons in the appropriate microenvironment. For instance, the detection of ligands derived from dead cells might signal through TLR-mediated pathways to promote death or process retraction in that neuron. This could act to ensure that neurons avoid growth near dead cells or noxious stimuli and to regulate the proper distribution of neurons in a given region.

1.6.3. Cytokines

Multiple CNS cell types are capable of producing cytokines at the steady state and during inflammatory events, with microglia and infiltrating immune cells being the primary sources.^{190,253–255} The role of cytokines in CNS infection, neurodegeneration, and injury are beginning to be elucidated, yet initial studies demonstrate that a complicated network is at play.^{256–259} It is clear that cytokines mediate diverse processes such as neurogenesis, controlling the switch to gliogenesis, migration, axon pathfinding, fate specification, differentiation, survival, and likely more.^{255,260,261} These processes are important in the CNS during homeostasis and pathogenesis in the developing brain as well as in the adult brain, and as a result, there is a wealth of literature describing various roles for cytokines in the brain. This section will focus on a few fundamental examples of the important roles that cytokines play during CNS development.

Box 3: Cytokines. Cytokines are an ancient and diverse class of small signaling proteins that exert pleiotropic effects on their target cells.^{257–261} Over 300 cytokines have been identified and can be secreted from a wide array of cell types—classically, those of the immune system—to signal in a receptor-dependent manner and activate JAK-STAT or MAPK downstream pathways.^{257,259,262} Cytokines can be classified into a variety of families which include interleukins (IL), growth factors, IFNs, tumor necrosis factors (TNF), colony stimulating factors, and chemokines.^{257,260,262,263} The nervous system also has a few unique families of cytokines which include the neurotrophins and neuropoietins.²⁶² Typically, cytokines are expressed at low levels in both the periphery and the CNS and are highly upregulated in response to immune challenge or injury.^{257,260,261,263} Cytokines can act as growth factors, pro-inflammatory mediators, anti-inflammatory mediators, instructors of immune cell differentiation and effector function mobilization, and more.^{257,258,261,262} Individual cytokines can exert complex effects on a given cell type, which may be further complicated by the interaction between multiple cytokine signals, the microenvironment, and the specific cell type.^{257,260}

Many of the essential growth factors for cells of the nervous system fall into cytokine families, for example, BMP and TGF- β .²⁶¹ Members of the neuropoietic (gp130) cytokine family—which is composed of CNTF, LIF, CT-1, OSM, and IL-6—also play diverse roles during neurodevelopment; particularly notable are functions in regulating neurogenesis, fate specification, and differentiation.^{262,263} IL-6 is a pro-inflammatory cytokine that stimulates acute immune responses²⁶⁴ and is also expressed in the developing brain,^{265–268} where it can protect against cytotoxicity, act as a neurotrophic factor, regulate dendrite growth, and influence neurotransmitter phenotype.^{269–277} The roles of the gp130 family of cytokines in such neurodevelopmental processes have been reviewed elsewhere^{262,263} and thus will not be covered in detail here.

The IL-1 family of cytokines includes IL-1 α , IL-1 β , and IL-33, among others, and are potent inflammatory mediators that classically act to activate and polarize many cell types of the immune system.²⁷⁸ IL-1 α and IL-1 β act on the same receptor, IL-1R1 in conjugation with IL-1R accessory protein (IL-1RAP), to initiate MyD88-dependent downstream signaling that typically activates MAPK and NF κ B pathways.²⁷⁸ IL-33 signals through the receptor ST2 which recruits the shared receptor subunit IL-1RAP to initiate downstream pathway activation.²⁷⁸ IL-1 α and IL-1 β both have known roles influencing neurogenesis.^{254,255,260} In some cases, IL-1 β and IL-1 α can promote neuronal proliferation and differentiation while in other contexts these cytokines are inhibitory to such processes.^{61,279–290} IL-1 β and IL-1 α have also been shown to influence astroglialogenesis,^{290,291} and therefore might

contribute to fate decisions during nervous system development. IL-1 β has also been shown to contribute to various other neurodevelopmental processes, including neuronal migration, neurite growth, and axon pathfinding.^{292–295} The role of IL-1 α and IL-1 β during neurodevelopment is complex, and each of these cytokines likely exerts effects that depend upon the cell type, microenvironment of the brain region, time point, and converging signaling cascades, among others. IL-RAP has been shown to act as a trans-synaptic organizer to modulate synapse formation.^{296–298} Intriguingly, mutations in IL-RAP have been linked to various forms of mental retardation.^{299,300} Null mutations in *Ilrap1* in mice are associated with decreased spine density, impaired excitatory synapse formation, and deficits in synaptic plasticity in the hippocampus.²⁹⁸ The same *Ilrap1*^{-/-} mice show impaired excitatory/inhibitory balance in the cerebellum and amygdala during development.^{301,302} These studies point toward an essential role for IL-RAP in organizing synapses during neurodevelopment.

IL-33 is an alarmin that is released during tissue damage but is also known to play homeostatic roles in tissue development and remodeling both in the periphery and the brain.^{303–305} Recently, a role for IL-33 in synaptic pruning by microglia during neurodevelopment has been reported.¹⁶¹ Astrocytes produce IL-33 in the vicinity of an unwanted synapse during the refinement stage of nervous system development, which acts as a signal to promote microglial engulfment (Figure 2).¹⁶¹ This is mediated in part by signaling through the IL-33 receptor, ST2, on microglia.¹⁶¹ Such signaling might be acting in concert with other microglial receptors that are also known to mediate synapse phagocytosis, such as CR3 and TREM2. This process is functionally important for proper circuit formation, as the loss of IL-33 results in a greater number of synapses which is correlated with circuit dysfunction, as demonstrated in the thalamus and spinal cord.¹⁶¹ *Il33*^{-/-} mice display lower levels of anxiety and impaired social recognition,³⁰⁶ further illustrating the importance for IL-33 in the proper formation of neuronal circuits.

Many other cytokines have also been described to influence neurodevelopment. The growth factor CSF1 and its receptor CSF1R are well accepted to be necessary for driving differentiation of tissue resident macrophages, among other immune cell types.^{27,307,308} It has recently been shown that IL-34, another ligand of CSF1R, produced by neurons is an essential factor for maintaining the microglial population in the brain.^{309,310} In the immune system, IL-4 is well known to promote T_H2 differentiation and to regulate proliferation and apoptosis of many immune cell types.³¹¹ In the brain, IL-4 acts to promote adult neurogenesis in the dentate gyrus,^{312–314} which is produced in part by meningeal CD4⁺ T cells in response to cognitive activity.^{315–318} It remains to be fully elucidated whether IL-4 plays a similar role to promote neurogenesis during development. IL-9 acts to promote T_H9 differentiation but is also greatly pleiotropic and exerts diverse effects on different immune cell subsets.³¹⁹ IL-9 acts on cortical neurons to reduce the expression of pro-apoptotic factor Bax and mediate a neuroprotective effect during the cell dieback phase of neurodevelopment.^{320–322} TNF- α , IFN- γ , and IFN- α have also been shown to influence neurogenesis, but the majority of these studies have been done *in vitro* or in the adult brain,²⁵⁵ thus, it remains uncertain whether these cytokines also regulate neurogenesis during brain maturation. In summary, cytokines are a diverse set of signaling molecules that mediate multiple arms of neurodevelopment through complex mechanisms. Just as in the immune system, the cytokine network in the developing brain is intricate and pleiotropic, and significant work to understand the diverse roles of individual cytokines is certainly warranted.

1.6.4. Chemokines

Chemokines offer a prime example of molecules that elicit similar responses in immune cells and nervous system cells alike, but also play distinct and unrelated roles in each system. Chemokines compose a subset of the cytokine family and are primarily secreted proteins.^{323,324} There are numerous chemokines that signal through different chemokine receptors, all of which are G-protein coupled receptors that typically promote actin reorganization and cell polarization once activated.^{323,324} The archetypal function of chemokines is in cell migration, whereby cells expressing a given chemokine receptor move along a gradient of a cognate chemokine and arrest at the site of highest concentration.^{323,324} This is typified in the immune system whereby leukocytes traffic according to chemokine signals during both homeostasis and inflammatory events.³²⁴ For instance, naïve T cells circulate through the bloodstream, lymph nodes, and lymphatics according to coordinated chemokine-mediated signaling.³²⁴ Once a T cell has encountered its antigen, the repertoire of chemokine receptors expressed will change, allowing the T cell to migrate toward sites of inflammation where different chemokine signals are rapidly and robustly produced.³²⁴

In a similar manner, chemokines control the trafficking of cells of the nervous system during development to control the patterning of nervous system tissue.^{261,323,325–327} The chemokine signaling pair CXCL12:CXCR4 has been extensively studied for its role in mediating neuronal migration in multiple brain regions.^{325–327} The contribution of CXCL12:CXCR4 signaling to the migration of cerebellar neurons during development will be briefly described here as an example, though this process has been extensively reviewed elsewhere and thus the discussion here will be kept brief.^{261,323,325–327} During cerebellar development, granule precursor cells (GPCs) migrate from the rhombic lip to the cerebellar surface where they proliferate to form the external granule layer (EGL), and eventually some cells migrate inward past the Purkinje cell layer to form the internal granule layer (IGL).^{261,325,326} Meningeal cells secrete CXCL12 which acts as a chemoattractant for GPCs expressing CXCR4 to migrate tangentially and form the EGL.^{328–333} The loss of CXCR4 or CXCL12 leads to abnormal cerebellum patterning, whereby granule cells migrate prematurely into the IGL.^{329,330,332,333} This demonstrates that meningeal CXCR4 drives the migration of GPCs along the EGL and keeps GPCs in the EGL to undergo proper proliferation prior to inward migration; thus, disruption leads to abnormal migration patterns and aberrant layering.^{261,325}

CXCL12 signaling through CXCR4 and its other receptor, CXCR7, has also been implicated the migration of other neuronal types in diverse brain regions; including granule cells of the dentate gyrus, Cajal-Retizius cells of the cortex, sensory neurons of the DRG, and more.^{334–340} CXCL12 signaling has been shown to be important for axon pathfinding during development.^{15,16,341–344} Chemokine signaling likely impacts proper glial proliferation and patterning during development as well, as the loss of CXCR4 or CXCR2 reduces the number of OPCs in the spinal cord and the loss of CXCR2 impairs proper oligodendrocyte patterning.^{345,346}

The transmembrane chemokine CX3CL1 (also known as fractalkine) and its receptor CX3CR1 are involved in the recruitment of various immune cell types to sites of inflammation, but this pair is also utilized by the nervous system to mediate neuron-microglia interactions.^{323,347,348} In the immune system, CX3CR1 is expressed by monocytes, macrophages, NK cells, T cells, and dendritic cells in a tissue-specific manner and acts to stimulate the migration of these cells via CX3CL1 to sites of tissue damage or infection.³⁴⁷ CX3CL1 can be cleaved by proteases, such as cathepsin S or ADAM10/17, to generate a soluble form of CX3CL1 that also acts as a ligand for CX3CR1.^{347,348} In both immune and nervous systems, activation of CX3CR1 stimulates downstream signaling pathways that promote the transcription factors CREB and NF κ B to mediate the production of inflammatory cytokines, among other activating functions.^{347,348} In the nervous system, CX3CL1 is primarily expressed by neurons and CX3CR1 is exclusively and constitutively expressed by microglia.^{348,349} Transmembrane neuronal CX3CL1 is cleaved and acts to recruit microglia to promote trophic support for neurons during development, for instance, by releasing factors such as IL-1 β , IL-6, TNF- α .^{80,81,323,348,350–352} CX3CL1:CX3CR1 signaling also contributes to proper circuit formation, as CX3CR1 modulates microglial motility and recruitment to synapses, which is necessary for proper synapse maturation.^{84,108,353,354} This signaling also likely plays a role in the recruitment of microglia to phagocytose unwanted synapses during pruning stages of circuit formation.⁹²

1.6.5. Inflammasomes

Inflammasomes are multi-protein complexes that assemble following the activation of PRRs and mediate the production of inflammatory cytokines which could also be accompanied by cell death.³⁵⁵ In the canonical model of inflammasome activation, cytosolic PRR sensors activate in response to intracellular PAMPs or DAMPs, which triggers oligomerization and promotes recruitment of caspase-1.³⁵⁵ Most inflammasomes use the adaptor protein ASC to bridge the sensor with caspase-1.³⁵⁵ Assembly of this platform facilitates activation of caspase-1, which then acts to cleave downstream target molecules that promote a pro-inflammatory state.^{356,357} Important effectors of inflammasome assembly include the activation of pro-inflammatory cytokines IL-1 β and IL-18, as well as cleavage of gasdermin D which can assemble to form pores in the plasma membrane.^{356,357} Gasdermin D pores facilitate cytokine release from the cell and can also lead to an inflammatory type of cell death known as pyroptosis, which may be avoided via ESCRT-mediated membrane repair.^{356,358}

Unsurprisingly, microglia and other CNS-resident myeloid lineage cells express the highest levels of inflammasome components. However, inflammasome activation in neurons and astrocytes has also recently been demonstrated.^{190,359} Inflammasome assembly in the CNS was first characterized in the context of microglia

and other cell types responding to danger signals associated with infection,^{360–364} injury,^{365,366} or neurodegeneration.^{367–371} For instance, inflammasome activation in the CNS has been shown to drive neurodegenerative diseases such as Alzheimer's disease, in which ASC specks, indicative of inflammasome activation, are released from microglia and can seed amyloid β oligomerization to drive disease progression.³⁷¹

The rapidly dividing state of cells during development engenders accumulation of genotoxic stress which can persist if improperly repaired by DNA damage repair pathways.^{372,373} The cytosolic dsDNA sensor AIM2 has been shown to coordinate inflammasome activation and incite pyroptotic cell death in neurons with DNA damage.^{374–380} Newly published work has demonstrated that AIM2 responds to neuronal DNA damage during development to mediate the removal of genetically compromised cells (Figure 3).⁵⁶ This process is dependent on the presence of gasdermin D, and the loss of AIM2 leads to a greater number of neurons in the adult brain which harbor higher amounts of DNA damage.⁵⁶ Altogether, these findings suggest that pyroptotic cell death during neurodevelopment, orchestrated by the AIM2 inflammasome, is necessary for proper brain formation.⁵⁶

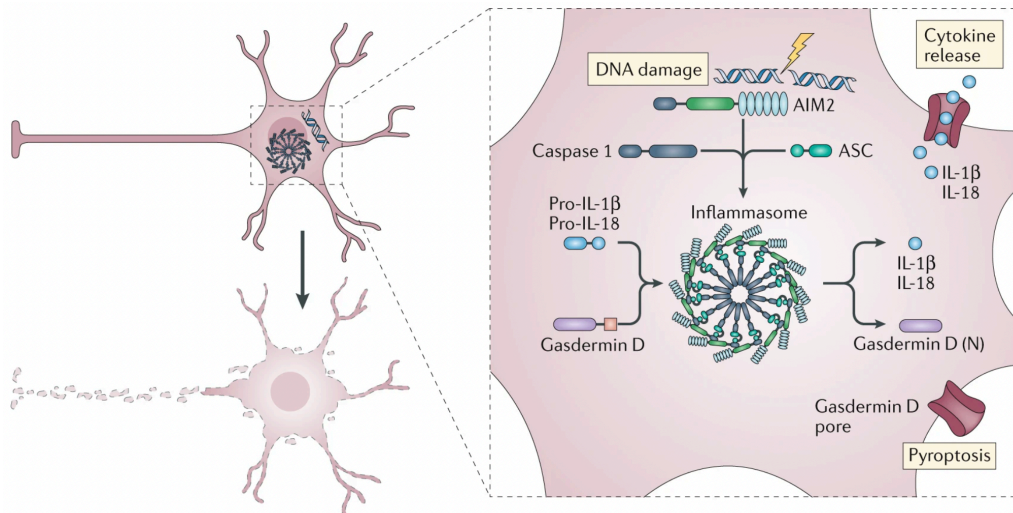


Figure 1.3. AIM2 inflammasome signalling contributes to CNS cell dieback.

Binding of AIM2 to cytosolic DNA initiates assembly of AIM2, ASC and caspase 1 to form the inflammasome multiprotein complex. Inflammasome activation cleaves gasdermin D, the N-terminal fragments of which assemble to generate pores in the membrane to promote cytokine release and pyroptosis. Activation of the inflammasome also cleaves pro-cytokines IL-1 β and IL-18 to generate active forms that can be released from the cell; however, cytokine signalling does not appear to be involved in the neurodevelopmental removal of genetically compromised cells.

The AIM2 inflammasome has also been demonstrated to regulate neuronal morphology *in vitro* in response to exogenous dsDNA and *in vivo* during development, though the effectors that incite inflammasome activation to mediate this effect during development remain unidentified.³⁸¹ Activation of the AIM2 inflammasome in neurons can alter dendritic length and branching and axonal length.³⁸¹ The loss of AIM2 leads to altered dendritic arborization in the developing and adult brain.³⁸¹ Interestingly, inflammasome-mediated cytokine production and signaling was found to be important for these changes in morphology induced by AIM2 activation,³⁸¹ raising the possibility that the inflammasome acts as a platform to generate cytokine mediators of neurite growth. This work suggests that the DNA sensor AIM2 might be important for proper neuronal process elaboration during development, though the mechanistic details remain to be delineated.

It has yet to be fully explored whether other inflammasomes (e.g. the NLRP3 inflammasome, the NLRP1 inflammasome, etc.) contribute to homeostatic neurodevelopment. Nevertheless, behavioral abnormalities seen in caspase-1 and AIM2 deficient mice are absent in NLRP3 deficient mice, suggesting that perhaps other inflammasomes are less necessary for proper nervous system formation.⁵⁶ Inflammasomes present an intriguing platform for sensing of internal cellular stress which can be commonplace during development. Additional work on this front will likely reveal additional roles for inflammasome function during the formation and maintenance of a properly functioning nervous system.

1.7 Maternal immune activation

Neurodevelopment is a beautifully coordinated and precise process that requires expert timing and organization for proper execution. Disruption at any stage could potentially have dire consequences from the molecular to the circuit level. Countless epidemiological studies in the past few decades have linked maternal infection during pregnancy with a heightened risk for neurodevelopmental disorders.^{382–384} Maternal infection with Rubella, influenza, *Toxoplasma gondii*, and many other diverse types of pathogens have been increasingly correlated with many complex multigenic cases of neurologic dysfunction.^{251,385,386} Maternal risk factors for abnormal immune system activation during pregnancy, such as autoimmune disease, diabetes, and certain genetic risk variants, have also been tied to offspring neurologic dysfunction.³⁸⁷ Environmental insults capable of causing inflammation, such as maternal stress, maternal obesity, pesticides, and pollution, are additional risk factors for future offspring neuropathology.¹³³ These studies paired with clinical observations have illustrated that maternal immune activation is a significant risk factor for neurodevelopmental disorders including ASD,^{101,384,388–391} schizophrenia,^{382,383,392–395} cerebral palsy,³⁹⁶ and epilepsy³⁹⁷ as well as being a potential precipitating factor for neurodegenerative disease.^{132,398,399}

In reality, many factors likely converge to contribute to disease onset which might include the level of immune activation and the type of immune response, as well as other factors such as genetic predisposition, maternal diet, prenatal stress, and more. Nevertheless, immune activation certainly accounts for a piece of the puzzle, and the commonalities in signaling pathway between the nervous and immune systems described in this review provide a basis for such interaction. For instance, neurons use many of the same signaling pathways as immune cells, such that immune infiltration and inflammatory signaling could possibly converge to incite dysfunction during development. Immune activation alone could alter the delicate signaling milieu of nervous system tissue enough to cause lifelong alterations. Furthermore, abnormal maternal immune activity might permanently alter the fetal immune system or prime it for dysfunction later in life. This is supported by the observation that autistic and schizophrenic patients often have immune dysfunction.^{101,400,401}

Studies conducted over the past two decades have provided direct links between MIA, offspring brain dysfunction, and behavioral abnormalities typical of ASD or schizophrenia.^{9,10,251,385,386,402} Mouse models of MIA are numerous with differences in immunogen challenge type, timing, and dose all contributing to distinct phenotypes.^{9,10,251,385,403} Importantly, maternal infection in humans does not always lead to neurodevelopmental disorders in offspring but instead might act as a primer for future "hits", including risk factors such as genetic predisposition, stress, or other environmental insults.^{9,10,133,134,404,405} Maternal inflammation likely acts as a primer for synergistic effects precipitating disease symptoms. The MIA mouse model is amenable to incorporating multiple hits, for instance, one version combines prenatal low-dose polyI:C exposure with postnatal sub-chronic stress.⁴⁰⁶ Such work using these heterogeneous models has begun to unravel the biological underpinnings of MIA-driven neurological dysfunction. The phenomenon of MIA-induced neurologic dysfunction and current animal models of MIA have been thoroughly reviewed in the past decade,^{9,10,99,251,385,387,403} thus, this review will highlight a few examples and key players. Though MIA has been linked to a wide array of neurological conditions, this review will provide an overview of MIA as a precipitating factor for ASD and schizophrenia as these disorders have been the most extensively studied mechanistically.

1.7.1. Autism spectrum disorder

Autism spectrum disorders are a group of multifactorial disorders in which a convergence of genetic and environmental risk factors is posited to contribute to the onset of neurological dysfunction as a result of developmental abnormalities.⁴⁰⁷ The symptoms of ASD, which are diverse in etiology and severity, are characterized in DSM-5 by deficits in social-emotional interactions and/or communication as well as stereotypical or repetitive behaviors.⁴⁰⁸ These symptoms typically appear during the early postnatal development period, but may not fully be apparent if mild or masked by learning, or might not manifest until later in life when social demands present a stressor.^{407,408} The disorder is also highly sex-biased with males being four times more likely to be diagnosed with ASD compared to females.¹³⁰ Maternal inflammation is a risk factor for ASD diagnosis and signs of neuroinflammation have been reported in individuals with ASD.^{9,101,409,410} For instance, elevated levels of TNF, IL-1 β , IL-6, IL-13, and CCL2 have been measured in the CSF of individuals with ASD.⁴¹¹

In the most frequently used mouse model of MIA-induced ASD, pregnant mothers are injected with the dsRNA viral mimetic polyI:C at or around E12 (Figure 4).^{9,10,251,385} Male offspring of these mice display core symptoms associated with ASD including communication deficits, impaired sociability, and repetitive behaviors (Figure 4).^{9,10,251,385} The baseline immunogenicity of dams, type of immune response induced, and polyI:C treatment regimen all additionally contribute to the susceptibility of the pregnancy to induce offspring behavioral phenotypes.⁴¹² These factors are notable as it speaks to the variability that is also associated with the human condition.

The gut not only tunes the immune compartment but also directly influences cognition, acting as a critical nexus of brain-immune interaction. Maternal microflora colonize the fetal gut and commensal bacteria influence immune system development by coordinating the maturation of specific immune cell subsets.^{413,414} Dysbiosis and gastrointestinal dysfunction, perhaps primed by maternal microflora, are common in ASD and may modulate immune and neurological dysfunction.⁴¹⁵⁻⁴¹⁹ Treating MIA offspring orally with *Bacteroides fragilis* is sufficient to correct gut dysfunction and many autistic-like behavioral abnormalities.⁴¹⁸ These studies point toward a critical gut immune-brain connection that is disrupted in ASD and may be influenced by MIA.

The first reports identified placental IL-6 as a key mediator of neuropathology and long-term behavioral deficits.^{252,420,421} Interestingly, human maternal IL-6 levels have been shown to predict child working memory performance.⁴²² IL-6 is a key cytokine necessary for T_H17 differentiation, a subset of helper T cells that respond to extracellular bacterial and fungal infection and characteristically produce high levels of IL-17a. Later work illustrated that maternal ROR γ t-expressing T_H17-mediated production of IL-17a is necessary and sufficient for the induction of offspring atypical cortical development and ASD behavioral phenotypes.⁴²³ Maternal gut microbiota that calibrate T_H17 responses, such as segmented filamentous bacteria (SFB), increase the risk for MIA-induced neurodevelopmental disease pathogenesis.^{419,424} Intestinal TLR3-expressing dendritic cells from pregnant mothers secrete IL-6, IL-1 β , and IL-23 which prompt IL-17a production from commensal SFB-induced T cells (Figure 4).⁴¹⁹ MIA induces alterations in fetal brain cytokine and cytokine receptor levels that differ in levels across brain regions in an age-dependent manner (Figure 4).^{425,426} MIA-induced increases in IL-6 promotes excess neurogenesis and contributes to an overabundance of cortical neurons, particularly in layers IV and V.^{427,428} MIA offspring also harbor atypical cortical patches that localize highly to the dysgranular zone region of the primary somatosensory cortex (S1DZ), and the size of these patches correlates with behavioral abnormalities.⁴²⁹ These patches contain fewer PV⁺ interneurons, which corresponds to hyperactivation in the region.⁴²⁹ Hyperactive S1DZ projections to the striatum and temporal association cortex accounted for abnormal repetitive and social behaviors, respectively.⁴²⁹

Some individuals with ASD experience ameliorated symptoms during the course of fever.⁴³⁰ Interestingly, MIA offspring challenged with LPS-induced systemic inflammation exhibit a temporary reduction S1DZ activity and rescue of behavioral deficits.⁴³¹ This effect is driven by a rise in brain IL-17a, and direct IL-17a injection but not LPS-induced fever is sufficient to also rescue social behavioral deficits in multiple monogenetic models of ASD, but not controls.⁴³¹ This work suggests that MIA might act to prime the immune system and that subsequent postnatal inflammation can serve beneficial effects.

The MIA response is also associated with disturbances beyond changes in immune cells and cytokines; for instance, polyI:C treatment induces changes in tRNA fragments early after injection.⁴³² The placenta itself undergoes extensive changes in gene expression following polyI:C treatment (Chapter 2). Interestingly, many of these changes are sex-dependent, which could provide a basis for explaining the sex-bias observed in both the MIA model and in the human condition of ASD (Chapter 2).

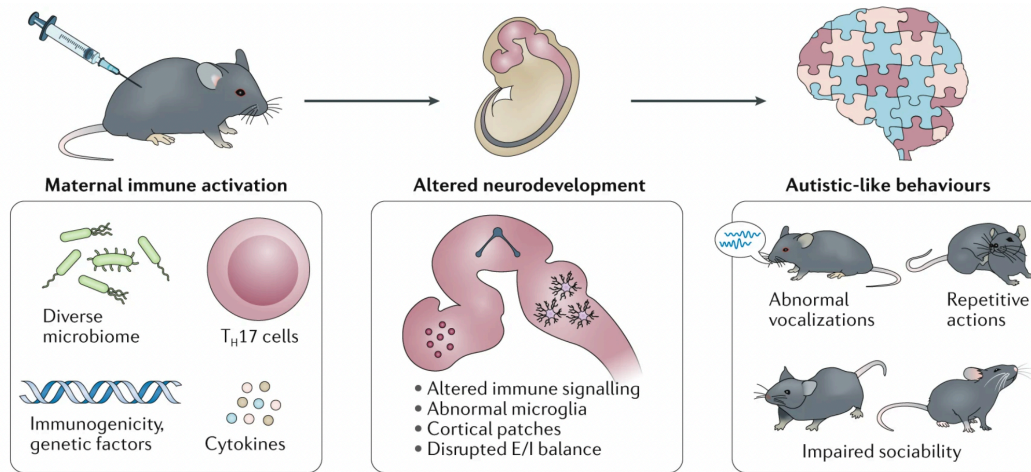


Figure 1.4. Maternal immune activation promotes abnormal brain development and autism-like behaviors

Induced inflammation during pregnancy promotes inflammatory signalling that can influence embryonic development. Many factors, including the maternal microbiome, the T helper 17 (T_H17) cell subset, baseline immunogenicity, genetic factors and cytokine response, may impact the susceptibility of the pregnancy to downstream offspring neurodevelopmental defects. Inflammatory mediators at the maternal–fetal interface may impact brain maturation through diverse mechanisms, including altered brain immune signalling, abnormalities in microglia and cortical malformations that contribute to an altered balance of excitatory to inhibitory neurons (E/I). Maternal immune activation offspring display autism-like behaviours characterized by abnormal communication, stereotyped/repetitive actions and impaired sociability.

1.7.2. Schizophrenia

The schizophrenia spectrum describes psychotic disorders characterized by hallucinations, delusions, disorganized thinking and/or speech, disorganized or abnormal motor behavior, and negative symptoms (including, for instance, diminished emotional expression, avolition, or anhedonia).⁴⁰⁸ Schizophrenic symptoms typically manifest in late adolescence or early adulthood and may correspond with cognitive impairments that include deficits in executive function, working memory, and attention.⁴³³ As with ASD, schizophrenia pathology is likely a result of the convergence of genetic and environmental risk factors.^{392,434} Maternal infection^{382,383,392–394} and elevated cytokine levels^{395,435–437} during pregnancy are significant risk factors for adult psychosis. Further support for an immune role in schizophrenia comes from observations that patients often also have susceptible immunity and/or neuroinflammatory pathology.^{59,251,400,438–440} Genome-wide association studies have also revealed associations between immune system components and schizophrenia.^{441,442}

The MIA model of schizophrenia is quite similar to that most commonly used for ASD whereby pregnant mothers are injected with polyI:C; however, a different injection protocol leads to behavioral abnormalities more similar to those typical of schizophrenia. Offspring of these mice display core symptoms associated with schizophrenia including deficits in pre-pulse inhibition (a measure of attention and distractibility), acoustic startle response (a measure of ability to ignore irrelevant stimuli), and exploratory behavior, again dependent on placental IL-6.^{420,421,443,444} Overexpression of the anti-inflammatory cytokine IL-10 during pregnancy also leads to the same behavioral abnormalities in offspring, but IL-10 overexpression paired with polyI:C treatment abrogates the development of such behaviors.⁴⁴⁵ This work suggests that the balance between anti-inflammatory and pro-inflammatory signaling during pregnancy is a critical determinant of offspring neurologic dysfunction.

It has not yet been extensively interrogated whether maternal cytokines are able to cross the placental barrier and enter the nervous system of the embryo. If this does occur, maternal cytokines could severely affect neurodevelopment, as baseline cytokine signaling is highly regulated and underlies diverse developmental programs. For example, IL-1 β , IL-6, and TNF- α have all been shown to inhibit dendrite outgrowth and branching in cortical neurons, which is consistent with the pathology of schizophrenia.²⁹⁵ Moreover, individuals with schizophrenia have elevated levels of serum IL-1 β , IL-6, and TNF.⁴⁴⁶ MIA may also impact innate immune molecules beyond cytokines in the developing brain; for example, neurons of MIA offspring have been shown to express heightened levels of MHC I, which corresponds to decreases in synaptic density and reduced connectivity.⁴⁴⁷ It stands to reason that altered immune signaling has the potential to impact neurodevelopmental processes such as neurogenesis, dendrite and axon outgrowth, synaptic pruning, and more. Altered brain

structure is consistently observed in schizophrenia and has been linked to maternal infection and cytokines;^{448–450} however, a mechanistic link between maternal inflammation and altered brain maturation has yet to be fully delineated. Finally, MIA has also been shown to impact neurotransmission, contributing to alterations in serotonergic, glutamatergic, and GABAergic signaling in different contexts, which might also underlie neurologic dysfunction in schizophrenia.^{451–453}

1.7.3. Microglia: A common thread

Further evidence for neuroinflammatory pathology is illustrated by the observation of abnormal activation of microglia and astrocytes in the brains of individuals with ASD or schizophrenia.^{99,101,102,106,440,454–457} Positron emission tomography studies conducted with autistic and schizophrenic patients have revealed various signs of neuroinflammation and microglial dysfunction.^{458–460} Microglia are essential players both in developmental processes as well as for adult homeostatic brain function. During neurodevelopment, microglia are essential sculptors of neuronal circuitry contributing to diverse processes such as neurogenesis and synaptic pruning.⁴⁶¹ Maternal inflammation could impact such microglia-mediated developmental processes through convergent immune-related signaling which might then alter brain wiring and function. Moreover, MIA also contributes to altered microglial development (Figure 5). Abnormal microglia, such as those observed in some schizophrenic and autistic individuals, may further aggravate processes for which microglia are accountable and contribute to lifelong neurologic dysfunction. Microglia can secrete effectors of neurogenesis, support synaptic pruning, as well as promote survival, apoptosis, differentiation, and more. Therefore, maternal inflammation that impacts microglia development and function may significantly contribute to the neurologic dysfunction observed in neurodevelopmental disorders.

Though some studies report that embryonic and adult microglia display few abnormalities after maternal polyI:C exposure,^{462,463} offspring microglia could still be primed by this event and display increased reactivity later in life. Other studies provide evidence of MIA-induced microglia abnormalities,^{33,112,113,464,465} for example, MIA has been shown to induce transcriptional changes in embryonic microglia toward a more differentiated state and suggest alterations in phagocytic capacity.^{33,464} Maternal type I interferon signaling in response to polyI:C challenge was found to reduce the proliferation of newborn microglia and heighten microglia sensitivity to stress later in life.¹¹² A few lines of evidence suggest that MIA can skew microglia toward a more activated phenotype that correlates with adulthood schizophrenic-like behaviors.^{466–468} Indeed, microglia-like cells derived from schizophrenic individuals were found to have a heightened capacity to phagocytose synapses.¹¹⁷ Further supporting a role for disrupted microglia in MIA offspring, depleting microglia and allowing for repopulation rescues deficits in some abnormal behaviors.¹¹³ MIA-induced immune system priming might impact microglia such that future inflammatory events incite an abnormal response to further exacerbate neuropathology.⁹

Dysbiosis and gastrointestinal issues observed in many individuals with ASD paired with the ability for gut microflora to modulate immune system composition raises the possibility that MIA-induced microbiota changes impact microglia. The absence of maternal microbiota has been shown to alter microglia chromatin landscape, transcriptional profile, and colonization of the fetal brain.^{33,39} Thus, evidence suggests that gut microflora may act as a linking factor between MIA, microglial dysfunction, and autistic behavioral abnormalities.

It is clear both that cytokines are a part of the maternal inflammatory signature and that these inflammatory mediators can significantly impact brain development; therefore, it follows that maternally derived cytokines might be key drivers of altered neurodevelopment in MIA. The brains of affected offspring do show altered cytokine receptor expression but the consequences of this still remain unclear. As covered in the first part of this review, immune players have diverse and significant roles during neurodevelopment. It therefore also seems possible that maternal inflammatory mediators able to cross the placenta and enter the fetal nervous system might hold the potential to cause convergent signaling on any of such implicated pathways. In addition, genetic risk factors or environmental second hits may also coalesce to precipitate changes in nervous system development. Such aberrations could conceivably contribute to impaired nervous system development.

Inflammatory signaling during neurodevelopment has the potential to impact the architecture and function of the brain, but beyond this, an inflammatory signature might also persist into adulthood, further exacerbating

dysfunction. Immune signaling components are also utilized by the mature CNS for similar homeostatic processes. For instance, adult neurogenesis and synaptic plasticity are essential hippocampal mediators of learning and memory which are also influenced by immune players such as cytokines.^{169,318} Baseline dysregulated inflammatory signaling initiated by MIA therefore could potentially contribute to lifelong neurological dysfunction, independent of distinct developmental priming events. Altogether, inflammation during development constitutes a crucial potential contributing factor to altered neurodevelopment which might underlie varied neurodevelopmental disorders. Further elucidation of the biologic underpinnings of such events will likely shed light on homeostatic functions of immunity in the nervous system as well as reveal potential treatment strategies for cases of dysfunction.

1.8 Conclusion

The long-held belief that the brain is an immune-privileged site has undergone a paradigm shift as a large body of work now illustrates that the immune and nervous systems are critically intertwined. Neural cells influence immune function and immune cells impact neurogenic processes from early developmental stages throughout the lifetime of an organism. Immune cells, such as microglia, are crucial sculptors of neural circuits during development and can influence nearly every process in nervous system assembly. Innate immune signaling mechanisms are widespread in controlling neurodevelopmental processes. Indeed, many signaling molecules are conserved among immune cell and CNS-resident cells, while some have unique functions in each system. Though these signaling molecules were first characterized in the immune system, their importance in homeostatic processes in the nervous system illustrates that such initial categorical definitions are immaterial. Moreover, immune cells and signaling molecules have been implicated in a wide array of neurodevelopmental disorders, further exemplifying the functional importance of immunity in nervous system formation and maintenance. Improper activation of the immune system during neurodevelopment can lead to severe and persistent impairments in physiologic processes ranging from gut microbiota composition to cognitive function. The future study of innate immunity in neurodevelopment will continue to shed light on homeostatic processes that sculpt the CNS and may also reveal therapeutic strategies to treat various neurodevelopmental disorders.

Chapter 2: SSRI treatment modifies the effects of maternal inflammation on *in utero* physiology and offspring neurobiology

2.1 Abstract

Perturbations to the *in utero* environment can dramatically change the trajectory of offspring neurodevelopment. Insults commonly encountered in modern human life such as infection, toxins, high-fat diet, prescription medications, and others are increasingly linked to behavioral alterations in prenatally-exposed offspring. While appreciation is expanding for the potential consequence that these triggers can have on embryo development, there is a paucity of information concerning how the crucial maternal-fetal interface (MFI) responds to these various insults and how it may relate to changes in offspring neurodevelopment. Here, we found that the MFI responds both to an inflammatory state and altered serotonergic tone in pregnant mice. Maternal immune activation (MIA) triggered an acute inflammatory response in the MFI dominated by interferon signaling that came at the expense of ordinary development-related transcriptional programs. The major MFI compartments, the decidua and the placenta, each responded in distinct manners to MIA. MFIs exposed to MIA were also found to have disrupted sex-specific gene expression and heightened serotonin levels. We found that offspring exposed to MIA had sex-biased behavioral changes and that microglia were not transcriptionally impacted. Moreover, the combination of maternal inflammation in the presence of pharmacologic inhibition of serotonin reuptake further transformed MFI physiology and offspring neurobiology, impacting immune and serotonin signaling pathways alike. In all, these findings highlight the complexities of evaluating diverse environmental impacts on placental physiology and neurodevelopment.

Kristine E. Zengeler^{1,2,3*}, Daniel A. Shapiro¹, Katherine R. Bruch¹, Catherine R. Lammert^{1,2}, Hannah Ennerfelt^{1,2,3}, and John R. Lukens^{1,2,3*}

¹Center for Brain Immunology and Glia (BIG), Department of Neuroscience, University of Virginia, Charlottesville, VA 22908, USA, ²Neuroscience Graduate Program, University of Virginia, Charlottesville, VA 22908, USA, ³Cell and Molecular Biology Graduate Training Program, University of Virginia, Charlottesville, VA 22908, USA. * Corresponding authors.

Author contributions:

K.E.Z. and J.R.L. designed the study; K.E.Z., C.R.L., and H.E. performed experiments; K.E.Z., D.A.S., and K.R.B. performed bioinformatics analyses; K.E.Z. analyzed data; K.E.Z. and J.R.L. wrote the manuscript; J.R.L. oversaw the project.

2023, Brain, Behavior, and Immunity, 108(80-97), <https://doi.org/10.1016/j.bbi.2022.10.024>.

2.2 List of abbreviations

ADD, anti-depressant drug; BBB, blood-brain barrier; DEG, differentially expressed gene; dNK, decidual natural killer cell; E, embryonic day; GO, gene ontology; GSEA, gene set enrichment analysis; hpi, hours post-injection; IFN, interferon; IGF, insulin growth factor; i.p., intraperitoneal; MACS, magnetic-activated cell sorting; MAO, monoamine oxidase; MFI, maternal-fetal interface; MIA, maternal immune activation; P, postnatal day; PCA, principal component analysis; polyI:C, polyinosinic-polycytidylic acid; RNA-seq, RNA-sequencing; SLC, solute carrier; scRNA-seq, single-cell RNA-sequencing; SSRI, selective serotonin reuptake inhibitor; TLR, Toll-like receptor; USV, ultrasonic vocalization.

2.3 Introduction

Not long ago, in the early 1900s, the fetus was viewed as a “perfect parasite” that was “afforded protection against nutritional damage that might be inflicted on the mother”⁴⁶⁹. This line of thinking emphasized a lack of

concern for environmental insults on fetal development. In the present day, it is generally well-accepted that perturbations to a pregnant mother's healthy physiology, such as with smoking or alcohol consumption, can negatively impact offspring development. Such environmental alterations may occur in states of malnutrition, obesity, infection, autoimmune conditions, mental health struggles, psychiatric conditions, and more^{9,10,469-473}. Insults that induce an altered immune state during pregnancy (e.g. infection, autoimmune condition, pollutants) have been linked to altered offspring neurodevelopmental trajectories^{9,10,474}. Stress and depression during pregnancy have also been shown to increase the risk of similar conditions or other psychiatric conditions in children^{475,476}. The common thread between these varied cases is an environmental trigger that causes a shift in maternal physiology which may propagate ill-affecting signaling cascades to the developing embryo.

Accumulating epidemiologic studies have linked maternal immune activation (MIA) to an increased penetrance of neurodevelopmental disorders, psychiatric conditions, and other neurologic disorders in offspring^{9,10,477-479}. Diverse immune triggers including viral or bacterial infection, autoimmune conditions, and exposure to environmental pollutants have all been associated with elevated rates of mental conditions including autism, schizophrenia, depression, and more^{9,10,133,477,479,480}. Further subtleties in this model exist, as not all cases of MIA may outright trigger neurologic alternations in offspring but could instead act as a primer for future insults which collectively spur symptom onset^{9,406}. Immune activation may heighten levels of inflammatory mediators that can impact the placental environment and the developing embryo^{9,10,479,481}. For example, heightened maternal serum levels of cytokines such as IL-6 and IL-17a can lead to offspring behavioral alterations in MIA animal models^{420,421,423,424}.

Another pertinent environmental trigger that merits further exploration is the impact of the use of antidepressant drugs (ADDs) during pregnancy. As the incidence of depression in the population has risen in past decades, so has the use of ADDs⁴⁸². ADDs constitute one of the most commonly prescribed group of drugs as they are currently prescribed to approximately 10% of the worldwide population⁴⁸². While adverse maternal mental health has been consistently linked to an increased rate of neurodevelopmental and psychiatric disorders in offspring^{472,482}, it is unclear how pharmacological treatment for these conditions in the mother may impact the developing embryo.

About 80% of pregnant women prescribed an ADD are given a selective serotonin reuptake inhibitor (SSRI), as this class of ADDs are known to be relatively safe to take during pregnancy⁴⁸². SSRIs work by blocking serotonin reuptake by serotonin transporters, thereby increasing extracellular serotonin concentrations and prolonging serotonin signaling^{483,484}. Though SSRIs are often used during pregnancy, there is some evidence to suggest that SSRIs can be teratogenic and that intake during pregnancy may increase the risk of premature delivery, low birth weight, neonatal cardiovascular abnormalities, and offspring metabolic and neurologic disorders^{472,483,484}. Given that the placenta is the sole source of serotonin for the developing embryo early in pregnancy, paired with the importance of serotonin for brain development, prenatal disruption of maternal serotonin levels could presumably alter offspring neurodevelopment^{483,485-492}.

A critical component of studying the impact of the maternal environment on the developing embryo is the maternal-fetal interface (MFI). The maternally-derived decidua and embryo-derived placenta constitute a temporary barrier organ that represents the first site of interaction between the mother and the embryo⁴⁹³. This interface allows for maternal support of the developing embryo with nutrients, gases, and hormones and also protection from harmful stimuli⁴⁹³. Therefore, the MFI must balance tolerogenic immune responses to a non-self-embryo, but also protect the developing embryo from deleterious consequences of infection or other triggers of maternal inflammation⁴⁹³⁻⁴⁹⁵.

Understanding how the MFI responds to a shift in a healthy baseline milieu in the maternal environment may be key in elucidating any impacts on fetal development. Studies into how perturbations to this important interface influence neurodevelopment are lacking. We therefore sought to investigate the murine MFI response to either MIA or SSRI exposure during pregnancy, as well as how these stressors impact offspring neurodevelopment. Given the evidence that combined stressors during pregnancy in a "two-hit" model have a greater impact on offspring development^{9,133}, we also aimed to examine whether a combinatorial effect of SSRI exposure and MIA exists.

To explore how environmental stressors impact *in utero* physiology and neurodevelopment, we exposed pregnant mice to a mimicked viral infection and/or treated them with SSRIs. We found that the MFI undergoes a rapid and robust immune response following MIA that was largely interferon-driven. Each MFI compartment (decidua and placenta) responded in distinct fashions to MIA. Moreover, we uncovered baseline transcriptional sex differences in the MFI that were subacutely eliminated following MIA. Offspring of these MIA pregnancies displayed altered sex-specific behaviors that were not accompanied by an appreciable transcriptional shift in microglia, the resident immune cells of the brain. Like exposure to MIA alone, we found that SSRI treatment on its own during pregnancy altered the MFI immune signaling landscape. Intriguingly, dual exposure to both MIA and SSRIs elicited combinatorial effects. Specifically, the MFI immune response to MIA was reshaped in the presence of SSRIs and the embryonic brain transcriptional response to either MIA or SSRIs alone was exacerbated when the treatments were combined. This study demonstrates that the maternal-fetal interface is sensitive to environmental insults such as MIA and SSRI exposure and that these triggers can impact offspring neurobiology in a complex fashion.

2.4 Results

2.5.1. MIA triggers a robust immune response acutely at the maternal-immune interface

There is now an abundance of evidence that inflammation during pregnancy is a significant risk factor for offspring neurodevelopmental disorders yet the response of the maternal-fetal interface to systemic inflammation is less well understood. We sought to better understand how inflammation during pregnancy impacts offspring neurodevelopment through characterizing the MFI transcriptional response to MIA in an unbiased manner. To this end, we employed a model of MIA in which pregnant dams were injected with the viral mimetic polyinosinic-polycytidylic acid (polyI:C) on embryonic day (E)11 and E12 (Supplemental Table 1; Lammert et al., 2018; Lammert and Lukens, 2019). This immune response is relatively mild, as polyI:C exposure did not significantly affect dam weight gain throughout pregnancy (Figure 2.1A), litter size, or offspring sex distribution (Figure 2.1B).

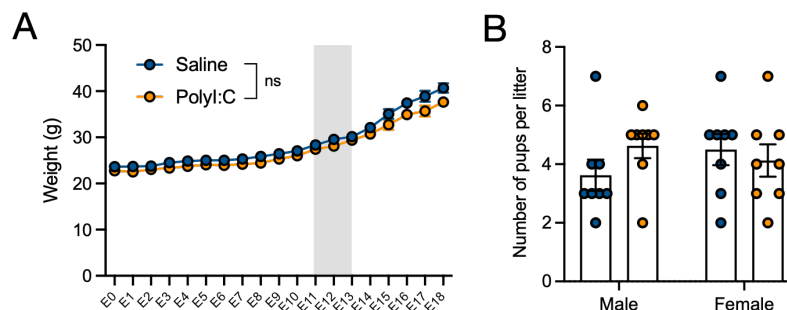


Figure 2.1. PolyI:C-induced MIA does not appreciably impact maternal weight or litter size.

Pregnant dams were injected intraperitoneally (i.p.) with 20 mg/kg polyI:C on embryonic day (E)11 and E12 to elicit maternal immune activation (MIA) or with saline as a control. (A) Dam weight through pregnancy. Grey box indicates i.p. injection timepoints. (B) Number of pups born to polyI:C and saline dams stratified by sex. Each point represents the average 14 pregnancies per group (A) or individual pregnancies (B). Statistical significance calculated by two-way ANOVA with Sidak's multiple comparisons test (A) or one-way ANOVA with Tukey's post-hoc comparison (B). Error bars indicate mean \pm s.e.m.

To illuminate the impact of MIA on the maternal-fetal interface in an unbiased manner, we employed bulk RNA-sequencing (RNA-seq) on MFI tissue (comprising both the decidua and placenta) from MIA and control pregnancies. We chose to evaluate the MFI at E12, 3 hours-post-injection (hpi), in which maternal serum IL-6 levels are highest in this MIA model, as well as E14, 48 hpi, in which IL-17a levels peak (Choi et al., 2016; Figure 2.2A). MFI samples were collected from time- and embryo-matched saline and polyI:C pregnancies. RNA extracted from MFI samples collected at E12 and E14 was pooled equally by sex within each litter, yielding four samples collected from independent saline and polyI:C pregnancies. Principal component analysis (PCA) of all E12 and E14 samples revealed significant clustering of samples by both timepoint and treatment (Figure 2.3A), indicating a substantial effect of both developmental stage and MIA on the placental transcriptome.

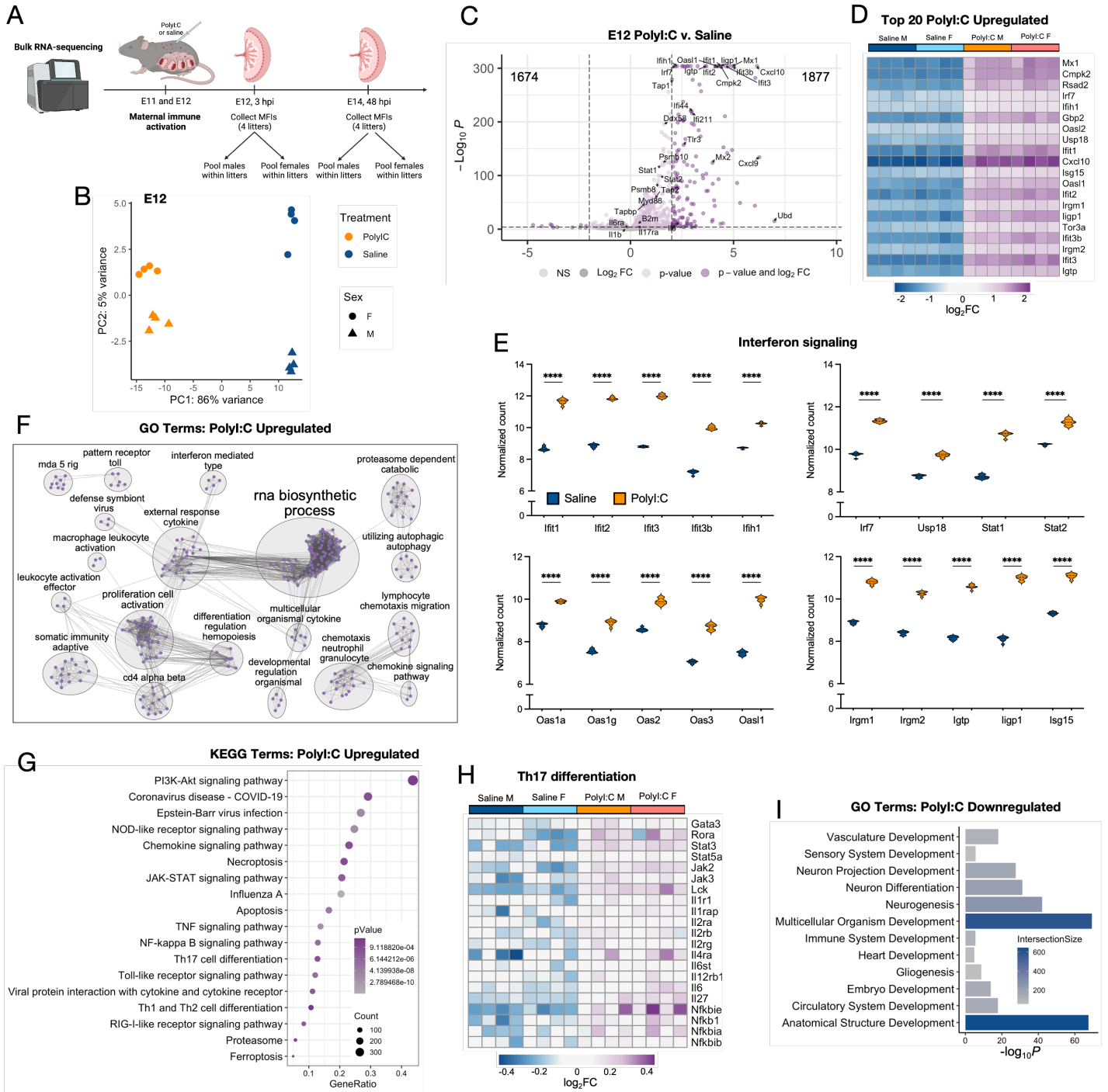


Figure 2.2. The maternal-fetal interface undergoes a robust immune response acutely after polyI:C exposure.

Pregnant dams were injected intraperitoneally (i.p.) with 20 mg/kg polyI:C on embryonic day (E)11 and E12 to elicit maternal immune activation (MIA) or with saline as a control. Bulk RNA-sequencing was conducted on maternal-fetal interface (MFI) tissue at E12 (3 hrs post-injection, hpi) and E14 (48 hpi). (A) Experimental design. 3- and 48-hpi placental tissue and fetal bodies were collected. Fetal bodies were genotyped by Sx PCR to demarcate placental extracts by sex. Sex-stratified samples were pooled within litters for E12 and E14 timepoints, $n = 4$ litters/group. (B-G) RNA was isolated from MFI tissue then bulk RNA-sequencing was conducted on the 4 experimental groups with 4 samples per group. (B) Principal component analysis (PCA) showing clustering of groups from E12 placental samples. (C) Volcano plot showing the number of differentially expressed genes in E12 MFI tissue comparing polyI:C to saline ($FDR < .1$) and combined by sex. Dark purple dots indicate genes that passed the combined p -value $< 1 \times 10^{-5}$ and $\log_2FC > 2$ cutoff of significance, light purple dots indicate genes with p -value $< 1 \times 10^{-5}$, and dark grey dots indicate genes with $\log_2FC > 2$. (D) Heatmap representation of the top 20 genes upregulated in the polyI:C group, combined by sex ($FDR < .1$). (E) Interferon pathway gene expression (rlog normalized counts) compared between polyI:C and saline groups, combined by sex. (F) Cytoscape network map illustrating select shared gene ontology (GO) terms. (G) Gene set enrichment analysis (GSEA) using KEGG pathways from genes upregulated ($FDR < .1$) in the polyI:C group. Dot plot of select enriched KEGG terms. (H) Genes related to Th17 differentiation compared between polyI:C and saline groups, combined by sex and expression levels visualized by heatmap. (I) GSEA of significantly downregulated genes in the polyI:C group ($FDR < .1$). Select GO terms shown. Statistical significance calculated by unpaired Student's t -test (E). **** $P < 0.0001$.

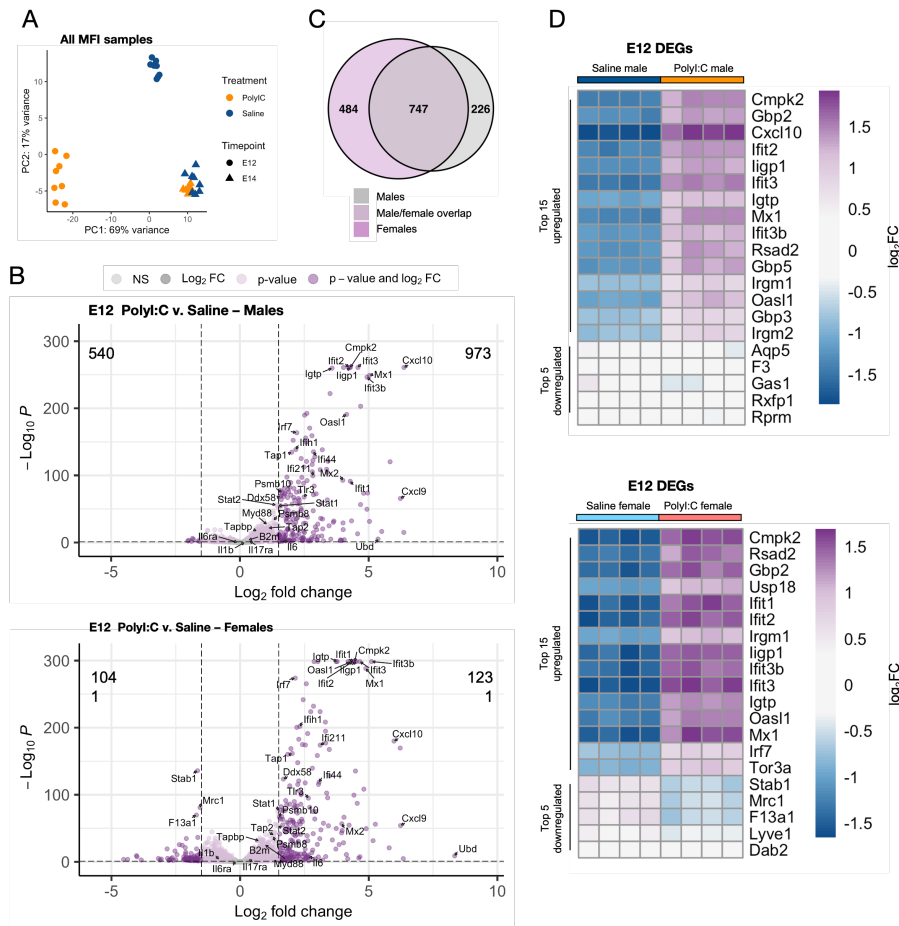


Figure 2.3. The E12 MFI response to polyI:C is similar between sexes.

Pregnant dams were injected i.p. with 20 mg/kg polyI:C on E11 and E12 to elicit MIA or with saline as a control. Bulk RNA-sequencing was conducted on MFI tissue at E12 (3 hpi) and E14 (48 hpi). (A) PCA showing clustering of groups by timepoint and treatment group. (B) Volcano plots showing the number of differentially expressed genes in E12 MFI tissue comparing polyI:C to saline (FDR<.1), separated by sex. Dark purple dots indicate genes that passed the combined p-value < 1×10^{-5} and \log_2 FC > 2 cutoff of significance, light purple dots indicate genes with p-value < 1×10^{-5} , and dark grey dots indicate genes with \log_2 FC > 2. (C) Venn diagram illustrating overlapping differentially expressed genes (DEGs) upregulated by polyI:C comparing the male and female response. (D) Heatmap representation of the top 15 upregulated and top 5 downregulated genes (FDR<.1) compared between saline and polyI:C E12 MFIs from male (top) and female (bottom) offspring.

We first wanted to define the acute response to MIA by comparing polyI:C to saline MFI samples at E12 (3 hpi) collapsed across sex. PCA at this timepoint revealed that saline and polyI:C MFI samples clustered in distinct groups along PC1, accounting for 86% of the variance, indicating that MIA causes a predominant shift in the MFI transcriptome (Figure 2.2B). The transcriptional response at the MFI was robust and quick at the initiation of MIA. We found 1,877 upregulated genes and 1,674 downregulated genes when comparing polyI:C to saline MFIs at E12 (Figure 2.2C). When looking at the top 20 polyI:C upregulated genes, we noticed a strong pro-inflammatory signature dominated by type I interferon (IFN) response genes including *Mx1*, *Cxcl10*, and *Ifit1*, among others (Figure 2.2C,D). Indeed, we found dramatically increased expression of many interferon-stimulated genes that included IFIT and OAS pattern recognition receptors, STAT transcription factors, and more (Figure 2.2E).

We next sought to glean an overall view of the immune response orchestrated at the MFI in response to polyI:C exposure. A cytoscape network analysis of polyI:C upregulated genes revealed an enrichment of immune terms related to cytokine signaling, lymphocyte and neutrophil migration, autophagy, and leukocyte activation (Figure 2.2F). Gene set enrichment analysis (GSEA) of polyI:C upregulated genes using KEGG pathways uncovered specific signaling cascades engaged which included PI3K-AKT, NOD-like receptors, Toll-like receptors (TLRs), RIG-1, and NF- κ B signaling, among others (Figure 2.2G). We also noted pathways related to T cell activation (Figure 2.2G) and were intrigued to see indication of a Th17 response, given that maternal Th17-mediated IL17a production is required for the onset of polyI:C offspring behavioral phenotypes^{423,497,498}. Indeed, we found a

broad upregulation of many genes related to Th17 differentiation acutely following polyI:C exposure in the MFI (Figure 2.2H). We also noted a shift toward anti-angiogenic signaling in which polyI:C induced the downregulation of many pro-angiogenic factors (i.e. *Fgf2*, *Pdgfa*, *Pdgfc*) concomitant with upregulation of anti-angiogenic factors (i.e. *Angpt1*, *Angpt2*, *Cxcl9*, *Cxcl10*, *Cxcl11*, *Thbs1*, *Thbs4*; Figure 2.4).

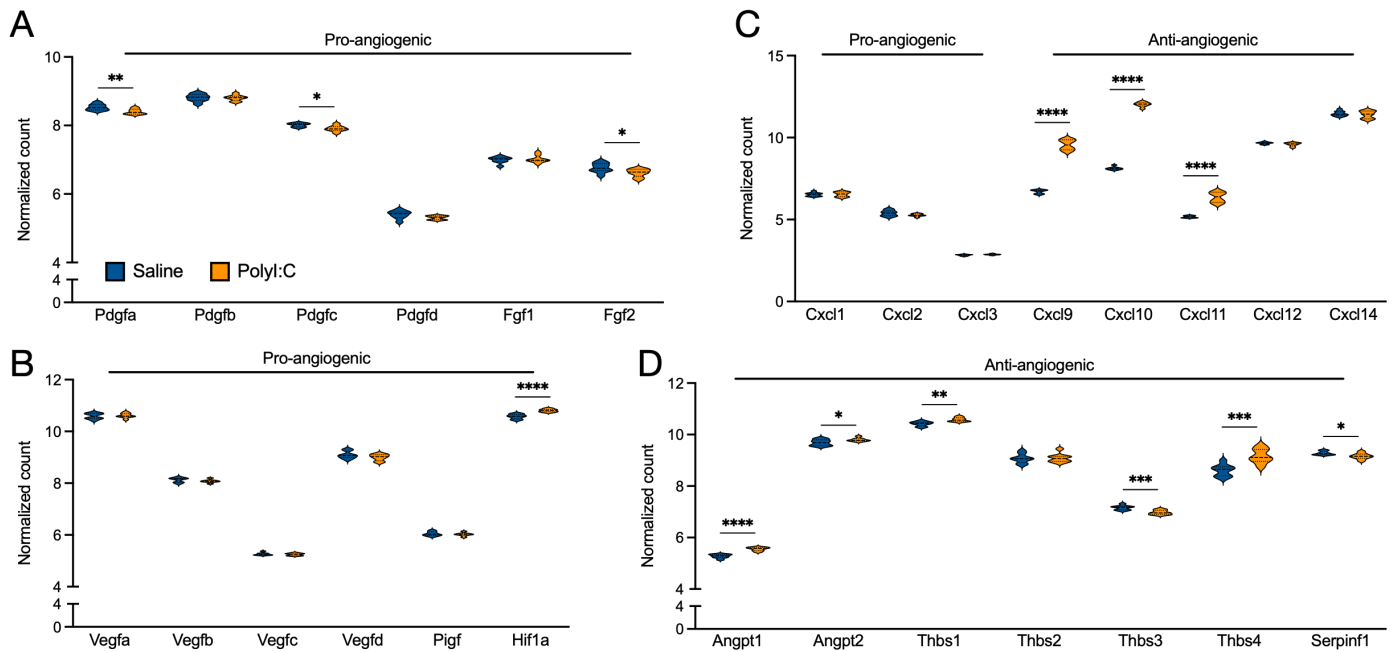


Figure 2.4. Expression of angiogenesis-related genes in the placenta 3 hours-post MIA.

Pregnant dams were injected i.p. with 20 mg/kg polyI:C on E11 and E12 to elicit MIA or with saline as a control. Bulk RNA-sequencing was conducted on MFI tissue at E12 (3 hpi). (A-D) Violin plots illustrating the expression (rlog normalized counts) of pro- and anti-angiogenic signals in the MFI 3 hpi. (A) Expression levels of pro-angiogenic platelet-derived growth factors and fibroblast growth factors. (B) Expression levels of pro-angiogenic vascular endothelial growth factors and other factors. (C) Expression levels of pro- and anti-angiogenic chemokines. (D) Expression levels of anti-angiogenic angiopoietins, thrombospondins, and plasminogen activator inhibitor-1. Statistical significance calculated by unpaired Student's t-test (A-D). * $P < 0.05$, ** $P < 0.01$, *** $P < 0.001$, **** $P < 0.0001$.

While the largest fold changes in gene expression were found in upregulated genes, we were still curious to explore the pathways disengaged in MIA-exposed MFIs. GSEA of polyI:C downregulated genes using the gene ontology (GO) database revealed an interesting dampening of pathways related to offspring development (Figure 2.2I). Such downregulated pathways were related to vascular, heart, and nervous system development in particular, which we were intrigued to find in MFI tissue that did not include the embryo itself. Given the central role of the MFI in providing embryo nutrition, it is possible that the inflammatory response detracts from this typical support. In all, the acute transcriptional response to MIA at the MFI engaged a robust immune response largely driven by type I IFN signaling at the expense of ordinary offspring developmental support.

Sex differences in the neurodevelopment of MIA offspring have been reported using multiple different models of infection^{499–503}. Thus, we were interested to see whether there were sex differences in the immune response at the placenta that could begin to explain some of the differences in offspring neurodevelopment. We therefore conducted differential gene expression analysis on E12 MFIs split by sex. We found 1,513 differentially expressed genes (DEGs) in males and 2,272 DEGs in females (Figure 2.3B), with the largest fold changes occurring in upregulated genes in both sexes. We found many of these upregulated genes to be similar between the sexes (Figure 2.3B,C) with the top 15 upregulated DEGs largely overlapping in male and female MFIs (Figure 2.3D). Taken together, this transcriptional analysis of the acute MFI response to MIA revealed an engaged immune response that is largely conserved between the sexes.

2.5.2. The pro-inflammatory response to polyI:C is distinct at the placenta and the decidua

To glean insight into whether this immune response is generated in dam-derived cells (decidua) or embryo-derived cells (placenta), we dissected apart decidua and placenta tissue. Successful dissociation of the decidua from the placenta was confirmed by relative expression of the placenta-enriched marker *Cdh1* (E-cadherin; Figure 2.5A). We additionally confirmed that deciduae from either male or female embryos were composed primarily of female (i.e. maternal) cells via expression of the X chromosome gene *Xist* (Figure 2.5B). Placentas from female embryos also expressed *Xist* but completely lacked expression of the Y chromosome gene *Uty* (Figure 2.5B-C). Accordingly, placentas from male embryos completely lacked *Xist* expression but highly expressed *Uty* (Figure 2.5B-C).

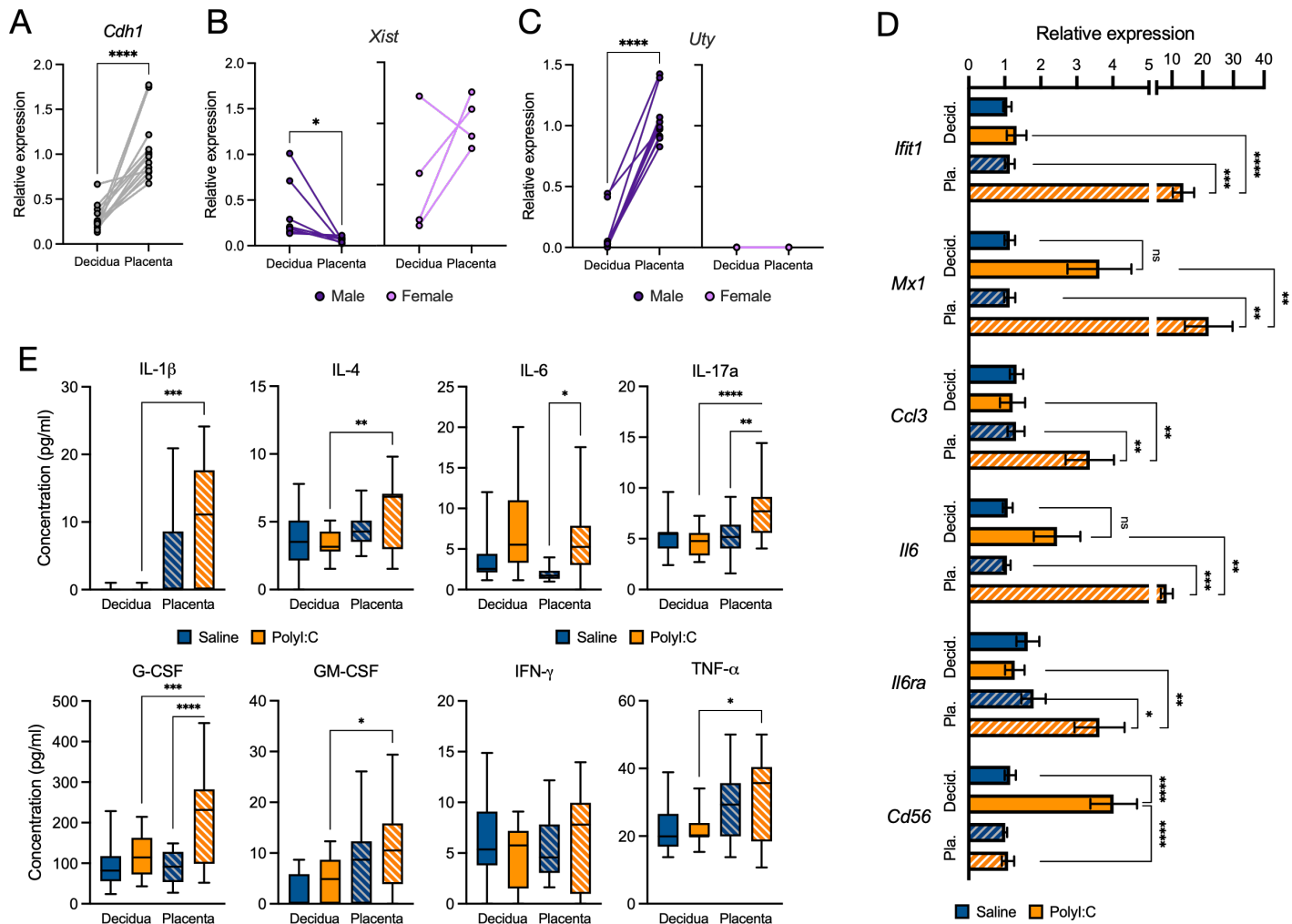


Figure 2.5. The effects of polyI:C in the decidua compared to the placenta.

Pregnant dams were injected i.p. with saline as a control on E11 and E12. Maternal-fetal interface tissue was collected at E12, 3 hpi, and the decidua was dissected away from the placenta. Relative gene expression was assessed in these tissues by qPCR. (A) Relative expression of the placenta-enriched marker, E-cadherin, in matched maternal-fetal interface samples, normalized to placenta expression. (B-C) Relative expression of sex chromosome genes *Xist* (X chromosome; B) and *Uty* (Y chromosome; C) in matched decidua and placenta samples collected from saline control pregnancies and split by sex. (B) Relative *Xist* expression, normalized to saline female placenta expression. (C) Relative *Uty* expression, normalized to male placenta expression. (D) Relative expression of pro-inflammatory genes, normalized to saline deciduae or saline placentas. (E) Cytokines levels assessed by multiplex cytokine array conducted on decidua and placenta homogenates from saline and polyI:C pregnancies. Samples were collected from at two independent pregnancies per group. Each point represents an individual decidua or placenta (A-C). Pla. = placenta, Decid. = decidua. Statistical significance calculated by paired Student's t-test (A-C) or one-way ANOVA with Tukey's post-hoc comparison (D-E). Error bars indicate mean \pm s.e.m. ns = not significant, * $P < 0.05$, ** $P < 0.01$, *** $P < 0.001$, **** $P < 0.0001$.

We next profiled the expression of pro-inflammatory genes by qPCR to understand the response to polyI:C in each MFI compartment. We previously found *Ifit1*, *Mx1*, and *Il6* to have increased expression in bulk maternal-fetal interface tissue (Figure 2.2). Strikingly, the placenta, but not the decidua, significantly upregulated expression of *Ifit1*, *Mx1*, and *Il6*, in addition to *Ccl3* and *Il6ra* 3 hpi (Figure 2.5D). Meanwhile, a well-characterized

marker of decidual NK (dNK) cells, *Cd56*, was exclusively upregulated in the decidua but not the placenta 3 hpi (Figure 2.5D).

These findings heightened our curiosity as to whether protein levels of pro-inflammatory cytokines were differentially enriched in either MFI compartment. We conducted a multiplex cytokine assay on dissected decidua and placenta tissue homogenates from pregnancies 3 hours post-saline or -polyI:C treatment. In comparing cytokine concentrations within each tissue, we found significantly elevated levels of IL-6, IL-17a, and G-CSF within the placenta but not the decidua (Figure 2.5E). No cytokines were found in significantly altered levels within the decidua (Figure 2.5E). Further, when comparing polyI:C deciduae to polyI:C placentas we found significantly elevated levels of IL-1 β , IL-4, IL-17a, G-CSF, GM-CSF, and TNF- α (Figure 2.5E). Other MIA studies have similarly reported increased levels of IL-6 and IL-17a following polyI:C treatment^{420,423,424} and we were intrigued to find this response exclusively in the placental compartment. Altogether, we find that both dam- and embryo-derived cells respond to polyI:C yet in distinct fashions.

2.5.3. The MFI immune response to MIA is largely absent by E14

We were next curious to see how long this inflammatory response at the MFI persisted after polyI:C exposure. To this end, we compared the transcriptome of polyI:C and saline MFI samples at E14 (48 hpi). PCA clustering revealed that saline and polyI:C samples still clustered in relatively distinct groups at this time point, though not to the same extent as at 3 hpi (Figure 2.2B, 2.6A). While there was a significant number of DEGs in response to MIA at 3 hpi, we found many fewer DEGs at 48 hpi (Figure 2.6B), indicating a potential resolution of the inflammatory response. Interestingly, we noticed that the male control MFIs clustered more closely with the polyI:C MFIs by PCA compared to the females (Figure 2.6A).

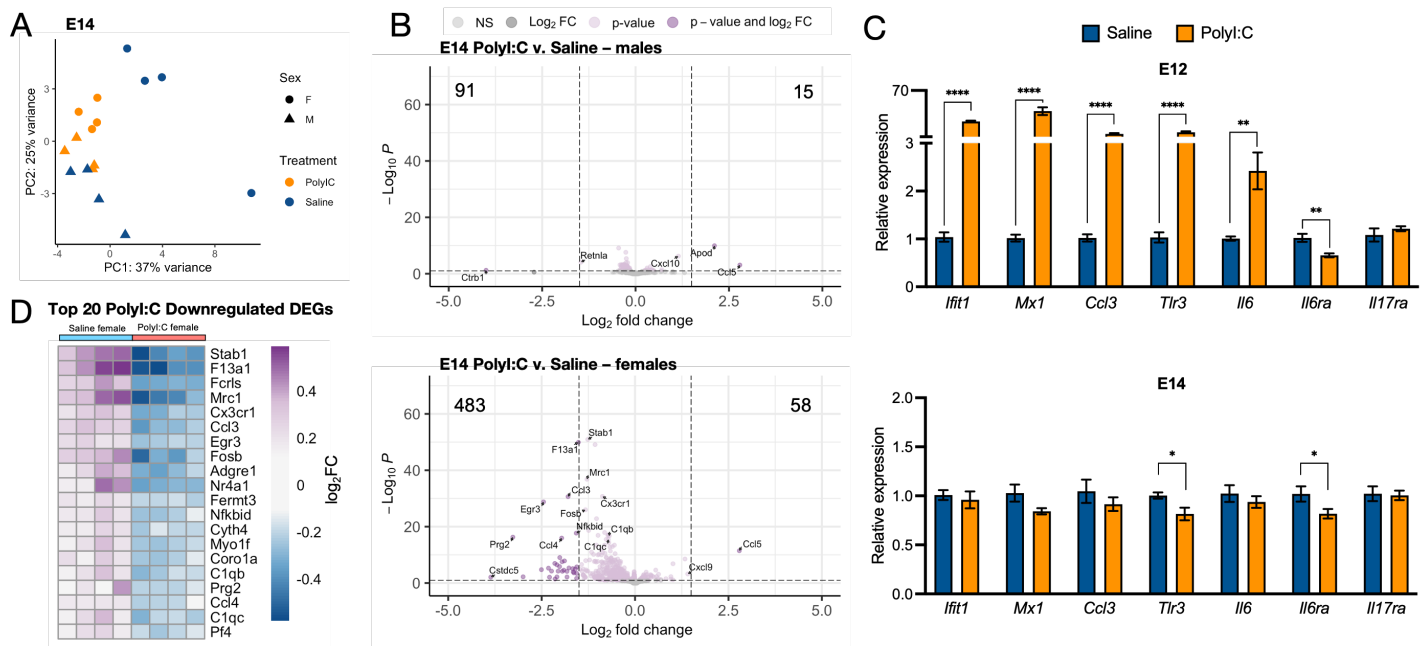


Figure 2.6. The MFI immune response is largely complete by 48 hpi.

Pregnant dams were injected i.p. with 20 mg/kg polyI:C on E11 and E12 to elicit MIA or with saline as a control. Bulk RNA-sequencing was conducted on MFI tissue at E14 (48 hpi). (A) PCA showing clustering of groups from E14 MFI samples. (B) Volcano plots showing the number of differentially expressed genes in E14 MFI tissue comparing polyI:C to saline (FDR<.1), separated by sex. Dark purple dots indicate genes that passed the combined p-value < 1x10⁻⁵ and log₂FC > 2 cutoff of significance, light purple dots indicate genes with p-value < 1x10⁻⁵, and dark grey dots indicate genes with log₂FC > 2. (C) qPCR comparing the expression of key MIA-related inflammatory mediator genes between polyI:C and saline MFI tissue at E12 (3 hpi) and E14 (48 hpi). (D) Heatmap representation of the top 20 genes downregulated in the polyI:C group (FDR<.1) compared between saline and polyI:C female MFIs. Statistical significance calculated by unpaired Student's t-test (C). Error bars indicate mean +/- s.e.m. *P < 0.05, **P < 0.01, ****P < 0.0001.

To further explore this pattern, we conducted differential expression analysis with the samples split by sex. Indeed, only 106 genes were significantly differentially expressed in the male MFI exposed to polyI:C compared

to controls (Figure 2.6B). We meanwhile uncovered 541 DEGs in female MFIs, 58 of which were upregulated and 483 of which were downregulated (Figure 2.6B). In both sexes, there was a striking lack of the immune response genes that were so strongly upregulated at 3 hpi (Figure 2.2C, 2.6B). We verified this effect by qPCR looking at a selection of relevant DEGs and indeed saw the same strong upregulation of immune-related genes at E12 which were no longer differentially expressed by E14 (Figure 2.6C). In fact, many of the top downregulated genes in females were related to the immune system, including *Stab1*, *Mrc1*, *Cx3cr1*, *Ccl3*, *C1qb*, and *C1qc* (Figure 2.6D). Altogether, the active MFI response to MIA occurring at E12 is largely over by E14 on the transcriptional level; moreover, the female MFI may even be further downregulating some immune-related genes.

2.5.4. Baseline sex differences in the MFI transcriptome are dampened subacutely by MIA

We noted in our PCA plots that samples clustered distinctly based on sex when comparing our saline controls at E12 (Figure 2.2B) and at E14 (Figure 2.6A), indicating significant baseline sex differences in the MFI transcriptome. We were fascinated to see that MIA appears to dampen these sex differences, as polyI:C male and polyI:C female MFI samples separate to a smaller degree on the PCA plots both at E12 (Figure 2.2B) and at E14 (Figure 2.6A). This finding spurred our curiosity to define any baseline transcriptional sex differences and whether MIA influences the expression of these genes.

We conducted differential gene expression analysis comparing male to female MFIs split by treatment and timepoint (Figure 2.7A). In saline control MFIs, we uncovered 701 genes at E12 and 868 genes at E14 that were differentially regulated by sex (Figure 2.7A,B). We were fascinated to see that nearly all of these sex-dependent genes were no longer differentially expressed by sex when comparing polyI:C male to polyI:C female MFIs both at E12 and E14 (Figure 2.7A,B). Specifically, there were only 15 genes at E12 and 75 genes at E14 that were differentially expressed when comparing between the sexes in polyI:C MFIs (Figure 2.7A,B), and many of these DEGs were sex chromosome genes (Figure 2.7A). In other words, the response to polyI:C is largely overlapping in male and female MFIs, consistent with our DEG findings (Figure 2.3).

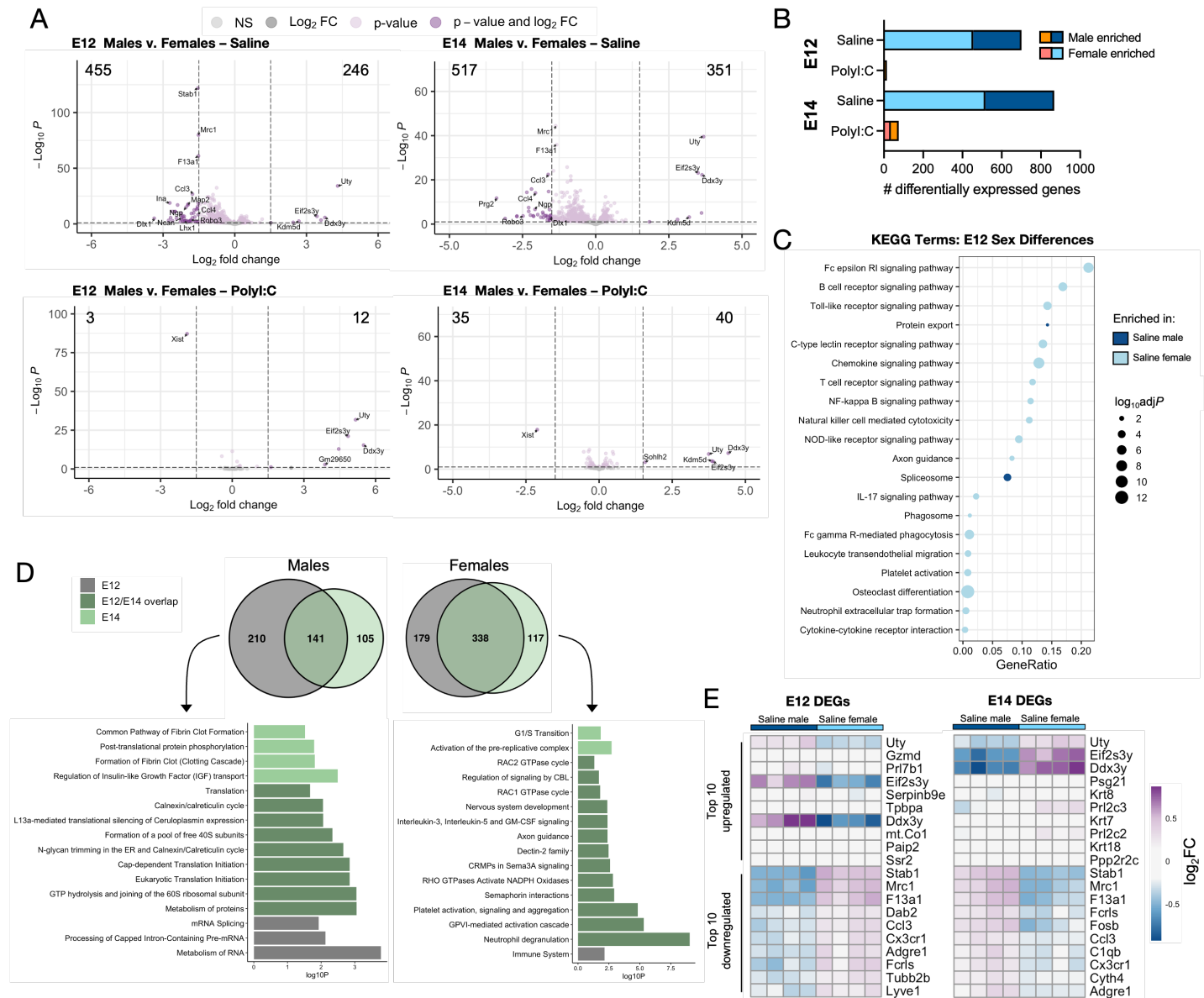


Figure 2.7. Baseline sex differences in the MFI transcriptome are dampened by MIA.

Pregnant dams were injected i.p. with 20 mg/kg polyI:C on E11 and E12 to elicit MIA or with saline as a control. Bulk RNA-sequencing was conducted on MFI tissue at E12 (3 hpi) and E14 (48 hpi). (A) Volcano plots showing the number of differentially expressed genes in E12 and E14 MFI tissue comparing males to females ($FDR < .1$), separated by treatment group. Dark purple dots indicate genes that passed the combined $p\text{-value} < 1 \times 10^{-5}$ and $\log_2FC > 2$ cutoff of significance, light purple dots indicate genes with $p\text{-value} < 1 \times 10^{-5}$, and dark grey dots indicate genes with $\log_2FC > 2$. (B) Numbers of differentially expressed genes ($FDR < .1$, $p\text{-value} < 1 \times 10^{-5}$ and $\log_2FC > 2$) enriched in either male or female samples within saline and polyI:C groups at E12 and E14. (C,D) Gene set enrichment analysis using (C) KEGG and (D) Reactome pathways from genes differentially expressed ($FDR < .1$) between males and females in the saline group. (C) Dot plot of select enriched KEGG terms in male and female E12 MFIs. (D) DEGs between saline males and females were compared at E12 and E14. Overlapping and non-overlapping DEGs are illustrated by Venn diagram and were subject to gene set enrichment analysis. (E) Heatmap representation of the top 10 upregulated and downregulated genes in saline offspring at E12 and E14 ($FDR < .1$).

To begin to understand these MFI transcriptional sex differences, we first wanted to better define the biological processes chiefly employed at each developmental stage assessed, as this may inform any perturbations that occur as a result of sex and/or MIA. Thus, we conducted PCA and differential expression analysis comparing subsequent developmental timepoints (E14 v. E12) in saline control samples. PCA revealed that time had the greatest influence on the transcriptional landscape (**Figure S4A**); PC1 accounted for 69% of the variance in which samples cluster along this principal component predominately by timepoint. Sex accounted for the second-most variance in transcriptome (14%), as samples clustered next by female and male along PC2 (**Figure S4A**).

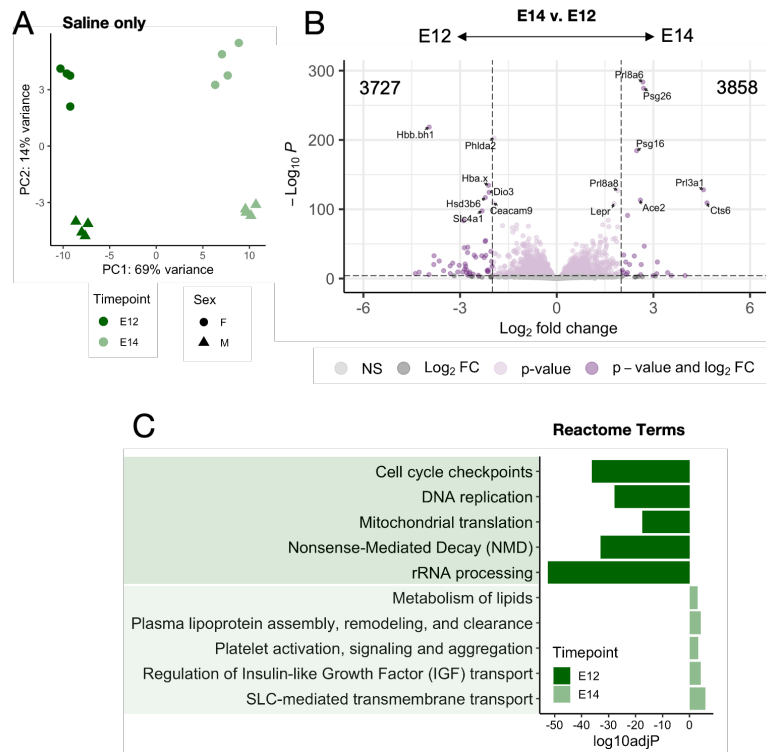


Figure 2.8. The developmental trajectory of the MFI transcriptome.

Pregnant dams were injected i.p. with saline as a control on E11 and E12. Bulk RNA-sequencing was conducted on MFI tissue at E12 (3 hpi) and E14 (48 hpi). (A) PCA plots including E12 and E14 samples showing clustering of groups. (B) Volcano plot showing the number of differentially expressed genes (FDR<.1) in control MFI tissue comparing E12 to E14 and combined by sex. Dark purple dots indicate genes that passed the combined p-value < 1×10^{-5} and $\log_2 \text{FC} > 2$ cutoff of significance, light purple dots indicate genes with p-value < 1×10^{-5} , and dark grey dots indicate genes with $\log_2 \text{FC} > 2$. (C) Reactome terms selected following gene set enrichment analysis of control MFIs comparing E12 to E14. Genes with negative $\log_{10} \text{adjP}$ values are enriched at E12 while genes with positive $\log_{10} \text{adjP}$ values are enriched at E14.

We identified 3,727 genes enriched at E12 and 3,858 enriched at E14 in the homeostatic MFI (Figure 2.8B). The top DEGs enriched at E12 included hemoglobin subunits *Hbb.bh1* and *Hba.x*, the cell cycle regulator *Phlda2*, and oxidoreductases *Dio3* and *Hsd3b6* (Figure 2.8B). GSEA of all E12 DEGs revealed that networks related to the cell cycle, mitochondrial translation, and rRNA processing dominated the transcriptional landscape at this time compared to E14 (Figure 2.8C). At E14, we identified prevailing enrichment for the prolactin genes *Prl3a1*, *Prl8a6*, and *Prl8a8*, pregnancy-specific glycoproteins *Psg16* and *Psg26*, which are known to be involved in immunoregulation and thromboregulation, as well as the cathepsin-encoding gene *Cts6*. Indeed, GSEA of all E14-enriched genes uncovered pathways related to lipid metabolism (likely related to lactation) and plasma/platelet-related processes, in addition to insulin growth factor (IGF)- and solute carrier (SLC)-mediated transport (Figure 2.8C). We also identified significant enrichment for *Ace2*, the angiotensin-converting enzyme that can also serve as a primary entry point into cells subverted by SARS-CoV-2 when ACE2 is present in a membrane-bound form (Yan et al., 2020; Figure 2.8B). This is consistent with studies showing that SARS-CoV-2 can infect placental syncytiotrophoblasts and initiate an inflammatory response at the placenta^{505,506}.

Males and females conceivably require different support in terms of nutrients, growth factors, and protection⁵⁰⁷⁻⁵⁰⁹. In addition, male embryos are immunologically viewed as significantly more foreign to the mother's immune system due to the presence of Y chromosome genes, perhaps necessitating an even more tolerogenic state^{507,509}. Moreover, differences in sex chromosome gene dosage (XX vs XY) could influence MFI function both at baseline and in response to a change in the maternal milieu, such as those triggered by environmental insults like MIA. We therefore first sought to more completely understand the gene modules that made up apparent sex-dependent DEGs. At E12, GSEA revealed an abundance of differentially regulated pathways in female MFIs, many of which were related to immune signaling pathways (Figure 2.7C). In particular, we noted enrichment of signaling modules involving Fc receptors, TLRs, chemokines, and activation of various immune cell subsets (Figure 2.7C). The male MFI at baseline were enriched for protein export and spliceosome pathway KEGG terms (Figure 2.7C).

We wondered whether these sex-dependent gene modules persisted at E14 and/or whether new sex-dependent gene modules appeared as pregnancy progressed. A comparison of genes differentially expressed in males at E12 and E14 revealed an overlap of 141 genes, with 210 genes uniquely expressed at E12 and 105 genes uniquely expressed at E14 (Figure 2.7D). The largest fold changes in male-enriched genes occurred in *Uty*, *Eif2s3y*, and *Ddx3y*, which were present at both E12 and E14 (Figure 2.7E). GSEA using the Reactome dataset found that male MFIs were enriched for mRNA processing-related pathways at E12 while at E14 male MFIs were enriched for fibrin signaling and insulin-like growth factor transport (Figure 2.7D). Male MFIs were enriched for pathways related to translation and the calnexin cycle at both E12 and E14 (Figure 2.7D).

We then repeated this analysis on female MFIs and found 338 overlapping genes at E12 and E14, with 179 genes unique to E12 and 117 genes unique to E14 (Figure 2.7D). The top 10 DEGs enriched in females were present at E12 and E14, including *Stab1*, *Mrc1*, and *F13a1* (Figure 2.7E). Consistent with our KEGG terms (Figure 2.7C), E12 female MFIs were enriched for immune signaling (Figure 2.7D). Some of these immune pathways were also apparent at E14, including Dectin- and neutrophil-related signaling (Figure 2.7D) and genes such as *Ccl3*, *Cx3cr1*, and *Fcrls* (Figure 2.7E). Female MFIs were also enriched for non-immune-related pathways at both E12 and E14 which included GTPases and modules related to the nervous system (Figure 2.7D). At E14 alone, female MFIs were enriched for cell cycle-related signaling (Figure 2.7D).

All of these gene modules that are typically employed in males and females separately during development are no longer apparent in polyI:C pregnancies (Figure 2.7A,B). Strikingly, though the immune response to polyI:C is largely complete by E14, these dampened sex differences continue to persist at this timepoint, which indicates of a prolonged imprint of polyI:C exposure (Figure 2.7A,B). While the female and male MFI immune response to MIA predominantly overlaps, it is possible that the lack of typical employment of sex-specific gene modules contributes to altered offspring development in a MIA environment.

2.5.5. MIA leads to sex-biased behavioral changes without an accompanying transcriptional shift in microglia

Given the quintessence of the maternal-fetal interface in supporting embryo development paired with the significantly shifted transcriptome triggered by MIA, we next sought to investigate the impact that maternal inflammation may have on offspring neurodevelopment. We wondered whether sex-biased differences in offspring behavior existed in our MIA model, given our findings that the MIA female MFI was found to downregulate many immune-related genes subacutely (Figure 2.6B,D) and that baseline transcriptional sex differences in the MFI are dampened by MIA (Figure 2.7).

Indeed, our MIA offspring displayed sex-biased behavioral alterations. More specifically, we found that male polyI:C offspring emitted fewer ultrasonic vocalizations (USVs) when briefly separated from their mother and littermates at postnatal day (P)10 (Figure 2.9A), indicating impaired communication ability compared to female polyI:C littermates and saline control offspring. Sex-biased behavioral alterations were also present in adulthood, as male polyI:C offspring buried more marbles (Figure 2.9B) and interacted equally with an object versus a novel mouse (Figure 2.9C) compared to female polyI:C offspring and saline controls; indicative of repetitive/stereotyped behaviors and sociability deficits, respectively. These sex-biased behavioral changes are consistent with published neurodevelopmental alterations using other MIA models ^{499–501,503}.

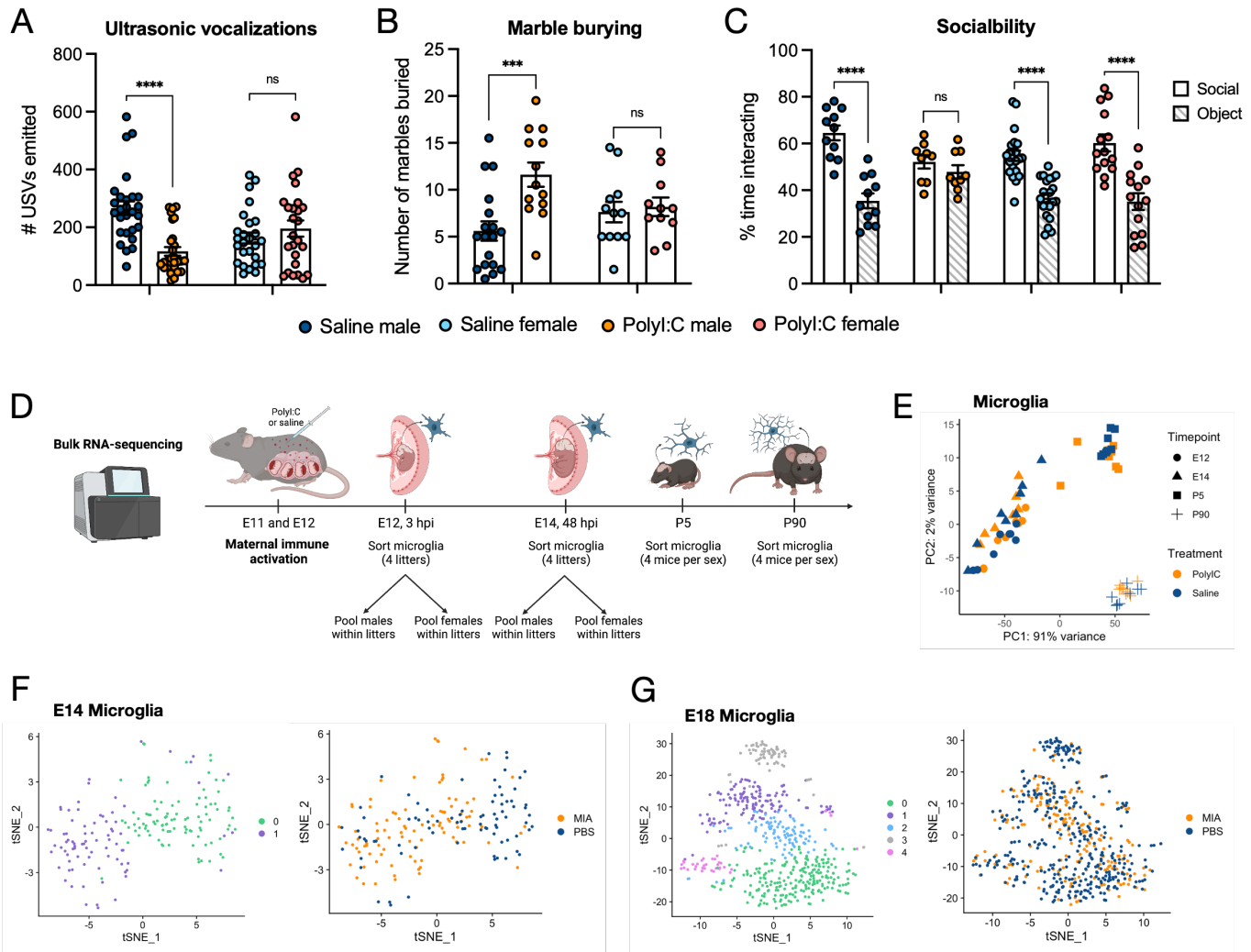


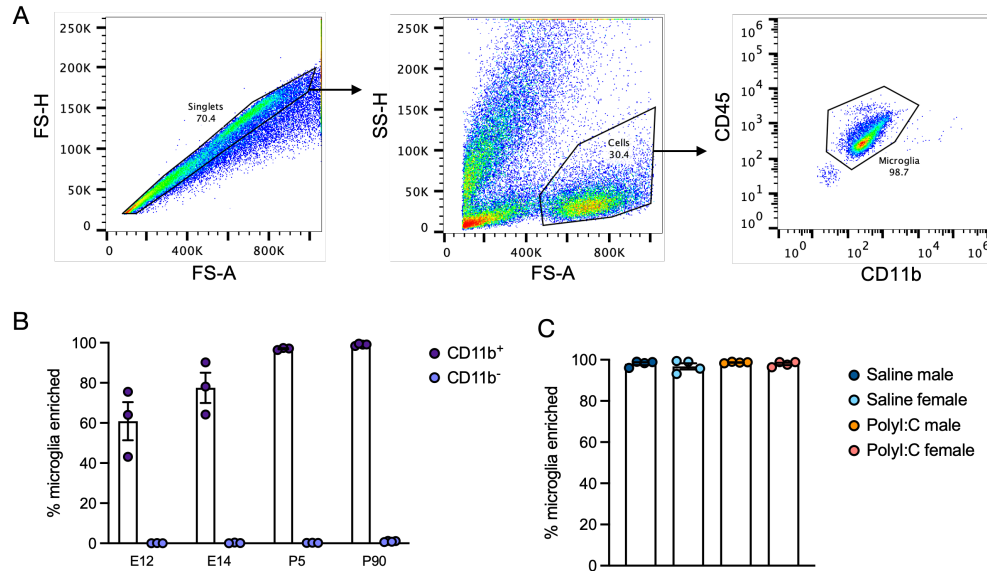
Figure 2.9. Maternal immune activation elicits sex-biased behavioral alterations in offspring but does not impact microglia on the transcriptional level.

Pregnant dams were injected i.p. with 20 mg/kg polyI:C on E11 and E12 to elicit MIA or with saline as a control. (A-C) Male and female offspring of MIA and control pregnancies were assessed for behavioral alterations including communication ability (A), stereotyped/repetitive actions (B), and sociability changes (C). (A) Number of ultrasonic vocalizations elicited during 3-min of separation from mother and littermates at postnatal day (P)10. (B) Number of marbles buried during a 10-min marble burying assay conducted at 8-10 weeks of age. (C) Percent time spent interacting with a novel mouse compared to a novel object during a 10-min three-chamber social preference test conducted at 8-10 weeks of age. (D) Microglia RNA-sequencing experimental design. 3- and 48-hpi embryos were collected and decapitated bodies were genotyped by Sx PCR to demarcate brain extracts by sex. Brains were also harvested from P5 and P90 offspring. Single cell suspensions of fresh brain tissue were subject to CD11b+ magnetic bead purification by magnetic-activated cell sorting (MACS) to isolate microglia. Sex-stratified samples were pooled within litters for E12 and E14 timepoints ($n = 4$ litters per group). Individual mice were used for P5 and P90 timepoints ($n = 4$ mice per group). RNA was isolated from purified microglia and then bulk RNA-seq was conducted on the 4 experimental groups with 4 samples per group at each timepoint. (E) PCA showing clustering of treatment groups from all timepoints. (F,G) Reanalysis of single cell RNA-sequencing data collected from MIA offspring and PBS control brains (Kalish et al. 2020) at E14 (48 hours-post-polyI:C) and E18 (96 hours-post-polyI:C). tSNE plots show microglia forming two clusters at E14 (F, left) and five clusters at E18 (G, left); however, MIA and PBS microglia do not fall into any distinct cluster at either timepoint or form any distinct clusters (F,G; right). Each point represents an individual mouse (A-C). Statistical significance calculated by one-way ANOVA with Tukey's post-hoc comparison (A-B) or multiple Student's t-tests (C). Error bars indicate mean \pm s.e.m. ns = not significant, * $P < 0.05$, *** $P < 0.001$, **** $P < 0.0001$.

The innate immune cells of the brain, microglia, constitute the first line of defense against brain pathogens and are also critically involved in homeostatic neurodevelopmental processes including circuit refinement, angiogenesis, and cell maturation/differentiation^{474,510,511}. All of these processes could conceivably be impacted by sex and/or inflammation during neurodevelopment. We therefore wondered whether microglia would be particularly sensitive to any immunologic and/or sex-specific stimuli that could be propagated from the placenta to the developing embryonic brain during MIA.

To investigate in an unbiased manner whether microglial gene expression is impacted by MIA, we conducted bulk RNA-seq on purified offspring microglia at select timepoints post-MIA (Figure 2.9D). Given our intriguing

findings from the MFI RNA-seq study, we chose to evaluate microglia at E12 (3 hpi) and E14 (48 hpi) in an effort to correlate any MFI findings to a potential impact on microglia. We additionally collected sorted microglia at P5, a timepoint in development in which microglial phagocytosis is distinctly relevant^{125,474,512}, as well as at P90 when neurodevelopment is largely complete. Microglia were isolated by generating single-cell suspensions of brain tissue and then selecting for CD11b⁺ cells by magnetic-activated cell sorting (MACS). This strategy was effective in purifying CD11b⁺ cells at all evaluated timepoints (E12, E14, P5, and P90; Figure 2.10A,B) and the purity and efficacy of this isolation technique was not impacted by either sex or treatment condition (Figure 2.10C).



Pregnant dams were injected i.p. with 20 mg/kg polyI:C on E11 and E12 to elicit MIA or with saline as a control. Brains were collected from offspring at ages E12, E14, P5, and P90, single-cell suspensions made, and microglia were purified by MACS using CD11b-coated magnetic beads. Microglia enrichment in CD11b⁺ fractions was evaluated by flow cytometry. (A) Representative gating strategy. Microglia were gated as CD11b⁺CD45^{low} single cells. (B,C) Quantification of the percent of single cells in the microglia gate in CD11b⁺ column fractions compared to CD11b⁻ column fractions at each of the four time points (B) and across experimental groups as evaluated at P90 (C).

Using the same strategy as with MFI samples, RNA extracted from microglia samples collected at E12 and E14 was pooled equally by sex within each litter from a total of four litters per group (Figure 2.9D). Given the larger brain size, samples isolated at P5 and P90 were collected from a full brain of sorted microglia RNA from four mice per group (Figure 2.9D). PCA of all microglia across these developmental points revealed that time had the greatest influence on the transcriptional landscape of microglia: groupings were spread out by timepoints across PC1 which accounted for 91% of the variance (Figure 2.9E, 2.11A). In looking at each time point individually, we found that microglia were largely unaffected by MIA whereby polyI:C and saline samples clustered together at E12, E14, P5, and P90 (Figure 2.9E). We noted very few differentially expressed genes when comparing saline to polyI:C microglia at each of these timepoints, with none passing the significance threshold (Figure 2.12). Moreover, we did not find any major sex differences in microglia at baseline (Figure 2.13) or when exposed to polyI:C (Figure 2.14) on the transcriptional level at any of the assessed timepoints.

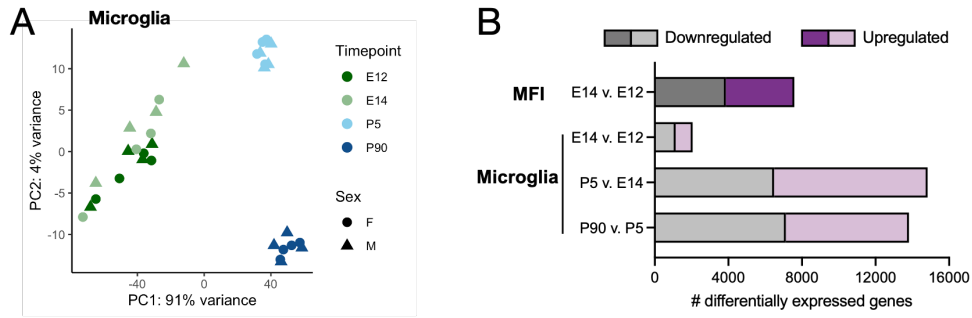


Figure 2.11. Microglia transcriptional maturation.

Pregnant dams were injected i.p. with saline as a control on E11 and E12. MFI tissue was collected at E12 and E14. Brains were collected from offspring at E12, E14, P5, and P90, single-cell suspensions made, and microglia were purified by MACS using CD11b-coated magnetic beads. RNA was isolated from MFIs and purified microglia then bulk RNA-seq was conducted on the 4 experimental groups with 4 samples per group at each timepoint. (A) PCA plots of all microglia samples showing clustering of groups by timepoint. (B) Number of upregulated and downregulated differentially expressed genes (FDR < .1, p-value < 1×10^{-5} and $\log_2FC > 2$) comparing subsequent timepoints in the MFI and microglia.

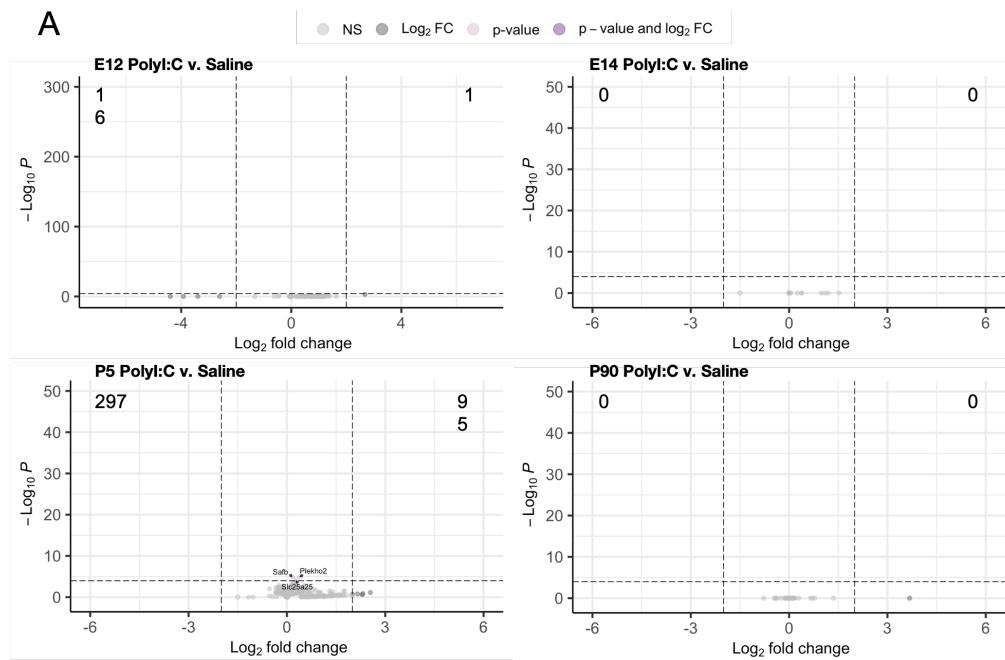


Figure 2.12. Microglia are not transcriptionally impacted by MIA.

Pregnant dams were injected i.p. with 20 mg/kg polyI:C on E11 and E12 to elicit MIA or with saline as a control. Brains were collected from offspring at ages E12, E14, P5, and P90, single-cell suspensions made, and microglia were purified by MACS using CD11b-coated magnetic beads. RNA was isolated from purified microglia and then bulk RNA-seq was conducted on the 4 experimental groups with 4 samples per group at each timepoint. (A) Volcano plots showing the number of differentially expressed genes in microglia comparing polyI:C to saline, broken down across the 4 developmental timepoints (FDR < .1) and combined by sex. Light purple dots indicate genes with p-value < 1×10^{-5} and dark grey dots indicate genes with $\log_2FC > 2$. No genes passed the combined p-value < 1×10^{-5} and $\log_2FC > 2$ cutoff of significance.

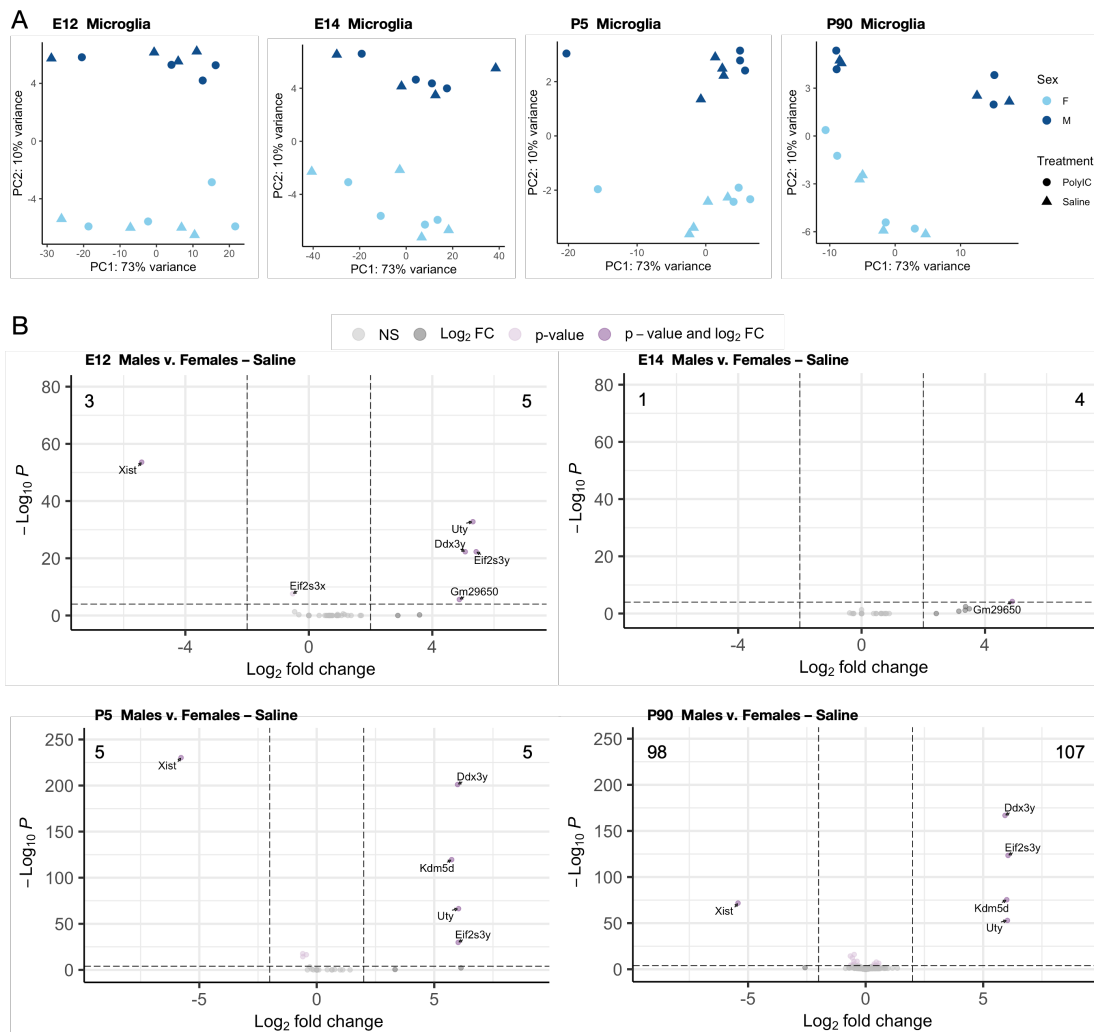


Figure 2.13. Lack of major transcriptional sex differences in microglia at baseline.

Pregnant dams were injected i.p. with saline as a control. Brains were collected from offspring at ages E12, E14, P5, and P90, single-cell suspensions made, and microglia were purified by MACS using CD11b-coated magnetic beads. RNA was isolated from purified microglia and then bulk RNA-seq was conducted on the 4 experimental groups with 4 samples per group at each timepoint. (A) PCA of microglial samples showing clustering of groups at each timepoint by sex. (B) Volcano plots showing the number of differentially expressed genes comparing males to females in saline control microglia ($FDR < .1$), separated by timepoint. Dark purple dots indicate genes that passed the combined $p\text{-value} < 1 \times 10^{-5}$ and $\log_2 FC > 2$ cutoff of significance, light purple dots indicate genes with $p\text{-value} < 1 \times 10^{-5}$, and dark grey dots indicate genes with $\log_2 FC > 2$.

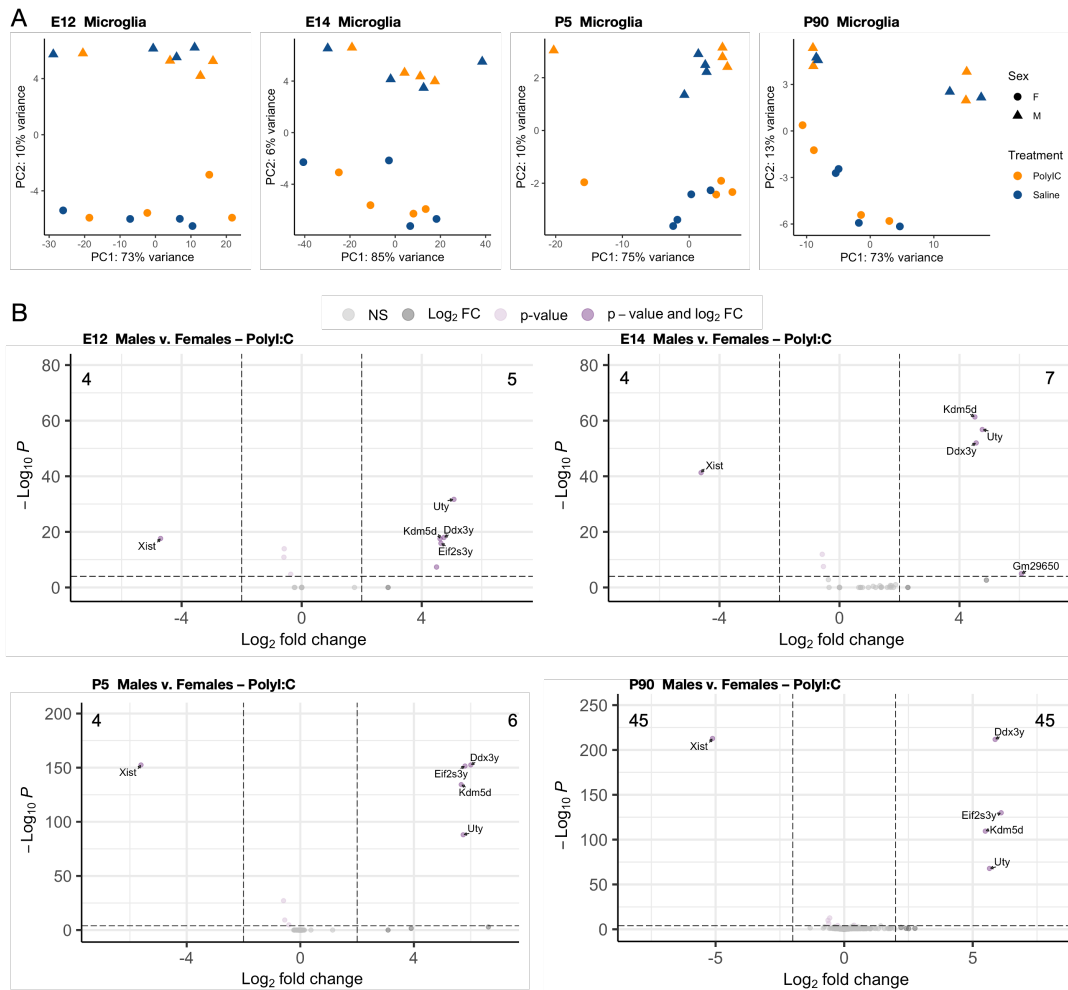


Figure 2.14. Lack of major transcriptional sex differences in MIA microglia.

Pregnant dams were injected i.p. with 20 mg/kg poly:I:C on E11 and E12 to elicit MIA or with saline as a control. Brains were collected from offspring at ages E12, E14, P5, and P90, single-cell suspensions made, and microglia were purified by MACS using CD11b-coated magnetic beads. RNA was isolated from purified microglia and then bulk RNA-seq was conducted on the 4 experimental groups with 4 samples per group at each timepoint. (A) PCA of microglial samples showing clustering of groups at each timepoint by treatment. (B) Volcano plots showing the number of differentially expressed genes comparing males to females in poly:I:C microglia (FDR < 0.1), separated by timepoint. Dark purple dots indicate genes that passed the combined p-value < 1×10^{-5} and $\log_2 \text{FC} > 2$ cutoff of significance, light purple dots indicate genes with p-value < 1×10^{-5} , and dark grey dots indicate genes with $\log_2 \text{FC} > 2$.

To verify the quality and robustness of our microglia RNA-seq dataset, we evaluated the baseline transcriptional landscape and developmental trajectory in control microglia collapsed across sex. We conducted differential expression analysis at subsequent developmental timepoints (E14 v. E12, P5 v. E14, and P90 v. P5) in saline control samples and identified a vast number of DEGs in each of these comparisons as we had found in the placenta (Figure 2.11B). We found microglia to be increasingly transcriptionally different at each comparison through our developmental time course (Figures 2.11, 2.15A-C) in which there was a coordinated loss of immature microglia genes and gain of mature markers (Figure 2.15D-G). Pathway analyses revealed that microglia progress through highly distinct neurodevelopmental phases: these cells first undergo robust replication, then progress to a role of sculpting the extracellular matrix and neuronal development, then become highly active in terms of metabolism, cell growth, and signaling cascades, and finally reach a mature maintenance state (Figure 2.15H). This transcriptional assessment of microglial maturation is consistent with published studies

33,35

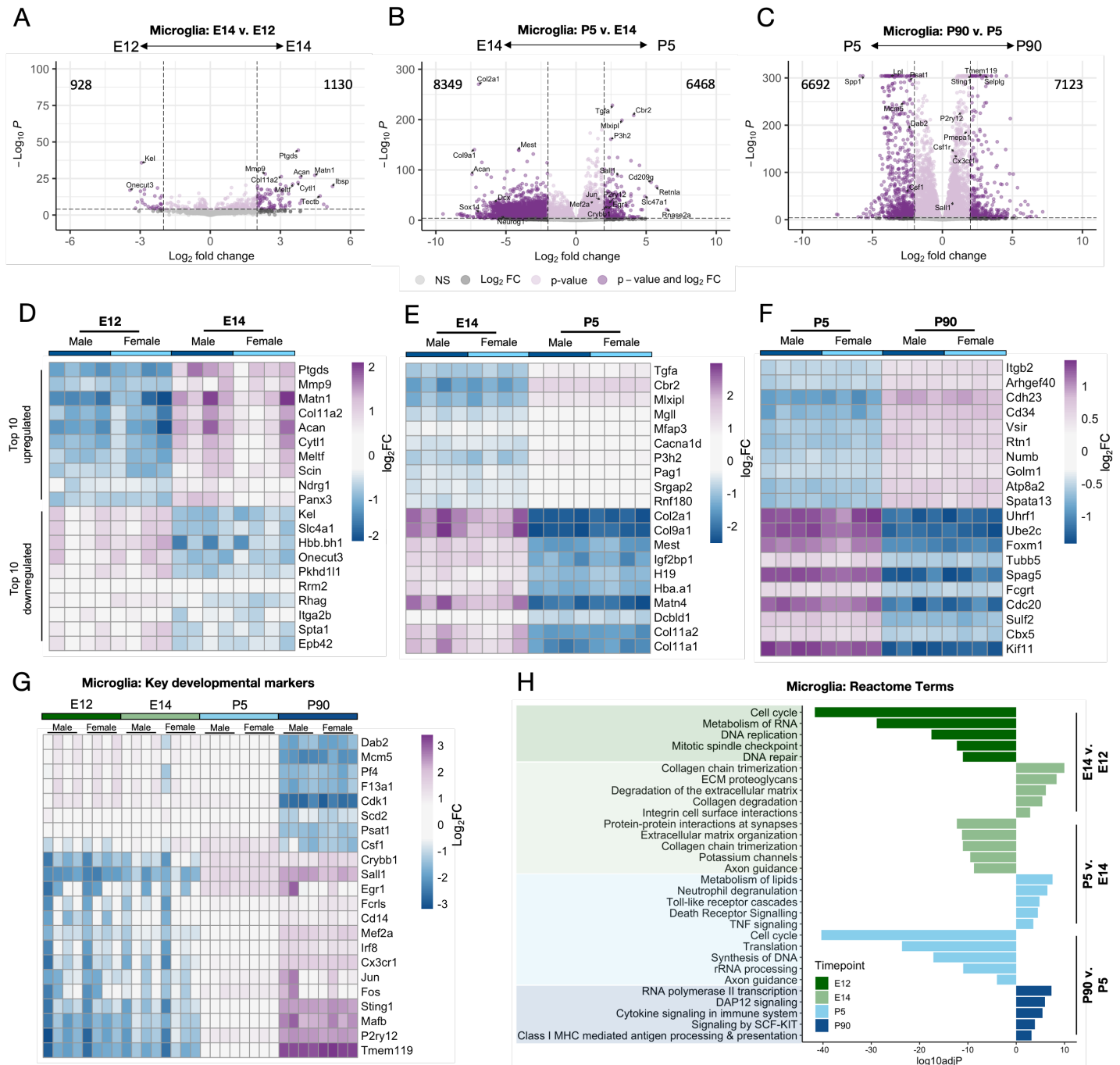


Figure 2.15. The microglial transcriptional development program.

Pregnant dams were injected i.p. with saline as a control on E11 and E12. Brains were collected from offspring at ages E12, E14, P5, and P90, single-cell suspensions made, and microglia were purified by MACS using CD11b-coated magnetic beads. RNA was isolated from purified microglia and then bulk RNA-seq was conducted on the 4 experimental groups with 4 samples per group at each timepoint. (A-C) Volcano plots showing the number of differentially expressed genes in microglia comparing polyI:C to saline combined by sex ($FDR < .1$). Plots shown for subsequent timepoint comparisons: E14 v. E12 (A), P5 v. E14 (B), and P90 v. P5 (C). Dark purple dots indicate genes that passed the combined p -value $< 1 \times 10^{-5}$ and $\text{log}_2\text{FC} > 2$ cutoff of significance, light purple dots indicate genes with p -value $< 1 \times 10^{-5}$, and dark grey dots indicate genes with $\text{log}_2\text{FC} > 2$. (D-F) Heatmap representations of the top 10 genes ($FDR < .1$) enriched at each subsequent timepoint comparison: E14 v. E12 (D), P5 v. E14 (E), and P90 v. P5 (F). (G) Heatmap representation of select key microglia development-related genes at each timepoint shows the progressive loss of immature markers and acquisition of mature markers. (H) Reactome terms selected following gene set enrichment analysis conducted at subsequent timepoint comparisons. For each comparison, genes with negative $\text{log}_{10}\text{adj}P$ values are enriched at the earlier timepoint while genes with positive $\text{log}_{10}\text{adj}P$ values are enriched at the later timepoint.

To independently corroborate these findings, we re-analyzed the transcriptional profile of MIA microglia from a published single-cell RNA-sequencing (scRNA-seq) dataset using a similar polyI:C model⁵⁰¹. Following clustering of all cells at E14 (48 hours post-polyI:C) and E18 (96 hours post-polyI:C), we selected for microglia based on enriched expression of *Cx3cr1* and *Tmem119* and low expression of other cell-type-specific markers

(Figure 2.16). tSNE re-clustering of microglia yielded two sub-clusters at E14 (Figure 2.9F) and 5 sub-clusters at E18 (Figure 2.9G). MIA and control PBS microglia did not fall into any distinct cluster at either E14 (Figure 2.9F) or E18 (Figure 2.9G). In addition, we found very few significantly differentially expressed genes between MIA and PBS microglia. There were no significant DEGs at E14 and only 4 DEGs at E18: *mt-Co2*, *Mrc1*, *Lyve1*, and *F13a1*. Taken together, these findings suggest that this model of MIA does not significantly affect the transcriptome of microglia during development or persisting into adulthood. Whether this MIA model alters microglia at the functional levels and/or primes microglia to respond differently to insults later in life will be important future areas of investigation.

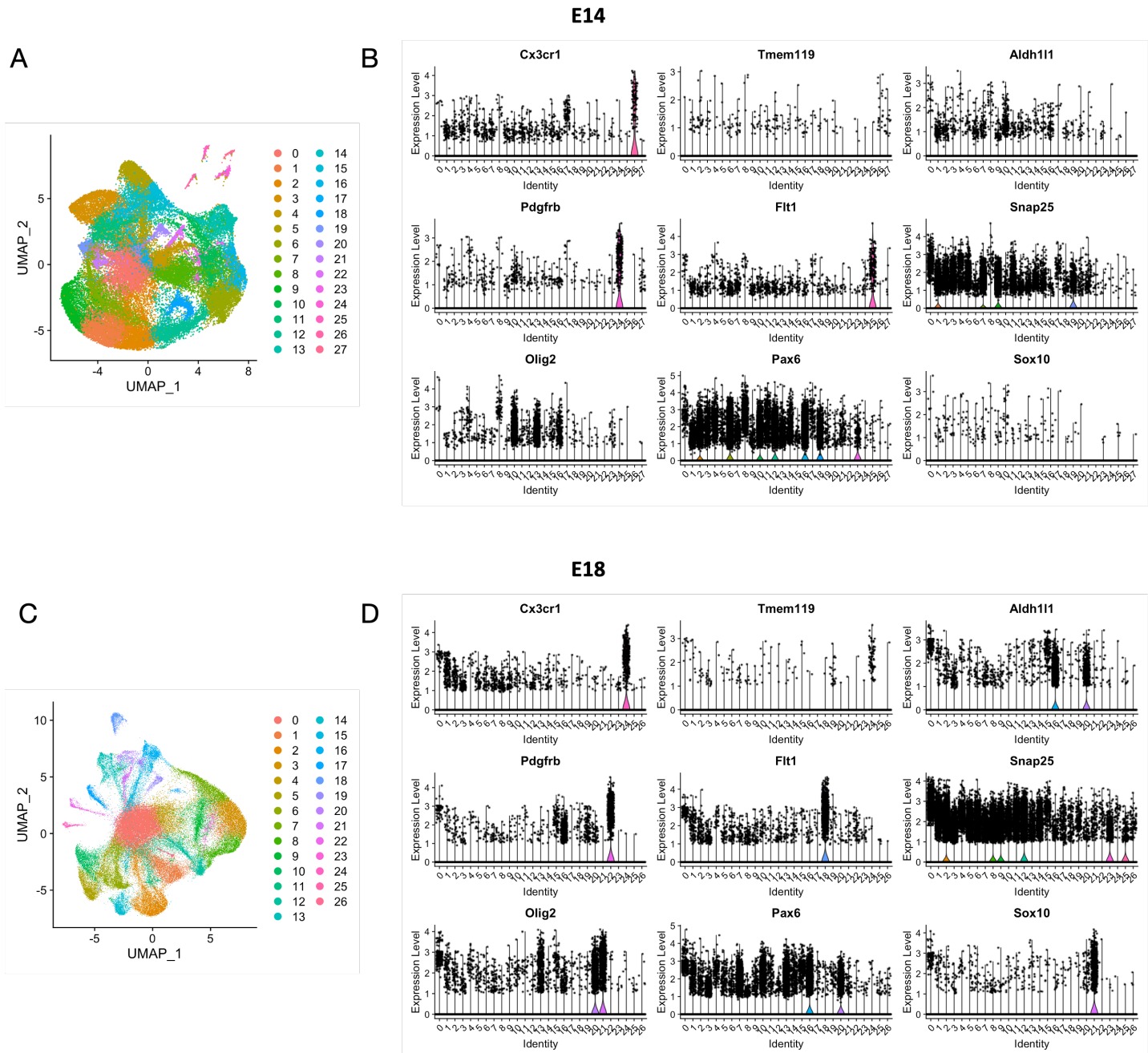


Figure 2.16. scRNA-seq clustering and cluster expression of cell-type-specific markers for selection of microglia.

Reanalysis of single cell RNA-sequencing (scRNA-seq) data collected from MIA offspring and PBS control brains (Kalish et al. 2020) at E14 (48 hours-post-poly:C, A and B) and E18 (96 hours-post-poly:C, C and D). All cells within each timepoint were clustered and cell-type-specific gene expression was assessed within each cluster. UMAP projections (A,C) and violin plots illustrating relative expression levels of cell type-specific markers (B,D) were used to identify microglia. Microglia were determined to be cluster #26 at E14 (A,B) and cluster #24 at E18 (C,D).

2.5.6. SSRI exposure reshapes the MFI response to MIA

A recent study found that inflammation during pregnancy due to maternal high-fat diet gave rise to sex-dependent behavioral alterations that were accompanied by reduced placental serotonin levels⁵¹³. We therefore wondered whether maternal inflammation in our polyI:C model also altered the serotonergic tone of the MFI. In addition, we were interested to see whether and how the MFI responds to a different type of environmental insult, and furthermore whether a combination of insults would differentially impact *in utero* physiology and offspring neurobiology. For this second insult, we used fluoxetine (a common SSRI, brand name Prozac), a medication used to treat depression in addition to other mental conditions, including obsessive compulsive disorder, panic attacks, some eating disorders, and premenstrual syndrome⁵¹⁴. A query study found that fluoxetine is among one of the top 20 most commonly prescribed medications during pregnancy⁵¹⁵.

For our study, we began treating female mice with fluoxetine at least two weeks prior to mating (Figure 2.17A) to investigate the impact on MFI health and offspring neurodevelopment. Control and fluoxetine-treated pregnant dams were then exposed to MIA or a saline control injection as before and then maternal sera, MFIs, and embryonic brains were harvested 3 hpi to compare differential responses to polyI:C and fluoxetine as well as to interrogate any combinational effects (Figure 2.17A). Fluoxetine exposure, like polyI:C, did not appreciably affect maternal weight gain during pregnancy (Figure 2.18A) nor the number of embryos when collected at E12 (Figure 2.18B). We did note a trend toward diminished dam weight gain and offspring numbers in double-hit fluoxetine polyI:C pregnancies (Figure 2.18A,B).

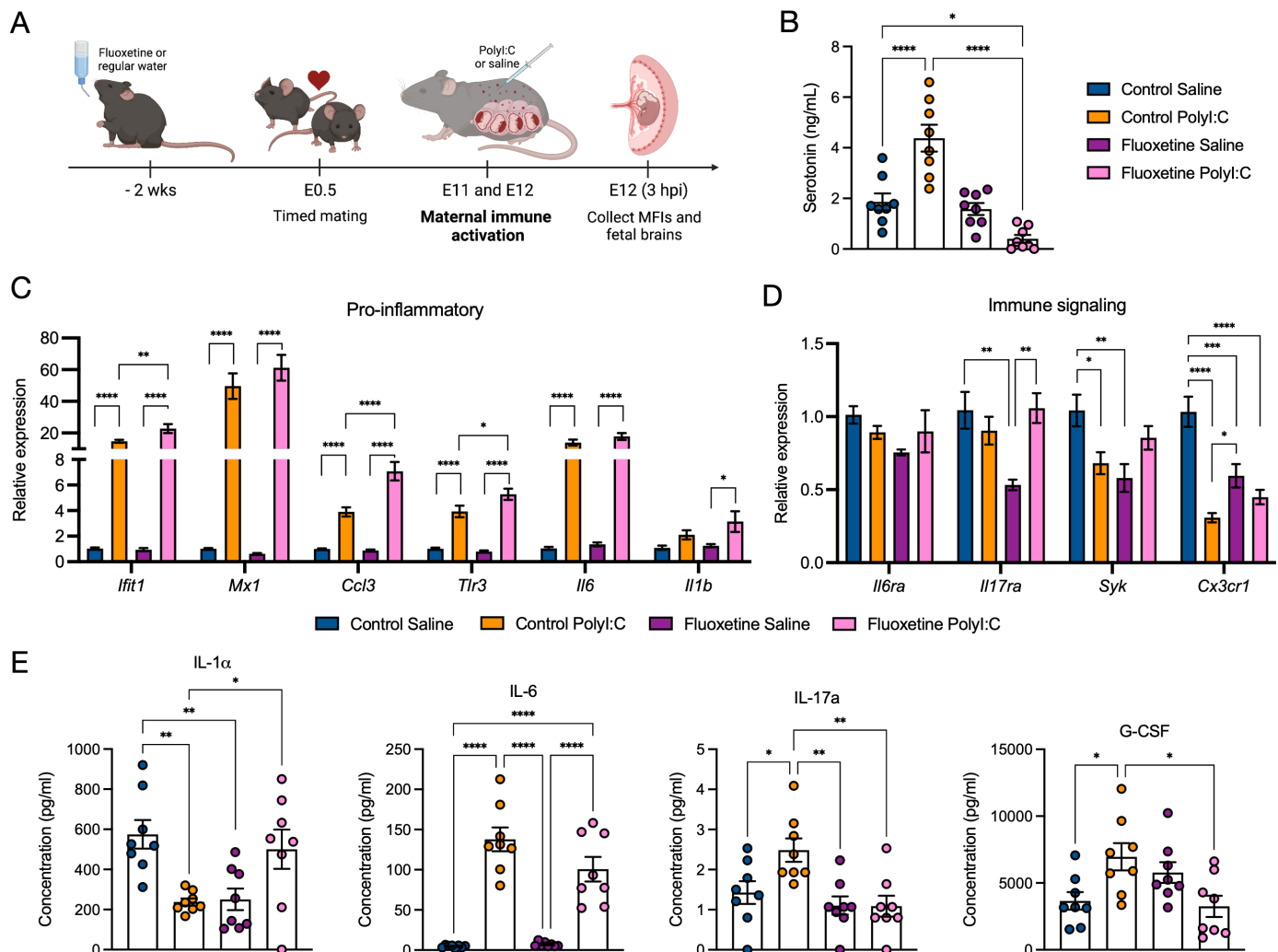


Figure 2.17. Fluoxetine exposure reshapes the MFI response to MIA.

Female mice were given fluoxetine in the drinking water (160 mg/L) for at least 2 weeks prior to addition of a male to the cage for mating. The presence of a vaginal plug was marked as E0.5. Pregnant dams were injected i.p. with 20 mg/kg polyI:C on E11 and E12 to elicit MIA or with saline as a control.

MFIs were collected 3 hpi on E12. (A) Experimental design. (B) Serotonin levels assessed by ELISA conducted on MFI homogenates. (C,D) Key pro-inflammatory immune response (C) and immune signaling (D) gene expression assessed by qPCR conducted on MFI RNA. (E) Cytokine levels assessed by multiplex cytokine array on MFI homogenates. Samples were collected from at least two independent pregnancies per group. Each point represents an individual MFI (B,E), n = 8 MFIs per group (B-E). Statistical significance calculated by one-way ANOVA with Tukey's post-hoc comparison (B-E). Error bars indicate mean \pm s.e.m. * $P < 0.05$, ** $P < 0.01$, *** $P < 0.001$, **** $P < 0.0001$.

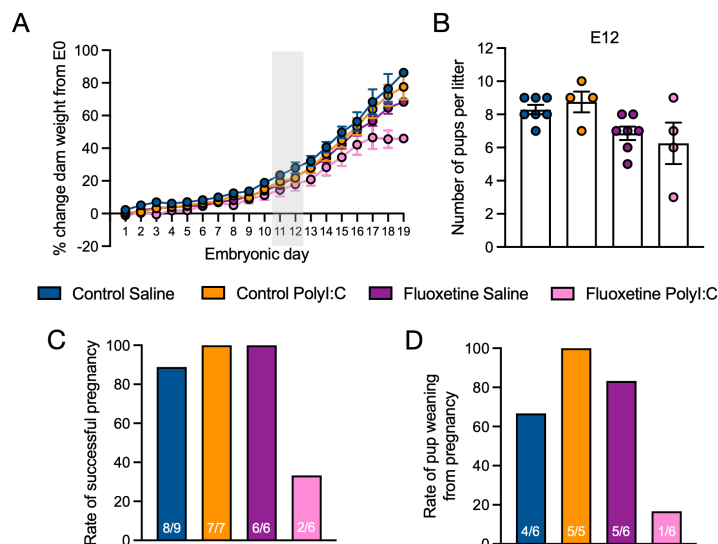


Figure 2.18. MIA impacts fluoxetine pregnancy progression.

Female mice were given fluoxetine in the drinking water (160 mg/L) for at least 2 weeks prior to addition of a male to the cage for mating. The presence of a vaginal plug was marked as E0.5. Pregnant dams were injected i.p. with 20 mg/kg polyI:C on E11 and E12 to elicit MIA or with saline as a control. (A) Dam weight through pregnancy. Plotted as percent change from baseline (E0 weight). Grey box indicates i.p. injection timepoints. (B) Number of pups *in utero* on E12. (C) Rate of successful pregnancy as assessed by the birth of at least one live pup. White ratio insets denote the quantity of pregnancies assessed. (D) Rate of successful pup weaning assessed on P21. White ratio insets denote the quantity of pregnancies assessed. Each point represents the average 3-6 pregnancies per group (A) or individual pregnancies (B). Statistical significance calculated by two-way ANOVA with Sidak's multiple comparisons test (A) or one-way ANOVA with Tukey's post-hoc comparison (B). Error bars indicate mean \pm s.e.m.

Serotonin in the developing embryo is supplied by the mother via placental production until the embryo is able to synthesize its own source of serotonin beginning around E15⁴⁸⁸. MIA exposure in the non-fluoxetine group caused MFI serotonin levels to increase two-fold (Figure 2.17B). We were fascinated to see the opposite effect of polyI:C on fluoxetine pregnancies, whereby MFI serotonin levels were nearly undetectable (Figure 2.17B).

Though serotonin is perhaps most well-known for its roles in the brain where it regulates cognition, mood, sleep, and appetite, serotonin also plays a significant part in peripheral immune responses⁵¹⁶. Nearly all immune cells express serotonin effector machinery and serotonin can influence cytokine secretion, leukocyte activation and migration, and more⁵¹⁶. We therefore questioned whether SSRI exposure, which is known to elevate peripheral serotonin levels, would reshape the MFI immune response to MIA. Indeed, qPCR of key inflammatory mediators identified in our RNA-seq dataset (Figure 2.2C-E) revealed that fluoxetine combined with polyI:C exposure significantly potentiated the expression levels of these pro-inflammatory genes at the placenta including *Ifit1*, *Ccl3*, and *Tlr3* (Figure 2.17C). Meanwhile, some of these pro-inflammatory genes remained unchanged by fluoxetine exposure alone (Figure 2.17C). Interestingly though, fluoxetine-only exposure diminished MFI expression of the immune signaling components *Ii17ra*, *Syk*, and *Cx3cr1*, some of which were restored to control levels in the case of dual treatment with both polyI:C and fluoxetine (Figure 2.17D).

These results led us to question whether cytokine levels were changed systemically in the mother or in the MFI in our treatment groups. To this end, we conducted a multiplex cytokine assay on maternal sera collected at 3 hpi. We found significantly elevated levels of IL-4 and IL-6 following polyI:C treatment alone and elevated IL-6 levels with polyI:C + fluoxetine, but no other significant differences were found in any of the other cytokines analyzed in this assay (Figure 2.19A, Supplemental Table 2). Instead, we found that the levels of IL-1 α , IL-6, IL-17a, and G-CSF in the MFI were considerably impacted by our treatments (Figure 2.17E). Consistent with other studies⁴²³, polyI:C exposure led to significantly higher levels of IL-6 in MFI tissue, yet these were not impacted by fluoxetine (Figure 2.17E). PolyI:C treatment also led to higher MFI levels of IL-17a and G-CSF and these were dampened to baseline levels in the presence of fluoxetine (Figure 2.17E). We also noted a decrease in IL-

1 α levels with polyI:C or fluoxetine exposure alone that were returned to baseline levels in two-hit fluoxetine + polyI:C MFIs (Figure 2.17E). In contrast to these effects on IL-1 α , IL-6, IL-17a, and G-CSF, we did not observe an appreciable impact of polyI:C and/or fluoxetine treatment on MFI levels of IL-1 β , IL-4, IL-10, GM-CSF, IFN- γ , or TNF- α at 3 hpi (Figure 2.19B, Supplemental Table 3). These collective findings illustrate that polyI:C and fluoxetine can impact the MFI cytokine milieu, and that the combination of these treatments can have multimodal effects.

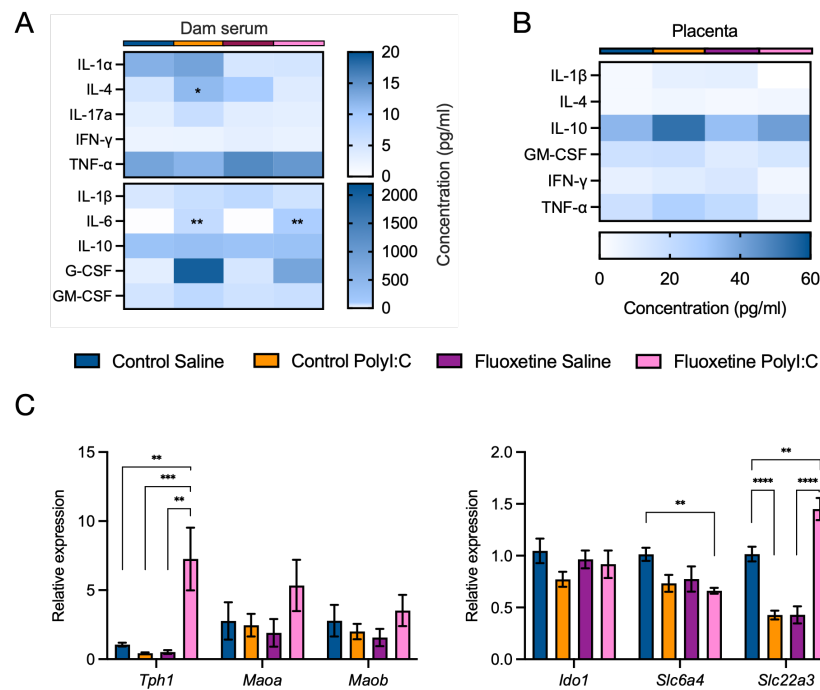


Figure 2.19. Fluoxetine and MIA do not largely impact maternal cytokine levels but elicit combinatorial effects on MFI serotonin signaling.

Female mice were given fluoxetine in the drinking water (160 mg/L) for at least 2 weeks prior to addition of a male to the cage for mating. The presence of a vaginal plug was marked as E0.5. Pregnant dams were injected i.p. with 20 mg/kg polyI:C on E11 and E12 to elicit MIA or with saline as a control. Maternal sera and MFI tissue were collected 3 hpi on E12. (A,B) Systemic (A) and MFI (B) cytokine levels assessed by multiplex cytokine array. (C) MFI gene expression of serotonin-related genes assessed by qPCR. Samples were collected from at least two independent pregnancies per group. n = 8 MFIs per group (B-C). Statistical significance calculated by one-way ANOVA with Tukey's post-hoc comparison (A-C). Error bars indicate mean \pm s.e.m. * P < 0.05, ** P < 0.01, *** P < 0.001, **** P < 0.0001.

We next questioned how fluoxetine treatment alone or in combination with polyI:C-induced MIA modulates MFI serotonin signaling. *Tph1*, coding for the major serotonin synthesis enzyme tryptophan hydroxylase 1, was significantly upregulated in fluoxetine polyI:C MFIs (Figure 2.19C), perhaps to compensate for the extremely low MFI serotonin levels in this double-hit group (Figure 2.17B). Next, we turned to the serotonin transporters 5-HTT (also known as SERT; *Slc6a4*) and OCT3 (*Slc22a3*). While there is little serotonin present in the two-hit placentas (Figure 2.17B), we were surprised to find diminished expression of *Slc6a4* and elevated expression of *Slc22a3* in fluoxetine polyI:C placentas (Figure 2.19C). PolyI:C treatment alone elevated serotonin levels (Figure 2.17B) and simultaneously decreased *Slc22a3* expression (Figure 2.19C).

Serotonin is synthesized from tryptophan and IDO1 is an essential tryptophan degrading enzyme producing kynurenine to shunt tryptophan resources away from serotonin production⁵¹⁷. We found no significant changes in MFI *Ido1* expression in any of our treatment groups (Figure 2.19C). Monoamine oxidase (MAO) enzymes can catalyze the oxidative deamination of serotonin which inhibits serotonin active signaling at 5-HT receptors. We did not find differential expression of either *Maoa* or *Maob* in MFI tissue 3 hpi in any of our treatment groups (Figure 2.19C), suggesting serotonin deactivation likely does not account for differential MFI serotonin levels at this timepoint (Figure 2.17B). Altogether, these data suggest that fluoxetine may reshape MFI serotonin signaling when combined with maternal inflammation.

2.5.7. SSRI exposure potentiates the offspring brain response to MIA

Given the significance of the placenta as a source of serotonin to the developing embryo^{488,489}, as well as the importance of serotonergic signaling during neurodevelopment^{484,489,518}, we next wanted to investigate the impact of MIA and SSRI exposure on the developing embryonic brain. MIA has been previously reported to decrease the expression of protein synthesis-related genes due to activation of the integrated stress response⁵⁰¹. We noticed a trending decrease in the expression of the translation initiation factor *Eif2s1* in polyI:C brains 3 hpi (Figure 2.20A). Conversely, the expression of *Eif2s1* as well as *Chd1*, a chromatin remodeler linked to the stress response, and *Rack1*, a core ribosomal subunit, were all strongly increased in polyI:C brains that were also exposed to fluoxetine (Figure 2.20A).

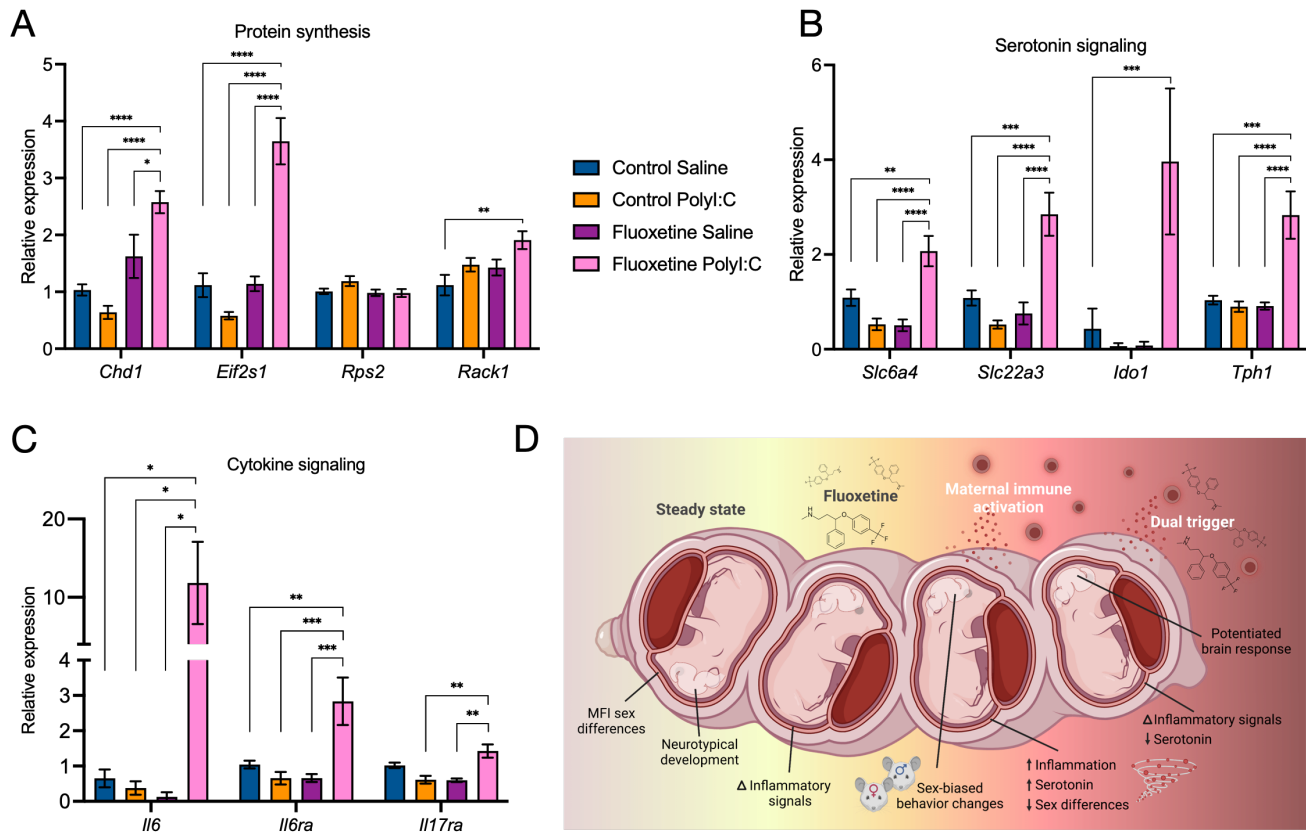


Figure 2.20. Fluoxetine exposure potentiates the embryonic brain response to MIA.

Female mice were given fluoxetine in the drinking water (160 mg/L) for at least 2 weeks prior to addition of a male to the cage for mating. The presence of a vaginal plug was marked as E0.5. Pregnant dams were injected i.p. with 20 mg/kg polyI:C on E11 and E12 to elicit MIA or with saline as a control. Fetal brains were collected 3 hpi on E12. (A-C) qPCR of bulk brain tissue assessing expression of genes related to protein synthesis (A), the serotonin signaling (B), and cytokine signaling (C). (D) Graphical abstract summarizing the findings from the present study. Samples were collected from at least two independent pregnancies per group. n = 6-8 mice per group (A-C). Statistical significance calculated by one-way ANOVA with Tukey's post-hoc comparison (A-C). Error bars indicate mean +/- s.e.m. * $P < 0.05$, ** $P < 0.01$, *** $P < 0.001$, **** $P < 0.0001$.

SSRIs, including fluoxetine, are known to cross the maternal-fetal interface barrier and blood-brain-barrier to enter the developing embryo^{483,519}. Moreover, maternal inflammatory mediators such as IL-6 and IL-17a can also influence offspring developmental neurobiology^{420,423,424}. Given this, we sought to investigate the impact of MIA and SSRI treatment on serotonin-related gene expression. Serotonin-related genes *Slc6a4*, *Slc22a3*, *Ido1*, and *Tph1* were all non-significantly diminished in expression with either fluoxetine or polyI:C exposure alone but dramatically increased when fluoxetine and polyI:C were combined (Figure 2.20B). These trends match that which we found for protein synthesis machinery and highlight the combinatorial impact of MIA and SSRI treatment on the developing brain.

The impact that we saw of MIA and SSRI treatment on MFI inflammatory signaling (Figure 2.17C-E) spurred us to see if a shift in cytokine signaling was occurring simultaneously in the embryonic brain. We focused on IL-6

and IL-17a signaling given the dependence of MIA-induced behavioral alterations on these molecules^{420,423,424}. We found significantly elevated expression of *Il6*, *Il6ra*, and *Il17ra* in embryonic brains exposed to combined fluoxetine polyI:C treatment, but not those exposed to either fluoxetine or polyI:C treatment alone (Figure 2.20C). Altogether, these results illustrate that pro-inflammatory agents combined with SSRI treatment may impact offspring neurobiology by shifting the transcription of protein synthesis, serotonin, and cytokine machinery.

The severe impact of polyI:C treatment on fluoxetine pregnancies was further noted when pregnancies were allowed to carry to term. While most control, polyI:C, and fluoxetine pregnancies successfully produced live pups, we found that a large fraction of fluoxetine pregnancies were lost following the second hit polyI:C treatment (Figure 2.18C). Moreover, only a few fluoxetine polyI:C pups made it to weaning age (P21; Figure 2.18D) while most pups from the other treatment groups were viable. In totality, our study reported herein finds that different manipulations of the maternal environment led to distinct responses at the maternal-fetal interface and in offspring neurobiology (Figure 2.20D).

2.5 Discussion

The placenta is a remarkable organ whose temporary existence is essential for eutherian mammal life. Maternal-fetal interface cells mediate indispensable nutrient and waste exchange between the mother and developing embryo⁴⁹³. Disturbed placental well-being can thus severely compromise embryo development. Knowledge of how the MFI supports offspring neurodevelopment during homeostasis and the impact of common environmental insults on *in utero* physiology and subsequent neurodevelopmental consequences are lacking. Expanding knowledge in these areas is important to achieve better understanding of both healthy neurodevelopment as well as the etiology of environmentally-triggered neurodevelopmental disturbances.

In the study reported herein, we investigated the impact of maternal inflammation and disruption in serotonergic tone via SSRI exposure on *in utero* physiology and offspring neurodevelopment. Our bulk RNA-seq dataset revealed that the MFI undergoes a notable pro-inflammatory response to MIA within 3 hpi that has lasting impacts on the placental transcriptome out to at least 48 hpi. A recent study found that maternal SARS-CoV-2 infection perturbed placental expression of IFN-stimulated genes and Fc receptors which was accompanied by impaired placental antibody transfer to the fetus⁵⁰⁶. Even brief disruption of the delicate maternal-fetal interface milieu has the potential to alter nutrient, waste, and gas exchange with the developing embryo which may have severe consequences.

We noted a strongly upregulated type I IFN signature in polyI:C MFIs. This is consistent with previous findings that type I IFNs are a large source of antiviral immunity in the placenta^{506,520,521}. We noted significantly elevated expression of *Ifitm1* and *Ifitm3* in MIA-exposed MFIs (Supplemental Gene Lists). IFITM can block viral entry into cells, yet it also can limit the fusion of placental cytotrophoblasts into syncytiotrophoblasts, a key step in placental barrier formation⁵²². While limiting viral spread into the developing embryo is essential, the generation of highly pro-inflammatory IFNs may negatively impact both placental physiology and offspring neurodevelopment.

Our MIA model recapitulated at the maternal-fetal interface the well-known IL-6 and IL-17a signatures that are necessary for the onset of MIA behavioral changes^{420,423,424}. While it is unclear whether cytokines can cross either the placental barrier and/or the blood-brain barrier (BBB), cytokine signaling at the placenta itself can contribute to ill-affecting neurodevelopmental consequences^{523,524}. For instance, impairing IL-6Ra function (thereby obstructing IL-6 signaling) in placental trophoblasts was shown to protect against MIA-induced offspring cerebellar pathologies and behavioral changes (Wu et al., 2017). In all, the MFI inflammatory response characterized with this dataset may help to illuminate some of the developmental effects of MIA.

One may be surprised to learn that the homeostatic MFI is jam packed with maternal immune cells; leukocytes constitute nearly 40% of all cells^{494,525}. The majority of these immune cells are dNK cells with the remainder largely being decidual macrophages and T cells⁴⁹⁴. This large immune population serves essential tolerogenic roles as well as homeostatic uterine and vascular remodeling functions^{494,520,525}. One could postulate that alterations in the immune landscape that occur in response to MIA, SSRIs, or other insults may ultimately disrupt the delicate tolerogenic state and potentially cause immune-driven harm to the embryo. We speculate that in

MIA pregnancies, immune cells generally dedicated to homeostatic functions in the maternal-fetal interface are instead concerned with engaging an inflammatory response. Perhaps a loss of homeostatic immune cell function contributes to altered MIA offspring outcomes.

Our current study is limited in that it lacks cell specificity. Future studies will be necessary to shed light on the specific cell types in which the signaling pathways identified herein are altered. For now, we may only speculate on potential responders based on known cell-type expression. dNK cells produce a variety of growth factors, angiogenic factors, and cytokines at baseline including VEGFa, IL-8, IFN- γ , and CXCL10 at the maternal-fetal interface⁴⁹⁴. We found dramatically elevated *Cxcl10* expression in polyI:C-exposed MFIs. Interferons can induce *Cxcl10* expression and CXCL10 can contribute to immune cell chemotaxis, T cell activation, and angiogenesis⁵²⁶. Correspondingly, we found an increase in the dNK cell marker *Cd56* specifically in the decidua following polyI:C treatment. Whether dNK cells are the source of CXCL10 and how CXCL10 contributes to the MFI immune response and neurodevelopment are important future areas of investigation.

Circulating cells present in the vasculature are another potential reservoir responsible for driving some of the DEGs in our maternal-fetal interface RNA-seq study. It is possible that the amount of peripheral blood (originating from either the mother or the embryo) in our MFI samples is changed upon initiation of the maternal immune response. Indeed, studies are beginning to reveal that maternal infection can lead to abnormal placental villous architecture and vascular remodeling⁵²⁷. Many immune molecules like cytokines and chemokines, including some of those which we found to have elevated expression at the MIA maternal-fetal interface, are known to impact placental vascular development and function. Mechanistically, these inflammatory mediators can cross-talk with angiogenic factors, such as sFlt-1 and VEGF⁵²⁷, which may cause improper placental vascular development and contribute to adverse offspring outcomes. dNK cells are a critical population involved in vascular remodeling⁵²⁵. It is possible that polyI:C exposure affects this homeostatic dNK function. Moreover, we found altered expression of many factors known to impact angiogenesis acutely after polyI:C exposure. Though beyond the scope of the current study, it would be interesting to more mechanistically evaluate how these blood transport processes are impacted by polyI:C, as this could explain some of the alterations to fetal development reported in this MIA model.

The transcriptional landscape is altogether transformed in the MIA environment, having the potential to alter typical transfer of oxygen, nutrients, antibodies, and more to the embryo. It is conceivable that male and female embryos are differentially sensitive to theoretic disruptions in typical placental support. One of the findings we were most surprised by in this study was that baseline MFI transcriptional sex differences are nearly eliminated by MIA. Even more striking to us was that this dampening of sex-specific signaling persisted beyond the cessation of the pro-inflammatory response to polyI:C. A few studies have begun to define sex differences in placental structure and function⁵⁰⁷⁻⁵⁰⁹ but there is yet much insight to be gleaned in this realm. We found that female control MFIs were enriched for immune- and neurodevelopment-related modules in addition to pathways related to the cell cycle, semaphorin interactions, and platelet activation. Male embryos are thought to be more metabolically demanding, requiring greater levels of immune tolerance and of nutrient transport to support larger growth requirements^{508,528}. Our dataset found that the male MFI was enriched for pathways related to protein export, the spliceosome, the fibrin clotting cascade, and translation. It is imaginable that a loss of sex-specific MFI support on its own disturbs embryo development beyond the known pro-inflammatory environment effects. Moreover, the sex of the embryo may render different responses to such conditions of stress, potentially precipitating some of the neurodevelopmental consequences commonly reported in MIA offspring.

We were initially surprised to find no major consequence of MIA on the transcriptome of offspring microglia. Other studies using different MIA models have indeed reported that MIA can impact microglia number, motility, and phagocytic capacity^{112,462,529,530}. It is possible that our relatively mild polyI:C-driven model is below a certain threshold for impacting microglia on the transcriptional level; an argument supported by the lack of transcriptional differences seen in the Kalish et al. 2021 dataset collected from a similar model. Microglia exposed to our MIA paradigm may have no resting transcriptional differences yet still harbor differences in protein levels, post-translational modification, or other aspects that contribute to alterations in form and function. Alternatively, microglia exposed to this type of MIA could exist in a “primed” state in which differences in function or response is revealed in the presence of a stimulus or second hit. Indeed, such was found to be the case in one study in which scRNA-seq analysis of control versus MIA-exposed microglia yielded only 7 DEGs at baseline, yet 401

DEGs following adult immune challenge⁵³¹. While MIA microglia may be similar to control microglia in terms of transcriptional state, density, morphology, and activation at baseline^{426,462,463,531–533}, new work suggests that epigenetic priming of MIA microglia leads to dysfunctional responses when confronted with stimuli later in life⁵³¹. The variability in the type and strength of the immune response generated with different MIA models, dam microbiome, developmental stage targeted, and other experimental considerations could all additionally account for different outcomes on microglia.

Stress, depression, and anxiety may also contribute to inflammation during pregnancy and have the potential to alter the maternal environment in other facets. Major depressive disorder has a devastating prevalence of 13% amongst pregnant women⁵¹⁸. SSRIs are the most commonly prescribed treatment for depression⁴⁸². 25% of women taking SSRIs continue use during pregnancy and another 0.5% of women begin taking an SSRI at some point during pregnancy⁴⁸³. Maternal SSRI intake can potentially lead to systemic disruption of serotonergic signaling. Circulating and tissue-resident immune cells, placental syncytiotrophoblasts and cytotrophoblasts, and developing neural cells all utilize serotonergic transporters and signaling^{483,516,534}. SSRI action on any or all of these populations could therefore potentially impact neurodevelopment. Our findings reveal that SSRI exposure alone can modulate the expression of genes involved in immune and serotonin signaling at the maternal-fetal interface.

Immune cell function can be directly impacted by SSRI exposure in the mother and embryo, both of which could potentially affect neurodevelopment given that maternal and embryonic immune cells contribute to both placental support and neurodevelopment^{474,494,525,535,536}. Serotonin can modulate immune cell activation including cytokine release, migration, adhesion, antigen presentation, phagocytosis, and more, in both pro- and anti-inflammatory ways⁵¹⁶. The serotonin transporter SERT, whose function is blocked by SSRIs, can be found on monocytes, macrophages, T and B cells, and mast cells, while serotonin receptors can be found on nearly all types of immune cells⁵¹⁶. Thus, SSRIs may broadly affect the immune system and have been investigated as immunomodulatory drugs^{537,538}. SSRIs have been shown to act in immunosuppressive or immunostimulatory manners depending on the underlying immunologic state^{537,538}.

Given that SSRIs can directly modulate immune cell function, it logically follows that our study finds a differential impact of polyI:C alone compared to combined fluoxetine and polyI:C treatment. We found that prenatal fluoxetine exposure influenced the MFI immune response to polyI:C by exacerbating the levels of some immunomodulatory factors while dampening others. These complex effects of combined fluoxetine and polyI:C exposures could partially be explained by the fact that SSRIs can have both pro- and anti-inflammatory effects^{537,538}; thereby, SSRI exposure may heighten some inflammatory response pathways while dampening others. For instance, we found heightened expression of *Ifit1*, *Ccl3*, and *Tlr3* in fluoxetine polyI:C MFIs when compared with polyI:C treatment alone. On the other hand, levels of IL-1 α , IL-17a, and G-CSF were returned to control levels in fluoxetine polyI:C MFIs compared to polyI:C alone. Meanwhile other pathways may be unaffected by fluoxetine exposure. For instance, we found no change in the MFI expression levels or protein levels of IL-6 comparing double-hit fluoxetine polyI:C to single-hit polyI:C alone. Similar effects can be seen when comparing fluoxetine-only exposure to combined fluoxetine polyI:C treatment. For example, fluoxetine alone dramatically dampened MFI expression of the cytokine receptor *Il17ra*, the critical pro-inflammatory mediator *Syk*, and the chemokine receptor *Cx3cr1*. In the presence of fluoxetine, polyI:C treatment restored the expression of *Il17ra* and *Syk* to control levels.

We found that polyI:C elicited heightened MFI levels of serotonin relative to controls, while the combination of polyI:C and fluoxetine exposure instead lowered MFI serotonin to nearly undetectable levels. A recent study also found heightened placental serotonin levels in a prenatal stress model that was accompanied by maternal inflammation⁵³⁹. The embryo is not capable of synthesizing its own source of serotonin until after E15 (Bonnin et al., 2011; Bonnin and Levitt, 2011) yet serotonin is used for a variety of developmental processes prior to E15⁴⁸³. Serotonin transfer from the mother via the placenta therefore acts as the sole source of serotonin until sufficient embryo-sourced serotonin synthesis is achieved (Bonnin et al., 2011; Bonnin and Levitt, 2011). Thus, disrupted serotonin tone in the maternal-fetal interface prior to E15, as we have detected at E12 following out environmental manipulations, have the potential to severely limit embryo serotonin levels. How disrupted placental serotonin signaling impacts offspring neurodevelopment is certainly underexplored and warrants future investigation.

While polyI:C has not been shown to be able to cross the placenta or BBB, many SSRIs are able to cross both of these barriers and may therefore directly influence serotonin signaling in the developing embryo^{483,519}. Serotonin is involved in a wide array of neurodevelopmental events including cell proliferation, migration, death, neurite guidance, dendrite maturation, and synaptogenesis⁴⁸³. Conceivably, any of these events may therefore be disrupted if embryonic brain serotonin levels are elevated by SSRIs. While serotonin transporters are only expressed by serotonergic neurons in the adult brain, a wider variety of neurons in developing brain express serotonin transporters and could potentially be affected by SSRIs⁴⁸³.

Longitudinal human studies tracking the outcomes of children from SSRI pregnancies are currently limited, but murine studies investigating the impact of prenatal SSRI exposure on offspring neural circuits and behavior have begun to uncover some notable consequences^{483,489,518}. While the impact of SSRIs on neural circuit formation and glial development are minimal, studies from *Slc6a4*^{-/-} mice have revealed that disruption of serotonin transporter function during neurodevelopment disrupts neuroanatomy in the somatosensory cortex and corticolimbic system^{483,540}. Altered function in these regions maps to the behavioral impacts of prenatal SSRI exposure in which treated offspring display delayed motor development, anxiety- and depressive-like behaviors, reduced impulsivity, improved spatial learning, and increased susceptibility to addictive-like behaviors⁵⁴⁰⁻⁵⁴³.

Our dual-environmental-hit studies revealed a complex brain transcriptional response following combined fluoxetine and polyI:C treatment compared to either fluoxetine or polyI:C exposure alone. In one case, MFI serotonin levels are significantly elevated following polyI:C treatment yet are almost undetectable following polyI:C treatment in fluoxetine pregnancies when compared to baseline control levels. Another stark example of this combinational effect is observed when looking at the embryonic brain transcriptome: while protein synthesis, serotonin-related, and cytokine-related transcription showed a trending reduction with either fluoxetine or polyI:C exposure alone, the combined exposure of fluoxetine and polyI:C significantly elevated expression above control levels across these modules. These findings highlight the critical importance of taking the entire maternal environment into account when assessing the impact of triggers on placental physiology and neurodevelopment.

Among eutherian mammals, the placenta has so far been found in at least 20 different variations, making it the most mutable organ⁴⁹³. Differences in cell type composition, maternal-fetal interface structure, and cellular function are known to exist between mice and humans^{493,494,520}. It is therefore imperative that reported findings from murine studies such as ours be investigated secondarily in a human setting, as any environmental impacts on the human placenta and downstream neurodevelopmental consequences could differ.

Our study suggests that SSRI intake during pregnancy could potentially have lasting consequences on offspring neurobiology. Yet, SSRI use provides necessary reprieve from detrimental mental health states. Untreated maternal stress, depression, and anxiety can all on their own perturb offspring neurodevelopment, contributing to adverse behavioral and cognitive outcomes⁵⁴⁴. It will therefore be of utmost importance to consider both the relative benefits and potential consequences of SSRIs as a therapeutic option during pregnancy.

2.6 Conclusions

Our findings illustrate that commonly encountered environmental insults have the potential to cause notable alterations to maternal-fetal interface physiology which may then impact offspring neurodevelopment. In particular, we found that prenatal inflammation and SSRI exposure reshape the signaling milieu of the maternal-fetal interface and offspring brain (Figure 2.20D). The placenta remains a highly understudied organ despite its absolute necessity for human life. Uncovering details concerning placental physiology during homeostasis and in response to environmental stressors will undoubtedly illuminate novel developmental biology, and in particular, that which concerns deviation from baseline.

2.7 Methods

2.7.1. Mice

All mouse experiments were performed in accordance with the relevant guidelines and regulations of the University of Virginia and approved by the University of Virginia Animal Care and Use Committee. 8-week-old C57BL/6J wild-type mice were obtained from Taconic Biosciences and housed in University of Virginia facilities for at least 1 week before use. Mice were housed in specific pathogen-free conditions under standard 12-hour light/dark cycle conditions in rooms equipped with control for temperature ($21 \pm 1.5^\circ\text{C}$) and humidity ($50 \pm 10\%$).

2.7.2. SSRI treatment and maternal immune activation

Virgin female wild type mice were placed on fluoxetine water (160 mg/L) or standard water as a control at least 2 weeks prior to mating. Duos of females were set up with male mice for mating and checked every morning for vaginal plugs. The presence of a vaginal plug was marked as embryonic day (E)0.5 and males were subsequently removed from the cage. Maternal immune activation was initiated by intraperitoneal (i.p.) injection of 20 mg/kg polyinosinic-polycytidylic acid (polyI:C) at E11 and E12 or saline was injected as a control⁴⁹⁶. Fluoxetine and control groups were kept their respective water treatments throughout the entirety of pregnancies.

2.7.3. Tissue collection

Mice were euthanized by i.p. Euthasol injection (440 mg/kg; Anada, 200-071). Maternal blood was immediately collected by cardiac puncture, incubated at room temperature for 10 minutes, and then spun down for 15 min at 1500 rpm. The top layer of serum was collected for downstream analyses. For sample isolation at embryonic timepoints, whole maternal-fetal interface tissue was dissected away from the embryo, flash frozen, and stored at -80°C . Unless otherwise noted, E12 or E14 maternal-fetal interface tissue was kept all together, including the decidua, placenta, and surrounding supportive uterine muscle tissue. For qPCR experiments comparing the decidua to the placenta, the surrounding supportive uterine muscle tissue was removed and the decidua was dissected away from the placenta. For all experiments fetal bodies were removed from the placenta, the top of embryo heads were isolated, and brains were scooped out. Embryonic brains were either placed in Buffer A (DMEM/F12 with 10% FBS, 0.1% GlutaMAX, and 0.1% antibiotic antimycotic) on ice for downstream magnetic-activated cell sorting (MACS) or were flash frozen and stored at -80°C . The remaining embryonic body was flash frozen and stored at -80°C for downstream sex genotyping. For postnatal brain collection (postnatal day (P)5 or P90) euthanized mice were perfused with 5 U/ml heparin in 1x PBS, brains were harvested, and meninges carefully removed. Brains were placed in Buffer A on ice for downstream MACS preparation.

2.7.4. Sex genotyping

Flash frozen fetal body tissue was incubated in 200 μl DirectPCR Lysis Reagent (Viagen Biotech, 102-T) with 4 μl Proteinase K (Thermo Fisher 3115879001) overnight at 55°C . Samples were heat shocked at 85°C for 45 minutes and then chilled at 4°C for 5 min and spun down at 16,000 rpm for 10 min. DNA supernatants were collected and stored at -20°C until use for PCR. PCR reactions were set up using MyTaq Red Mix (Meridian Bioscience BIO-25043) and Sx primer pair (sequences below) with extracted DNA, and then run on an agarose gel.

Rev: 5' CTT ATG TTT ATA GGC ATG CAC CAT GTA 3'
Fwd: 5' GAT GAT TTG AGT GGA AAT GTG AGG TA 3'

2.7.5. RNA extraction

Frozen tissues (whole MFIs, placentas, deciduae, or whole brains) were thawed on ice and then mechanically homogenized in Tissue Protein Extraction Reagent (T-PER; Thermo Fisher, 78510) containing phosphatase inhibitor cocktail PhosSTOP (Roche, 04906845001) and protease inhibitor cocktail cOmplete (Roche, 11873580001). Whole maternal-fetal interface tissue, placentas, and deciduae were homogenized in 500 μ l and whole E12 or E14 brains in 250 μ l of this TPER cocktail. Slurries (50 μ l of placenta/decidua slurry or the entire embryonic brain slurry) were then added to 500 μ l TRIzol (Life Technologies, 15596018) and stored at -80°C until further use. For RNA extraction, TRIzol-supended samples were thawed on ice, vortexed, and 100 μ l of chloroform (Fisher Scientific, BP1145-1) was added. Samples were incubated at room temperature for 5 minutes and then spun down at 14,000 rpm at 4°C for 15 minutes. The clear aqueous top layer was collected and an equal volume of isopropanol (Sigma, I9516) was added then vortexed vigorously. Samples were then incubated at room temperature for 10 minutes and spun down at 12,000 rpm at 4°C for 5 minutes. The resulting RNA pellet was then washed with 1 ml of 70% ethanol in RNase-/DNase-free water and spun down at 14,000 rpm at 4°C for 5 min. This wash step was then repeated and finally the RNA pellet was air dried at room temperature and resuspended in 30 μ l of DNase-/RNase-free water. RNA quality and quantity were evaluated using NanoDrop 2000 Spectrophotometer (Thermo Scientific).

2.7.6. Magnetic-activated cell sorting

Fresh brains held in Buffer A (DMEM/F12 with 10% FBS, 0.1% GlutaMAX, and 0.1% antibiotic antimycotic) on ice were transferred to Buffer B (HBSS + Ca + Mg with 4 U/ml papain, and 50 U/ml DNase I) at room temperature. For embryonic timepoints (E12 and E14) brains were added to 1.5 ml Buffer B. For postnatal timepoints (P5 and P90) brains were added to 5 ml Buffer B. Samples were triturated using a 5 ml serologic pipette and incubated for 15 min at 37°C . Samples were then triturated using a 1 ml pipette and incubated again for 15 min at 37°C . This step was repeated twice (giving a total of 3 trituration steps and 45 minutes of incubation at 37°C) to yield a smooth single cell suspension. Samples were triturated once more with a 1 ml pipette and then filtered through a 70 μm cell strainer into a clean tube. 20 ml Buffer A was then added and cells were spun down at 300 g at 4°C for 10 min (fast acceleration, slow brake). Supernatants were aspirated and the remaining cell pellets were resuspended in 180 μ l 1x MACS buffer (Miltenyi Biotec, 130-0910376) in PBS. 90 μ l of CD11b magnetic microbeads (Miltenyi Biotec, 130-093-634) were added and samples were incubated for 15 min at 4°C . Samples were then washed with 1 ml MACS buffer and spun down at 300 g at 4°C for 10 min (fast acceleration, fast brake). Supernatants were aspirated and the remaining cell pellets were resuspended in 500 μ l MACS buffer. LS columns (Miltenyi Biotec, 130-042-401) and a QuadroMACS magnet (Miltenyi Biotec, 130-091-051) were used to isolate CD11b⁺ cells according to the manufacturer's instructions. Column-bound microglia (CD11b⁺ cells) were then spun down at 300 g at 4°C for 10 min. Cell pellets were either added to 200 μ l TRIzol reagent for RNA extraction or resuspended in 1x PBS for flow cytometry.

2.7.7. Flow cytometry

Flow cytometry was employed to validate MACS purification efficacy. CD11b-positive and -negative fractions in 1x PBS were transferred to a 96-well round bottom plate and spun down at 1500 rpm for 5 minutes at 4°C . Cells were then stained with fixable viability dye (eBioscience, 65-0866-14) at 1:1000 for 30 minutes at 4°C . Cells were washed with FACS buffer (1x PBS, 1 mM EDTA, and 1% BSA) and spun down at 1500 rpm at 4°C . Cells were then stained 1:200 with CD11b (APC), CD45 (PE-Cy7), and TCR β chain (Brilliant Violet 510) flow antibodies (all from eBioscience) in FACS buffer for 15 minutes at 4°C . Cells were washed once with FACS buffer, spun down at 1500 rpm at 4°C , then resuspended in 100 μ l of FACS buffer. Microglia were identified as CD45^{int} and CD11b^{hi} after gating for single cells. Data were acquired using a Gallios flow cytometer (10 colors, 3 lasers, B5-R1-V2 Configuration with Kaluza Acquisition; Beckman Coulter) and analyzed using FlowJo software (Becton, Dickinson, & Company).

2.7.8. RNA-sequencing procedure and data analysis

Isolated maternal-fetal interface RNA and sorted microglia resuspended in TRIzol were sent to GENEWIZ Next Generation Sequencing for sample preparation and bulk RNA-sequencing. The raw sequencing reads (FASTQ files) were aligned to the UCSC mm39 mouse genome build using the splice-aware read aligner HISAT2. Samtools was used for quality control filtering. Reads were sorted into feature counts with HTSeq. DESeq2 (v1.30.0) was used to normalize the raw counts based on read depth, perform principal component analysis, and conduct differential expression analysis. The p-values were corrected with the Benjamini-Hochberg procedure to limit false positives arising from multiple testing. Significantly downregulated and upregulated genes were assayed using GProfiler (<https://biit.cs.ut.ee/gprofiler/gost>) to generate KEGG, GO, and Reactome terms. Network maps were generated using Cytoscape (3.9.1). Analyses were performed and plots were generated in RStudio using the following packages: lattice, DESeq2, pheatmap, GSA, ggplot2, ggrepel, dplyr, tidyverse, ggprofiler2, pals, EnhancedVolcano, stringr, data.table, and VennDiagram.

2.7.9. cDNA synthesis and qPCR

Isolated RNA was converted to cDNA using a Sensifast cDNA Synthesis kit (Bioline, BIO-65054). Gene expression levels were determined using Taqman Gene Expression Assay primer/probe mix (Thermo Fisher), Sensifast Probe No-ROX kit (Bioline, BIO-86005), and a CFX384 Real-Time PCR System (BioRad, 1855484). All kits were used according to manufacturer's instructions. The following primers (Thermo Fisher Scientific) were used: *Ifit1* (Mm00515153_m1), *Mx1* (Mm00487796_m1), *Ccl3* (Mm00441259_g1), *Tlr3* (Mm01207404_m1), *Il1b* (Mm00434228_m1), *Il6* (Mm00446190_m1), *Il17a* (Mm00439619_m1), *Il6ra* (Mm01211445_m1), *Il17ra* (Mm00434214_m1), *Cx3cr1* (Mm02620111_s1), *Sykb* (Mm01333035_m1), *Chd1* (Mm00514308_m1), *Eif2s1* (Mm00782766_s1), *Rps2* (Mm01971861_g1), *Rack1* (Hs00272002_m1), *Slc6a4* (Mm00439391_m1), *Slc22a3* (Mm00488294_m1), *Ido1* (Mm00492590_m1), *Tph1* (Mm01202614_m1), *Maoa* (Mm00558004_m1), *Maob* (Mm00555412_m1), *Cdh1* (Mm01247357_m1), *Cd56* (Mm01149710_m1), *Uty* (Mm00447710_m1), *Xist* (Mm01232884_m1), and *Gapdh* (Mm99999915_g1). Relative expression levels were calculated based upon *Gapdh* expression.

2.7.10. Serotonin ELISA

Serotonin concentrations in maternal sera or MFI homogenates were determined using a serotonin ELISA kit (Enzo Life Sciences, ADI-900-175). Frozen MFI tissues were thawed on ice and then mechanically homogenized in 500 μ l TPER cocktail (Tissue Protein Extraction Reagent T-PER (Thermo Fisher, 78510) containing phosphatase inhibitor cocktail PhosSTOP (Roche, 04906845001) and protease inhibitor cocktail cOmplete (Roche, 11873580001)). Slurries were then spun down at 16,000 rpm for 10 minutes and the soluble supernatants were collected. Serotonin ELISA was conducted on undiluted maternal sera or 1:10 diluted MFI tissue extracts according to the manufacturer's instructions. The plate was read on an Epoch microplate spectrophotometer (Agilent) at 405 nm.

2.7.11. Multiplex cytokine assay

Cytokine concentrations in maternal sera and homogenates from MFI, placenta, and decidua were determined using a Bio-Plex multiplex cytokine assay. Frozen tissues (bulk MFI or dissected placenta/decidua tissues) were thawed on ice and then mechanically homogenized in Tissue Protein Extraction Reagent T-PER (Thermo Fisher, 78510) containing phosphatase inhibitor cocktail PhosSTOP (Roche, 04906845001) and protease inhibitor cocktail cOmplete (Roche, 11873580001). Whole MFIs and placentas were homogenized in 500 μ l and deciduae in 250 μ l of this TPER cocktail. Slurries were then spun down at 16,000 rpm for 10 minutes and the soluble supernatants were collected. A multiplex cytokine assay was conducted on undiluted samples. All reagents were used according to the manufacturer's instructions: Bio-Plex Pro Reagent Kit III (Bio-Rad, 171304090M), Bio-Plex Pro Coupled Magnetic Beads (from Mouse Cytokine 23-plex Assay, Bio-Rad, M60009RDPD), Group I Cytokine standards (Bio-Rad, 171150001). The plate was read on a Bio-Plex 200 System with HTS (Bio-Plex, 171000205).

2.7.12. Behavior

All behavior experiments were performed between 8 am and 5 pm in a blinded fashion. Mice were transported from their home vivarium room to the behavior core and allowed 30 minutes to habituate before beginning each test. All behavior experiments were conducted as previously described⁴²⁴.

Ultrasonic vocalization recording

Communication following maternal separation was conducted on P10 male and female mice. Pups were separated from their mother with their littermates and allowed to habituate in the testing room for 10 min. Mice were then placed one-by-one in a clean 1 L plastic cup with a microphone suspended overhead. Ultrasonic vocalizations (USVs) were recorded using UltraSoundGate GM16/CMPA microphone (Avisoft Bioacoustics) and analyzed with SASLab Pro software (Avisoft Bioacoustics). USVs were measured between 25 and 125 kHz and background recordings shorter than 0.02 ms were excluded.

Marble burying assay

Repetitive/stereotyped behaviors were assessed on adult male and female mice (8-10 weeks of age) using the marble burying assay. Mice were acclimated to wood chip bedding in their home cages overnight prior to testing. Experimental mice were placed into a clean cage (12 x 7 x 5 in) filled with 3 in tightly packed wood chip bedding with 20 glass marbles arrayed in rows of 4 and columns of 5 equally spaced throughout the cage. Mice were allowed to explore the cage for 15 min and then an index score of marbles buried was calculated. A score of 0-1 was given for each marble (0 = < 50% buried, 0.5 = ~ 50% buried, 1 = > 50% buried) to yield a maximum score of 20 for this assay.

Social preference test

Sociability was assessed on adult male and female mice (8-10 weeks of age) using the social preference test. Two chamber habituation sessions were conducted in which mice were allowed to explore the entire 3-chamber arena with empty wire cages added for 5-min each session. Mice were then housed in solo overnight before testing. The social preference test began with placing the mice in the center of the 3-chamber arena with the portals blocked off in which mice were allowed to explore only the center chamber for 5 min. Then, the barriers were removed and the mice had free access to the entire arena, with the top chamber containing an empty wire cage holding a novel mouse (age and sex-matched) and the bottom chamber containing another empty wire cage holding a novel object (aqua syringe suction balls). Mice were allowed to explore for 10 min and activity was tracked using EthoVision XT (Noldus).

2.7.13. Statistics

Sample sizes were chosen on the basis of standard power calculations (with $\alpha = 0.05$ and power of 0.8). Statistical tests for RNA-seq analyses were conducted using R (4.0.4 GUI 1.74 Catalina build (7936)) in RStudio (1.4.1106). For all other analyses, Prism software (GraphPad, 9.4.0) was used to calculate mean and s.e.m. values and to conduct unpaired Student's t test, one-way ANOVA, and two-way ANOVA. *P* values less than 0.05 were considered significant.

Declaration of competing interest

The authors declare no competing financial interests.

Data availability

All data are available from the authors upon request. Raw gene counts from bulk RNA-seq of maternal-fetal interface tissue and isolated microglia are publicly available on Mendeley [DOI: 10.17632/sj6384j77p.1] and GitHub [<https://github.com/LukensLab/MIA-RNAseq.git>]. All code used to process RNA-seq data is also publicly available on GitHub [<https://github.com/LukensLab/MIA-RNAseq.git>].

Acknowledgements

We thank members of the Lukens lab and the Center for Brain Immunology and Glia (BIG) at the University of Virginia for valuable discussions. This work was supported by The National Institutes of Health/National Institute of Neurological Disorders and Stroke (R01NS106383; awarded to J.R.L.), The National Institutes of Health/National Institute of Mental Health (R21MH120412-01; awarded to J.R.L.), The Simons Foundation Autism Research Initiative (Pilot Award 515305 to J.R.L.), and The Owens Family Foundation (Awarded to J.R.L.). K.E.Z. and H.E. were supported by a Cell and Molecular Biology Training Grant (1T32GM139787-01-35, awarded to K.E.Z.; T32GM008136, awarded to H.E.), Wagner Fellowships, and Double Hoo Awards. D.S. was supported by a Harrison Fellowship.

Chapter 3: Astrocyte inflammasome signaling mediates neuronal physiology and memory

3.1 Abstract

Precise control over synaptic connections underlies the capability of neurons to modify circuit processing throughout the lifetime of an organism. A given experience activates and induces dynamic modification in hippocampal physiology, imparting this brain region with the ability to encode experiences as memories. Consequently, impaired hippocampal synaptic plasticity is associated with deficits in memory function which has been linked to a myriad of neurologic disease states such as Alzheimer's disease and dementia. Mounting evidence demonstrates that molecular mediators originally characterized in the immune system are also expressed by nervous system cells and underlie important neurological processes. Interestingly, we find that the innate immune-based multiprotein inflammasome complex assembles in the healthy adult brain. Perturbations to an animal's environment, including environmental enrichment and a spatial learning task, dampened baseline levels of inflammasome activity in the hippocampus. Inhibition of inflammasome activation promoted synapse abundance and memory recall. Assembled hippocampal inflammasomes were found primarily in astrocytes. The loss of inflammasome activation specifically within astrocytes promoted hippocampal IL-33 production, perineuronal net turnover, and neuronal plasticity in the short-term. Prolonged loss of astrocyte inflammasome activity elicited opposing effects on these processes. These findings reveal an unexpected physiologic role for inflammasome activity in regulating memory function.

Kristine E. Zengeler^{1,2,3}, Ava Hollis¹, Hannah Ennerfelt^{1,2,3}, Joshua D. Samuels^{1,2}, Katelyn A. Moore¹, and John R. Lukens^{1,2,3}

¹Center for Brain Immunology and Glia (BIG), Department of Neuroscience, University of Virginia, Charlottesville, VA 22908, USA, ²Neuroscience Graduate Program, University of Virginia, Charlottesville, VA 22908, USA, ³Cell and Molecular Biology Graduate Training Program, University of Virginia, Charlottesville, VA 22908, USA.

Author contributions:

K.E.Z. and J.R.L. designed the study; K.E.Z., A.H., H.E., and J.D.S. performed experiments; K.A.M. oversaw animal husbandry and conducted genotyping; K.E.Z. analyzed data; K.E.Z. and J.R.L. wrote the manuscript; J.R.L. oversaw the project.

3.2 List of abbreviations

ASC, apoptosis-associated speck-like protein containing a caspase activation and recruitment domain; CA, Cornu Ammonis; CARD, caspase activation and recruitment domain; CNS, central nervous system; DG, dentate gyrus; ECM, extracellular matrix; EE, enriched environment; FOV, field of view; GSDMD, Gasdermin-D; i.p., intraperitoneal; MWM, Morris water maze; ROS, reactive oxygen species; rpm, rotations per minute; PNN, perineuronal net; PRR, pattern recognition receptor; WFA, Wisteria floribunda agglutinin.

3.3 Introduction

The burgeoning field of neuroimmunology has brought the study of immune signaling to the forefront of neurologic disease treatment investigation. Beyond pathogenic states, there is an expanding understanding that molecules and pathways involved in immune responses can also be exploited to support physiologic brain

development and function^{69,70,474,545}. For instance, pattern recognition receptors (PRRs), cytokines, the complement system, phagocytic machinery, and more have been tied to homeostatic central nervous system (CNS) processes such as neurogenesis, cell migration, and synaptic pruning^{69,70,474,545}.

The inflammasome is a multiprotein signaling complex assembled following detection of intracellular danger signals which contributes to the innate immune response⁵⁴⁶⁻⁵⁴⁸. Inflammasomes come in a variety of flavors but canonically consist of a PRR acting as a sensor, an effector caspase, and often the bridging adaptor molecule ASC (apoptosis-associated speck-like protein containing a caspase activation and recruitment domain (CARD))⁵⁴⁶⁻⁵⁴⁸. An array of inflammasome PRR sensors exist and can sense a broad spectrum of intracellular danger signals ranging from pathogen components such as flagellin, to nucleic acids, to reactive oxygen species (ROS), and beyond⁵⁴⁶⁻⁵⁴⁸. Sensor recognition of its obligate ligand initiates oligomerization and recruitment of the adaptor molecule ASC for sensors lacking a CARD, which binds together these components and provides a platform for complex assembly⁵⁴⁶⁻⁵⁴⁸. Nucleated ASC recruits an effector caspase (canonically, Caspase-1) which then undergoes autocatalytic cleavage⁵⁴⁶⁻⁵⁴⁸.

The assembled inflammasome provides a platform for cleaved Caspase-1 to proteolytically process a variety of downstream targets to propagate an immune response⁵⁴⁶⁻⁵⁴⁸. The most well-known inflammasome cleavage targets include cytokines, such as pro-IL-1 β and pro-IL-18, which require cleavage to elicit their pro-inflammatory signaling properties⁵⁴⁶⁻⁵⁴⁸. Inflammasomes can also cleave the protein Gasdermin-D (GSDMD), of which the N-terminal fragment can self-oligomerize within the plasma membrane, creating pores which can ultimately lead to cell lysis³⁵⁶. Inflammasome-initiated active cytokine release and cell lysis constitutes a pro-inflammatory type of cell death known as pyroptosis^{549,550}. Notably, cytokine release and cell death can be limited by ESCRT-III-mediated membrane repair³⁵⁸.

While originally characterized in the peripheral immune system in the context of infections, the inflammasome has more recently been recognized to contribute to immune activation in sterile contexts within the CNS^{359,551-553}. Neuroinflammation is increasingly recognized as a factor of CNS pathology, including neurodegenerative diseases, stroke, depression, and more, which has either beneficial or detrimental effects depending on the context^{25,259,554-557}. The resident immune cells of the CNS, microglia, have historically been interrogated as inflammasome activators in these contexts; however, reports of inflammasome activation in other CNS cells are beginning to emerge^{359,551-553}. CNS inflammasome activation is typically associated with pro-inflammatory cytokine release and cell death that propagate neurologic disease^{359,551-553}. As such, pathogenic inflammasome signaling has been linked to age-related cognitive decline, Alzheimer's disease, Parkinson's disease, amyotrophic lateral sclerosis, multiple sclerosis, stroke, traumatic brain injury, epilepsy, and more⁵⁵³.

The inflammasome has rarely been studied outside of disease states in the CNS. Our lab recently found that the AIM2 inflammasome eliminates cells harboring DNA damage during development and that inflammasome-dependent cell removal is necessary for proper brain development⁵⁵⁸. Beyond orchestrating cell death, AIM2 can also modulate neuronal morphology³⁸¹. The NLRP3 inflammasome plays a role in sleep, as mice lacking NLRP3 exhibit increased wakefulness at baseline and maladaptively responded to sleep deprivation and bacterial-induced sleep modulation⁵⁵⁹. IL-1 β , which requires inflammasome-mediated cleavage for active signaling, is found in low levels in the healthy brain and has been linked to control of long-term potentiation, neurogenesis, and synaptic pruning⁵⁶⁰.

In this study, we found that the inflammasome is activated in the healthy adult brain and contributes to homeostatic CNS cell function. In the hippocampus, astrocytes harbored the highest concentration of assembled ASC nucleation, and relative inflammasome activation was modulated by physiologic environmental alterations. Short-term pharmacologic inhibition or genetic ablation of inflammasome function in astrocytes altered synapse abundance and contributed to memory function. Conversely, long-term ablation of astrocyte Caspase-1 activity was detrimental to synapse health and hippocampal-dependent memory. Caspase-1 function specifically in astrocytes regulated astrocyte reactivity, hippocampal IL-33 levels, perineuronal net abundance, and relative neuronal plasticity. These findings reveal an important role for physiologic inflammasome activity in maintaining healthy memory function.

3.4 Results

3.4.1. The inflammasome is physiologically activated in the healthy adult brain

The inflammasome is typically assembled in response to danger signals within a cell. The ASC^{Citrine} reporter mouse provides for *in situ* localization of active inflammasome assembly, as diffuse ASC becomes aggregated into bright ASC specks upon oligomerization into multimeric complexes⁵⁶¹. We noticed a striking presence of ASC specks throughout the brain in healthy adult mice (Figure 3.1A). ASC specks were highly concentrated within the hippocampus and cerebellum, with lower levels distributed throughout the brain including the olfactory bulb, cortex, substantia nigra, and nucleus accumbens (Figure 3.1B-C).

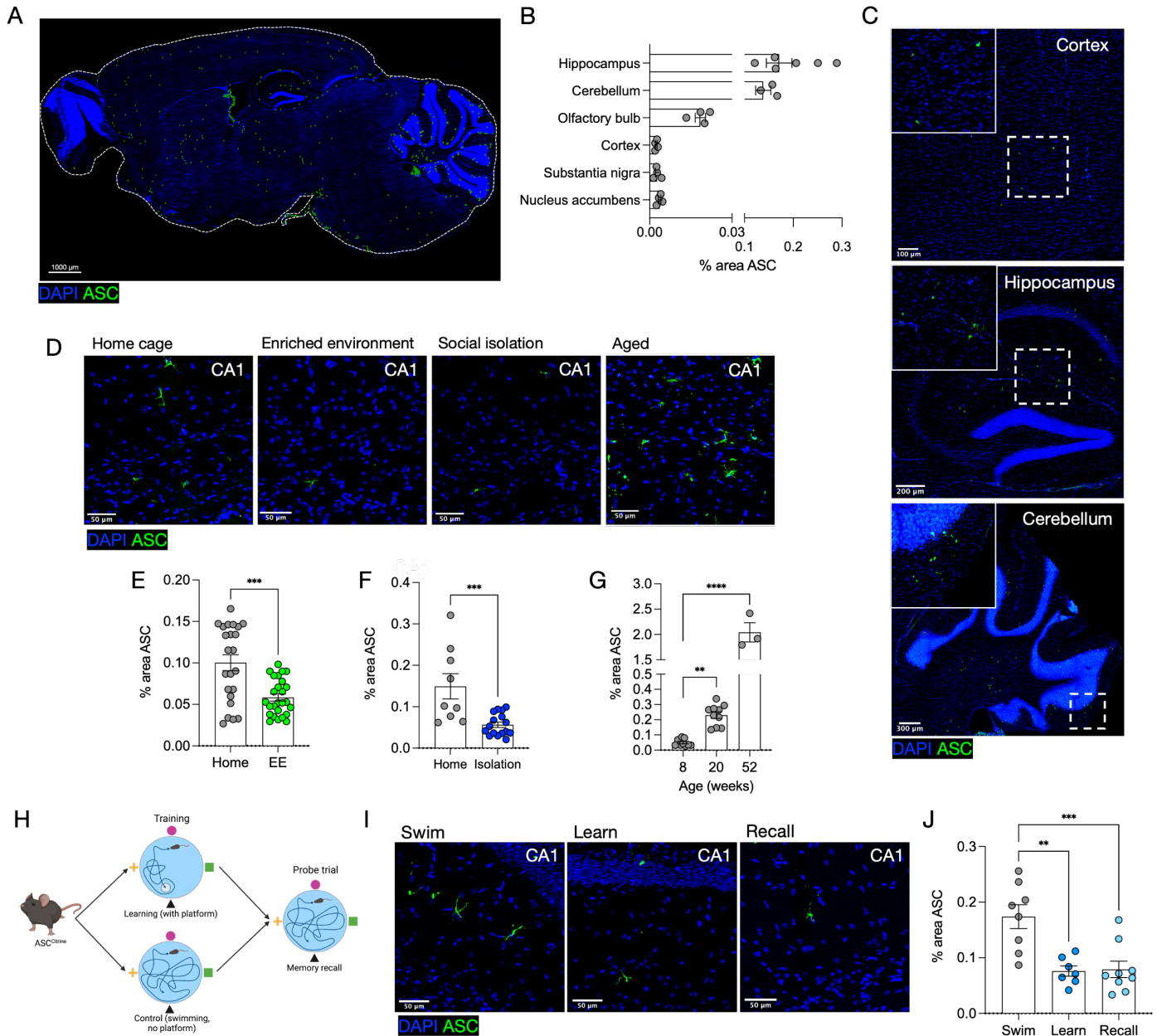


Figure 3.1. Inflammasome activation is dynamically regulated by experience.

(A) Representative sagittal brain section from an adult ASC^{Citrine} mouse demonstrating widespread inflammasome activation at baseline. (B) Quantification of ASC distribution by brain region, where % area is the total area ASC+ divided by the total area of the given region. (C) Representative images of inflammasome activation in the cortex (top), hippocampus (middle), and cerebellum (bottom) from an adult ASC^{Citrine} mouse. Insets show magnification. (D-G) Physiologic regulation of hippocampal inflammasome activation was assessed in adult ASC^{Citrine} mice that were either exposed to an enriched environment (EE) or social isolation at 8-12 weeks-old, or that were left to age. 8-12 week-old ASC^{Citrine} mice left in their home cages were used as controls. (D) Representative images of ASC specks in the CA1 hippocampal region following these treatments. (E) Quantification of % area ASC over the entire hippocampus following immediately following 48 hr EE exposure relative to home cage controls. (F) Quantification of % area ASC over the entire

hippocampus following immediately following 48 hr social isolation relative to home cage controls. (G) Quantification of % area ASC over the entire hippocampus over adult age. (H-J) Adult (8-12 week-old) ASC^{Citrine} mice were trained on the Morris water maze spatial learning and memory task, and brains were harvested immediately following 2 days of training (“Learn” group) or after the probe trial (“Recall” group). Mice that underwent the same treatment but without a hidden platform to guide learning were used as controls and harvested following the probe trial (“Swim” group). (H) Experimental design. (I) Representative images of ASC in the CA1 hippocampal region following these treatments. (J) Quantification of % area ASC over the entire hippocampus following these treatments. Each point represents an individual mouse. Statistical significance calculated by unpaired Student’s t-test (E-G) or one-way ANOVA (J). Error bars indicate mean +/- s.e.m. ***P* < 0.01, ****P* < 0.001, *****P* < 0.0001.

In peripheral immune cells, it is typical for a single inflammasome complex to form in a cell in a clear punctate ASC speck⁵⁶¹. While single ASC puncta were observed in the healthy brain (Figure 3.1C), we also noticed an array of unique inflammasome morphological states in ASC^{Citrine} brains (Figure 3.2). ASC specks could be found in groups of multiple specks, in larger “splotchy” assemblies, and also in “spindle”-like formations in the Cornu Ammonis 1 (CA1; Figure 3.2A) and dentate gyrus (DG; Figure 3.2B) hippocampal subregions. Live imaging in the cortex revealed that these assemblies remained morphologically stable up for up to one hour (Supplemental Videos; data not shown in document).

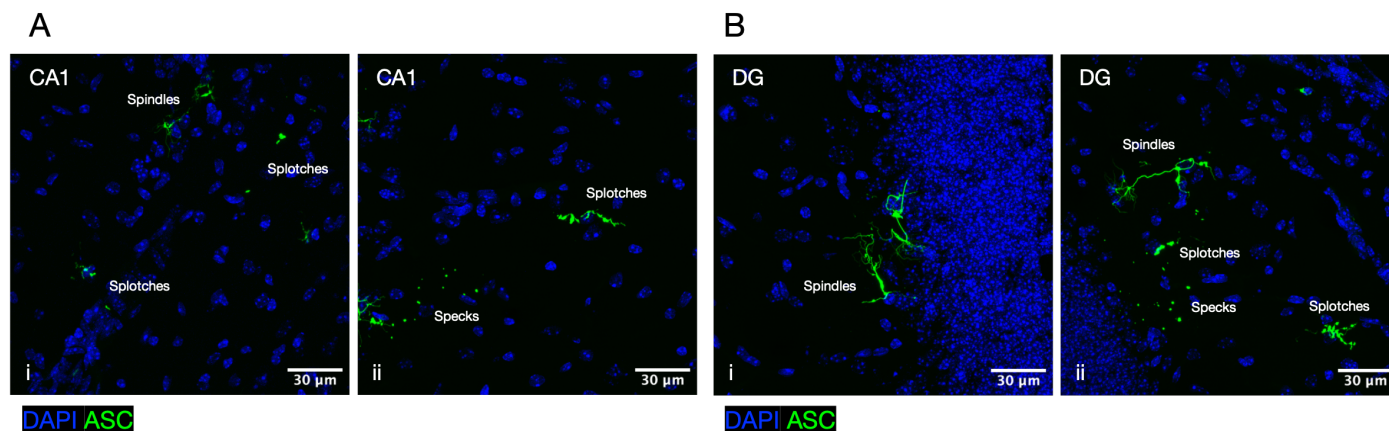


Figure 3.2. The different morphological states of brain ASC specks.

Physiologic presence of ASC specks was assessed in adult ASC^{Citrine} mice. ASC specks were found in three distinct morphological states, including clouds of prototypical specks, larger splotch-like formations, and more complex spindle-like structures. Representative images taken in hippocampal subregions CA1 (A) and dentate gyrus (DG; B) are shown. Two example fields of view (FOV; i, ii) are shown for each region.

Given the high density of ASC specks observed in the hippocampus at homeostasis (Figure 3.1A-C), we wondered whether altered engagement of this brain region would alter inflammasome assembly. Environmental enrichment (EE) is well characterized to activate hippocampal neurons, promote synaptic plasticity, and improve learning and memory^{562–567}. We found that EE significantly dampened hippocampal ASC speck levels (Figure 3.1D,E). Inflammasome activation was coordinately lowered across hippocampal subregions; in particular, the DG, CA1, CA2, and CA3 (Figure 3.3A). This was accompanied by a reduction in markers of gliosis including IBA1 (Figure 3.3B,C), GFAP (Figure 3.3D,E), and S100β (Figure 3.3F,G) in the hippocampus. Moreover, gene expression of the inflammasome sensor *Nlrp3* and the inflammasome-associated cytokine *Il1b* were moderately but significantly reduced following EE (Figure 3.3H).

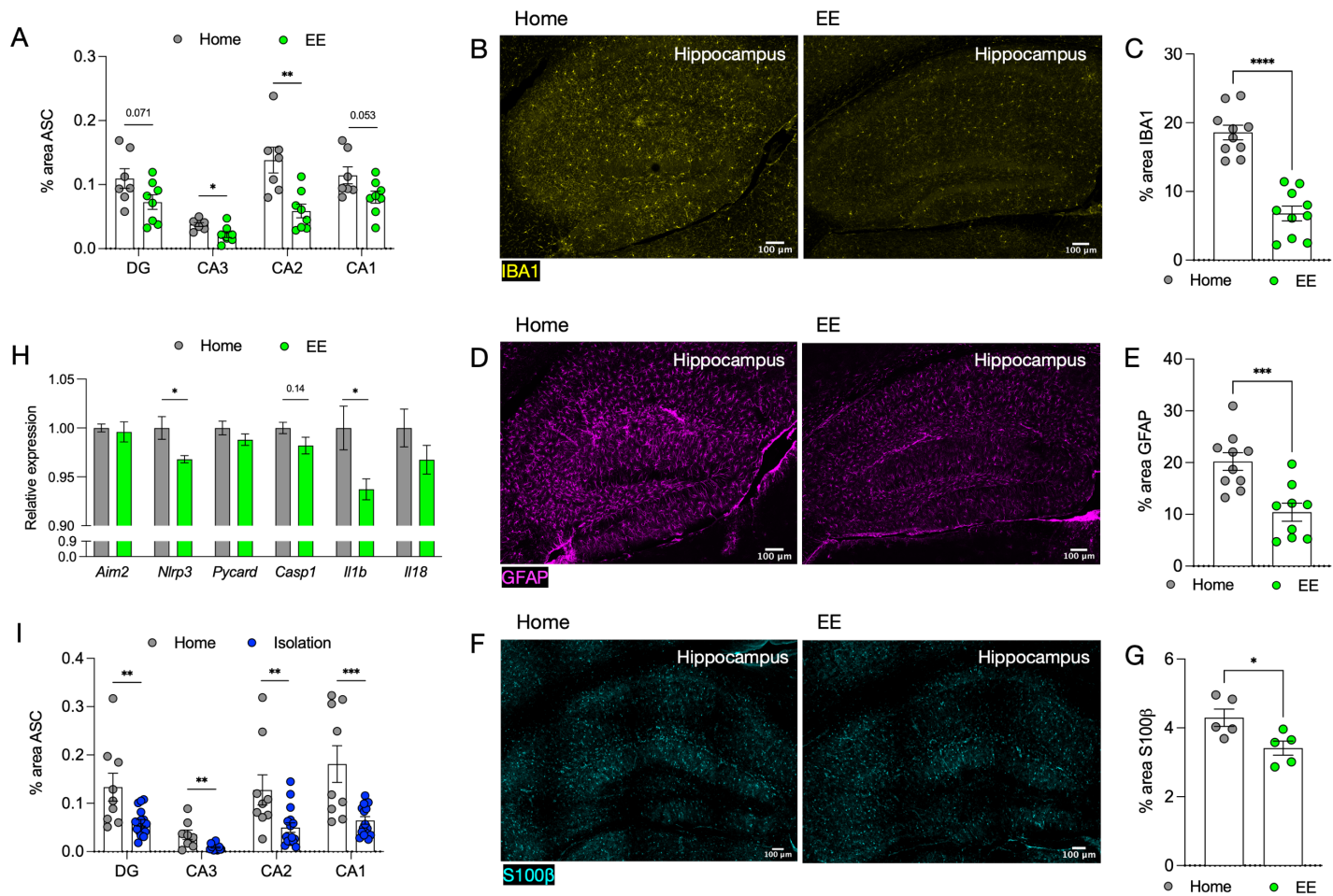


Figure 3.3. Environmental changes dampen inflammasome activation across hippocampal subregions, dampen expression of inflammasome components, and diminish hippocampal gliosis.

Physiologic regulation of hippocampal inflammasome activation was assessed in adult (8-12 week-old) ASC^{Citrine} mice that were either exposed to an enriched environment (EE; A-H) or social isolation (I) for 48 hrs. ASC^{Citrine} mice left in their home cages were used as controls. (A) Quantification of % area ASC in different hippocampal subregions immediately following EE exposure relative to home cage controls. (B-C) Representative images (B) and quantification (C) of hippocampal IBA1 levels following EE. (D-E) Representative images (D) and quantification (E) of hippocampal GFAP levels following EE. (F-G) Representative images (F) and quantification (G) of hippocampal S100β levels following EE. (H) Relative expression levels of various inflammasome components assessed by qPCR conducted on half-brain homogenates from EE-exposed or home cage control mice. (I) Quantification of % area ASC in different hippocampal subregions immediately following social isolation relative to home cage controls. Each point represents an individual mouse. Statistical significance calculated by multiple unpaired t-tests (A,H,I) or unpaired Student's t-test (C,E,G). Error bars indicate mean +/- s.e.m. **P* < 0.05, ***P* < 0.01, ****P* < 0.001, *****P* < 0.0001.

Conversely to EE, social isolation is known to negatively impact hippocampal physiology and memory^{568,569}. Interestingly, singly housed mice also displayed dampened the levels of ASC specks within the hippocampus (Figure 3.1D,F). Similar to exposure to the enriched environment, single housing also dampened inflammasome activation across the hippocampal regions DG, CA1, CA2, and CA3 (Figure 3.3I). These findings paired with the EE results suggest that any acute perturbation to the animal's environment, independent of the valence and downstream impact on memory function, may lower inflammasome activation.

Hippocampal aging is also known to diminish synapse numbers, synaptic plasticity, and learning and memory function^{570,571}. As opposed to acute social isolation, we found that hippocampal levels of ASC specks increased with age (Figure 3.1D,G, 3.4A,B). This increase in inflammasome activation was also noted in the cerebellum (Figure 3.4C,D). This finding is particularly notable given that pathogenic inflammasome activation is increasingly found to be a driver of neurodegenerative diseases, for many of which age is a primary risk factor⁵⁷². Indeed, the aged brain harbored marked hippocampal gliosis (Figure 3.4E-J) that accompanied greater inflammasome activation within astrocytes as well as microglia (Figure 3.4G,K). Intracellular ASC speck volume significantly positively correlated with IBA1 reactivity (Figure 3.4G,L) but not GFAP reactivity (Figure 3.4G,M) in the hippocampus across young and old mice. Thus, while microglia and astrocyte reactivity both track with

heightened inflammasome activation in the aged brain, microglia reactivity may be a better predictor of the corresponding level of inflammasome activation.

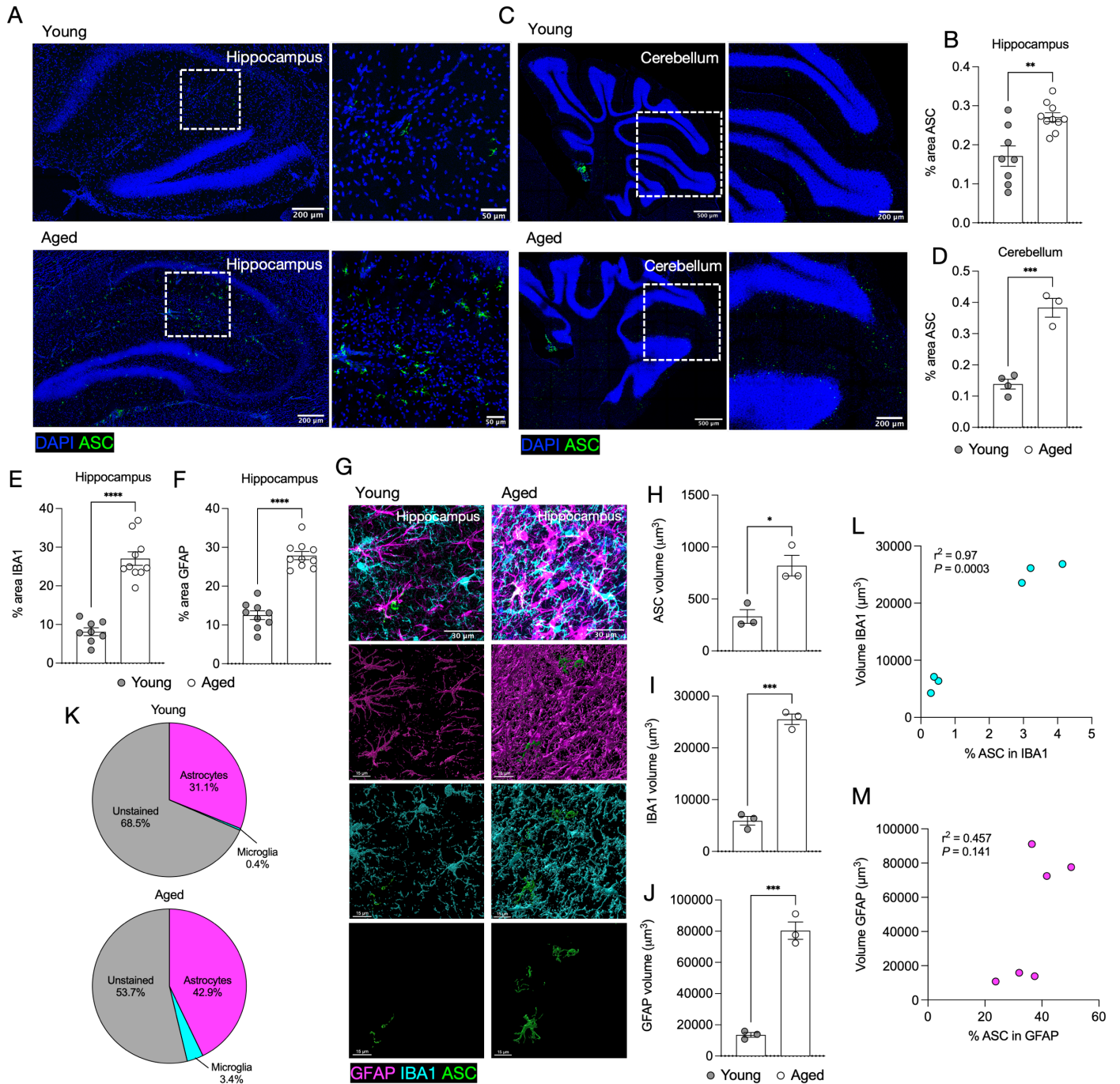


Figure 3.4. Increased ASC speck formation activation and gliosis in the aged ASC^{Citrine} brain.

Inflammasome activation and associated gliosis were assessed in young (10-12 week-old) and aged (20 week-old) ASC^{Citrine} mice. (A-D) Relative ASC levels were assessed in the hippocampus (A,B) and cerebellum (C,D). Representative images (A) and quantification of % area ASC (B) in the hippocampus in young and aged ASC^{Citrine} mice. Representative images (C) and quantification of % area ASC (D) in the cerebellum in young and aged ASC^{Citrine} mice. (E-M) Microglia and astrocyte activation was assessed in the hippocampus of young and aged mice by IBA1 and GFAP reactivity, respectively. (E) Quantification and (G, top row) representative images of relative IBA1 levels in the hippocampus of young and aged mice. (F) Quantification and (G, top row) representative images of relative GFAP levels in the hippocampus of young and aged mice. (G-M) 3D renderings of hippocampal ASC specks, microglia (IBA1+ cells), and astrocytes (GFAP+ cells) were generated from young and aged ASC^{Citrine} mice. (G) Representative 2D projections (top row) and 3D rendered surfaces (bottom three rows) of ASC specks, IBA1, and GFAP. (H-J) Total volume per FOV of ASC (H), IBA1 (I), and GFAP (J). (K-M) ASC volume within GFAP volume or IBA1 volume was calculated, then divided by the total volume of ASC per FOV. The percent volume of ASC within astrocytes (GFAP volume) or microglia (IBA1 volume) was then calculated. The remaining volume of ASC not within GFAP or IBA1 volume was counted as “unstained” volume. (K) Distribution of ASC volume within astrocytes and microglia in young compared to aged mice. (L,M) Correlations between the percent of ASC within and the total volume of IBA1 (L) or GFAP (M). Each point represents an individual mouse. Statistical significance calculated by

unpaired Student's t-test (B,D,E,F,H-J) or Pearson correlation test (L,M). Error bars indicate mean +/- s.e.m. * $P < 0.05$, ** $P < 0.01$, *** $P < 0.001$, **** $P < 0.0001$.

We next sought to assess the involvement of inflammasome assembly in the hippocampus as it relates to the processes of learning and memory in a more direct fashion. To this end, we utilized the Morris water maze (MWM) in which mice learn to locate an escape platform submerged beneath opaque water using spatial cues. We trained ASC^{Citrine} mice on this hippocampus-dependent spatial learning task for 4 days and then assessed their memory of the hidden platform location using a probe trial on day 5 in which the platform is removed (Figure 3.1H). Control mice were left to swim in the pool with spatial cues but without any hidden platform to guide learning for 4 days (Figure 3.1H). Mice were harvested after 2 days of training ("learn" group) or after the probe trial on day 5 ("recall" group for those trained with the hidden platform, "swim" group for controls) and hippocampal ASC speck levels were assessed.

We found that learning a spatial task or recalling the learned escape location both significantly reduced ASC speck levels relative to swim-only controls (Figure 3.1I-J). Importantly, this effect was unique to the hippocampus, the key region engaged in this spatial task, as cerebellum levels of ASC specks were unchanged after spatial memory recall (Figure 3.5). These results reveal that active engagement of the hippocampus in a learning or memory recall task is sufficient to dampen ASC speck formation.

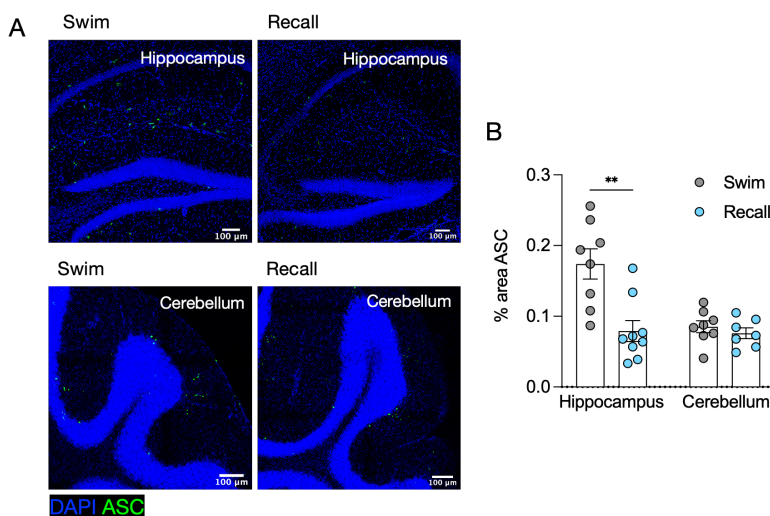


Figure 3.5. Spatial memory recall dampens inflammasome activation in the hippocampus but not the cerebellum.

Adult (8-12 week-old) ASC^{Citrine} mice were trained on the Morris water maze spatial learning and memory task, and brains were harvested immediately following the probe trial ("Recall" group). Mice that underwent the same treatment but without a hidden platform to guide learning were used as controls and harvested following the probe trial ("Swim" group). (A-B) Relative ASC speck levels were assessed in the hippocampus and cerebellum after memory recall. Representative images (A) and quantification (B) of percent area ASC over the entire hippocampus and cerebellum. Each point represents an individual mouse. Statistical significance calculated by multiple unpaired t-tests (B). Error bars indicate mean +/- s.e.m. ** $P < 0.01$.

3.4.2. Blocking inflammasome function improves synaptic plasticity

We next sought to functionally assess whether inflammasome activation influences memory and associated underlying neural plasticity. Given that Caspase-1 is a central effector component of the majority of inflammasomes, we inhibited Caspase-1 to block downstream target cleavage. The Thy1^{YFP} reporter mouse allows for the assessment of neuronal morphology by virtue of the sparse labeling of neurons throughout the brain. We treated adult Thy1^{YFP} mice with VX-765, a Caspase-1 inhibitor that is known to penetrate the blood-brain barrier^{573,574}, to assess memory and neuron morphology following the blockade of inflammasome activation (Figure 3.6A). Our treatment regimen led to a modest but significant weight gain in mice (Figure 3.7A), but did not affect baseline locomotion or exploratory behavior in the open field test (Figure 3.7B,C) or anxiety-like behavior in the elevated plus maze (Figure 3.7D).

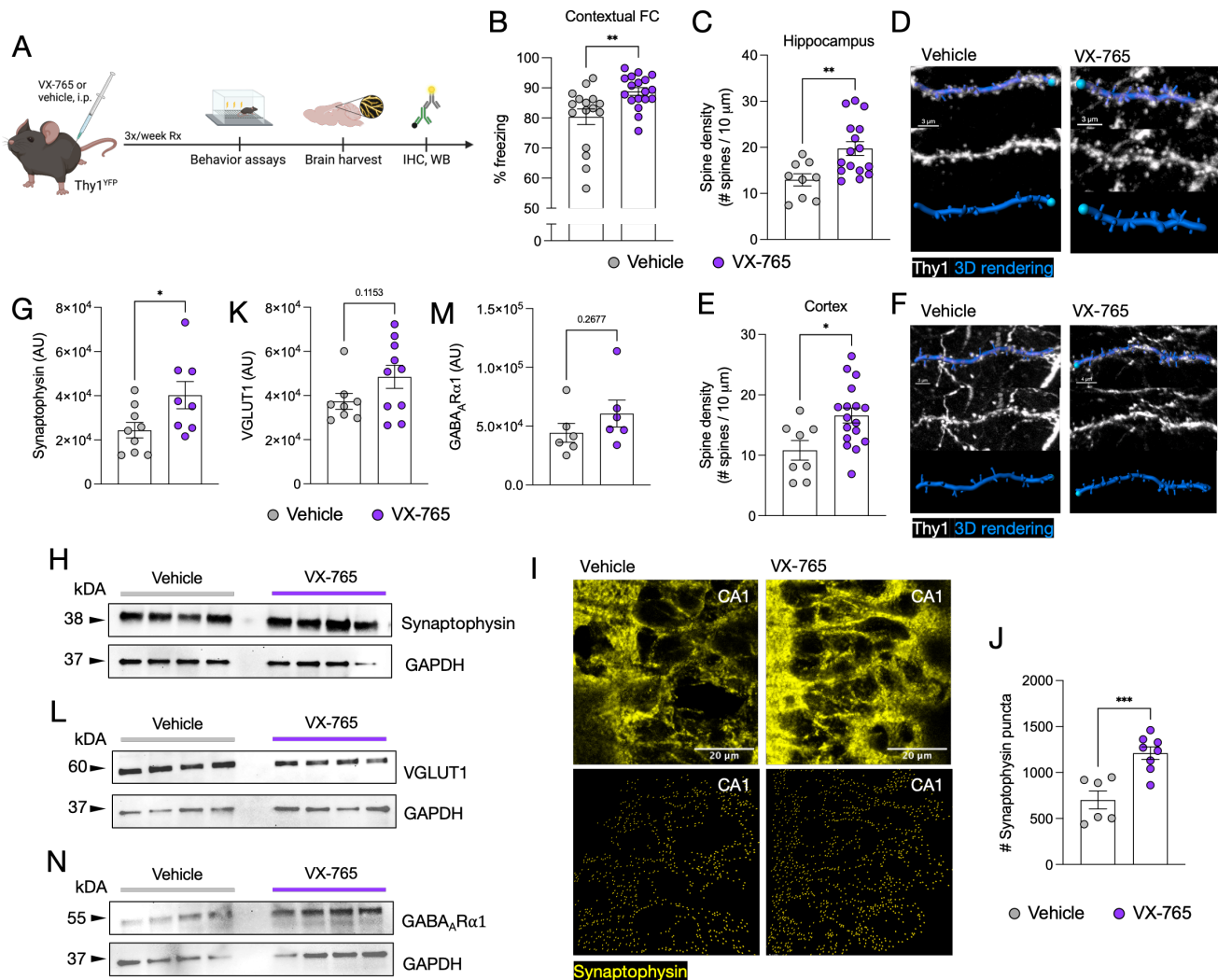


Figure 3.6. Caspase-1 inhibition improves long-term memory and hippocampal synapse formation.

Adult Thy1^{YFP} mice were treated with the Caspase-1 inhibitor VX-765 (30 mg/kg) or vehicle control by i.p. injection. Mice were injected 3x/week beginning at least two weeks prior to behavioral analysis and continuously throughout behavioral assessment until harvesting. (A) Experimental design. (B) Hippocampal-dependent memory was assessed using a contextual fear conditioning (FC) recall test conducted 3 weeks after tone-shock training. (C-F) Neuronal spine density was assessed by 3D rendering of Thy1+ processes. Neuronal processes in the hippocampus (C,D) and cortex (E,F) of vehicle- or VX-765-treated mice were reconstructed in Imaris and average spine density (number of spines per 10 μm) was quantified. At least 5 process segments per FOV were analyzed, and all segments in 3 FOVs per mouse per brain region were averaged. Quantification (C,E) and representative images and 3D renderings (D,F) are shown. (G,H) Synaptophysin protein levels were assessed by Western blot conducted on hippocampal lysates from vehicle- or VX-765-treated mice. Quantification (G) and representative blot (H) are shown. (I,J) Synaptophysin protein levels were assessed in the CA1 hippocampal subregion of vehicle- or VX-765-treated mice by immunohistochemistry. Stained brain sections were imaged and Synaptophysin+ puncta were quantified using Imaris reconstructions. Representative images (I, top), Imaris puncta reconstructions (I, bottom), and quantification (J) are shown. (K,L) VGLUT1 protein levels were assessed by Western blot conducted on hippocampal lysates from vehicle- or VX-765-treated mice. Quantification (K) and representative blot (L) are shown. (M,N) GABA_ARα1 protein levels were assessed by Western blot conducted on hippocampal lysates from vehicle- or VX-765-treated mice. Quantification (M) and representative blot (N) are shown. Each point represents an individual mouse. Statistical significance calculated by unpaired Student's t-test (B,C,E,G,J,K,M). Error bars indicate mean +/- s.e.m. **P* < 0.05, ***P* < 0.01, ****P* < 0.001.

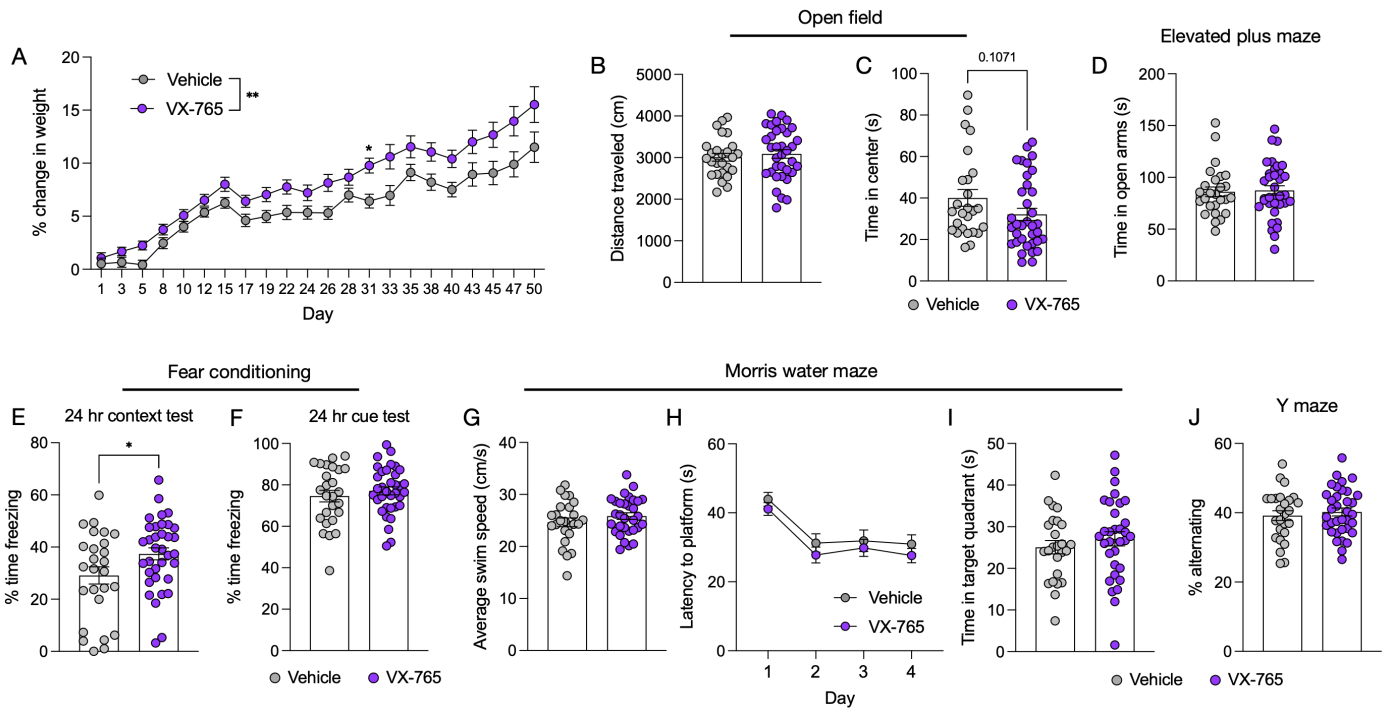


Figure 3.7. Caspase-1 inhibition contributes to moderate weight gain, but does not impact general locomotion, exploratory behavior, anxiety-like behavior, or spatial learning in mice.

Adult $Thy1^{YFP}$ mice were treated with the Caspase-1 inhibitor VX-765 (30 mg/kg) or vehicle control by i.p. injection. Mice were injected 3x/week beginning at least two weeks prior to behavioral analysis and continuously throughout behavioral assessment until harvesting. (A) Mouse weight (g) from beginning treatment until harvest was measured before i.p. injection. (B,C) General locomotion and exploratory behavior was assessed using the open field test. (B) Distance traveled over the entire test period. (C) Time spent in center of the arena. (D) Anxiety-like behavior was assessed using the elevated plus maze. Total time spent in the open arms of the arena were quantified. (E,F) Short-term memory was assessed by fear conditioning. 24 hr after training, hippocampal-dependent memory was assessed using a context test (E) and hippocampal-independent memory was assessed using a cue test (F). (G-I) Spatial learning and memory was assessed using the Morris water maze. (G) Swim speed averaged over the four training trials on day 1. (H) Latency to locate the hidden platform over four days of training. Latency was averaged over the four trials conducted on each day. (I) Time spent in the target quadrant during the probe test conducted on day 5 in which the hidden platform was removed. (J) Spatial working memory was assessed using the Y maze. Total number of alternations was divided by the total number of arm entries to calculate the measure of percent alternating. Each point represents the average of all mice in the treatment group (A,H) or an individual mouse (B-G,I,J). Statistical significance calculated by two-way ANOVA with Sidak's multiple comparisons test (A,H) or unpaired Student's t-test (B-G,I,J). Error bars indicate mean \pm s.e.m. * $P < 0.05$, ** $P < 0.01$.

Given the central importance of the hippocampus in memory formation and the dynamic modulation of inflammasome activation that we observed in this region, we next assessed learning and memory behavior in mice treated with the Caspase-1 inhibitor. Mice treated with VX-765 displayed significantly higher levels of freezing in a contextual fear conditioning test (Figure 3.6B, Figure 3.7E), a hippocampus-dependent test. Meanwhile, freezing was unchanged in a cued fear conditioning task (Figure 3.7F), a hippocampus-independent test. We did not find any differences in performance in the Morris water maze (Figure 3.7G-I), a spatial learning and memory task, and the Y maze (Figure 3.7J), a spatial working memory task. These results reveal that inhibition of inflammasome activation in healthy adult mice does not vastly impact motor function and anxiety-like behaviors but can improve certain types of spatial memory.

Synaptic plasticity is an obligatory process allowing for the formation of new neuronal connections during memory formation⁵⁷⁵⁻⁵⁷⁷. Our finding that Caspase-1 inhibition can improve memory led us to question whether synaptic plasticity may be affected by the inflammasome. Our treatment with $Thy1^{YFP}$ mice allowed for visualization of neuronal spines which we assessed to measure memory-related plasticity. We found that mice treated with the Caspase-1 inhibitor VX-765 had a significantly higher density of spines in both the hippocampus (Figure 3.6C,D) and cortex (Figure 3.6E,F). The morphology of spines can lend information as to the plasticity of these structures^{578,579}. We found sex-dependent alterations in different subsets of neuronal spines, including filopodia, long thin, mushroom, and stubby spines (Figure 3.8), yet these changes were quite subtle.

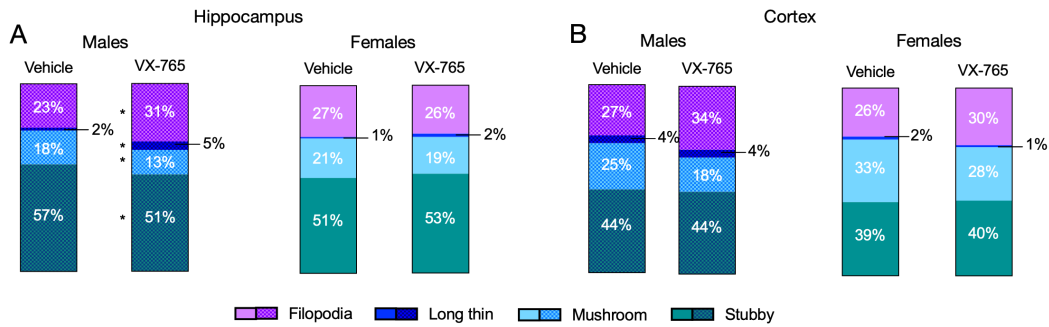


Figure 3.8. Caspase-1 inhibition shifts spine morphology.

Adult Thy1^{YFP} mice were treated with the Caspase-1 inhibitor VX-765 (30 mg/kg) or vehicle control by i.p. injection. Mice were injected 3x/week beginning at least two weeks prior to behavioral analysis and continuously throughout behavioral assessment until harvesting. Neuronal spine types were assessed by 3D rendering of Thy1+ processes. Neuronal processes in the hippocampus (A) and cortex (B) of vehicle- or VX-765-treated mice were reconstructed in Imaris. Imaris quantifications of the total spine length (“Length”, μm), maximum spine head diameter (“MaxHead”, μm), and mean spine neck diameter (“MeanNeck”, μm) were noted for each spine reconstructed along a dendrite. These measurements were then used to classify each spine into one of the following categories: stubby (Length < 1), mushroom (Length < 3 and MaxHead > MeanNeck), long thin (MaxHead >= MeanNeck), or filopodia (any yet-uncategorized spine). At least 5 segments per FOV were analyzed, and all segments in 3 FOVs per mouse per brain region were averaged. The average distribution of each spine type is plotted a bar graph, split by sex and treatment group. Statistical significance calculated by unpaired Student’s t-test (A,B) comparing groups within each sex and within each spine category. *P < 0.05.

Given the striking increase in post-synaptic spines, we wondered whether presynaptic terminals were coordinately increased under Caspase-1 inhibition. We found significantly higher levels of the presynaptic marker Synaptophysin in hippocampal extracts from VX-765-treated mice (Figure 3.6G,H). We confirmed this result through immunohistochemistry in which we observed significantly more Synaptophysin puncta in the CA1 of mice treated with the Caspase-1 inhibitor VX-765 (Figure 3.6I,J). These collective results reveal that both presynaptic and postsynaptic terminals are increased following the blockade of inflammasome activation, consistent with the improved memory function of these mice (Figure 3.6B).

Next, we sought to further characterize the characteristics of synapses impacted by blocking inflammasome function. We found a trend toward heightened hippocampal levels of VGLUT1 (Figure 3.6K,L), a marker of excitatory glutamatergic presynaptic terminals. There was no significant change in the levels of hippocampal GABA_ARα1 (Figure 3.6M,N), a receptor enriched on post-synaptic inhibitory terminals, though we did note a trend toward higher levels. Given our findings that post- and presynaptic structures increase in VX-765-treated mice, it is possible that this collective heightening is driven by slight increases in both excitatory and inhibitory subsets.

3.4.3. Inflammasome activity in astrocytes regulates synaptic plasticity and memory function

Inflammasome activation has primarily been witnessed in peripheral immune cells as a part of the innate immune response to a wide variety of pathogens^{355,546}. Similarly, states of sterile CNS pathology have also been linked to inflammasome activation in the brain resident immune cells, microglia^{359,551}. We next sought to determine the cellular location of inflammasomes in the adult CNS at homeostasis. As the hippocampus and cerebellum were the regions containing the highest density of ASC specks (Figure 3.1A-C), we stained for cell-type specific markers in these regions. Assembled inflammasomes were found primarily in astrocytes (GFAP+ cells) in the hippocampus rather than microglia (IBA1+ cells; Figure 3.9A,B, 3.10A).

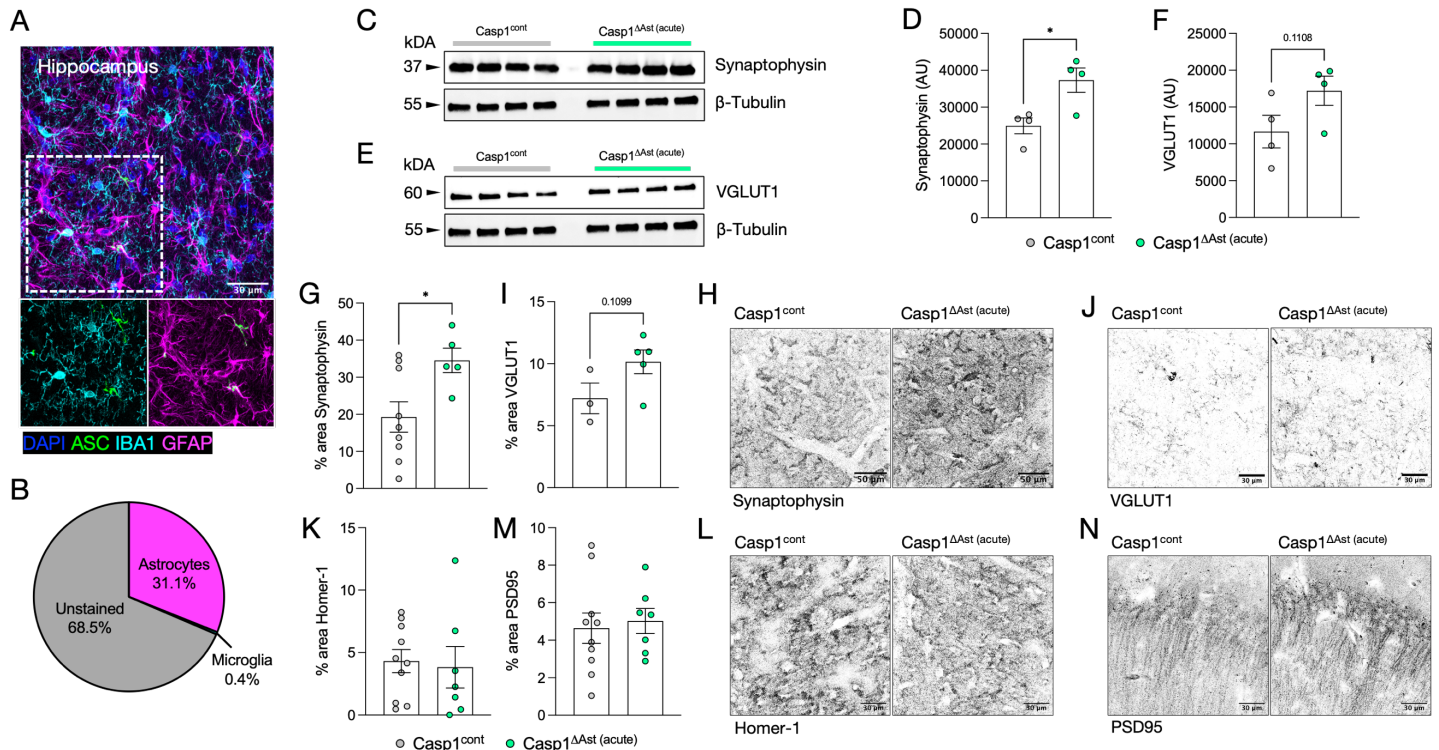


Figure 3.9. Astrocyte inflammasome activity regulates neuronal synapses.

The impact of astrocyte inflammasome activity on hippocampal synapses was assessed. (A-B) Inflammasome cell type localization was assessed in the hippocampus of adult (10-12 week-old) ASC^{Citrine} mice. 3D renderings of ASC, IBA1, and GFAP surfaces were generated in Imaris. Masks were created to assess the ASC signal within each cell surface, and the ASC volume within total IBA1 and GFAP surfaces in the FOV were recorded. (A) Representative images showing the colocalization of ASC in IBA1+ microglia relative to GFAP+ astrocytes. (B) Pie chart depicting the relative presence of ASC specks within astrocytes (GFAP+ surface) compared to microglia (IBA1+ surface). Percentages were calculated based upon total ASC volume within the FOV. Unstained area refers to ASC volume not directly within either the IBA1 or GFAP surface for any given FOV. 3-5 FOVs were analyzed per mouse, and 3 mice total were analyzed in the aggregated data. (C-N) *Casp1^{fl/fl};Aldh111^{Cre-ERT2}* (*Casp1^{ΔAst (acute)}*) mice and Cre-negative *Casp1^{fl/fl}* littermate controls (*Casp1^{cont}*) received tamoxifen food beginning at 3 weeks-old and continuing until two weeks prior to beginning behavior assessment (8-10 weeks-old). Brains were harvested from these animals after behavioral assessment at 4-6 months of age. Hippocampal synapse markers were assessed by Western blot (C-F) and immunohistochemistry (IHC; G-N). (C-F) Western blots were conducted on hippocampal lysates from *Casp1^{cont}* and *Casp1^{ΔAst (acute)}* mice to assess Synaptophysin (C,D) and VGLUT1 (E,F) protein levels. Representative blots (C,E) and quantification (D,F) are shown. (G-N) IHC was conducted in the CA1 of *Casp1^{cont}* and *Casp1^{ΔAst (acute)}* mice to assess Synaptophysin (G,H), VGLUT1 (I,J), Homer-1 (K,L), and PSD95 (M,N) protein levels. Quantification of average percent area coverage per FOV (G,I,K,M) and representative images (H,J,L,N) are shown. Each point represents an individual mouse. Statistical significance calculated by unpaired Student's t-test (D,F,G,I,K,M). Error bars indicate mean \pm s.e.m. * $P < 0.05$.

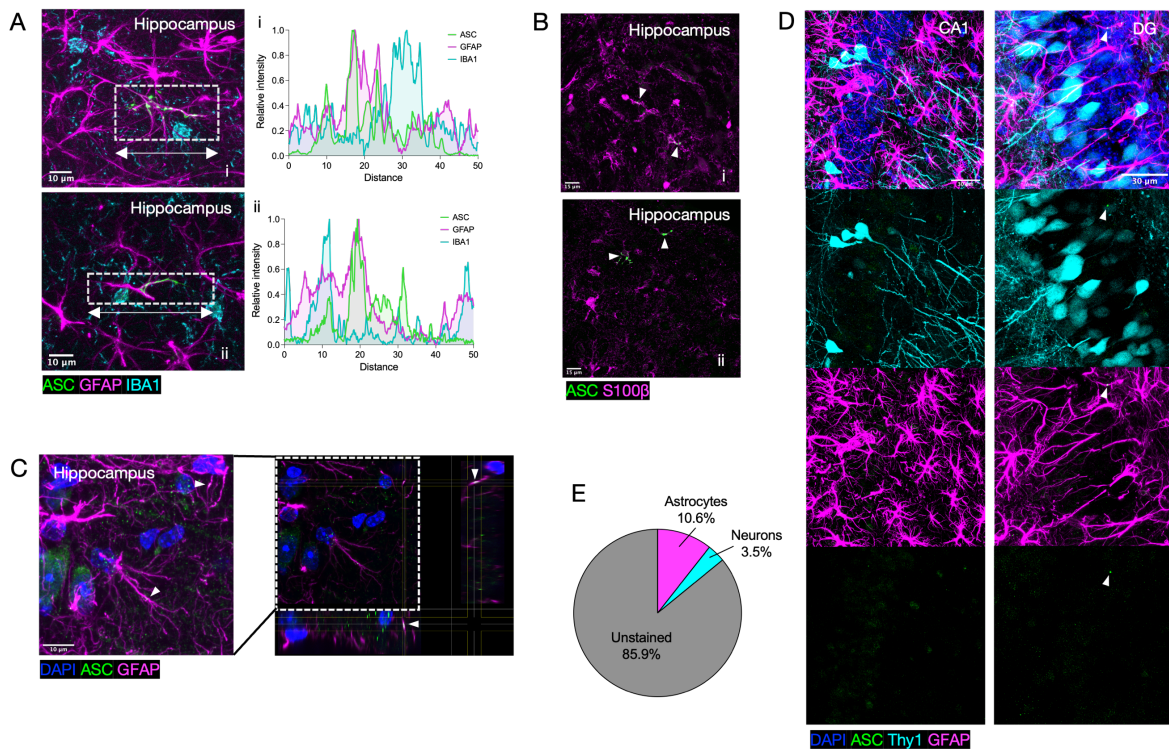


Figure 3.10. ASC specks can be found within astrocytes and neurons in the hippocampus.

Inflammasome cell type localization was assessed in the hippocampus of adult (10-12 week-old) ASC^{Citrine} and Thy1^{YFP} mice. (A) Colocalization of ASC within GFAP+ astrocyte area and not within IBA1+ microglia area. Fluorescent signal was collapsed across the y-axis in the indicated inset box (left) and then plotted as relative intensity over the x-axis distance (right). ASC^{Citrine} reporter signal peaks overlap with GFAP+ signal peaks but not with IBA1 signal peaks. Two examples (i, ii) of this analysis conducted in the hippocampus are shown. (B) Colocalization of ASC with S100β+ astrocytes within the hippocampus of ASC^{Citrine} mice. Two examples (i, ii) are shown. (C) Colocalization of exogenously stained ASC with GFAP+ astrocytes within the hippocampus. A 2D slice of the z-stack was taken to visualize ASC speck presence within the process of an astrocyte. (D,E) Thy1^{YFP} mice were used to assess the presence of ASC specks within hippocampal neurons and astrocytes. 3D renderings of ASC, Thy1, and GFAP surfaces were generated in Imaris. Masks were created to assess the ASC signal within each cell surface, and the ASC volume within total Thy1 and GFAP surfaces in the FOV were recorded. (D) Representative images showing the colocalization of ASC in Thy1+ neurons relative to GFAP+ astrocytes. (E) Pie chart depicting the relative presence of ASC specks within neurons (Thy1+ surface) relative to astrocytes (GFAP+ surface). Percentages were calculated based upon total ASC volume within the FOV. Unstained area refers to ASC volume not directly within either the Thy1 or GFAP surface for any given FOV. 3-5 FOVs were analyzed per mouse, and 3 mice total were analyzed in the aggregated data.

We confirmed that these GFAP+ cells were bonified astrocytes, rather than neural precursors, by labeling with the astrocyte marker S100β (Figure 3.10B). We additionally confirmed that this localization was not purely a product of the ASC^{Citrine} reporter line by using an antibody against ASC in wild type mice, in which we found ASC specks within hippocampal astrocytes (Figure 3.10C). Using this antibody, we also noticed assembled inflammasomes within the processes of some Thy1+ neurons, though to a much lesser extent than that of astrocytes (Figure 3.10D-E).

Meanwhile in the cerebellum, Purkinje cells (Calbindin+ cells) housed ASC specks, which were seen in both the soma and dendrites (Figure 3.11A). Purkinje cells in the healthy cerebellum also expressed the inflammasome cleavage target GSDMD. Interestingly, GSDMD was found throughout the entire Purkinje cell in both the soma and dendrites (Figure 3.11B). In peripheral immune cells, cleavage of GSDMD by the inflammasome leads to the formation of pores in the plasma membrane which can ultimately cause lysis^{355,356}. It is unlikely that every Purkinje cell is undergoing cell lysis and therefore possible that GSDMD is performing a different function in this cell type during baseline physiology.

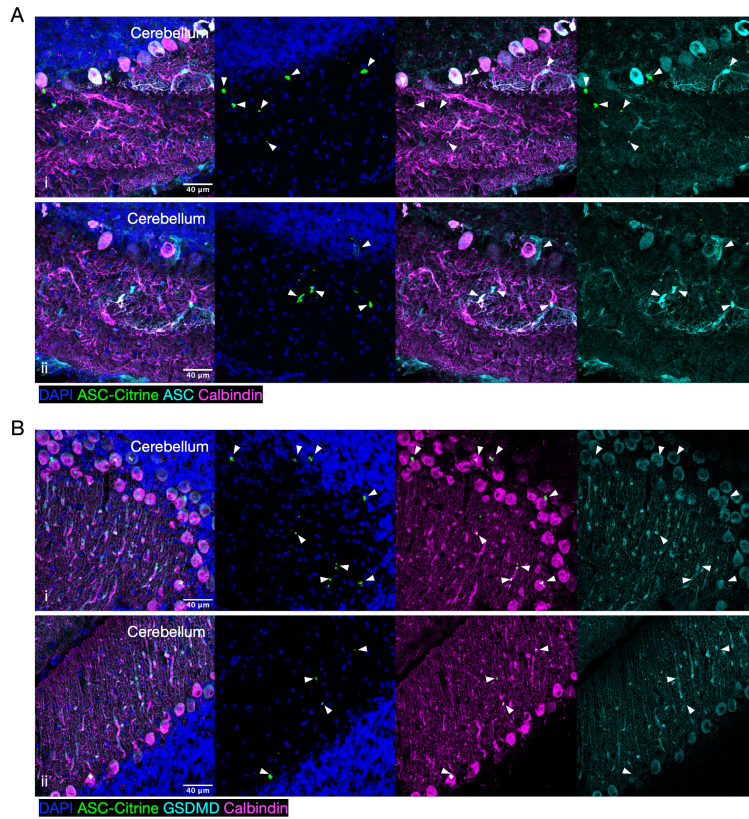


Figure 3.11. ASC specks are found in Purkinje cells in the cerebellum.

Inflammasome cell type localization was assessed in the cerebellum of adult (10-12 week-old) ASC^{Citrine} mice. (A) Co-localization of ASC in Calbindin+ Purkinje cells, assessed by ASC reporter signal as well as exogenous ASC antibody staining. Two examples (i, ii) are shown. (B) Colocalization of ASC and GSDMD with Calbindin+ Purkinje cells. ASC can be found within the soma and dendrites of Purkinje cells. GSDMD can be found throughout the body of the Purkinje cells. Two examples (i, ii) are shown.

We decided to further investigate the involvement of inflammasome in hippocampal astrocytes, given the sensitivity of these inflammasomes to physiological environmental alterations (Figure 3.1) and involvement in memory function (Figure 3.6). Relative GFAP levels are commonly used as a general readout of astrocyte reactivity. We wondered whether astrocytes harboring assembled inflammasomes were more reactive than those without inflammasomes. Using 3D reconstructions of total GFAP volume for individual astrocytes in the hippocampus, we found that in fact astrocytes with ASC specks did not have greater GFAP levels than those lacking ASC specks (Figure 3.12A-B). However, GFAP volume and ASC volume were significantly positively correlated for individual astrocytes (Figure 3.12C). These data convey that for astrocytes harboring inflammasomes, a larger inflammasome assembly corresponds to a greater level of GFAP reactivity.

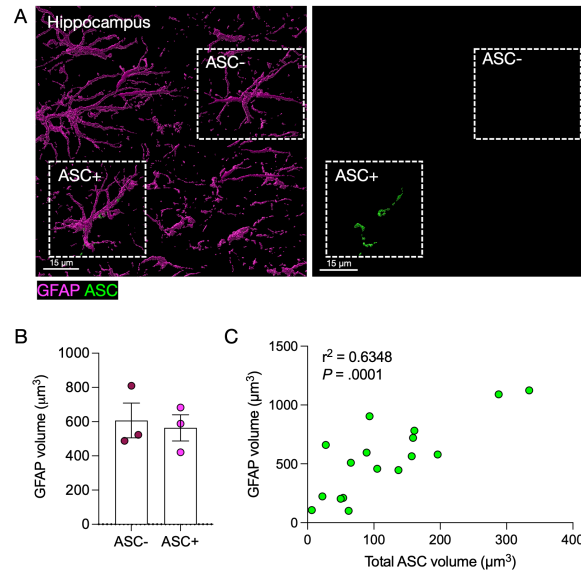


Figure 3.12. Astrocytes harboring inflammasomes are not differentially activated, but GFAP and ASC speck levels are correlated.

The association between inflammasome activation and astrocyte GFAP levels was assessed in the hippocampus of adult (10-12 week-old) *ASC^{Citrine}* mice. 3D renderings of ASC and GFAP surfaces were generated in Imaris, and individual astrocytes were then sorted into ASC+ or ASC- bins. The entire GFAP volume of each astrocyte was recorded as well as the ASC volume within each GFAP surface. (A) Representative surfaces, showing an ASC+ astrocyte and ASC- astrocyte in the same FOV. (B) Quantification of average GFAP volume of a given astrocyte, given its ASC +/- status. (C) Correlation between total ASC volume and the corresponding GFAP volume of a given astrocyte. Only ASC+ astrocytes are included. Each FOV contained at least one ASC+ and one ASC- astrocyte. 2-5 cells were analyzed per FOV, 3-5 FOVs were analyzed per mouse, and 3 mice total were analyzed. For B, each point represents the average of all cells analyzed per mouse. For C, each point represents an individual ASC+ astrocyte. Statistical significance calculated by unpaired Student's t-test (B) or Pearson correlation test (C). Error bars indicate mean +/- s.e.m.

We next sought to functionally probe the importance of astrocyte inflammasome activation in the homeostatic adult brain. To accomplish this, we generated *Casp1^{fl/fl};Aldh11^{Cre-ERT2}* mice (hereafter referred to as *Casp1^{ΔAst}*) which we fed tamoxifen food upon weaning to genetically ablate Caspase-1 function in adult astrocytes. We used Cre-negative littermates as controls (hereafter referred to as *Casp1^{cont}*). We verified reduction of *Casp1* transcript only in astrocytes via magnetic bead sorting of ACSA2+ cells (Figure 3.13).

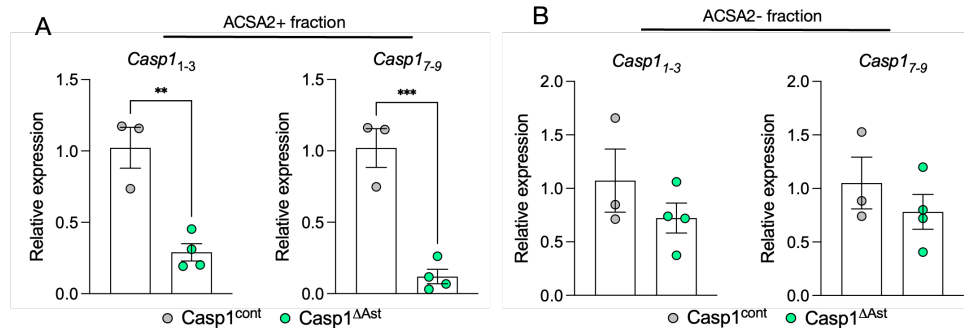


Figure 3.13. Loss of *Casp1* expression specifically in astrocytes in *Casp1^{ΔAst}* mice.

Casp1^{fl/fl};Aldh11^{Cre-ERT2} (*Casp1^{ΔAst}*) mice and Cre-negative *Casp1^{fl/fl}* littermate controls (*Casp1^{cont}*) received tamoxifen food beginning at 3 weeks-old and continuing until brain harvest. Mice were perfused and fresh whole brains were prepared into a single cell suspension for positive selection of astrocytes (ACSA-2+ cells) by magnetic-activated cell sorting. RNA was then extracted from each fraction for qPCR. Relative expression levels of *Casp1* were assessed within ACSA-2+ (A) and ACSA-2- (B) fractions using primers for exons 1-3 (left) and exons 7-9 (right). Each point represents an individual mouse. Statistical significance calculated by unpaired Student's t-test (A,B). Error bars indicate mean +/- s.e.m. ***P* < 0.01, ****P* < 0.001.

We did not detect any differences in locomotion, exploratory behavior, or anxiety in *Casp1^{ΔAst}* mice as assessed by the open field test and elevated plus maze (Figure 3.14A-C). *Casp1^{ΔAst}* mice also did not display differences in baseline motor function or motor learning as assessed on the rotarod (Figure 3.14D), highlighting the lack of importance of astrocyte inflammasome signaling within the cerebellum.

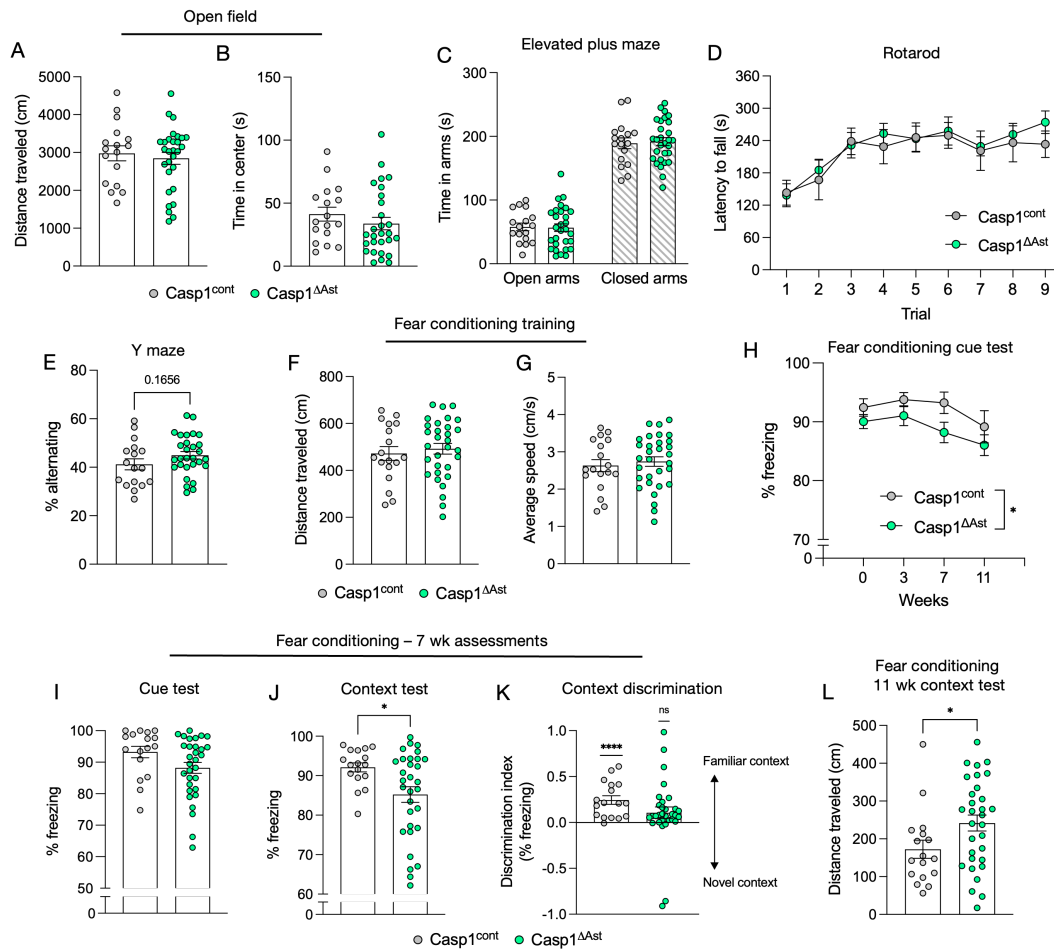


Figure 3.14. Astrocyte Caspase-1 ablation does not impact baseline locomotion, motor learning, spatial working memory, or associative fear memory, but improves long-term spatial memory flexibility.

Casp1^{fl/fl};Aldh111^{Cre-ERT2} (Casp1^{ΔAst}) mice and Cre-negative Casp1^{fl/fl} littermate controls (Casp1^{cont}) received tamoxifen food beginning at 3 weeks-old and continuing until two weeks prior to beginning behavior assessment (8-10 weeks-old). (A,B) General locomotion and exploratory behavior was assessed using the open field test. (A) Distance traveled over the entire test period. (B) Time spent in center of the arena. (C) Anxiety-like behavior was assessed using the elevated plus maze. Total time spent in the open and closed arms were quantified. (D) Motor coordination and learning were assessed on the rotarod apparatus. Latency to fall over from the rotating rod was measured on each trial. Three trials per day were conducted over three consecutive days. (E) Spatial working memory was assessed using the Y maze. Total number of alternations was divided by the total number of arm entries to calculate the measure of percent alternating. (F-L) Short-term and remote memory was assessed by fear conditioning. (F-G) Baseline locomotion and exploratory behavior within the conditioning chamber were measured by distance traveled (F) and average speed (G) during a habituation period. After tone-shock training, hippocampal-independent memory was assessed by cue testing (H,I) and hippocampal-dependent memory was assessed by context testing (J-L). Mice were assessed on these metrics 0 weeks (24 hours), 3 weeks, 7 weeks, and 11 weeks post-training. (H) Percent time spent immobile during the cue test as assessed on consecutive test sessions. (I) Percent time spent immobile during the cue test conducted 7 weeks after training. (J) Percent time spent immobile during the context test conducted 7 weeks after training. (K) Discrimination between the trained (familiar) context and an untrained (novel) context was assessed 7 weeks after training. Percent time spent immobile in each context was used to calculate a discrimination index where 1 indicates full relative immobility in the familiar context and -1 indicates full relative immobility in the novel context. (L) Total distance traveled during the context test conducted 11 weeks after training. Each point represents the average of all mice in the group (D,H) or an individual mouse (A-C,E-G,I-L). Statistical significance calculated by unpaired Student's t-test (A-C,E-G,I,J,L), two-way ANOVA with Sidak's multiple comparisons test (D,H), or one-sample t and Wilcoxon test against zero (K). Error bars indicate mean +/- s.e.m. **P* < 0.05, *****P* < 0.0001.

Given our findings that Caspase-1 inhibitor treatment significantly improved synaptic plasticity and memory function (Figure 3.6), we sought to determine if astrocyte inflammasomes sufficiently contribute to physiologic hippocampal function. In particular, we wondered whether the increase in synapse density resulting from widespread Caspase-1 inhibition (Figure 3.6C-J) was cell intrinsic to neurons or if it could be a downstream consequence of inflammasome activation within astrocytes. Thus, we assessed relative levels of synaptic markers in the hippocampi of Casp1^{ΔAst} mice compared to Cre-negative littermate controls. In line with our findings from Caspase-1 inhibitor-treated mice (Figure 3.6G,H,I,J), mice lacking astrocyte Caspase-1 function had significantly higher levels of the presynaptic marker Synaptophysin compared to controls (Figure 3.9C,D,G,H). We also noted a trend toward increased levels of the presynaptic glutamate transporter VGLUT1 in Casp1^{ΔAst} mice (Figure 3.9E,F,I,J), a similar trend to which we noted in Caspase-1 inhibitor-treated mice (Figure 3.6K,L).

Caspase-1 inhibition via VX-765 treatment also increased postsynaptic spine density (Figure 3.6C-F) concomitant with increased presynaptic density (Figure 3.6G,H,I,J). We therefore also analyzed postsynaptic markers in our Casp1^{ΔAst} mice. However, we found no change in the levels of the postsynaptic markers Homer-1 (Figure 3.9K,L) or PSD95 (Figure 3.9M,N) in Casp1^{ΔAst} mice compared to Cre-negative controls. These results suggest that presynaptic densities can be regulated cell-extrinsically by astrocyte inflammasome activity, and that inflammasome-mediated postsynaptic density is either regulated cell-intrinsically or cell-extrinsically by non-astrocytic cells.

Caspase-1 can function as an executioner Caspase that promotes pyroptotic cell death^{356,549,580}. We wondered whether the loss of Caspase-1 function in astrocytes limited pyroptosis in these cells, and if that led to altered number and/or density of astrocytes in the hippocampus. We indeed found significantly highest volume of the astrocyte marker GFAP in the hippocampus of Casp1^{ΔAst} mice (Figure 3.15A,B). Given that GFAP levels can be altered by astrocyte reactivity alone, we counted the number of nuclei per field of view (FOV) that were GFAP+ as a more accurate assessment of astrocyte numbers. We found no difference in the number of astrocytes in the CA1 region of the hippocampus of Casp1^{ΔAst} mice compared to Casp1^{cont} mice (Figure 3.15A,C). We also assessed relative astrocyte coverage using Aldh1l1 levels and found no change in the abundance of this astrocyte marker in the CA1 of Casp1^{ΔAst} mice (Figure 3.15D,E). Therefore, the loss of Caspase-1 in astrocytes can promote astrocyte reactivity but does not appear to affect astrocyte numbers or coverage.

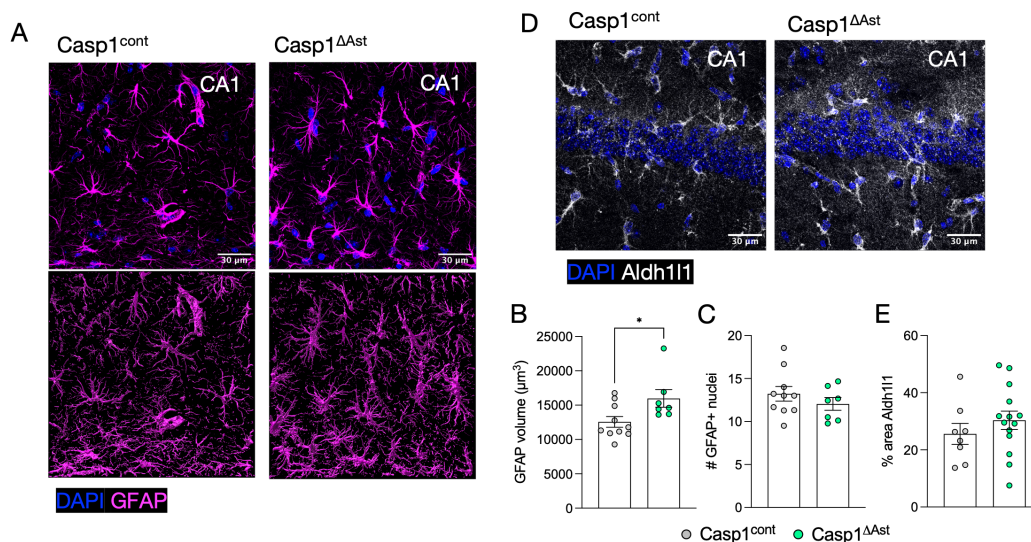


Figure 3.15. The acute loss of Caspase-1 function promotes reactivity but does not affect astrocyte numbers.

Casp1^{fl/fl};Aldh1l1^{Cre-ERT2} (Casp1^{ΔAst}) mice and Cre-negative Casp1^{fl/fl} littermate controls (Casp1^{cont}) received tamoxifen food beginning at 3 weeks-old and continuing until two weeks prior to beginning behavior assessment (8-10 weeks-old). Brains were harvested from these animals after behavioral assessment at 4-6 months of age. Astrocytes were assessed by IHC for GFAP (A-C) and Aldh1l1 (D,E) in the CA1 region of the hippocampus. (A-C) Astrocyte reactivity and numbers were assessed using GFAP signal per FOV. (A) 3D renderings of GFAP surfaces were generated in Imapris (bottom) to determine reactivity, and 2D projections overlaid with DAPI (top) were used to determine astrocyte numbers per FOV. Representative max projections (top) and corresponding 3D surfaces (bottom). (B) Quantification of average GFAP volume per FOV. (C) Quantification of the number of astrocytes per FOV. (D,E) Astrocyte coverage was assessed by percent area Aldh1l1 per FOV. Representative images (D) and quantification (E) are shown. Each point represents an individual mouse. 6-9 FOVs across 3 brain sections were analyzed per mouse to generate an average. Statistical significance calculated by unpaired Student's t-test (B,C,E). Error bars indicate mean ± s.e.m. *P < 0.05.

Given our results that astrocyte inflammasome activity can alter hippocampal neuron presynaptic density (Figure 3.9C-J), we wondered whether this relationship functionally contributed to memory processes. We conducted the Y maze test for spatial working memory on Casp1^{ΔAst} mice and found that these animals trended towards improved performance on this hippocampus-dependent task (Figure 3.14E). Given the enhancement in spatial memory in contextual fear conditioning test conducted with VX-765-treated mice, we next repeated this test with Casp1^{ΔAst} mice. We found no difference in memory recall in a 24 hr contextual fear conditioning task when comparing freezing behavior of Casp1^{ΔAst} animals and Cre-negative controls (Figure 3.16A). Importantly, Casp1^{ΔAst} mice had comparable baseline locomotion to controls during the training phase of this task (Figure 3.14F-G).

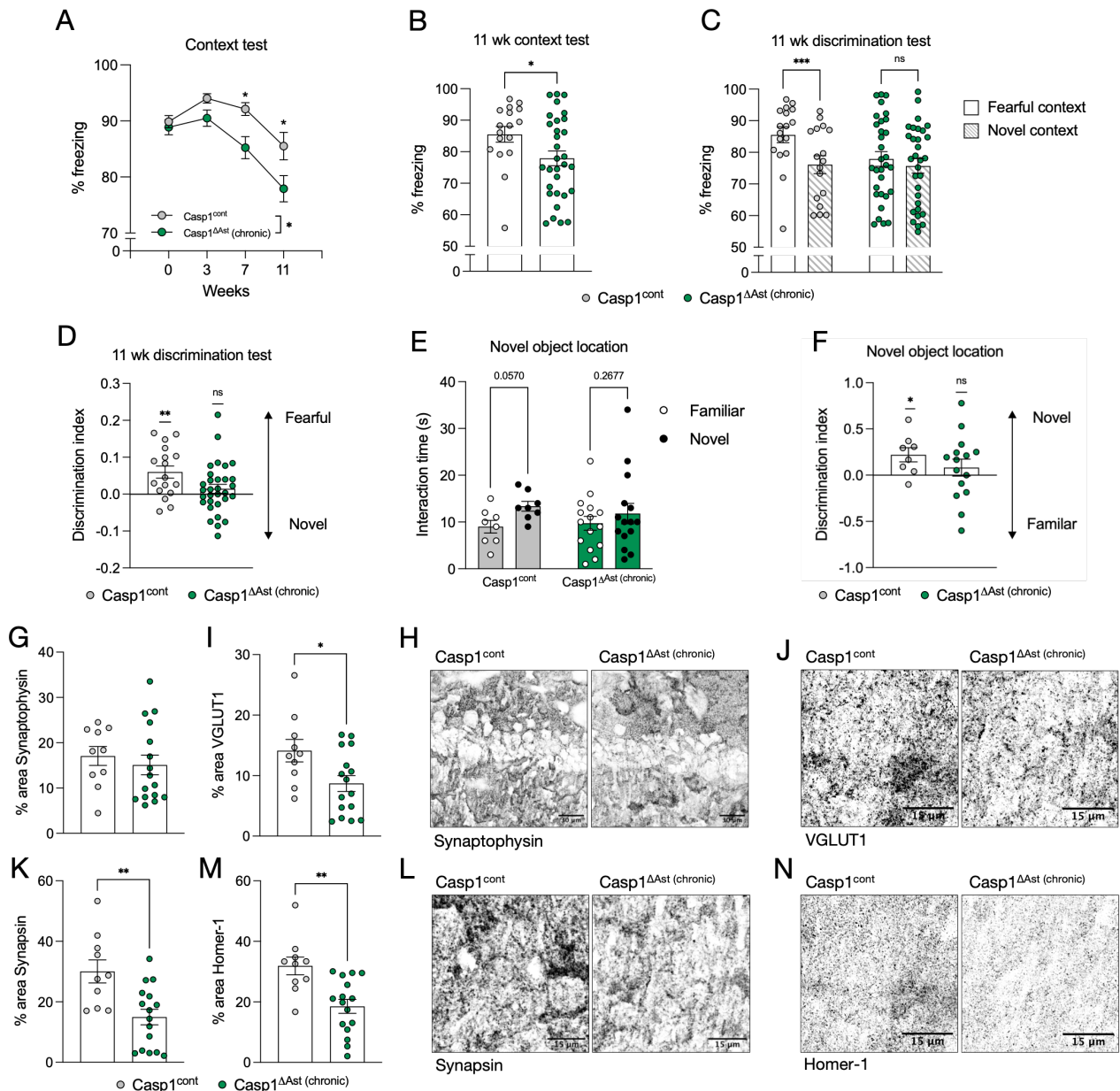


Figure 3.16. Prolonged loss of astrocyte inflammasome function is detrimental to memory retention and synaptic health.

Casp1^{fl/fl};Aldh11^{Cre-ERT2} (Casp1^{ΔAst (chronic)}) mice and Cre-negative Casp1^{fl/fl} littermate controls (Casp1^{cont}) received tamoxifen food beginning at 3 weeks-old and continuing until two weeks prior to beginning behavior assessment (8-10 weeks-old). Brains were harvested from these animals after behavioral assessment at 8 months of age. (A-D) Remote memory was assessed by fear conditioning. After tone-shock training, hippocampal-dependent memory was assessed by repeated context testing. Freezing behavior was assessed for 3-min in the trained context and a novel, untrained context 0 weeks (24 hours), 3 weeks, 7 weeks, and 11 weeks post-training. (A) Percent time spent immobile during the trained context test as assessed on consecutive test sessions. (B) Percent time spent immobile during the trained context test conducted 11 weeks after training. (C,D) Discrimination between the trained (fearful) context and the untrained (novel) context as assessed 11 weeks after training. (C) Percent time spent immobile during the trained context test compared exploration of a novel untrained context. (D) Percent time spent immobile in each context was used to calculate a discrimination index where 1 indicates full relative immobility in the familiar context and -1 indicates full relative immobility in the novel context. (E-F) Short-term spatial memory was assessed using the novel object location task, in which animals were presented with two identical objects in the training phase and then tested when one object was moved to a new location 2 hr later. (E) Time spent interacting with the objects in the familiar and novel locations during the 5-min test period. (F) A discrimination index was calculated based on time spent interacting with each object in which 1 indicates full preference for the novel location and -1 indicates full preference for the familiar location. (G-N) Hippocampal synapse markers were assessed by IHC in the CA1 region of the hippocampus of Casp1^{cont} and Casp1^{ΔAst (chronic)} mice. Relative Synaptophysin (G,H), VGLUT1 (I,J), Synapsin (K,L), and Homer-1 (M,N) protein levels were analyzed. Quantification of average percent area coverage per FOV (G,I,K,M) and representative images (H,J,L,N) are shown. 6-9 FOVs across 3 brain sections were analyzed per mouse to generate an average per mouse. Each point represents the average of all mice in the group (A) or an individual mouse (B-G,I,K,M). Statistical significance calculated by two-way ANOVA with Sidak's multiple comparisons test (A,C,E), unpaired Student's t-test (B,G,I,K,M), or one-sample t and Wilcoxon test against zero (D,F). Error bars indicate mean +/- s.e.m. **P* < 0.05, ***P* < 0.01, ****P* < 0.001.

Given our findings that ASC speck density decreased following environmental perturbations (Figure 3.1D-J) we posited that astrocyte inflammasome activity may be dispensable in these short-term memory tasks. In this case, astrocyte inflammasome activation may occur prior-to and/or at long-term intervals after learning. We thus continued to conduct fear conditioning recall tests repeatedly for weeks after initial fear training to assess whether the loss of astrocyte Caspase-1 function in the long-term affected memory consolidation and/or remote recall. Indeed, we found that over consecutive context testing, animals lacking astrocyte Caspase-1 function froze significantly less than controls (Figure 3.16A).

By the most remote time points tested, control animals still froze in the trained context, while mice lacking astrocyte Caspase-1 had nearly returned to baseline activity levels (Figure 3.14J,L, 3.16B). We assessed activity levels in these animals compared to controls in a novel, untrained context relative to the fearful, trained context. While control mice still identified the trained context as fearful relative to a novel context, mice lacking astrocyte Caspase-1 froze the same amount within the trained and novel arenas (Figure 3.14K, 3.16C,D). The results of this remote context discrimination test indicate that mice lacking astrocyte Caspase-1 are no longer able to distinguish the feared arena from a novel arena and may therefore have an impairment in long-term spatial memory.

To assess how relevant astrocyte inflammasome function in the hippocampus specifically is to memory function in adulthood, we also conducted consecutive cue testing following fear conditioning. We found no significant difference in short-term or remote memory recall in the hippocampus-independent cue test (Figure 3.14H-I). Lending to the idea that the worsened memory recall in astrocyte Caspase-1-deficient mice is primarily dependent on hippocampus-related effects, we also conducted an independent hippocampus-dependent spatial memory task, namely, the novel object location test. As expected, control animals spent significantly more time interacting with a familiar object placed in a novel location in the arena compared to the same object placed in a familiar location (Figure 3.16E,F). Yet, mice lacking astrocyte Caspase-1 spent equal amounts of time with the two objects (Figure 3.16E,F) which is indicative of impaired hippocampus-dependent memory.

These long-term memory impairments observed in astrocyte Caspase-1-deficient mice were surprising to us at first because our results thus far indicated that blocking inflammasome activation in adulthood is beneficial for memory function. Yet, inflammasome activity was clearly apparent in homeostatic physiologic states, lending to the concept that some baseline inflammasome activity does contribute to normal brain function. We therefore reasoned that the prolonged loss of inflammasome activity during these intermittent states between learning is what may largely contribute to proper memory consolidation and long-term recall.

Given this reasoning, we sought to determine the extent of hippocampal physiologic perturbation that occurs after prolonged loss of astrocyte Caspase-1 function. To this end, we waited until $Casp1^{\Delta Ast}$ were 8-months of age before conducting brain histopathologic studies (hereafter referred to as $Casp1^{\Delta Ast (chronic)}$ mice). Control mice in these studies were age-matched littermate controls ($Casp1^{cont}$ mice). $Casp1^{\Delta Ast}$ animals that were harvested at 3-4 months of age as previously assessed will hereafter be referred to as $Casp1^{\Delta Ast (acute)}$ mice to distinguish these two groups.

We first repeated the analyses of synaptic health in mice lacking astrocyte Caspase-1 function long-term. While we had previously noted that $Casp1^{\Delta Ast (acute)}$ mice had heightened levels of Synaptophysin (Figure 3.9C,D,G,H), the long-term loss of Caspase-1 ablated this effect (Figure 3.16G,H). In other words, hippocampal Synaptophysin levels were comparable to $Casp1^{cont}$ levels in $Casp1^{\Delta Ast (chronic)}$ mice, suggesting that presynapses were lost due to the chronic deficiency of Caspase-1 in these mice. Supporting this idea, we found significantly lower levels of the presynaptic markers VGLUT1 (Figure 3.16I,J) and Synapsin (Figure 3.16K,L) as well as postsynaptic marker Homer-1 (Figure 3.16M,N) in the $Casp1^{\Delta Ast (chronic)}$ hippocampus. These findings together reveal profound synapse loss in mice chronically lacking proper Caspase-1 function in astrocytes and support the behavioral findings of impaired memory in these animals (Figure 3.16A-F). Thus, while the short-term loss of inflammasome activity is necessary for proper memory function, the prolonged loss of inflammasome activity becomes detrimental for hippocampal physiology and memory function.

3.4.4. Astrocyte inflammasomes regulate neuronal plasticity through IL-33 and perineuronal nets

Our findings that inflammasome activity within astrocytes can modulate neuronal synapses led us to question the mechanism by which this cell-to-cell communication is happening. In particular, we sought to probe potential underlying neurobiology lending to the acute positive regulation of synapses as well as the chronic negative regulation of synapses by astrocyte inflammasomes. We therefore studied both Casp1^{ΔAst (acute)} and Casp1^{ΔAst (chronic)} mice paired with their age-matched Cre-negative littermate controls, Casp1^{cont} mice. All analyses were first split by age for respective control mice, but no differences were seen across any measures between differently aged Casp1^{cont} mice (data not shown). Thus, age-matched controls were grouped together as a single control group referred to as Casp1^{cont} from this point forward.

One study of synapse remodeling found that the IL-1 family cytokine IL-33 directs the engulfment of extracellular matrix (ECM) materials by microglia⁵⁸¹. In this work, the loss of IL-33 production in neurons led to heightened ECM levels concomitant with reduced synaptic plasticity⁵⁸¹. Interestingly, astrocytes in the hippocampus can also generate IL-33, a source that also contributes to synaptic plasticity⁵⁸². We wondered whether this IL-33-ECM-neuron plasticity axis was perturbed by the loss of astrocyte Caspase-1, and whether this signaling cascade could explain the relative gain and loss of synapses in our Casp1^{ΔAst} mice.

In alignment with our synapse data and with published reports^{581,582}, we found significantly higher levels of IL-33 in Casp1^{ΔAst (acute)} mice and a strong trend toward lower IL-33 levels in Casp1^{ΔAst (chronic)} mice compared to controls (Figure 3.17A,B, 3.18A-C). These findings match with the concept that IL-33 promotes synaptic plasticity, such that short-term Caspase-1-deficiency promotes IL-33 production and synapse formation while long-term Caspase-1-deficiency is detrimental to IL-33 production and synapse formation.

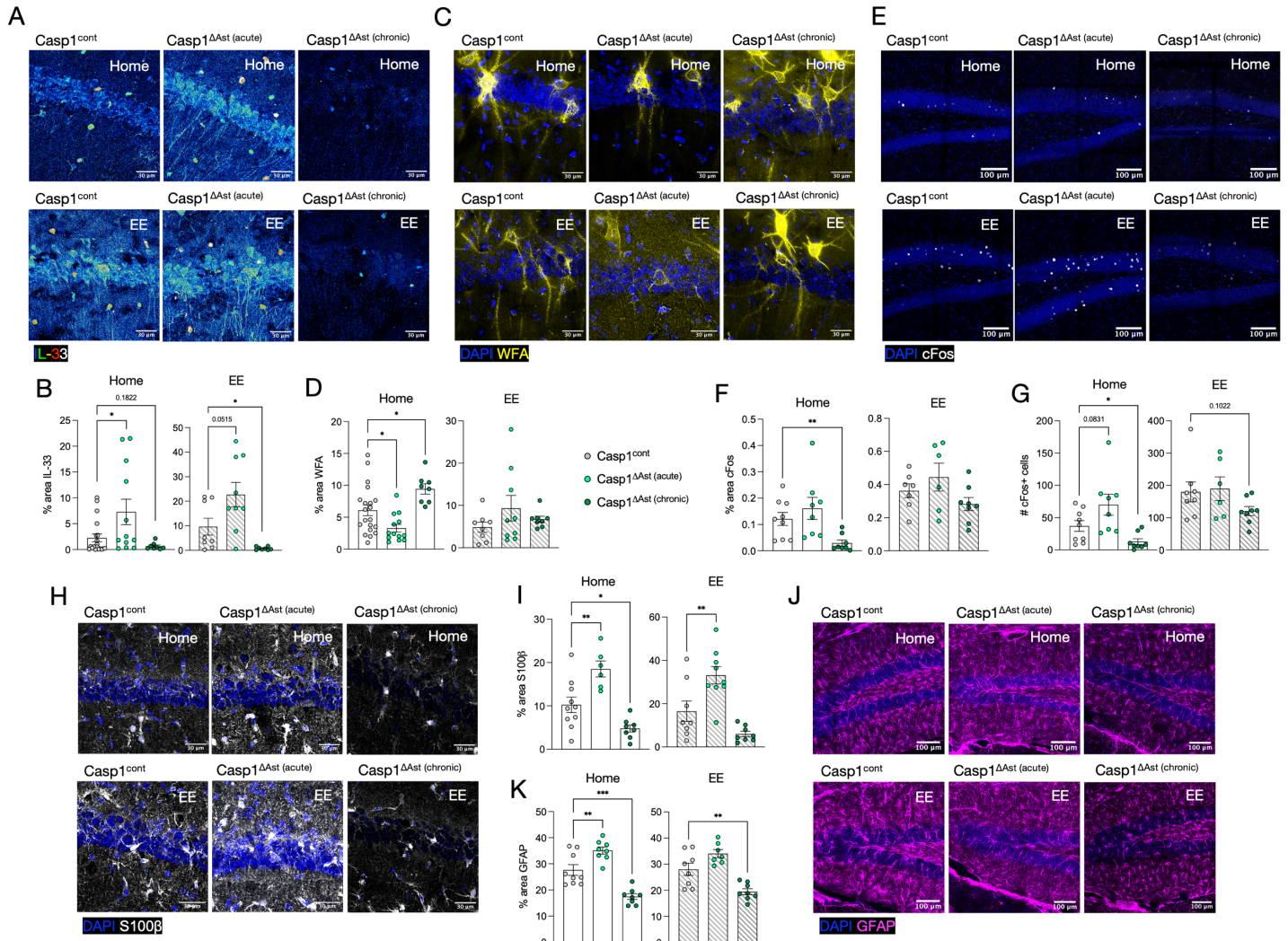


Figure 3.17. Astrocyte Caspase-1 modulates IL-33 production, perineuronal net coverage, and neuronal plasticity.

Casp1^{fl/fl};Aldh11^{Cre-ERT2} (*Casp1^{ΔAst}*) mice and Cre-negative *Casp1^{fl/fl}* littermate controls (*Casp1^{cont}*) received tamoxifen food beginning at 3 weeks-old and continuing until two weeks prior to beginning behavior assessment (8-10 weeks-old). Brains were harvested from these animals after behavioral assessments were complete at either 4-6 months of age (*Casp1^{ΔAst (acute)}*) or 8 months of age (*Casp1^{ΔAst (chronic)}*). Mice were randomly assigned for immediate perfusion and harvest ("Home") or were exposed to a novel enriched environment for 90 min prior to perfusion and harvest ("EE"). Hippocampal physiology was assessed by IHC in *Casp1^{cont}*, *Casp1^{ΔAst (acute)}*, and *Casp1^{ΔAst (chronic)}* brain section using various markers and percent area per FOV was quantified (B,D,F,G,I,K). (A,B) Relative IL-33 levels in the CA1 region. (A) Representative images using a thermal gradient to illustrate intense areas of IL-33 production. Dark blue indicates very low IL-33, green indicates low IL-33, red indicates high IL-33, and white indicates very high IL-33. (B) Quantification of relative IL-33 levels across genotypes at baseline or after EE exposure. (C,D) Perineuronal net coverage was assessed by WFA staining in the CA1 region. (E) Representative images and (F) quantification of relative WFA levels across genotypes at baseline or after EE exposure. (E-G) Neuronal activity was assessed by staining for the immediate early gene cFos in the entire hippocampus. (E) Representative images and (F) quantification of relative cFos percent area (F) and number of puncta (G) across genotypes at baseline or after EE exposure. (H,I) Astrocyte reactivity was assessed by S100β staining in the CA1 region. (H) Representative images and (I) quantification of relative S100β levels across genotypes at baseline or after EE exposure. (J,K) Astrocyte reactivity was secondarily assessed by GFAP staining in the CA1 region. (J) Representative images and (K) quantification of relative GFAP levels across genotypes at baseline or after EE exposure. Each point represents an individual mouse. 6-9 FOVs across 3 brain sections were analyzed per mouse to generate averages. Statistical significance calculated by unpaired Student's t-tests (B,D,F,G) or one-way ANOVA (I,K). Error bars indicate mean \pm s.e.m. * $P < 0.05$, ** $P < 0.01$, *** $P < 0.001$.

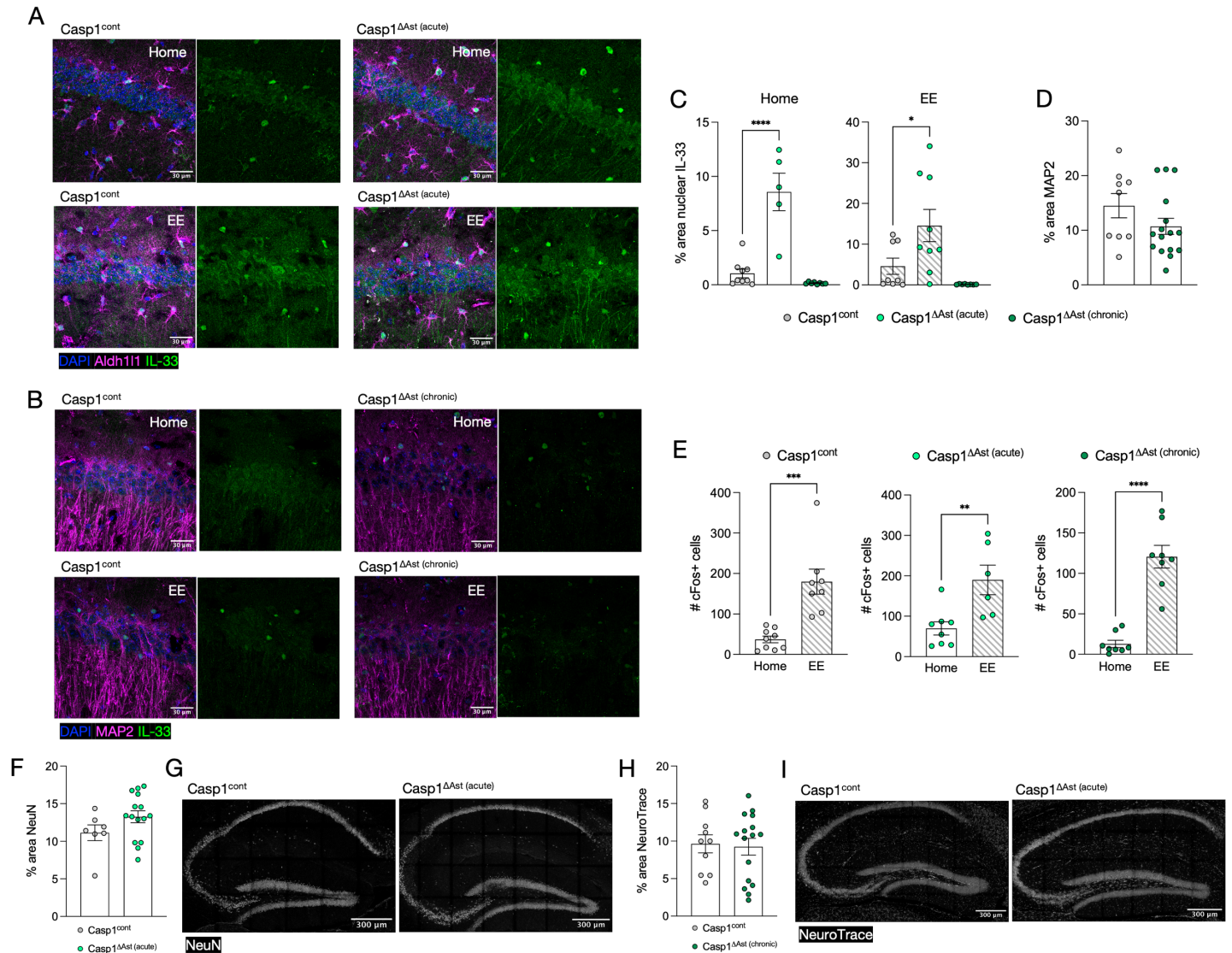


Figure 3.18. Astrocyte Caspase-1 regulates cellular IL-33 levels but does not impact neuron numbers or ability to respond to stimuli.

Casp1^{fl/fl};Aldh111^{Cre-ERT2} (Casp1^{ΔAst}) mice and Cre-negative Casp1^{fl/fl} littermate controls (Casp1^{cont}) received tamoxifen food beginning at 3 weeks-old and continuing until two weeks prior to beginning behavior assessment (8-10 weeks-old). Brains were harvested from these animals after behavioral assessments were complete at either 4-6 months of age (Casp1^{ΔAst} (acute)) or 8 months of age (Casp1^{ΔAst} (chronic)). Mice were randomly assigned for immediate perfusion and harvest ("Home") or were exposed to a novel enriched environment for 90 min prior to perfusion and harvest ("EE"). Hippocampal physiology was assessed by IHC in Casp1^{cont}, Casp1^{ΔAst} (acute), and Casp1^{ΔAst} (chronic) mice using various markers and percent area per FOV was quantified. (A-C) Relative IL-33 levels in the CA1 region and the cellular localization. (A,B) Representative images show IL-33 within astrocytes and neurons. Aldh111 was used to mark astrocytes (A) and MAP2 was used to mark neuron processes (B). (C) Quantification of IL-33 per FOV using strict thresholding for large particle size as a proxy for nuclear localization. (B,D) The density of neuronal processes was assessed by MAP2 staining in the CA1 region. (B) Representative images and (D) quantification of relative MAP2 levels in Casp1^{cont} and Casp1^{ΔAst} (chronic) mice collapsed across exposure (home and EE). (E) Neuronal activity was assessed by staining for the immediate early gene cFos in the entire hippocampus. Data in Figure 3.17G is plotted broken down across genotypes here to better illustrate the relative effects of EE treatment on cFos levels. (F,G) Neuron numbers were assessed by NeuN staining in the entire hippocampus. (F) Quantification of relative NeuN levels Casp1^{cont} and Casp1^{ΔAst} (acute) mice collapsed across exposure (home and EE) and (G) representative images are shown. (H,I) Neuron numbers were assessed by NeuroTrace staining in the entire hippocampus. (H) Quantification of relative NeuroTrace levels Casp1^{cont} and Casp1^{ΔAst} (chronic) mice collapsed across exposure (home and EE) and (I) representative images are shown. Each point represents an individual mouse. 6-9 FOVs across 3 brain sections were analyzed per mouse to generate averages. Statistical significance calculated by unpaired Student's t-tests (C,D,E,F,H). Error bars indicate mean +/- s.e.m. **P* < 0.05, ***P* < 0.01, ****P* < 0.001, *****P* < 0.0001.

IL-33 production is ramped up upon the induction of neuronal activity, for instance, after exposure to an enriched environment⁵⁸¹. We wondered whether this change in IL-33 production was at all related to astrocyte inflammasome activity, and therefore exposed Casp1^{ΔAst} (acute), Casp1^{ΔAst} (chronic), and control mice to an enriched environment prior to brain harvest. We found that IL-33 levels were higher in all three groups following EE exposure compared to controls left in their home cages prior to brain harvest (Figure 3.17A,B, 3.18A-C). Moreover, it remained consistent that IL-33 levels were higher in Casp1^{ΔAst} (acute) mice and significantly lower in

Casp1^{ΔAst (chronic)} mice compared to controls (Figure 3.17A,B, 3.18A-C). These data suggest that activity-induced IL-33 production may be largely attributed to a source outside of astrocyte inflammasome function.

Published studies indicate that IL-33 can be produced by both neurons and astrocytes in the hippocampus^{581,582}. We confirmed that IL-33 staining colocalized with markers for both astrocytes (Aldh111) and neurons (MAP2) in our control animals (Figure 3.18A,B). Moreover, acute or chronic Caspase-1 deficiency did not abrogate IL-33 production from either cell source (Figure 3.18A,B).

It has been well documented that the extracellular matrix, of which perineuronal nets (PNNs) constitute a subset, is diminished in quantity following a learning experience⁵⁸³⁻⁵⁸⁵. This reduction in PNN coverage allows for the remodeling of synapses to occur that is necessary to encode a learning experience as a memory⁵⁸³⁻⁵⁸⁵. Subsequently, PNNs are solidified around the newly formed synapses to encode that connection as a part of the memory⁵⁸³⁻⁵⁸⁵. Thus, perturbation of baseline PNN coverage and PNN plasticity can significantly impair proper memory encoding and recall.

Given that IL-33 can regulate ECM turnover⁵⁸¹, and that IL-33 levels were bidirectionally perturbed in astrocyte Caspase-1-deficient mice (Figure 3.17A,B), we next sought to evaluate potential ECM disruption that may occur following the loss of inflammasome activity. We assessed PNN coverage in the hippocampus using Wisteria floribunda agglutinin (WFA) staining, a well-characterized method to fluorescently label N-acetylglucosamine components of PNNs. We found that short-term loss of Caspase-1 function in astrocytes significantly reduced PNN coverage in the CA1 region of the hippocampus compared to controls (Figure 3.17C,D).

This effect also extended to other brain regions, in which there was a significant reduction in PNN coverage in the subiculum and trends toward reduced PNN coverage in the cortex and dentate gyrus (Figure 3.19A,B). Importantly, there were no baseline differences in the number of nuclei in the neuron cell body layer of the CA1 in Casp1^{ΔAst (acute)} mice compared to controls (Figure 3.19C,D). Thus, any differences in PNN coverage are likely not due to differences in the absolute number of neurons in this region.

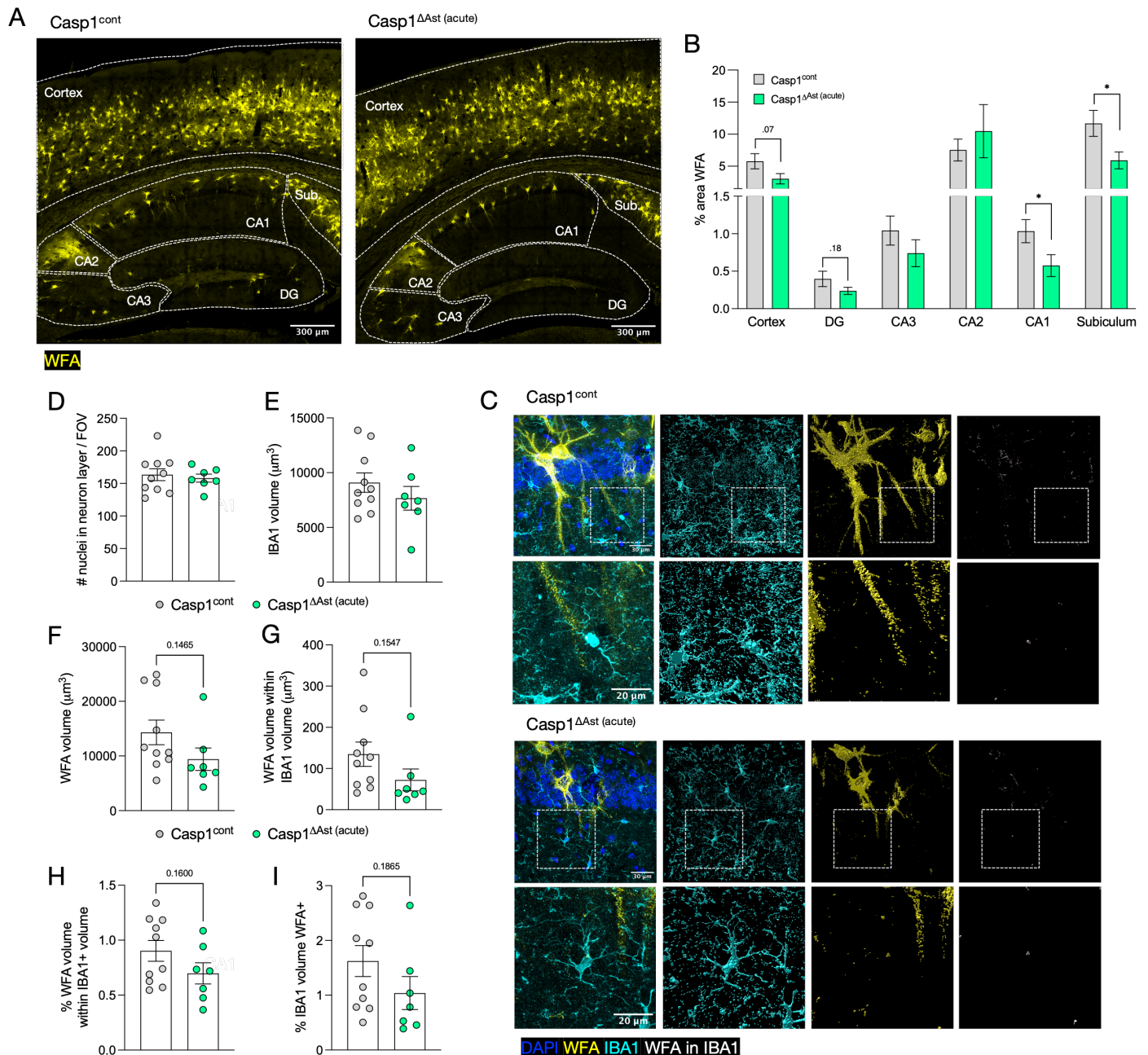


Figure 3.19. Astrocyte Caspase-1 acutely limits perineuronal net coverage through a mechanism independent of microglial engulfment.

Casp1^{fl/fl};Aldh11^{Cre-ERT2} (Casp1^{ΔAst (acute)}) mice and Cre-negative Casp1^{fl/fl} littermate controls (Casp1^{cont}) received tamoxifen food beginning at 3 weeks-old and continuing until two weeks prior to beginning behavior assessment (8-10 weeks-old). Brains were harvested from these animals after behavioral assessment at 4-6 months of age. Perineuronal net coverage and microglial engulfment was assessed using combined WFA and IBA1 staining. (A-B) Perineuronal net coverage was assessed across the cortex and hippocampal subregions. (A) Representative images and (B) quantification illustrating WFA levels in Casp1^{cont} and Casp1^{ΔAst (acute)} mice. (C-I) Microglial engulfment of perineuronal net material was assessed in the CA1 region. 3D renderings of WFA and IBA1 surfaces were generated in Imaris. Masks were created to assess the WFA signal within IBA1 surface, and the WFA volume within total IBA1 surfaces in the FOV was recorded. (C) Representative 2D max projections (left) and 3D surface renderings (right set of three). (D) Quantification of the number of nuclei in the neuron cell body layer of the CA1 region per FOV. The DAPI channel was used to mark individual nuclei in Imaris. (E) Relative IBA1 volume per FOV. (F) Relative WFA volume per FOV. (G) Relative masked WFA volume contained within IBA1 volume per FOV. (H) Quantification of the percent of total WFA volume that is contained within IBA1 volume per FOV. (I) Quantification of the percent of total IBA1 volume that contains WFA volume per FOV. Each point represents an individual mouse. 6-9 FOVs across 3 brain sections were analyzed per mouse to generate averages. Statistical significance calculated by multiple unpaired t-tests (B) or unpaired Student's t-test (D-I). Error bars indicate mean +/- s.e.m. **P* < 0.05.

Following the trends of our other findings, we found that the long-term loss of Caspase-1 in astrocytes led to opposite results of that of short-term loss with respect to PNNs. Specifically, PNN coverage was significantly enhanced in the Casp1^{ΔAst (chronic)} hippocampus compared to controls (Figure 3.17C,D). Interestingly, EE

treatment abrogated both of these differences in PNN coverage, as there were no significant changes in PNN coverage between the three groups that were exposed to the novel environment (Figure 3.17C,D). This finding reveals that new experiences can rescue the perturbations to PNN levels associated with the loss of astrocyte Caspase-1 function.

One mechanism by which PNN turnover can occur is via engulfment by the professional phagocytes of the brain, microglia. We wondered whether the reduction in PNN levels following short-term astrocyte Caspase-1-deficiency could be attributed to increased microglial engulfment of PNN components. To address this idea, we assessed the internalization of WFA within IBA1+ microglia in the CA1 region of the hippocampus of Casp1^{cont} and Casp1^{ΔAst (acute)} mice. We first confirmed that there were no overt differences in microglial numbers (Figure 3.20A,B), coverage area (Figure 3.20A,C), or volume (Figure 3.19C,E) in Casp1^{ΔAst (acute)} mice that could confound any engulfment analyses.

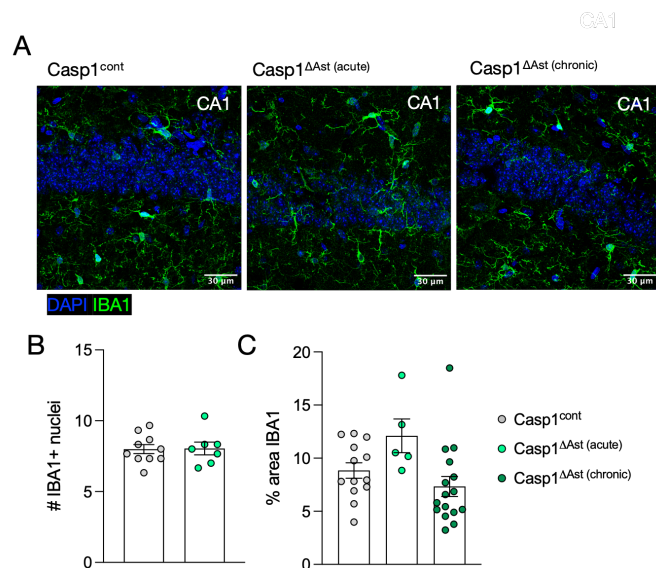


Figure 3.20. The loss of Caspase-1 in astrocytes does not overtly impact microglia.

Casp1^{fl/fl};Aldh111^{Cre-ERT2} (Casp1^{ΔAst}) mice and Cre-negative Casp1^{fl/fl} littermate controls (Casp1^{cont}) received tamoxifen food beginning at 3 weeks-old and continuing until two weeks prior to beginning behavior assessment (8-10 weeks-old). Brains were harvested from these animals after behavioral assessments were complete at either 4-6 months of age (Casp1^{ΔAst (acute)}) or 8 months of age (Casp1^{ΔAst (chronic)}). Microglia were assessed by IHC for IBA1 in the CA1 region of the hippocampus. (A) Representative images. (B) Quantification of the number of microglia per FOV assessed by counting the number of nuclei positive for IBA1. (C) Quantification of percent area of IBA1 coverage per FOV. Each point represents an individual mouse. 6-9 FOVs across 3 brain sections were analyzed per mouse to generate an average. Statistical significance calculated by unpaired Student's t-test (B) or one-way ANOVA (C). Error bars indicate mean ± s.e.m.

In line with our previous analysis, the short-term loss of astrocyte Caspase-1 function tended to decrease PNN density per FOV in Casp1^{ΔAst (acute)} mice (Figure 3.19C,F). We next assessed the volume of WFA within IBA1 volume to determine whether any differences in microglial PNN engulfment occurred in Casp1^{ΔAst (acute)} mice. We noted a trend toward reduced WFA volume contained within microglia (Figure 3.19C,G) similar to that of total WFA levels (Figure 3.19C,F), suggesting that microglial PNN phagocytosis is unaltered following the loss of astrocyte Caspase-1. Indeed, the percent of total WFA volume that was contained within microglia was not significantly changed in Casp1^{ΔAst (acute)} mice (Figure 3.19C,H). Moreover, the percent of microglia volume that contained WFA was also not changed (Figure 3.19C,I). These data suggest that changes to PNN coverage dependent upon inflammasome activity are likely not majorly driven by microglial phagocytosis of PNN material.

Our data thus far indicate that inflammasome activation within astrocytes can regulate hippocampal plasticity in part through modulation of IL-33, PNN coverage, and synapse density. Yet, whether astrocyte inflammasome activation alters the hippocampal network activity that underlies proper memory function remains a gap in understanding. Given that IL-33 and PNN plasticity can both contribute to altered hippocampal neuronal plasticity⁵⁸¹, we reasoned that ablating astrocyte inflammasome function in the short- and long-term may substantially impact hippocampal neuron activation and plasticity. To address this idea, we stained for the immediate early gene cFos, which is substantially upregulated following the induction of neuronal activity.

In line with our reasoning, we noted a strong trend toward increased cFos levels in the hippocampus of Casp1^{ΔAst (acute)} mice compared to controls and a significant decrease in cFos levels in Casp1^{ΔAst (chronic)} mice (Figure 3.19E-G). These data match with the concept of enhanced neuronal plasticity following the short-term loss of Caspase-1 function but impaired hippocampal plasticity following prolonged Caspase-1 deficiency. Importantly, the short- or long-term loss of Caspase-1 did not significantly affect neuron process coverage (Figure 3.18D), EE-induced cFos upregulation (Figure 3.18E), or baseline neuron numbers (Figure 3.18F-I) in the hippocampus. In line with our WFA results, we found that exposure to a novel environment completely abrogated these changes in cFos levels (Figure 3.19E-G). Thus, novel experiences are sufficient to rescue the baseline impact triggered by the loss of Caspase-1 deficiency in astrocytes.

While the impact of astrocyte inflammasome activation on hippocampal plasticity and memory function is better understood with our data, it remains an open question as to how Caspase-1 acts cell-intrinsically to ultimately change astrocyte biology and downstream network function. We noted that relative astrocyte reactivity was altered by the loss of inflammasome activity. In particular, short-term astrocyte Caspase-1 deficiency enhanced astrocyte reactivity in which strikingly heightened levels of S100β (Figure 3.18H,I) and GFAP (Figure 3.18J,K) were observed in Casp1^{ΔAst (acute)} mice compared to controls. Moreover, long-term astrocyte Caspase-1 deficiency dampened astrocyte reactivity whereby Casp1^{ΔAst (chronic)} mice displayed significantly lower levels of S100β (Figure 3.18H,I) and GFAP (Figure 3.18J,K) compared to controls. Exposure to a novel environment did not largely impact these trends (Figure 3.18H-K). Thus, Caspase-1 can alter the baseline inflammatory state of astrocytes, which may then feedforward to contribute to changes in IL-33, PNNs, neuron plasticity, and memory function. Altogether, this study reveals that inflammasome biology contributes significantly to healthy neurobiology and proper memory function.

3.5 Discussion

In the studies presented here, we have identified a novel unexpected function for the immune-based inflammasome complex in regulating the astrocyte-neuron communication underlying memory function. We report a baseline distribution of ASC specks throughout the adult brain at homeostasis, with the highest concentration of ASC specks coalescing in the hippocampus within astrocytes. ASC speck levels could be dynamically modulated by experience and age. We find that acute pharmacologic inhibition of Caspase-1 or genetic deletion specifically in astrocytes was sufficient to promote an increase in synaptic protein abundance and memory recall. Conversely, the prolonged loss of Caspase-1 in astrocytes was detrimental to synaptic health and memory function. We identified that astrocyte Caspase-1 regulates hippocampal IL-33 levels, PNN coverage, and neuronal plasticity bidirectionally short- and long-term.

These studies break new ground in our understanding that immune-based signaling molecules are hijacked for use in homeostatic contexts. While the inflammasome is typically thought to lead to cell lysis and pro-inflammatory cytokine release, we find here that the inflammasome is subtly modulated in the adult brain for dynamic physiologic benefit. These findings are notable as they contribute to our knowledge of the mechanisms underlying astrocyte biology, neuronal plasticity, and proper memory function. Moreover, these data may inform treatment strategies for neurologic diseases associated with perturbed inflammasome activation, as targeting this complex may be more nuanced than once thought.

We still lack knowledge as to the precise mechanism(s) by which inflammasome activity within astrocytes has such broad impacts on neurons and memory function as a whole. Future work will reveal what aspects of astrocyte biology are regulated by the inflammasome. Whether this astrocyte-neuron communication is solely regulated by IL-33 remains to be understood. It is possible that the inflammasome is activating other cytokines, such as IL-1β and IL-18, whose release from astrocytes could signal onto nearby neurons. Other mediators, such as ROS, ADP/ATP, neurotransmitters, or ion fluxes, could also have a level of inflammasome-dependent release which may then signal to neurons.

Astrocyte processes are well understood to wrap synapses leading to the “tripartite synapse” concept⁵⁸⁶. Indeed, astrocytes are in close contact with neuron soma, dendrites, axons, and synapses, among other parenchymal structures such as blood vessels⁵⁸⁷. A single mouse astrocyte can be in contact with several neuronal soma,

about 600 dendrites, and around 100,000 synapses⁵⁸⁸. As such, astrocytes are known to control synapse formation, maintenance, and elimination⁵⁸⁷. How the inflammasome fits into this picture of astrocyte-mediated synapse control will remain an area for future investigation.

Similarly, it is not known how PNNs are perturbed following the loss of Caspase-1. IL-33 is one potential explanation, as greater levels of IL-33 are linked to increased clearance of ECM materials and positive synaptic plasticity⁵⁸¹. Our first line evidence suggests that the changes to PNN coverage dependent upon Caspase-1 may not be mediated by microglial phagocytosis. Whether neurons or glia alter secretion of ECM components or ECM breakdown enzymes in processes related to Caspase-1 remains to be determined.

Along these lines, the cell source of IL-33 which alters production following astrocyte Caspase-1 knockout is unknown. Our evidence confirms that both neurons and astrocytes contain IL-33 in the adult hippocampus. Moreover, astrocyte Caspase-1 deficiency did not abrogate IL-33 production from either source. Yet, whether one cell source of IL-33 is primarily affected by astrocyte Caspase-1 loss is unknown. It is possible that Caspase-1 acts cell intrinsically to modulate IL-33 release, as this cytokine is within the IL-1 family whose activation is inflammasome-controlled⁵⁸⁹. One report claimed that IL-33 could be inactivated by Caspase-1⁵⁹⁰, while others claim IL-33 could be activated by the inflammasome⁵⁹¹, both of which would be consistent with parts of our data.

Our studies are surprising given that the presence of pro-inflammatory cytokines is canonically thought to be detrimental to CNS cell health and cognition. Yet, there is a growing appreciation for a balance in inflammatory signaling in the brain. Complete abrogation of inflammatory signaling can be detrimental to brain function. For instance, controlled levels of IL-1 β are known to be necessary for synaptic plasticity, as blocking IL-1 β is detrimental for long-term potentiation while supraphysiologic IL-1 β levels also suppress long-term potentiation⁵⁹²⁻⁵⁹⁴. Thus, a delicate middle ground of inflammatory signaling in the brain may be necessary to maintain a balanced homeostatic state.

The inflammasome has been a center point of interest as a druggable target for many neurologic disease states, including neurodegenerative disease, epilepsy, stroke, and others⁵⁵¹. Our work raises a point of caution in these endeavors, as complete blockade of the inflammasome may have unintended consequences on healthy brain function. The inflammasome represents an intricate and dynamic platform for responding to changes in the cellular environment and orchestrating appropriate responses. The present study places a spotlight on a homeostatic role for the inflammasome in contributing to healthy neurobiology and brain function, which raises a litany of remaining questions and opens the door for countless future studies.

3.6 Methods

3.6.1. Mice

All mouse experiments were performed in accordance with the relevant guidelines and regulations of the University of Virginia and approved by the University of Virginia Animal Care and Use Committee. Mice were housed in specific pathogen-free conditions under standard 12-hour light/dark cycle conditions in rooms equipped with control for temperature ($21 \pm 1.5^\circ\text{C}$) and humidity ($50 \pm 10\%$). Adult sex- and age-matched mice were assigned to experimental groups. Unless age is explicitly noted, mice were assessed beginning at 8-weeks of age. Male and female mice were included for all studies, and data was analyzed first separated by sex to check for any significant sex differences before combining. ASC^{Citrine} (strain #030744), Thy1^{YFP} (strain #003782), and Aldh111^{EGFP} (strain #030247) were obtained from The Jackson Laboratory. Casp1^{fl/fl} were generously provided by R. Flavell⁵⁹⁵ and crossed to Aldh111^{Cre-ERT2} (strain #031008) obtained from The Jackson Laboratory to generate Casp1^{fl/fl};Aldh111^{Cre-ERT2} (denoted Casp1 ^{Δ Ast}) and Cre-negative littermate controls (denoted Casp1^{cont}). Upon weaning, Casp1 ^{Δ Ast} and Casp1^{cont} littermates were fed tamoxifen diet (Envigo Teklad #TD.130858) *ad libitum* until two-weeks prior to behavioral analysis (about 6 weeks of age) and then returned to normal chow for the remainder of experimentation.

3.6.2. Caspase-1 inhibitor treatment

Mice were injected i.p. with the Caspase-1 inhibitor VX-765 prepared 6.25 mg/ml in 25% DMSO or vehicle (25% DMSO) as a control. Thy1^{YFP} received i.p. injections of 30 mg/kg VX-765 or vehicle control 3x/week (Mondays, Wednesdays, and Fridays) beginning two-weeks prior to behavioral testing and continuing for the entirety of experimentation. Mice were always weighed prior to injection.

3.6.3. Environmental enrichment

Mice were brought into a separate room and placed into an enriched environment (EE; rat cages with crushed corn cob bedding) or left in their home cages (11 x 7 x 6 inch mouse cages with crushed corn cob bedding) in the vivarium as a control. ASC^{Citrine} mice were EE housed for 48 hours under standard 12-hour light/dark cycle conditions in rooms equipped with control for temperature ($21 \pm 1.5^\circ\text{C}$) and humidity ($50 \pm 10\%$). Cages of Casp1^{cont}, Casp1 ^{Δ Ast (acute)}, and Casp1 ^{Δ Ast (chronic)} mice were randomly selected for immediate perfusion or 90 min environmental enrichment exposure prior to perfusion. Cage-mates were given the same housing treatments in these experiments. EE housing conditions consisted of a mix of colored igloos (Bio-Serv #K3570, #K3327), crawl balls (Bio-Serv #K3329, #K3330), and tunnels (Bio-Serv #K3322, #K3323) with *ad libitum* access to standard chow and water. Mice were euthanized, perfused, and brains harvested immediately following all EE treatments (see 3.6.6 "Tissue collection").

3.6.4. Social isolation

Mice were socially isolated in the home vivarium in standard mouse cages (11 x 7 x 6 inch with crushed corn cob bedding) for 48 hours via individual housing, with the addition of an enrichment nestlet. Mice were blocked from viewing neighboring cages. Control mice were kept housed in their standard housing arrangements (groups of 3-5 sex-matched mice) without blocked views of neighboring cages, with the addition of an enrichment nestlet. All housing provided *ad libitum* access to standard chow and water under standard 12-hour light/dark cycle conditions in rooms equipped with control for temperature ($21 \pm 1.5^\circ\text{C}$) and humidity ($50 \pm 10\%$).

3.6.5. Behavior

All behavior experiments were performed between 8 am and 5 pm in a blinded fashion. Mice were transported from their home vivarium room to the behavior core and allowed 20 minutes to habituate before beginning each test. All training apparatuses were cleaned with 70% ethanol before and after each mouse was tested.

Open field test

General locomotion, exploratory, and anxiety-related behaviors were assessed using the open field test. The opaque white plexiglass test arenas ($35 \times 35 \text{ cm}^2$) were evenly illuminated. Mice were placed into the center of the arena and allowed to explore for 10 min. All trials were tracked and scored using an overhead camera and video monitoring software (Ethovision XT Noldus). A central square ($20 \times 20 \text{ cm}^2$) was demarcated to quantify time spent in the center.

Elevated plus maze

Exploratory and anxiety-related behaviors were assessed using the elevated plus maze. The maze consisted of two open arms (uncovered, $35 \times 6 \text{ cm}^2$) and two closed arms (20 cm tall opaque black plexiglass, $35 \times 6 \text{ cm}^2$) extending from a common center square, elevated 121 cm above the floor. Mice were placed onto the opaque white plexiglass floor in the center facing a closed arm, and then allowed to explore the entire raised platform for 5 min. All trials were tracked and scored using an overhead camera and video monitoring software (Ethovision XT Noldus).

Rotarod

Gross motor function and motor learning were assessed on the rotarod. The rotarod apparatus consists of five separate compartments on a rotating rod (MED Associates Inc, ENV-575M). Each mouse was placed onto the rod at a speed of 4 rotations per minute (rpm). The rod accelerated from 4 rpm to 40 rpm over the span of 5 min. Each mouse was allowed to walk on the rotating rod until one of the three trial endpoints was reached: falling off to disrupt a laser at the base, 5 rotations hanging on the rod without ambulating, or elapsing 6 min of testing. Three trials were performed with at least 30 min between each trial for three consecutive days. Latency to fall was recorded by the rotarod-controlling software (Rotarod version 1.4.1, MED Associates Inc).

Y maze

Spatial working memory was assessed using the Y maze. The apparatus is made of opaque white plexiglass and composed of three identical arms extending from a common center triangle. Mice were placed into the center and allowed to explore the entire arena for 8 min. All trials were tracked and scored using an overhead camera and video monitoring software (Ethovision XT Noldus). Percent alternation was calculated as the total number of alternations (three entries into a unique arm) divided by the total number of arm entries made, multiplied by 100.

Morris water maze

Spatial learning and memory were assessed using the Morris water maze. The white plastic pool (1 m in diameter) contained water kept at $22 \pm 2^\circ\text{C}$ and made opaque with non-toxic white tempura paint. A hidden platform (10 cm in diameter) was placed 1 cm below the water surface. Four distinct visual cues within each quadrant were placed equally spaced around the walls of the pool. A dim light source evenly illuminated the test room.

The training phase of this task consisted of four 60 s trials per day for four days, and the probe trial consisted of a single 60 s trial in which the hidden platform was removed from the pool. If the mouse was unable to locate the platform within the trial time allotted, then it was manually placed onto the platform. Mice were allowed 2 min to sit on the platform following the very first training trial, and 5 s to sit on the platform for every trial afterwards. Mice were removed from the pool, dried, and returned to their home cages set upon heating pads between each trial on training days. At least 30 min was given between each training trial. All trials were tracked and scored using an overhead camera and video monitoring software (Ethovision XT Noldus).

For the Morris water maze task using ASC^{Citrine} mice, animals were harvested immediately following the fourth trial on training day 2 or immediately following the probe trial on day 5. Control mice for these experiments underwent identical testing procedures except without any hidden platform within the pool during the entire training phase. Control mice were harvested immediately following the probe trial on day 5.

Fear conditioning and extinction

Spatial memory, associative memory, and cognitive flexibility were assessed using fear conditioning paradigms. The training chamber (MED Associates Inc) consisted of an arena (28 x 21 x 22 cm) with clear plexiglass walls and a floor made of 18 stainless steel rods (4 mm in diameter) spaced 1.5 cm apart and wired to a shock generator. The chamber was kept inside a sound-proof box which was evenly lit with a white fluorescent light and supplied with background noise.

For fear conditioning training, mice were placed into the center of the arena and allowed to habituate for 3 min. Mice then received three pairs of cue-aversive stimuli over 3 min consisting of tone(18 s, 5 kHz, 75 dB)-shock(2 s, 5 mA) pairings separated by 40 s inter-trial-intervals. Mice were assessed in a context and/or cue test on the following day (24 hr later).

For the contextual fear conditioning test, mice were placed into the center of the arena as it appeared during the training session and allowed to explore freely for 3 min. No tone or shock were presented during this session. At least two hours after the context test, a cued fear conditioning test was conducted. For this session, the arena was altered in appearance such that black-and-white striped paper was placed over the walls, a white plastic insert covered the floor, and the chamber was scented with vanilla. Mice were placed into the center of the arena and allowed to explore this novel context for 3 min. Then, the same cue-aversive tone (18 s, 5 kHz, 75 dB) from the training session was played constantly for the next 3 min. For extinction testing, mice underwent these same context and cue tests at successive time points (3, 7, and 11 weeks) after the original training session. Mice were kept in their home cages in the vivarium without any additional behavioral interventions during the entirety of this extinction period.

All trials were tracked and scored using an overhead camera and video monitoring software (Ethovision XT Noldus). Percent freezing was calculated as the cumulative time immobile divided by the total test time (180 s), multiplied by 100. The discrimination index was calculated as $(A-B)/(A+B)$, where A = [% freezing in the trained context (i.e. the context test)] and B = [% freezing in the novel context (i.e. the habituation phase in the cue test)].

Novel object location test

Spatial memory was assessed using the novel object location test. The opaque white plexiglass test arenas (35 x 35 cm²) were evenly illuminated, and a 3-inch piece of tape was placed flush against the floor on the center of one wall for spatial orientation purposes. Mice were first habituated to these arenas for two 5 min exploration sessions. This habituation protocol was repeated for an additional two days, yielding a total of six 5 min habituation sessions.

For object location training, mice were placed into the center of the arena and allowed to explore for 10 min. During this phase, two rubber ducks were placed equidistant from the center piece of tape and away from the edges of the arena on the half closest to the piece of tape. Mice were then returned to their home cages for 2 hr. After this inter-trial-interval, mice were placed into the center of the arena for a novel location test in which one rubber duck was moved to a novel spot and the other rubber duck was kept in the same familiar location. The newly located duck was placed in line with the center piece of tape on the opposite side of the arena from the tape and away from the arena wall. Mice were allowed to interact with these two objects during the test phase for 5 min before being returned to their home cages.

All trials were tracked and scored using an overhead camera and video monitoring software (Ethovision XT Noldus). Time spent interacting with each object in the training and test phases were manually scored. It was confirmed that no baseline bias in time spent interacting with objects in either location existed (data not shown). The discrimination index was calculated as $(A-B)/(A+B)$, where A = [Time spent interacting with the novel object] and B = [Time spent interacting with the familiar object]. As such, a DI of zero indicates equal time with each object, a DI of -1 indicates full preference for the object in the familiar location, and a DI of 1 indicates full preference for the object in the novel location.

3.6.6. Tissue collection

Mice were euthanized by CO₂ asphyxiation and cervical dislocation, then transcardially perfused with 20 ml 1x PBS and brains were harvested. For all experiments involving IHC, Western blotting, cytokine analysis (multiplex cytokine array, ELISA), and qPCR, brains were cut down the midline, and the right hemisphere was optionally microdissected to remove the hippocampus, cortex, and cerebellum which were flash-frozen on dry ice. Microdissected samples were stored at -80°C until downstream processing for protein or RNA extraction. The left hemisphere was kept intact for downstream immunohistochemistry and drop-fixed in 4% PFA on ice, then stored overnight at 4°C. The following day, PFA was decanted, brains were washed in 1x PBS, and then 10 ml 30% sucrose was added. Brains were kept in 30% sucrose at 4°C until sinking to the bottom of the container (at least 48 hours) at which point they were prepped for cryosectioning (see 3.6.7 “Brain sample preparation”). For MACS studies, harvested brains were placed into HBSS on ice prior to processing (see 3.6.8 “Magnetic-activated cell sorting”).

3.6.7. Brain sample preparation

Drop-fixed half-brains sufficiently dehydrated in 30% sucrose (see 3.6.6 “Tissue collection”) were washed with 1x PBS and frozen in Tissue-Tek OCT compound (Sakura #4583). Frozen blocks were sectioned at 40 μ m using a cryostat (Leica) and sections were stored in 0.05% sodium azide in 1x PBS at 4°C for downstream IHC (see 3.6.9 “Immunofluorescence”). Flash-frozen half-brains or microdissected brain regions were minimally thawed on ice and mechanically homogenized in Tissue Protein Extraction Reagent (T-PER; Thermo Fisher, 78510) containing phosphatase inhibitor cocktail PhosSTOP (Roche, 04906845001) and protease inhibitor cocktail cOmplete (Roche, 11873580001). Half-brains or half-hippocampi were homogenized in 500 μ l or 200 μ l of this TPER cocktail, respectively. 50 μ l of these slurries were then added to TRIzol (500 μ l for half-brains or 250 μ l for half-hippocampi; Life Technologies, 15596018) and stored at -80°C until further use (see 3.6.10 “RNA isolation, cDNA synthesis, qPCR”). The remainder of the slurries were then spun down at 16,000 rpm for 10 minutes and the soluble supernatants were collected and stored at -80°C until further use (see 3.6.11 “Western blotting”).

3.6.8. Magnetic-activated cell sorting

Fresh whole brains held in HBSS on ice were dissociated using a Papain Dissociation System (Worthington #LK003150) according to manufacturer’s instructions with some modifications. Briefly, tissue was transferred into the Papain Solution (EBSS with 20 U/ml papain and 0.005% DNase) and triturated gently using a 5 ml serologic pipette. The mixture was incubated at 37°C on a shaker for 30 min in which it was triturated gently every 10 min (3x). The cloudy cell solution was then filtered through a 70 μ m cell strainer and spun down at room temperature at 300 g for 5 min. The resulting cell pellet was resuspended in the Inhibitor Solution (EBSS with papain/ovomucoid inhibitor solution and DNase). This cell solution was then layered atop fresh Inhibitor Solution and centrifuged at 70 g for 6 min at room temperature. The supernatant containing debris was discarded, and the remaining cell pellet was resuspended in 160 μ l 1x MACS buffer (Miltenyi Biotec, 130-0910376) in PBS.

Astrocytes were positively selected using ACSA-2 magnetic microbeads (Miltenyi Biotec, 130-097-678) according to manufacturer’s instructions with some modifications. Briefly, the cell suspension was incubated with 40 μ l FcR-blocking reagent for 25 min at 4°C. Then, 40 μ l anti-ACSA-2 magnetic microbeads were added, mixed well, and allowed to incubate for 15 min at 4°C. Cells were washed by adding 1 ml 1x MACS buffer and centrifuged at 300 g for 10 min at 4°C. Supernatants were aspirated and the remaining cell pellet was resuspended in 500 μ l 1x MACS buffer. LS columns (Miltenyi Biotec, 130-042-401) and a QuadroMACS magnet (Miltenyi Biotec, 130-091-051) were used to positively select for ACSA-2+ cells. Positive and negative fractions were spun down at 300 g for 10 min at 4°C. ACSA-2+ and ACSA-2- pellets were then resuspended in 200 μ l or 500 μ l TRIzol reagent, respectively, for downstream RNA extraction (see 3.6.10 “RNA isolation, cDNA synthesis, qPCR”).

3.6.9. Immunofluorescence

Brain sections stored in PBS with 0.05% sodium azide were blocked for 1 hour at room temperature in blocking solution (2% donkey serum, 1% BSA, 0.1% Triton-X, 0.05% Tween-20 in 1x PBS). Sections were then incubated with primary antibodies diluted in the blocking solution overnight at 4°C. The following antibodies were used: Aldh111 (E712Q, Cell Signaling, 1:300), ASC (AL177, AdipoGen, 1:300), Calbindin (D-28K, Millipore Sigma, 1:1000), cFos (ab190289, Abcam, 1:1000), GFAP (2.2B10, Thermo Fisher, 1:1000), GSDMD (ab209845, Abcam, 1:1000), Homer-1 (160 003, Synaptic Systems, 1:500), IBA1 (ab5076, Abcam, 1:300), IL-33 (AF3626, R&D, 1:100), NeuN (MAB377, Millipore Sigma, 1:500), PSD95 (2507, Cell Signaling, 1:200), S100 β (15146-1-AP, Proteintech, 1:500), Synapsin1/2 (106 004, Synaptic Systems, 1:1000), Synaptophysin (ab32594, Abcam, 1:1000), Synaptophysin (ab16659, Abcam, 1:300), VGLUT1 (135 511, Synaptic Systems, 1:500), WFA (B-1355-2, Vector Laboratories, 1:500). Samples were washed for 10 min three times with 0.5% Tween-20 in 1x PBS at

room temperature. Then, samples were incubated with secondary antibodies diluted in the blocking solution for 2 hrs at room temperature. Matched donkey Alexa Fluor-488, -568, -594, -647 anti-rabbit, -goat, -mouse, -rat, and -streptavidin antibodies were used (Thermo Fisher, 1:1000). Samples were washed again for 10 min three times with 0.5% Tween-20 in 1x PBS at room temperature and then incubated with DAPI (Millipore Sigma, 1:1000) for 10 min at room temperature. Samples were stored in 1x PBS prior to mounting on slides with ProLong Gold anti-fade mountant (Thermo Fisher, P36930) with coverslips. Slides were stored in the dark at 4°C. Images were acquired using LAS AF software (Leica microsystems) on a Leica TCS SP8 confocal microscope or Leica Stellaris confocal microscope. Images were analyzed using Fiji and Imaris (9.9.1) software.

For sections stained with NeuroTrace, secondary antibody stained was completed and well as final wash steps. Then, sections were washed once with 0.1% Triton-X in 1x PBS for 10 min and then twice in 1x PBS for 5 min all at room temperature. Sections were incubated with NeuroTrace 500/525 (N21480, Thermo Scientific, 1:100) diluted in 1x PBS for 20 min at room temperature. Sections were removed from this stain and then washed once with 0.1% Triton-X in 1x PBS for 10 min and then once in 1x PBS for 2 hr at room temperature. Following this last wash step, DAPI counterstaining was conducted as usual prior to section mounting.

3.6.10. RNA isolation, cDNA synthesis, qPCR

Brain samples or primary cells stored in TRIzol (see 3.6.7 “Brain sample preparation”) were thawed on ice and vortexed. 100 µl of chloroform (Fisher Scientific, BP1145-1) was added, and then samples were thoroughly vortex and incubated at room temperature for 5 minutes. Samples were spun down at 14,000 rpm at 4°C for 15 minutes. The clear aqueous top layer was collected into a clean tube and then an equal volume of isopropanol (~ 400 µl; Sigma, I9516) was added then vortexed vigorously. Samples were then incubated at room temperature for 10 minutes and spun down at 12,000 rpm at 4°C for 5 minutes. The resulting RNA pellet was then washed twice using 1 ml of 70% ethanol in RNase-/DNase-free water, spinning down at 14,000 rpm at 4°C for 5 min between washes. The resulting RNA pellet was air dried at room temperature and finally resuspended in 30 µl of DNase-/RNase-free water. Samples were stored at -80°C prior to cDNA synthesis. RNA quality and quantity were evaluated using NanoDrop 2000 Spectrophotometer (Thermo Scientific).

Isolated RNA was converted to cDNA using a Sensifast cDNA Synthesis kit (Bioline, BIO-65054). Gene expression levels were determined using Taqman Gene Expression Assay primer/probe mix (Thermo Fisher), Sensifast Probe No-ROX kit (Bioline, BIO-86005), and a CFX384 Real-Time PCR System (BioRad, 1855484). All kits were used according to manufacturer’s instructions. The following primers (Thermo Fisher Scientific) were used: *Aim2* (Mm01295720_m1), *Nlrp3* (Mm00840904_m1), *Pycard* (Mm00445747_g1), *Casp1* (Mm00438023_m1; exons 1-3), *Casp1* (Mm01243908_m1; exons 7-9), *Il1b* (Mm00434228_m1), *Il18* (Mm00434226_m1), and *Gapdh* (Mm99999915_g1). Relative gene expression levels to *Gapdh* were calculated using the delta-delta Ct method.

3.6.11. Western blotting

Soluble brain sample homogenates (see 3.6.7 “Brain sample preparation”) were diluted in 1x PBS. Protein concentration was determined according to a standard curve using Pierce 600 nm Protein Assay Reagent (Thermo Fisher, 22-660). Laemelli Sample Buffer (Bio-Rad, #1610747) was added at 1x to 20 µg protein lysates per sample and heated to 95°C for 5 min. Samples were loaded onto a 4–20% Mini-PROTEAN TGX Stain-Free Protein Gel (Bio-Rad, #4568093) and run at 120 V for 1.5 h using Mini-PROTEAN Tetra Cell (Bio-Rad, 1658004) in 1x Tris/Glycine/SDS Buffer (Bio-Rad, #1610732). Proteins were then transferred onto a Trans-Blot Turbo Midi 0.2 µm PVDF membrane (Bio-Rad, #1704157) for 21 min using a Trans-Blot Turbo Transfer System (Bio-Rad, #1704150) set to “2 mini gels” of “mixed MW”.

Membranes were blocked for 1 hr at room temperature using blocking solution (50% SuperBlock T20 TBS Blocking Buffer (Thermo Scientific, #37536), 50% BSA block (5% BSA + 0.05% Tween-20 in 1x TBS)). Membranes were then stained overnight at 4°C in primary antibodies diluted in blocking solution. The following

antibodies were used: Synaptophysin (ab32594, Abcam, 1;1000), VGLUT1 (135 511, Synaptic Systems, 1:500), GABA_AR α 1 (N95/35, Antibodies Inc, 1:500), GAPDH (14C10, #3683, Cell Signaling, 1:1000), β -Tubulin (9F3 #5346, Cell Signaling, 1:1000). Membranes were then washed for 5 min four times with 1x TBS, and then incubated with secondary antibodies diluted in blocking solution for 45 min at room temperature. Matched anti-rabbit (Cell Signaling, 7074P2, 1:5000) or anti-mouse (Cell Signaling, 7076S, 1:5000) secondary antibodies were used. Membranes were then washed for four times with 1x TBS over the course of 1-2 hrs. Membranes were coated in SuperSignal West Pico PLUS Chemiluminescent Substrate solution prepared according to manufacturer's instructions (Thermo Scientific, #34580) for 5 min in the dark prior to imaging. Stained membranes were imaged on a ChemiDoc MP Imaging System (Bio-Rad, #12003154). Protein levels were quantified using Fiji. Membranes were stored in 1x TBS-T (0.05% Tween-20 in 1x TBS) at 4°C.

For re-blotting, stained membranes were stripped for 10 min at room temperature using Restore PLUS Western Blot Stripping Buffer (Thermo Fisher, #46430). Membranes were then washed with 1x TBS and then blocked for 1 hr at room temperature using blocking solution. The staining procedure followed from this step.

3.6.12. Statistics

Sample sizes were chosen on the basis of standard power calculations (with $\alpha = 0.05$ and power of 0.8). Statistical tests for RNA-seq analyses were conducted using R (4.0.4 GUI 1.74 Catalina build (7936)) in RStudio (1.4.1106). For all other analyses, Prism software (GraphPad, 9.4.0) was used to calculate mean and s.e.m. values and to conduct unpaired Student's t test, one-way ANOVA, and two-way ANOVA. *P* values less than 0.05 were considered significant.

Declaration of competing interest

The authors declare no competing financial interests.

Data availability

All data are available from the authors upon request.

Acknowledgements

We thank members of the Lukens lab and the Center for Brain Immunology and Glia (BIG) at the University of Virginia for valuable discussions. This work was supported by The National Institutes of Health/National Institute of Neurological Disorders and Stroke (R01NS106383; awarded to J.R.L.), The National Institutes of Health/National Institute of Mental Health (R21MH120412-01; awarded to J.R.L.), The Simons Foundation Autism Research Initiative (Pilot Award 515305 to J.R.L.), and The Owens Family Foundation (Awarded to J.R.L.). K.E.Z. and H.E. were supported by Cell and Molecular Biology Training Grants (1T32GM139787-01-35, awarded to K.E.Z.; T32GM008136, awarded to H.E.), Wagner Fellowships, and Double Hoo Awards. A.H. was supported by a Double Hoo Award.

Chapter 4: Discussion and future directions

4.1 Dissertation discussion

This dissertation has highlighted the contribution of innate immune signaling to brain homeostasis and pathology. A delicate balance exists between healthy and disruptive inflammatory signaling in the brain. We find that perturbations to a mother's internal environment can trigger aberrant immune responses in the placenta (Chapter 2). These pro-inflammatory states impacted offspring brain development and behavior, stressing the potential consequences of deviant immune responses (Chapter 2). Meanwhile, we also find that the immune-based inflammasome complex is dynamically regulated in physiologic contexts in the brain (Chapter 3). Long-term blockade of astrocyte inflammasome signaling was detrimental to neuronal plasticity and memory function, emphasizing the important contribution of this immune-based complex to maintaining proper brain health (Chapter 3). Characterizing both the homeostatic and pathogenic roles of innate immune signaling in the brain will continue to reveal underlying neurobiology of brain function and neurologic disease, which can inform treatment strategies. This discussion will consider a few of the outstanding questions spurred by these dissertation studies and underscore some future areas of related research.

4.2.1. *The maternal-fetal interface response to environmental changes.*

Compromised placental function is a well-known contributor to perturbed fetal development^{421,505,513,522,525,596}. In particular, the essential roles of the placenta in providing barrier protection, nutritional support, gas exchange, and more to the developing fetus places it in a critical support position^{421,505,513,522,525,596}. Disruptions to a healthy maternal bodily environment including poor nutrition, infection, obesity, autoimmune disease, and stress can all alter fetal development^{421,505,513,522,525,596}. Yet, how these changes to the maternal environment are translated into changes in the fetus are not well understood. The maternal-fetal interface, including the placenta and decidua, represent the first and primary site of interaction between a mother and her offspring⁴⁹³. Probing the response of this critical juncture to environmental changes in the mother may therefore reveal fundamental biology underlying associated fetal developmental alterations in these conditions.

In the studies presented in this dissertation, we sought to characterize the maternal-fetal interface response to inflammation and/or selective serotonin reuptake inhibitor (SSRI) exposure and then correlate any of these changes to fetal neurodevelopmental outcomes (Chapter 2). We found that the maternal-fetal interface underwent a robust and rapid immune response to a viral mimetic that was largely characterized by interferon pathways. This immune response dampened baseline sex differences in the placenta sub-acutely and was associated with sex-dependent behavioral changes similar to those of autism spectrum disorder. We also found that SSRI treatment alone altered the immune signaling landscape of the maternal-fetal interface, which contributed to a reshaped response of the maternal-fetal interface when challenged with an inflammatory stimulus. Likewise, SSRI exposure potentiated the fetal brain response to inflammation alone. This study highlights the importance of taking the entire maternal-fetal interface signaling landscape into account when assessing changes to the maternal environment, and also emphasizes the critical role of the maternal-fetal interface in fostering healthy fetal development.

The precise cellular responses and molecular signaling pathways involved in the maternal-fetal interface response to inflammation and SSRI exposure, among diverse other stressors, remains largely unexplored. The maternal-fetal interface is made up of a very large population of immune cells that play both homeostatic and inflammatory-response roles. Whether and how this diverse immune population, including decidual natural killer (dNK) cells, decidual T cells, placental Haufbauer macrophages, and more respond to stimuli, and how this contributes to altered maternal-fetal interface physiology requires more research. Do these cells secrete inflammatory cytokines such as IL-6 and IL-17a that are known to contribute to behavioral changes in the offspring? Is there a long-term impact on their homeostatic functions, such as dNK-mediated arteriole remodeling that is necessary for proper nutrient and gas transport? Or T cell-mediated tolerance to the fetus?

Another major outstanding question in the field is what the exact source of cytokines is that then influence fetal neurodevelopment. Are placental cells responsible for cytokine secretion? Are these cytokines transported into fetal tissue? Or is the fetus generating its own cytokine response to inflammatory stimuli in the maternal-fetal interface or blood? One study ablated IL-6R function in placental trophoblasts which was sufficient to protect against the behavioral alterations in offspring that typically appear after *in utero* IL-6 exposure⁵²³. This shows the importance of the placenta as a source of IL-6R signaling in this model, but whether similar signaling pathways apply in more complicated changes to the maternal environment remains to be determined. Addressing these big picture questions will reveal novel targets to help prevent negative consequences on fetal development that may otherwise ensue when mothers are not in ideal health.

4.2.2. *Inflammasome signal cascades in homeostatic brain states.*

There is an increasing appreciation for the contribution of the immune system to brain homeostasis and well as neurologic disease. Immune signaling molecules can be used by central nervous system (CNS) cells for ordinary functions ranging from cell proliferation, to migration, to synaptic pruning⁴⁷⁴. Activation of brain immune signaling and infiltration of immune cells can also change the course of pathology in disease states including neurodegeneration, autoimmunity, infection, stroke, psychologic stress, neurodevelopmental disorders, and more^{195,400,474,557,597}. In the work presented in Chapter 3 of this dissertation, we highlight a novel role for the innate immune-based inflammasome signaling complex in regulating astrocyte-neuron communication and proper memory function.

It is unclear from our studies whether the changes in synapse density resulting from inhibition of the inflammasome are a result of perturbation of synapse growth, retraction, phagocytosis, or some other process. Astrocytes have been shown to directly promote synapse formation⁵⁸⁷, can actively phagocytose adult hippocampal synapses⁵⁹⁸, and maintain proper synapse function through structural support, ion buffering, neurotransmitter recycling, and more⁵⁸⁷. Which of these functions exactly could be contributed to by the inflammasome is yet unknown.

It would be extremely interesting to investigate the potential cleavage substrates of Caspase-1 in physiologic contexts. While Caspase-1 is primarily characterized to cleave pro-inflammatory cytokines and GSDMD, a litany of other substrates has also been identified whose function post-cleavage is not yet understood. For instance, Caspase-1 can cleave an array of ribosomal proteins, actin itself and actin polymerization factors, vimentin, and DNA replication factors, among others⁵⁹⁹. Intriguingly, many of these factors could relate to the structural complexity of astrocytes and astrocyte-synapse communication.

For one, astrocytes are known to locally translate transcripts in their distal processes⁶⁰⁰⁻⁶⁰². This process allows for precise control over protein trafficking to individual synapses and the maintenance of synaptic heterogeneity under contact from the umbrella of a single astrocyte⁶⁰⁰⁻⁶⁰². It would be interesting to determine whether inflammasome-mediated cleavage of ribosome components is related to these local translation events, and whether that could explain the Caspase-1-dependent control of synapse abundance that we identified in the present study.

Secondly, vimentin is thought to be specifically enriched in astrocytes and epithelial cells in the brain⁶⁰³. Like GFAP, vimentin is an intermediate filament protein that contributes to astrocyte morphology, process motility, protein scaffolding, and vesicle trafficking, which can ultimately influence learning and memory^{604,605}. The actin cytoskeleton of astrocytes likewise performs a similar set of critical functions⁶⁰⁶. The idea that the inflammasome can cleave vimentin and actin given the importance of these proteins for astrocyte biology certainly warrants the further investigation of this potential connection. Indeed, our studies report preliminary evidence that astrocyte reactivity (measured by GFAP and S100 β levels) is affected by the loss of Caspase-1.

It is quite likely that the Caspase-1 substrate cleavage profile is different based upon the cell type harboring the assembled inflammasome and/or brain region of interest. The inflammasome cleavage targets could be different based upon cell state to allow for dynamic modulation of inflammasome function. These factors could dictate the functional consequence of inflammasome activation in the brain.

Beyond the downstream impacts of inflammasome activation discussed thus far, it also remains to be determined what the physiologic endogenous triggers of the inflammasome might be in the brain. What's more, the obligate sensor also remains anonymous. Recent attention has fallen on the finding that astrocytes express the inflammasome sensor NLRP2, and that astrocyte NLRP2 responds to physiologic changes in brain state including depression and persistent pain⁶⁰⁷⁻⁶⁰⁹.

In one such study, kynurenine, a metabolite of tryptophan, upregulated NLRP2 in astrocytes, which activated the NLRP2 inflammasome in astrocytes upon pairing with ATP⁶⁰⁹. Indeed, studies in human astrocytes further support the idea that NLRP2 can be activated by ATP due to close association with purinoreceptors and pannexin channels⁶⁰⁸. These studies identify potential endogenous triggers of astrocyte inflammasomes, namely, neurotransmitter/metabolic byproducts and ATP, which could potentially explain some of the inflammasome activation we report in astrocytes that contributes to hippocampal physiology and memory function.

Another inflammasome sensor worth exploring is the promiscuous NLRP3. Of all inflammasome sensors, NLRP3 has been the most widely explored to date in the brain. NLRP3 can respond to a wide variety of stimuli, including oxidative stress, reactive oxygen species (ROS), lysosomal damage, ion fluxes, mitochondrial disruption, and ribosomal stress⁶¹⁰. Environmental stressors can trigger oxidative stress, which may generate ROS and oxidized mitochondrial DNA that can activate the NLRP3 inflammasome⁶¹¹. Ribotoxic stress can also trigger inflammasome activation^{612,613}, which is interesting given the potential that the inflammasome may also cleave ribosomal proteins⁵⁹⁹, suggestive of a possible feedback loop.

The identification of a homeostatic role for the inflammasome in the brain opens the door wide for many future studies probing the more precise signal cascades involved. Such studies will continue to reveal the neurobiology underlying important functional states in the brain, as well as inform future treatments for neurologic disease.

4.2 Future directions

4.2.1. Homeostatic Neuronal Inflammasome Activation

Our studies at present have only investigated inflammasome activation in a specific manner within astrocytes. Yet, immunohistochemistry reveals that ASC specks can be found within neurons as well as surrounding neuronal projections (Figure 3.10, 3.11). To what extent are the reported changes in neuronal physiology (i.e. higher spine density, increased in synapse marker abundance, dampened neuronal activity) following VX-765 treatment attributed to neuron-intrinsic inflammasome activation relative to neuron-extrinsic inflammasome activation in astrocytes? The function of homeostatic inflammasome activation within neurons compared to astrocytes remains a ripe area for future study.

Indeed, blocking inflammasome activation specifically in astrocytes via Caspase-1 knockout did not fully phenocopy the results we found after treating mice with the Caspase-1 inhibitor, VX-765. In particular, acute blockade of the inflammasome actually heightened neuronal activation in Casp1^{ΔAst (acute)} mice as assessed by relative baseline cFos levels (Figure 3.17E-G). Meanwhile, VX-765 treatment dampened physiologic neuronal activity in studies conducted outside of Chapter 3 (see Chapter 4, Figure 4.6). Moreover, Casp1^{ΔAst (acute)} mice did not display significantly enhanced spatial memory in a 24 hr contextual fear conditioning test (Figure 3.16A) as VX-765-treated mice did (Figure 3.6B). This discrepancy in results could be explained by a multitude of factors, including inhibitor specificity, effects on peripheral cells outside of the CNS, and inhibitor potency. One potential explanation, however, is that inhibition of neuronal inflammasomes in the case of VX-765 treatment contributes in part to the reported phenotypes.

To address the question of whether inflammasomes have homeostatic function within neurons, we have generated inducible neuron-specific Caspase-1 knockout mice. We crossed Casp1^{fl/fl} mice with Camk2a^{Cre-ERT2} mice to ablate Caspase-1 function in excitatory neurons following tamoxifen treatment (Casp1^{ΔExNeur}). We will repeat all key experiments conducted thus far in these Casp1^{ΔExNeur} mice compared to Cre-negative littermate

controls (Casp1^{cont}), including memory assessments, western blots for synapse markers, cFos staining at baseline and following novel environment exposure, and immunohistochemistry for synapse markers, astrocyte reactivity, and extracellular matrix. Comparing these results to those generated using Casp1^{ΔAst} mice will reveal relative cell-intrinsic and -extrinsic roles for Caspase-1 during adult homeostasis.

Beyond these proposed experiments, deeper questions still remain as to homeostatic inflammasome signal cascades. What stimuli are triggering inflammasome activation at baseline? What putative sensor(s) are becoming activated? What protein targets are cleaved? What is the consequence of Caspase-1-mediated cleavage events? Are the answers to these questions dependent upon the cell type, and/or brain region? Our studies have only begun to scratch the surface of the underlying biology of homeostatic inflammasome function in the brain.

4.2.2. The Relative Contribution of IL-33 to Inflammasome-Mediated Control of Neuronal Plasticity

Our study found that loss of Caspase-1 function in astrocytes led to heightened production of the alarmin IL-33. IL-33 can be produced by astrocytes and neurons alike in the adult hippocampus^{581,582}. Interestingly, the loss of Caspase-1 activity specifically in astrocytes appeared to increase the production of IL-33 by both astrocytes and neurons (Figure 3.18). This result points toward both a cell-intrinsic role of inflammasome-mediated IL-33 production in astrocytes, as well as a cell-extrinsic role in which some yet-unidentified factor produced by astrocyte inflammasomes modulates neuronal IL-33 production.

To what extent does astrocyte-derived versus neuron-derived IL-33 alter neuronal physiology? One study found that neuronal IL-33 release signals via microglial ST2 to direct engulfment of the extracellular matrix by microglia, and that this process underlies neuronal plasticity and memory function⁵⁸¹. Another study found that changes in neuronal activity can trigger astrocyte IL-33 release, which then feeds back to promote synapse formation and memory function⁵⁸². In particular, the loss of IL-33 production by astrocytes and ST2 activation prevents activity-dependent synapse formation⁵⁸². In both studies, IL-33 promotes synaptic plasticity, no matter the cellular source.

Notably, astrocytes and neurons produce distinct isoforms of IL-33 in the adult hippocampus, whereby neurons express *Il33a* and astrocytes express *Il33b*⁵⁸¹. This dichotomy could underlie the diverse roles of IL-33 in the hippocampus. Yet, there has only been a single IL-33 receptor, ST2, that has been identified to date. Therefore, each isoform may converge upon the same surface receptor upon release. Whether each isoform leads to distinct downstream signaling cascades due to binding affinity or co-receptor signaling is yet to be determined within the CNS.

We have generated mice with loss of astrocyte IL-33 function (*Il33^{fl/fl};Aldh111^{Cre-ERT2}*) to address whether the changes in neuronal physiology that we observed in our Casp1^{ΔAst} mice are phenocopied. We will repeat all key experiments (immunohistochemistry for cFos, synapse markers, astrocyte reactivity, and extracellular matrix; memory assessments) in these *Il33^{fl/fl};Aldh111^{Cre-ERT2}* (*Il33^{ΔAst}*) mice compared to littermate Cre-negative controls (*Il33^{cont}*). This will answer the question as to whether the inflammasome largely regulates astrocyte IL-33 release, or if another mechanism of release is also at play. Moreover, these experiments will help to address whether astrocyte inflammasome-mediated release of IL-33 is largely responsible for the changes to astrocyte and neuron physiology, or whether another cleavage product also contributes to these effects.

4.2.3. Inflammasome Function Within the Hippocampus

Our experiments conducted and proposed thus far target Caspase-1 in cells broadly throughout the brain. Yet, we have generally assessed the impact of this Caspase-1 ablation centrally in the hippocampus. As the hippocampus receives inputs from many regions (i.e. entorhinal cortex, various cortical regions, amygdala, olfactory bulb) it remains a possibility that our Caspase-1 ablation is not acting directly within the hippocampus,

but instead affects cell biology in hippocampus-projecting region which then has downstream effects on the hippocampus. Thus, the ideal experiment would target Caspase-1 function in a cell- and region-specific manner to address how inflammasome activation locally modulates hippocampal neuron physiology and memory function.

To address this question, we utilized adeno-associated virus (AAV)-driven genetic ablation of Caspase-1 function in either astrocytes or neurons via intrahippocampal injection. More specifically, we injected bilaterally into the hippocampus of $Thy1^{YFP};Casp1^{fl/fl}$ mice either AAV9-GFAP-mCherry-Cre to target astrocytes, AAV9-eSyn-mCherry-Cre to target neurons, or respective Cre-lacking control vectors (AAV9-GFAP-mCherry, AAV9-eSyn-RFP). This strategy allows for cell-type specific Caspase-1 ablation in the hippocampus paired with the ability to assess neuronal structure using the $Thy1^{YFP}$ transgene. Mice were allowed two weeks to recover from surgery and were then subject to behavior studies and downstream brain immunohistochemistry.

We first verified that the AAVs correctly targeted the cells of interest and remained within the hippocampus (Figure 4.1) by AAV-driven fluorescent reporter mCherry/RFP expression. Hippocampi of mice injected with AAV9-GFAP-mCherry-Cre ($Casp1^{AAV-\Delta Ast}$) only showed reporter labeling in $Aldh111+$ astrocytes with no infection of $Thy1+$ neurons (Figure 4.1A). Similarly, hippocampi of mice injected with AAV9-eSYN-mCherry-Cre ($Casp1^{AAV-\Delta Neur}$) only showed reporter labeling in $Thy1+$ neurons with no infection of GFAP+ astrocytes (Figure 4.1B). Thus, Caspase-1 expression could successfully be ablated in the targeted cell populations using these AAVs.

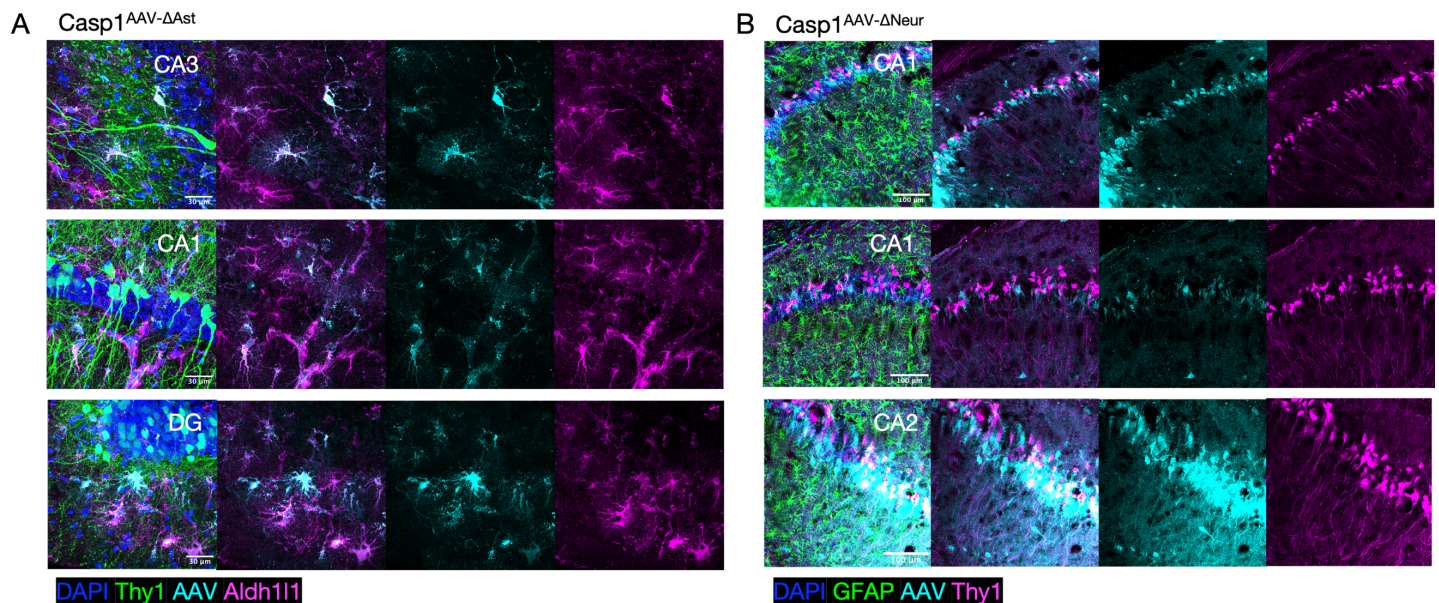


Figure 4.1. Verification of AAV targeting specificity in the hippocampus.

Bilateral hippocampal AAV injections were conducted in $Thy1^{YFP};Casp1^{fl/fl}$ mice 8-10 weeks of age. AAVs were designed to knock out *Casp1* in astrocytes (AAV9-GFAP-mCherry-Cre; $Casp1^{AAV-\Delta Ast}$) or neurons (AAV9-eSYN-mCherry-Cre; $Casp1^{AAV-\Delta Neur}$), paired with respective Cre-lacking control vectors (AAV9-GFAP-mCherry or AAV9-eSYN-RFP; $Casp1^{AAV-cont}$). Mice were allowed two weeks to recover prior to behavioral studies and brain harvest. Immunohistochemistry was conducted to verify AAV cell targeting specificity in the hippocampus. (A) AAV9-GFAP-mCherry-Cre is specific for $Aldh111+$ astrocytes and does not infect $Thy1+$ neurons. (B) AAV9-eSYN-mCherry-Cre is specific for $Thy1+$ neurons and does not infect GFAP+ astrocytes.

Behavioral studies were then conducted on $Casp1^{AAV-\Delta Ast}$ and $Casp1^{AAV-\Delta Neur}$ mice paired with their respective Cre-lacking AAV controls (AAV9-GFAP-mCherry or AAV9-eSYN-RFP; $Casp1^{AAV-cont}$). $Casp1^{AAV-\Delta Ast}$ showed no significant changes in baseline locomotory behavior on the open field (Figure 4.2A,B) or anxiety-related behavior on the open field and elevated plus maze tasks (Figure 4.2A-C). $Casp1^{AAV-\Delta Ast}$ mice were also able to distinguish between a novel and a familiar object to similar levels as controls on the novel object recognition task (Figure 4.2D). $Casp1^{AAV-\Delta Ast}$ mice also showed no difference in short-term spatial memory as assessed by the novel object location task (Figure 4.2E) and Y maze (Figure 4.2F). Meanwhile, $Casp1^{AAV-\Delta Ast}$ mice forgot the fear associated with the trained context faster than controls in a fear extinction paradigm (Figure 4.2G). This was specific to the context itself, as testing the trained cue at the final time point 11 weeks post-training revealed no

difference in freezing behavior between $Casp1^{AAV-\Delta Ast}$ mice and controls (Figure 4.2H). Indeed, $Casp1^{AAV-\Delta Ast}$ mice were no longer able to distinguish between fear associated with the trained context compared to an untrained novel context when assessed 11 weeks post-training (Figure 4.2I).

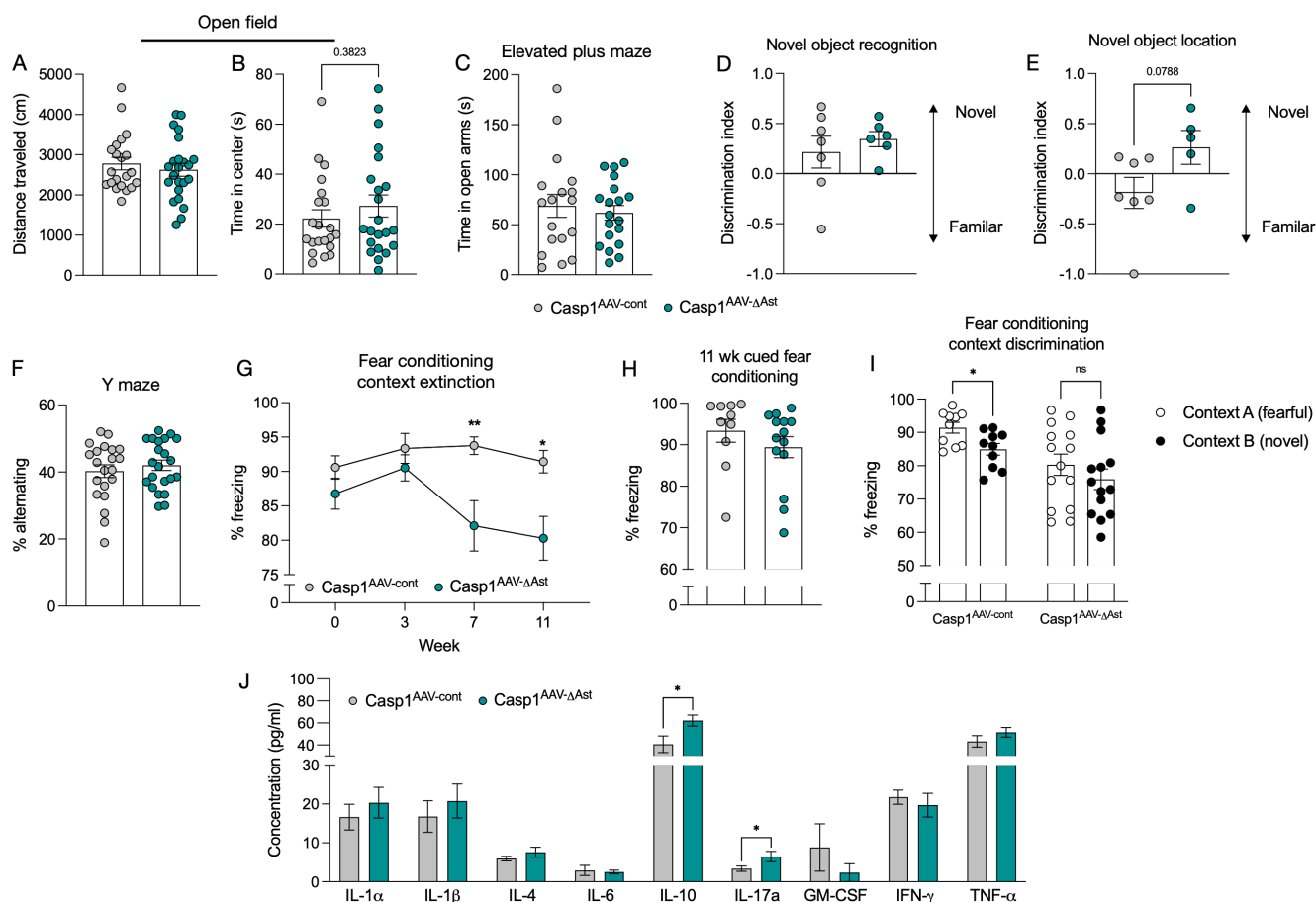


Figure 4.2. Behavioral and hippocampal cytokine analyses of $Casp1^{AAV-\Delta Ast}$ mice.

Bilateral hippocampal AAV injections were conducted in $Thy1^{YFP};Casp1^{fl/fl}$ mice 8-10 weeks of age. AAVs were designed to knock out $Casp1$ function in astrocytes (AAV9-GFAP-mCherry-Cre; $Casp1^{AAV-\Delta Ast}$) paired with a respective Cre-lacking control vector (AAV9-GFAP-mCherry; $Casp1^{AAV-cont}$). Mice were allowed two weeks to recover prior to behavioral studies and brain harvest. (A,B) General locomotion and exploratory behavior was assessed using the open field test. (A) Distance traveled over the entire test period. (B) Time spent in center of the arena. (C) Anxiety-like behavior was assessed using the elevated plus maze. Total time spent in the open arms were quantified. (D) Object recognition was assessed using the novel object recognition task, in which animals were presented with two identical objects in the training phase and then tested with that familiar object against a novel object 2 hr later. A discrimination index was calculated based on time spent interacting with each object in the 5-min test phase. (E) Short-term spatial memory was assessed using the novel object location task, in which animals were presented with two identical objects in the training phase and then tested when one object was moved to a new location 2 hr later. A discrimination index was calculated based on time spent interacting with each object in the 5-min test phase. (F) Spatial working memory was assessed using the Y maze. Total number of alternations was divided by the total number of arm entries to calculate the measure of percent alternating. (G-I) Short-term and remote memory was assessed by fear conditioning. (G) After tone-shock training, hippocampal-dependent memory was assessed by context testing and mice were assessed 0 weeks (24 hours), 3 weeks, 7 weeks, and 11 weeks post-training. Percent time spent immobile during the context test as assessed on consecutive test sessions. (H) After tone-shock training, hippocampal-independent memory was assessed by cue testing. Percent time spent immobile during the cue test conducted 11 weeks after training. (I) Discrimination between the trained (familiar) context and an untrained (novel) context was assessed 11 weeks after training. Percent time spent immobile in each context was used to calculate a discrimination index where 1 indicates full relative immobility in the familiar context and -1 indicates full relative immobility in the novel context. (J) A BioPlex multiplex cytokine array was conducted on hippocampal homogenates collected from $Casp1^{AAV-\Delta Ast}$ and $Casp1^{AAV-cont}$ mice 90 days post-AAV injection. Relative cytokine concentration levels are shown. Each point represents an individual mouse (A-F,H,I) or the average of all mice in the group (G). Statistical significance calculated by unpaired Student's t-test (A-F,H), two-way ANOVA with Sidak's multiple comparisons test (G), multiple paired t-tests (I), or multiple unpaired t-tests (J). Error bars indicate mean \pm s.e.m. * $P < 0.05$, ** $P < 0.01$.

Brains were then harvested from $Casp1^{AAV-\Delta Ast}$ and control mice, homogenized, and cytokine levels were measured using a multiplex cytokine array. Most tested cytokines could be detected at least at low levels in these hippocampal homogenates (Figure 4.2J). $Casp1^{AAV-\Delta Ast}$ hippocampi has significantly higher levels of IL-10 and IL-17a compared to controls (Figure 4.2J).

We next repeated select behavior assays on $Casp1^{AAV-\Delta Neur}$ mice and their respective Cre-lacking AAV controls (AAV9-eSYN-RFP; $Casp1^{AAV-cont}$). $Casp1^{AAV-\Delta Neur}$ showed no significant changes in baseline locomotory behavior

or anxiety-related behavior on the open field (Figure 4.3A,B). While not reaching significance, *Casp1*^{AAV-ΔNeur} mice trended towards hyperactive and impaired spatial working memory phenotypes when tested in the Y maze (Figure 4.3C-E). Specifically, *Casp1*^{AAV-ΔNeur} mice appeared to travel a greater distance during the task (Figure 4.3C) and revisit recently visited arms more frequently (Figure 4.3E) without noticeable changes in arm alternations (Figure 4.3D). *Casp1*^{AAV-ΔNeur} mice also displayed a trend toward short- and long-term spatial memory impairments in a fear conditioning task (Figure 4.3F-J). In particular, they tended to freeze less in the context test conducted 24 hours and 3 weeks after training (Figure 4.3G,I) even though they tended to move more than controls in the context prior to training (Figure 4.3F). Meanwhile, associative memory was not impacted in these animals, as *Casp1*^{AAV-ΔNeur} mice froze to similar levels as controls in the cue test conducted 24 hours and 3 weeks post-training (Figure 4.3H,J).

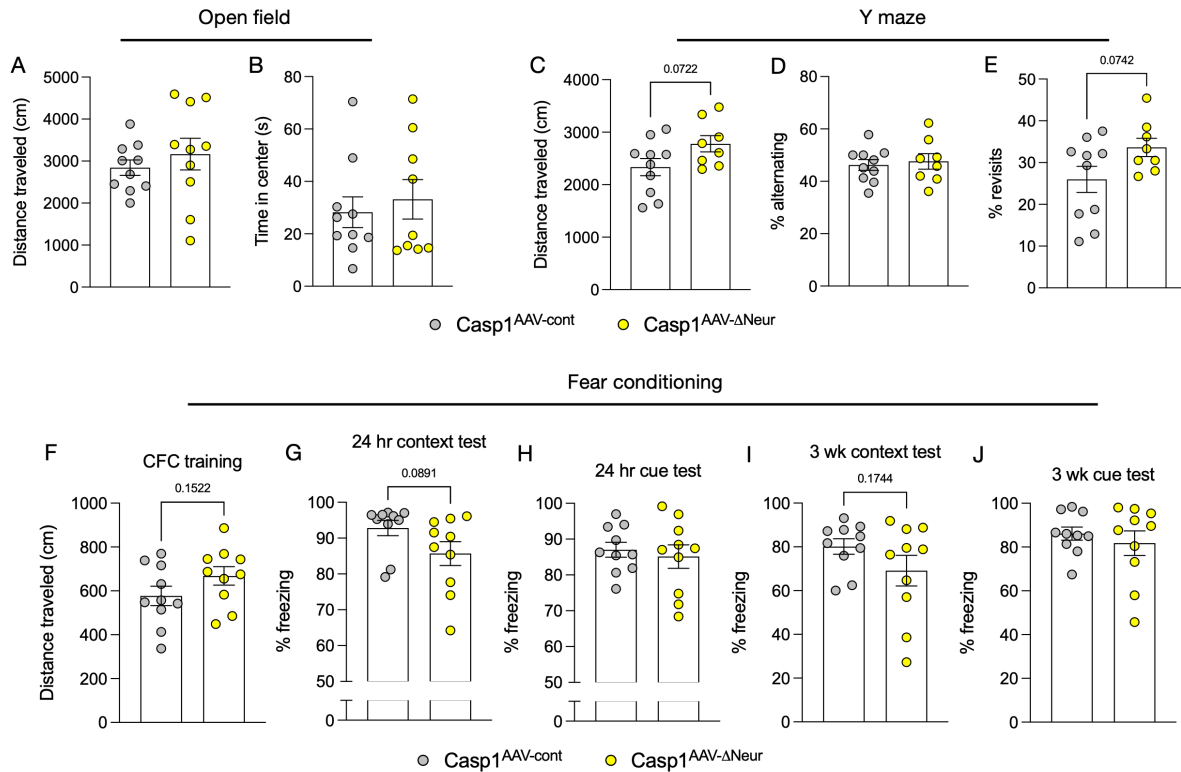


Figure 4.3. Behavioral analysis of *Casp1*^{AAV-ΔNeur} mice.

Bilateral hippocampal AAV injections were conducted in *Thy1*^{YFP};*Casp1*^{fl/fl} mice 8-10 weeks of age. AAVs were designed to knock out *Casp1* function in neurons (AAV9-eSYN-mCherry-Cre; *Casp1*^{AAV-ΔNeur}) paired with a respective Cre-lacking control vector (AAV9-eSYN-RFP; *Casp1*^{AAV-cont}). Mice were allowed two weeks to recover prior to behavioral studies and brain harvest. (A,B) General locomotion and exploratory behavior was assessed using the open field test. (A) Distance traveled over the entire test period. (B) Time spent in center of the arena. (C-E) Spatial working memory was assessed using the Y maze. (C) Distance traveled over the entire test period. (D) Total number of alternations was divided by the total number of arm entries to calculate the measure of percent alternating. (E) Total number of arm revisits was divided by the total number of arm entries to calculate the measure of percent revisits. (F-J) Short- and long-term memory was assessed by fear conditioning. (F) Baseline locomotory behavior was assessed for 3 min prior to tone-shock pair training. Distance traveled over this entire test period is shown. (G-J) After tone-shock training, hippocampal-dependent memory was assessed by context testing (G,I) and hippocampal-independent memory was assessed by cue testing (H,J). Mice were assessed 24 hours (G,H) and 3 weeks (I,J) post-training. (G) Percent time spent immobile during the context test conducted 24 hours after training. (H) Percent time spent immobile during the cue test conducted 24 hours after training. (I) Percent time spent immobile during the context test conducted 3 weeks after training. (J) Percent time spent immobile during the cue test conducted 3 hours after training. Each point represents an individual mouse. Statistical significance calculated by unpaired Student's t-test. Error bars indicate mean \pm s.e.m.

These results of possible memory impairments in both groups of Cre-injected mice led us to wonder the extent to which infected cells persisted in the hippocampus long-term after AAV injection. Immunohistochemistry was conducted on brains collected from all treatment groups 60- and 90-days post-injection (dpi) to answer this question. We first verified that control vectors lacking Cre could be detected 60 dpi in the hippocampi of *Thy1*^{YFP};*Casp1*^{fl/fl} (*Casp1*^{AAV-cont}) mice in which reporter fluorescence was visible (Figure 4.4A,C; left). In *Casp1*^{AAV-cont} mice injected with either AAV9-GFAP-mCherry or AAV9-eSYN-RFP, GFAP+ astrocytes and *Thy1*+ neurons were also present 60 dpi in the hippocampus (Figure 4.4A,C; left, insets). Surprisingly, mice injected with either AAV9-GFAP-mCherry-Cre or AAV9-eSYN-mCherry-Cre eventually lost reporter expression and the targeted cell type over time (Figure 4.4). While mCherry+GFAP+ astrocytes were observed 60 dpi (Figure 4.4A,

right), by 90 dpi there were no longer any mCherry+Aldh111+ astrocytes in the hippocampus (Figure 4.4B, bottom). While Aldh111+ astrocytes persisted in the hippocampi of AAV9-GFAP-mCherry control animals 90 dpi, there was marked loss of Aldh111+ astrocytes in Cre-injected mice by this time point (Figure 4.4B). Similarly, reporter expression was low-to-undetectable 60 dpi in mice injected with AAV9-eSYN-mCherry-Cre, which was associated with an almost complete loss of Thy1+ neurons in the hippocampus (Figure 4.4C, right). Thus, Cre-expressing target cell populations appeared to undergo ablation long-term following AAV injection. These findings likely explain the memory impairments observed in $Casp1^{AAV-\Delta Ast}$ and $Casp1^{AAV-\Delta Neur}$ mice (Figure 4.2, 4.3).

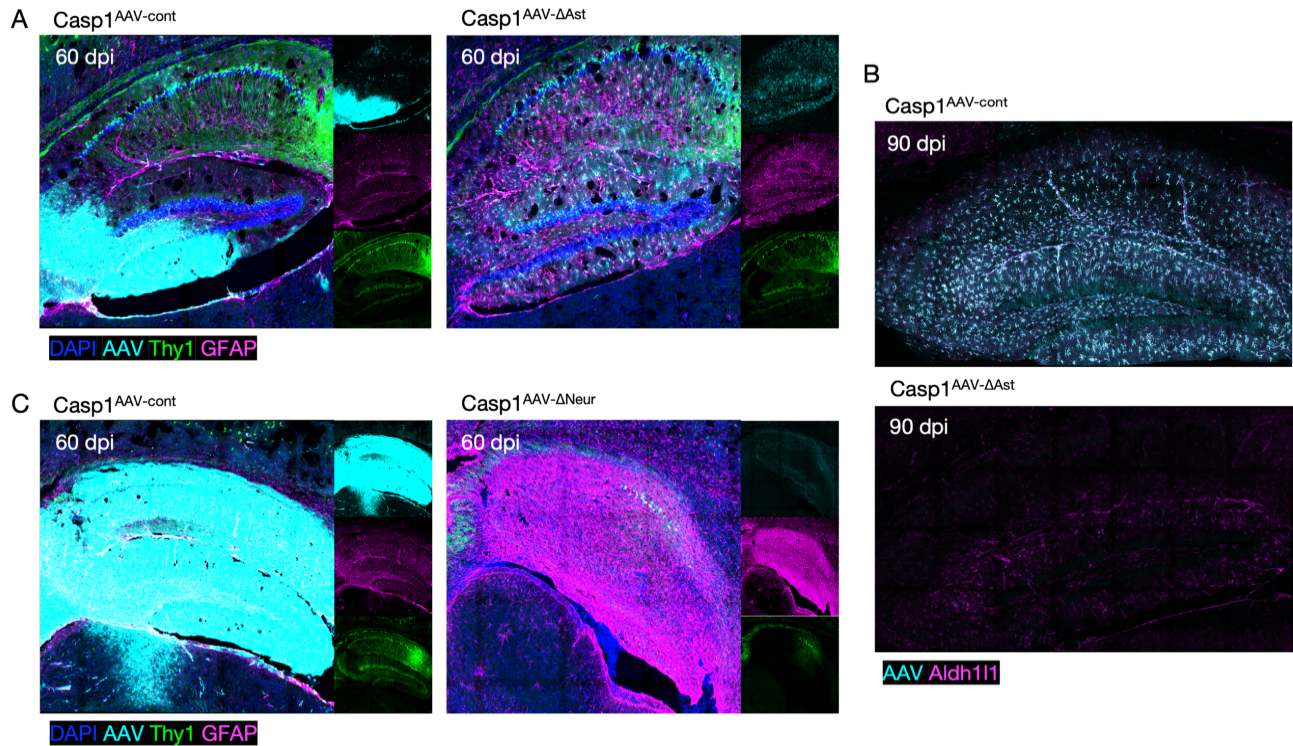


Figure 4.4. Long-term AAV presence in the hippocampus of $Casp1^{AAV-\Delta Ast}$ and $Casp1^{AAV-\Delta Neur}$ mice.

Bilateral hippocampal AAV injections were conducted in $Thy1^{YFP};Casp1^{fl/fl}$ mice 8-10 weeks of age. AAVs were designed to knock out *Casp1* in astrocytes (AAV9-GFAP-mCherry-Cre; $Casp1^{AAV-\Delta Ast}$) or neurons (AAV9-eSYN-mCherry-Cre; $Casp1^{AAV-\Delta Neur}$), paired with respective Cre-lacking control vectors (AAV9-GFAP-mCherry or AAV9-eSYN-RFP; $Casp1^{AAV-cont}$). Mice were allowed two weeks to recover prior to behavioral studies and brain harvest. Immunohistochemistry was conducted to assess long-term AAV presence 60- and 90-days post-injection (dpi). (A-B) AAV9-GFAP vectors are specific for GFAP+ and Aldh111+ astrocytes and do not infect Thy1+ neurons. (A) mCherry+ astrocytes can be observed in $Casp1^{AAV-cont}$ and $Casp1^{AAV-\Delta Ast}$ hippocampi 60 dpi. Right insets show individual channels. (B) mCherry+ astrocytes can be observed in $Casp1^{AAV-cont}$ hippocampi 90 dpi, but mCherry+ astrocytes no longer detectable in $Casp1^{AAV-\Delta Ast}$ hippocampi 90 dpi. Further, Aldh111 expression is markedly reduced in $Casp1^{AAV-\Delta Ast}$ hippocampi 90 dpi. (C) AAV9-eSYN vectors are specific for Thy1+ neurons and do not infect GFAP+ astrocytes. RFP+ neurons can be observed in $Casp1^{AAV-cont}$ hippocampi 60 dpi (left) but mCherry+ neurons are not observable in $Casp1^{AAV-\Delta Neur}$ hippocampi 60 dpi (right). Further, Thy1 expression is markedly reduced in $Casp1^{AAV-\Delta Neur}$ hippocampi 60 dpi. Right insets show individual channels.

How exactly Cre-driven ablation of target cell types occurred is unknown. One potential explanation is that AAV-harboring cells require Caspase-1 for survival after infection. Another possibility is that the titer of AAV injected was too high and the level of Cre within infected cells reaches a critical threshold for toxicity. Injecting these AAV-Cre constructs into wild type (non- $Casp1^{fl/fl}$) mice will help distinguish between these two potential possibilities. Until then, it remains a question as to whether inflammasome activity in regions projecting to the hippocampus impact neuronal physiology in the region.

4.2.4. Inflammasomes in Seizure Propagation

Seizures are caused by sudden bursts of neuronal firing which can lead to involuntary movements (i.e. jerks, convulsions, stiffness) sometimes accompanied by loss of awareness, consciousness, sensation, and/or bowel function⁶¹⁴. Severe seizures can cause death⁶¹⁴. If an individual has two or more unprovoked seizures then they

are categorized as having epilepsy⁶¹⁴. More than 50 million people worldwide are affected by epilepsy with 80% of cases being in low- and middle-income countries⁶¹⁴. A wide range of factors can contribute to the development of epilepsy including genetics, congenital brain malformations, brain trauma (loss of oxygen, head injury, stroke), CNS infections, metabolic diseases, brain tumors, and more^{614,615}.

Anti-seizure medications can control up to 70% of epilepsy-related seizures and surgery may be an option for certain refractory cases⁶¹⁴. Yet, anti-seizure medications have unwanted side effects, may eventually cause drug-resistance, or be completely ineffective for some individuals⁶¹⁶. Thus, a need for alternative seizure treatment strategies exists.

Inflammation is increasingly found to both contribute to bouts of neuronal hyperactivity, the primary cause of seizures, as well as be a consequence of such⁶¹⁵. Various inflammatory pathways have been linked to seizures, of which, pro-inflammatory cytokine release stands at the forefront⁶¹⁵. One such family of cytokines is the IL-1 family which is potently pro-inflammatory and is consistently linked to many forms of epilepsy^{615,617}. Indeed, blocking IL-1 can provide protection in various seizure models^{615,617-619}. However, delivering IL-1 neutralizing antibodies into the brain has proven difficult and global IL-1 blocking strategies can increase susceptibility to infections⁶¹⁷.

Given the necessity of the inflammasome in orchestrating active IL-1 cytokine release, this innate immune complex is becoming an investigation focus for novel anti-seizure targets⁶¹⁵. A body of literature has found NLRP1 and NLRP3 inflammasomes contribute to seizure severity and epilepsy development in an array of model systems⁶¹⁵. As such, inhibition of proper inflammasome function is consistently found to lower seizure susceptibility and improve symptoms of epilepsy⁶¹⁵. Indeed, the Caspase-1 inhibitor VX-765 entered phase 2b clinical trial for the treatment of epilepsy⁶²⁰.

Consistent with published studies, we found inflammasome activation to be associated with seizure activity in our own studies. We used a kainic acid (KA) model in which seizures are caused by neuronal hyperexcitability driven by glutamate receptor agonism, particularly in the hippocampus^{621,622}. qPCR probing various inflammasome components revealed elevated brain expression levels of *Nlrp3* and *Il1b* after seizure induction (Figure 4.5A). No changes in ASC speck levels were seen 2.5 hr after seizure induction (Figure 4.5B,C). Future experiments will probe inflammasome component expression and ASC speck levels during active seizures by harvesting mice upon seizure onset. As well, mice will be harvested 6- and 24-hrs post-KA administration to assess inflammasome activation sub-acutely following a bout of seizure activity but once baseline behavior has resumed.

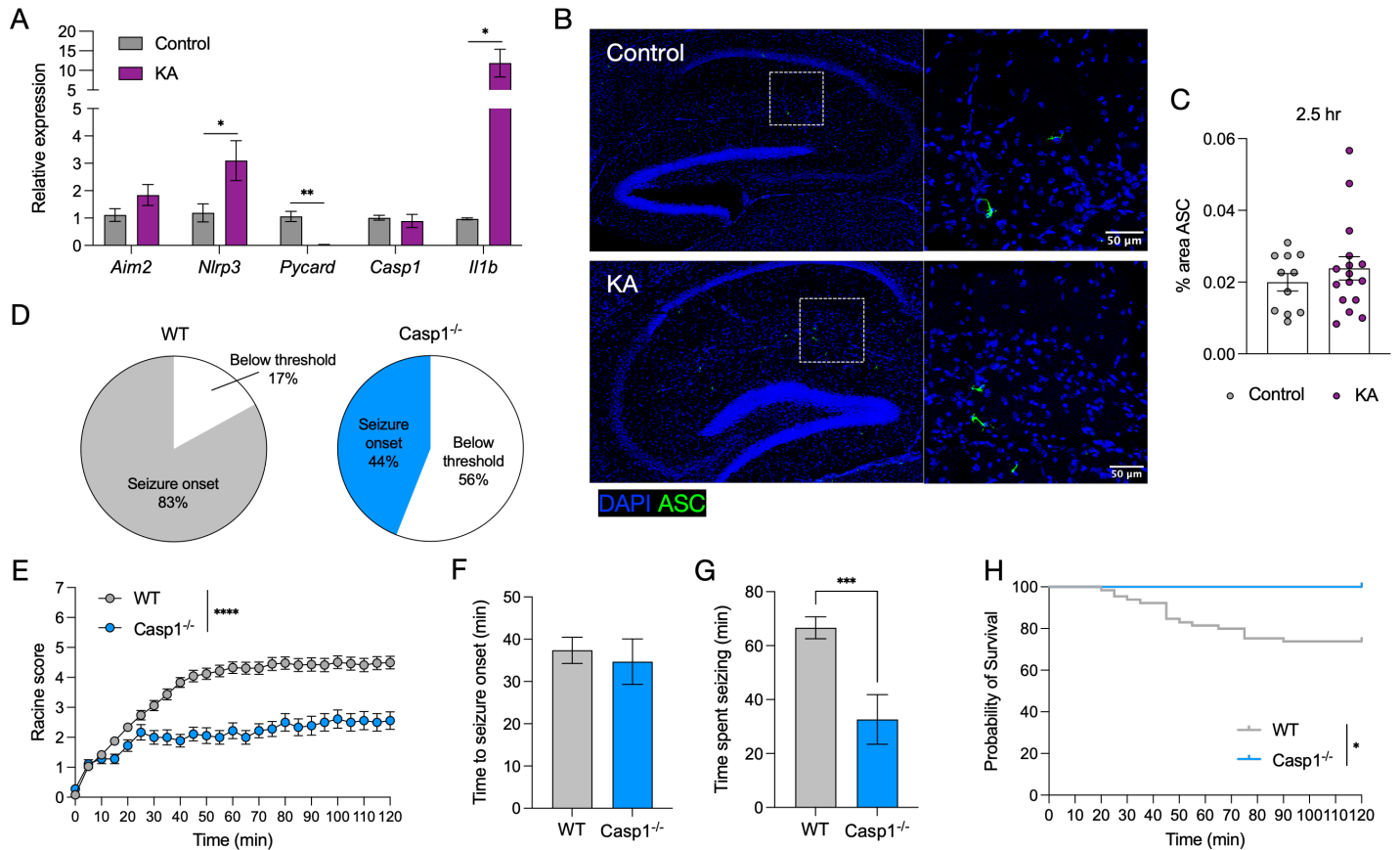


Figure 4.5. Inflammation activation propagates seizure progression.

Six-week old wild type (WT), ASC^{Citrine}, Casp1^{-/-} mice were injected i.p. with 24 mg/kg kainic acid (KA) to induce seizures. (A) Brains were harvested from WT mice 2.5 hrs after KA injection or from age-matched WT no treatment controls. RNA was extracted from half-brain homogenates, cDNA synthesized, and qPCR conducted to assess relative expression of inflammasome complex components. N = 2-5 per group. (B,C) Brains were harvested from ASC^{Citrine} mice 2.5 hrs after KA injection or from age-matched ASC^{Citrine} no treatment controls. Representative images (B) and quantification (C) of ASC specks in the hippocampus after seizure compared to baseline. N = 11 (No seizure controls), N = 16 (KA). (D-H) WT and Casp1^{-/-} mice were scored for seizure severity for 2 hrs beginning immediately after KA injection. Seizure severity was scored over time assessed using a modified Racine scale, with a score of 0 indicating baseline activity and a score of 7 indicating death. N = 65 (WT), N = 18 (Casp1^{-/-}). (D) Pie charts showing relative rates of seizure onset in WT compared to Casp1^{-/-} mice. A Racine score of 3 was used to indicate seizure onset, such that “below threshold” indicates a score of 3 was never reached within the 2 hrs of scoring time. (E) Seizure activity was scored every 5 min and severity plotted over time. (F) Time to seizure onset (Racine score 3) for mice that actively seized during the two-hour scoring time post-KA administration. (G) Once a Racine score of 4 was reached, mice were scored at a minimum of a score of 4 from that point forward. The sum of this time is summarized as time spent seizing. (H) Survival curve over two hours post-administration of KA, where Racine score 7 indicates death. Data combined from at least three independent experiments (D-H). Each data point represents an individual mouse (C), or the average of every mouse within the group (E). Male and female mice were used for all experiments. Statistical significance calculated by multiple unpaired Student’s t-test (A), unpaired Student’s t-test (C,F,G), two-way ANOVA (E), or Gehan-Breslow-Wilcoxon test (H). Error bars indicate mean +/- s.e.m. *P < 0.05, **P < 0.01, ***P < 0.001, ****P < 0.0001.

Given the correlation between inflammasome activation and seizure onset that we observed, we next investigated whether blocking inflammasome activation could protect from seizure propagation in our KA mouse model, consistent with similar studies⁶¹⁵. We injected wild type (WT) and Caspase-1-deficient mice (Casp1^{-/-}) with KA to induce seizure activity and scored seizure severity using a modified Racine scale⁶²³. In these studies, we found that Casp1^{-/-} mice were largely protected from severe seizures compared to WT controls (Figure 4.5D-H). While 83% of control animals exhibited significant seizure activity following KA injection, only 44% of Casp1^{-/-} animals reached this level of seizure activity (Figure 4.5D). Casp1^{-/-} mice had dramatically lower seizure severity over the course of scoring (Figure 4.5E), though the time to reach seizure onset was not impacted (Figure 4.5F). Indeed, Casp1^{-/-} mice spent markedly reduced time seizing during this scoring period compared to controls (Figure 4.5G) and were completely protected from seizure-induced death (Figure 4.5H).

These results showing that Caspase-1 can modulate neuronal hyperexcitability that drives kainic acid-induced seizures led us to question whether a feedback loop exists between neuronal activity and inflammasome activation. To first test whether blocking inflammasome activation indeed limits neuronal activity in the hippocampus, we leveraged the cFos^{Cre-ERT2} LSL-tdTomato (“TRAP2”, denoted as TRAP;tdTomato hereafter) in

which activated neurons can be fluorescently marked in a time-dependent manner. We sought to determine whether blocking inflammasome activation using the Caspase-1 inhibitor VX-765 would subsequently block hippocampal neuron activation. As such, we injected TRAP;tdTomato mice with VX-765 or vehicle control prior to tamoxifen administration, and then exposed these mice to a novel enriched environment to induce hippocampal neuronal activity in a physiologic manner (Figure 4.6A). As expected, 48 hr exposure to the enriched environment induced robust neuron activity in the hippocampus, which was fluorescently trapped in control mice (Figure 4.6B-D). Mice treated with the Caspase-1 inhibitor VX-765 were found to have significantly less tdTomato+ trapped area in the hippocampus (Figure 4.6B,C) corresponding to a lower number of trapped neurons (Figure 4.6B,D) compared to vehicle controls. Thus, blocking inflammasome activation is sufficient to dampen neuronal activity, even at physiologic levels. These data suggest that VX-765 treatment for epilepsy may work by limiting the pathogenic neuronal activity driving seizure propagation.

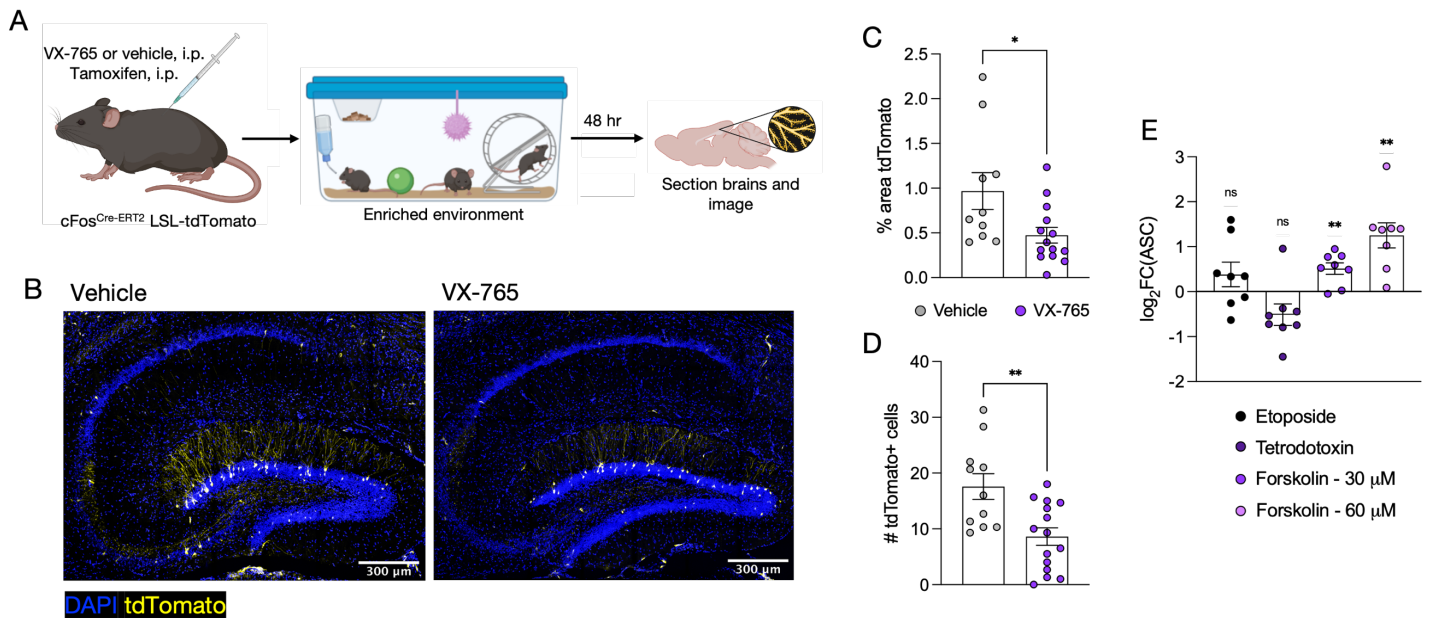


Figure 4.6. The inflammasome and neuronal activity are bidirectionally modulated.

The relationship between neuronal activity and inflammasome activation in the hippocampus was studied by manipulating inflammasome function or neuronal activity levels. (A-D) 8-10-week old TRAP;tdTomato (cFos^{Cre-ERT2} LSL-tdTomato) mice were injected i.p. with 50 mg/kg VX-765 or vehicle control, left to rest for 10 min, and then injected with 150 mg/kg tamoxifen. After 30 min, mice were placed into an enriched environment for 48 hrs. Mice were then perfused and brains were harvested for immunofluorescence microscopy to assess relative levels of neuronal activity. (A) Experimental design. (B-D) tdTomato signal was assessed in the entire hippocampus of VX-765 and vehicle control mice. (B) Representative images. Quantification of the percent area of total hippocampal coverage of tdTomato+ area (C) and count of the number of tdTomato+ neurons (D). (E) Primary mixed hippocampal cultures collected from ASC^{Citrine} pups were treated with etoposide to induce DNA damage (as a positive control), tetrodotoxin to block neuronal activity, or forskolin to induce neuronal activity for 12 hr. Cultures were fixed, stained, and imaged by confocal microscopy to assess ASC speck levels per FOV. The presence of ASC specks was determined relative to untreated control cultures. Relative ASC speck levels within each treatment are plotted as log₂FC, where zero indicates equal expression, positive numbers indicate elevated ASC speck levels, and negative numbers indicate lower ASC speck levels relative to untreated control cultures. Each point represents an individual mouse (C,D) or an individual well (E). Statistical significance calculated by unpaired Student's t-test (C,D) or one sample t and Wilcoxon test against zero (E). Error bars indicate mean +/- s.e.m. **P* < 0.05, ***P* < 0.01.

Seizures are considered to be driven by feedback loops of neuronal activity that drive a hyperexcitable network state^{615,622}. Many stimuli that are released during this process have the potential to activate the inflammasome, which our experiments show can further propagate neuronal activity. We therefore wondered whether the converse is true in that neuronal activity states are related to inflammasome activation. To assess this question, we treated primary ASC^{Citrine} mixed neuron/glia cultures with modulators of neuronal activity and then assessed ASC speck density relative to untreated control cultures. Our previous studies noted that etoposide-induced DNA damage is effective at inducing ASC speck formation and pyroptosis in this experimental set-up⁵⁶, which we used as a positive control for the present studies. We found that blocking neuronal activity with tetrodotoxin led to a trend in decreased inflammasome assembly while inducing neuronal activity with forskolin significantly increased inflammasome assembly (Figure 4.6E).

Notably, forskolin-induced ASC speck formation appeared to occur in a dose-dependent manner (Figure 4.6E), indicating that increasing levels of neural network activity can ramp up inflammasome activation levels. These

findings lend to the concept that neuronal activity induced by kainic acid, or other excitatory receptor activation, can induce inflammasome activation, which can itself induce more neuronal activity. Thus, a bidirectional feedback loop may exist between neuronal activity and inflammasome activation which could partially underlie pathogenic network excitability and seizure propagation.

These results confirm the importance of Caspase-1 and the inflammasome in seizure propagation. Yet, the CNS cell type harboring these pathogenic inflammasomes remains unknown. Defining a more precise mechanism of inflammasome activation during seizure will help to pinpoint a target cell type for more refined therapeutic intervention. To address this question, we generated mice deficient for Caspase-1 in defined CNS cell types and assessed relative seizure severity in these animals.

Microglia, being the primary resident immune cell type within the brain, are most frequently implicated in pathogenic inflammasome activation. Indeed, preliminary evidence exists that microglia activate the NLRP3 inflammasome in an *ex vivo* model of epilepsy^{624,625}. We conducted KA seizure experiments in microglia-specific Caspase-1 conditional knockouts, $Casp1^{fl/fl};Cx3cr1^{Cre}$ ($Casp1^{\Delta MG}$) and Cre-negative $Casp1^{fl/fl}$ littermate controls ($Casp1^{cont}$) to assess the importance of microglia inflammasome in acute seizure propagation *in vivo*. In this model, we found that there was no difference in seizure severity (Figure 4.7A), onset (Figure 4.7B), duration (Figure 4.7C), or survival (Figure 4.7D) in $Casp1^{\Delta MG}$ mice compared to controls. These findings suggest that the protection against severe seizure that we found in Caspase-1 deficient mice (Figure 4.5D-H) is not due to Caspase-1 activity within microglia.

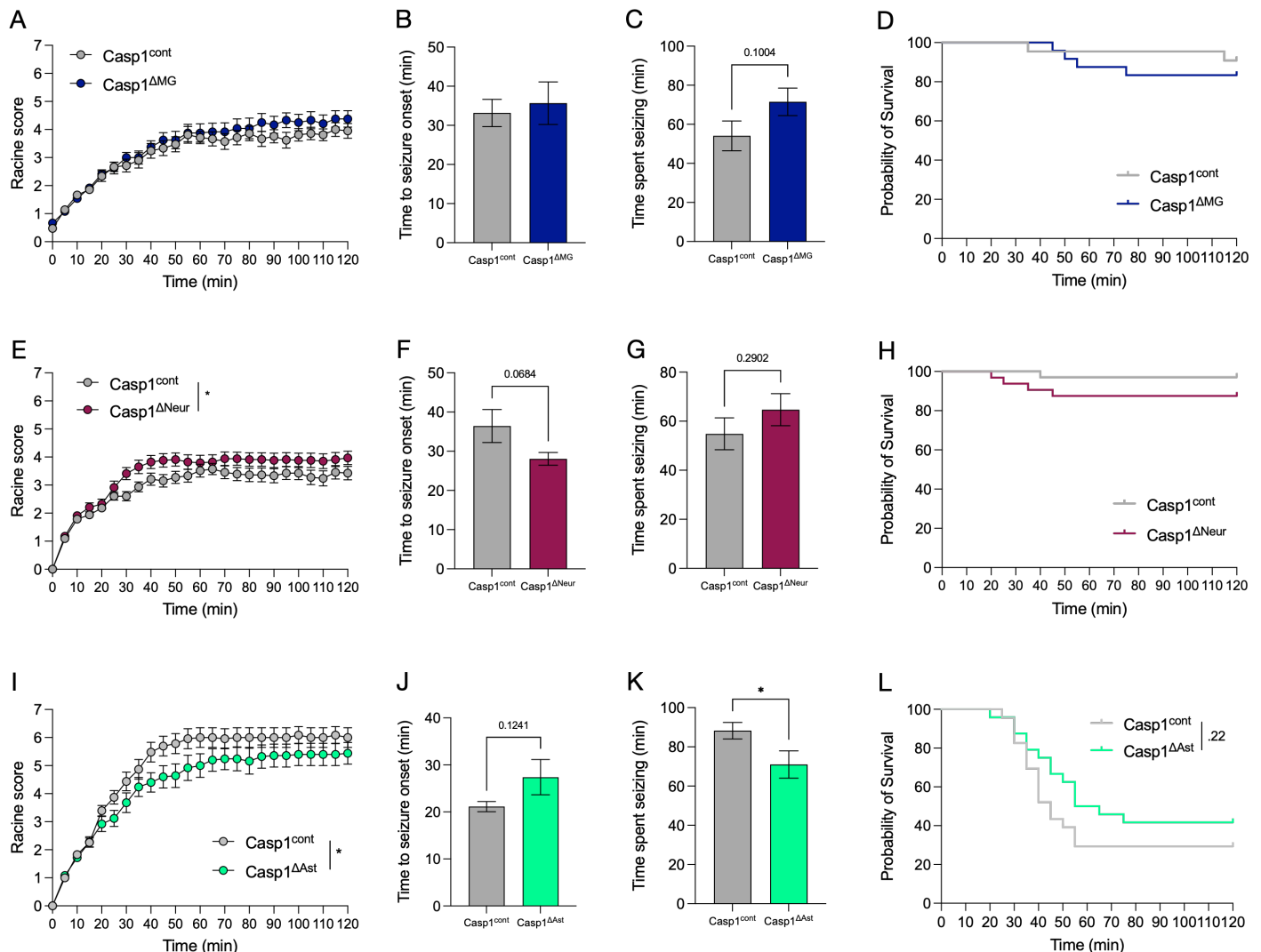


Figure 4.7. Cell-type-specific inflammasome activation contributes to seizure severity.

Six-week-old experimental mice were injected i.p. with 24 mg/kg kainic acid (KA) to induce seizures and scored for seizure severity beginning immediately after KA injection. Seizure severity was scored for 2 hrs using a modified Racine scale, with a score of 0 indicating baseline activity and a score of 7 indicating death. (A-D) Microglia-specific Caspase-1 conditional knockouts, $Casp1^{fl/fl};Cx3cr1^{Cre}$ ($Casp1^{\Delta MG}$, N = 24), and Cre-negative $Casp1^{fl/fl}$ littermate controls ($Casp1^{cont}$, N = 21) were assessed for relative seizure severity. (E-H) Neuron-specific Caspase-1 conditional knockouts, $Casp1^{fl/fl};Synapsin^{Cre}$ ($Casp1^{\Delta Neur}$, N = 33), and Cre-negative $Casp1^{fl/fl}$ littermate controls ($Casp1^{cont}$, N = 34) were assessed for relative seizure severity. (I-L) Astrocyte-specific Caspase-1 inducible conditional knockouts, $Casp1^{fl/fl};Aldh11^{Cre-ERT2}$ ($Casp1^{\Delta Ast}$, N = 16), and Cre-negative $Casp1^{fl/fl}$ littermate controls ($Casp1^{cont}$, N = 15) received tamoxifen food from 3 weeks of age until 6 weeks of age. Mice were injected with KA at 6 weeks of age and assessed for relative seizure severity. (A,E,I) Seizure activity was scored every 5 min and severity plotted over time. (B,F,J) Time to seizure onset (Racine score 3) for mice that actively seized during the two hour scoring time post-KA administration. (C,G,K) Once a Racine score of 4 was reached, mice were scored at a minimum of a score of 4 from that point forward. The sum of this time is summarized as time spent seizing. (D,H,L) Survival curve over two hours post-administration of KA, where Racine score 7 indicates death. Data combined from at least two independent experiments (A-L). Each data point represents the average of every mouse within the group (A,E,I). Male and female mice were used for all experiments. Statistical significance calculated by two-way ANOVA (A,E,I), unpaired Student's t-test (B,C,F,G,J,K) or Gehan-Breslow-Wilcoxon test (D,H,L). Error bars indicate mean \pm s.e.m. * $P < 0.05$.

Inflammasome activation can be triggered by a wide variety of danger-associated molecular patterns (DAMPs) which could be found within hyperexcitable neurons themselves, such as elevated ATP, calcium, reactive oxygen species, ruptured lysosome contents, and more. Thus, it is possible that pathogenic inflammasome activation in the context of seizure could be driven by neurons themselves, rather than in glia responding to the release of inflammasome-stimulating DAMPs. We therefore turned to neuron-specific Caspase-1 conditional knockouts, $Casp1^{fl/fl};Synapsin^{Cre}$ ($Casp1^{\Delta Neur}$) mice, and respective Cre-negative $Casp1^{fl/fl}$ littermate controls ($Casp1^{cont}$) to assess the importance of neuron inflammasomes in acute seizure propagation *in vivo*. Opposite to full-body Caspase-1-deficient mice which were protected from severe seizures (Figure 4.5D-H), we found that mice lacking Caspase-1 specifically in neurons were more susceptible to KA-induced seizures (Figure 4.7E-H). In particular, seizure severity was heightened in $Casp1^{\Delta Neur}$ mice compared to controls (Figure 4.7E). This was accompanied by trends in faster times to seizure onset (Figure 4.7F) and longer duration of seizures (Figure 4.7G) without any change in mortality (Figure 4.7H).

These findings suggest that neuronal Caspase-1 may actually have protective functions in the context of KA-induced seizures. This result could account for the fact that mice completely lacking Caspase-1 were not fully protected from seizures altogether (Figure 4.5D-H). These data also highlight the importance of investigating inflammasome activation on a cell type-specific basis to achieve optimal targeting strategies when designing inflammasome blocking drugs for the treatment of epilepsy, as not all inflammasome function could be pathogenic.

Astrocytes have a vital importance in neurotransmitter reuptake and recycling and also play key roles in buffering ion concentrations around synapses^{626,627}. These functions place astrocytes in an optimal position to regulate neuronal hyperexcitability. Paired with our findings that astrocytes in the adult hippocampus harbor inflammasomes (Chapter 3; Figure 3.9A,B, 3.10), we next sought to investigate a potential role for astrocyte inflammasome activation in seizure propagation. To address this, we generated astrocyte-specific Caspase-1 inducible conditional knockouts, $Casp1^{fl/fl};Aldh11^{CreERT2}$ ($Casp1^{\Delta Ast}$) mice and subjected these animals to KA seizure experiments alongside respective Cre-negative $Casp1^{fl/fl}$ littermate controls ($Casp1^{cont}$). We found a trend toward protection against severe seizures in $Casp1^{\Delta Ast}$ mice compared to controls (Figure 4.7I) without any change in time to seizure onset (Figure 4.7J) or seizure duration (Figure 4.7K).

We noted that seizures were dramatically more severe in the control mice for these studies as compared to other control groups (Figure 4.7E-H, 4.5). Indeed, most $Casp1^{cont}$ mice in these experiments succumbed to seizure-induced death (Racine score 7) within the scoring period (Figure 4.7I,L). We reasoned that the heightened seizure severity in these experiments was driven by diminished baseline health of the experimental mice which were kept on tamoxifen food for the three weeks prior to seizure studies. Nonetheless, the loss of Caspase-1 function within astrocytes did provide a significant level of protection against these deadly seizures (Figure 4.7I-L) in which $Casp1^{\Delta Ast}$ mice had significantly lower Racine scores (Figure 4.6I) and seized for less time (Figure 4.7K) compared to controls. In addition, there was a trend toward lengthened time to seizure onset (Figure 4.7J) and lower mortality (Figure 4.7L) in $Casp1^{\Delta Ast}$ mice compared to controls. Altogether, these studies reveal that inflammasome activation within astrocytes may in part contribute to seizure propagation. Future studies will use lower doses of KA to scale back the severity of seizures in this transgenic line to better assess relative seizure onset and duration in a more clinically relevant model.

While conducting studies to collect brains from ASC^{Citrine} mice for downstream immunohistochemistry of ASC specks in the hippocampus, we made the unexpected observation that these mice are slightly but significantly

protected from KA seizures (Figure 4.8). More specifically, ASC^{Citrine} mice had lower scores for seizure severity (Figure 4.7A) without any change in the time to seizure onset (Figure 4.8B) that was accompanied by a reduction in the duration of time spent seizing (Figure 4.8C) compared to WT control mice. While this was the case, we did not note any significant protection against seizure-related death in ASC^{Citrine} mice (Figure 4.8D).

This mild level of protection against seizure severity in ASC^{Citrine} mice could be explained by many potential factors. For one, the WT control mice used in these studies are not proper littermate controls of the ASC^{Citrine} mice. Thus, the slight difference in seizure activity could be explained by differences in strain, parenting, and/or microbiome. Another possible explanation is that Citrine-tagged ASC is knocked into the germline interferes with normal inflammasome function in this reporter line⁵⁶¹. The Citrine fluorophore tagged onto ASC could reasonably inhibit proper ASC oligomerization which is essential for robust inflammasome platform construction. What's more, the supraphysiologic levels of ASC may have a slight protective effect in these mice.

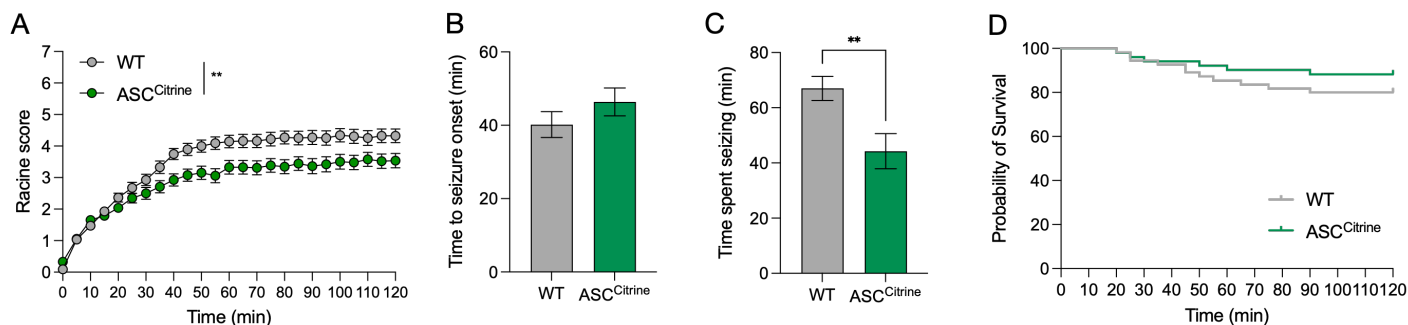


Figure 4.8. ASC^{Citrine} mice exhibit mild protection from seizures.

Six-week-old WT mice (N = 55) and ASC^{Citrine} mice (N = 52) were injected i.p. with 24 mg/kg kainic acid (KA) to induce seizures and scored for seizure severity beginning immediately after KA injection. Seizure severity was scored for 2 hrs using a modified Racine scale, with a score of 0 indicating baseline activity and a score of 7 indicating death. (A) Seizure activity was scored every 5 min and severity plotted over time. (B) Time to seizure onset (Racine score 3) for mice that actively seized during the two hour scoring time post-KA administration. (C) Once a Racine score of 4 was reached, mice were scored at a minimum of a score of 4 from that point forward. The sum of this time is summarized as time spent seizing. (D) Survival curve over two hours post-administration of KA, where Racine score 7 indicates death. Data combined from at least three independent experiments (A-D). Each data point represents the average of every mouse within the group (A,E,I). Male and female mice were used for all experiments. Statistical significance calculated by two-way ANOVA (A), unpaired Student's t-test (B,C) or Gehan-Breslow-Wilcoxon test (D). Error bars indicate mean +/- s.e.m. **P < 0.01.

While Caspase-1 constitutes one potential target for inflammasome blockade as an anti-seizure therapeutic target, it is yet worthwhile to investigate other target proteins in the inflammasome. One such component necessary for initiating inflammasome activation is the sensor. Many inflammasome sensors exist and two, namely, NLRP1 and NLRP3, have already been implicated in epilepsy⁶¹⁵. Elevated NLRP1 inflammasome activation has been noted in patients with temporal lobe epilepsy⁶²⁸. In a rat model of status epilepticus, blockade of NLRP1 protected against neuron pyroptosis⁶²⁸. Knockdown of NLRP3 similarly protected rats against severe status epilepticus⁶²⁹.

To extend these findings, we sought to investigate seizure severity in our KA mouse model using NLRP1-deficient mice. At first, we noted no difference in seizure severity in *Nlrp1*^{-/-} mice compared to WT controls (data not shown). Upon separating the data by sex, we noticed a stark sexually dimorphic phenotype in seizure severity (Figure 4.9). We found that female *Nlrp1*^{-/-} mice were protected against severe seizures as characterized by a significant reduction in Racine scores over the scoring period (Figure 4.8A). This was not associated with a change in the time to seizure onset (Figure 4.9B) but was accompanied by trends in shorter seizure duration (Figure 4.9C) and reduced mortality (Figure 4.9D) in female *Nlrp1*^{-/-} mice compared to controls. Meanwhile, no significant differences in seizure scores (Figure 4.9E), onset (Figure 4.9F), duration (Figure 4.9G), or mortality (Figure 4.9H) were noted in male *Nlrp1*^{-/-} mice. In fact, Male *Nlrp1*^{-/-} mice displayed trends toward more severe seizures across some of these measures as compared to controls (Figure 4.9E-H).

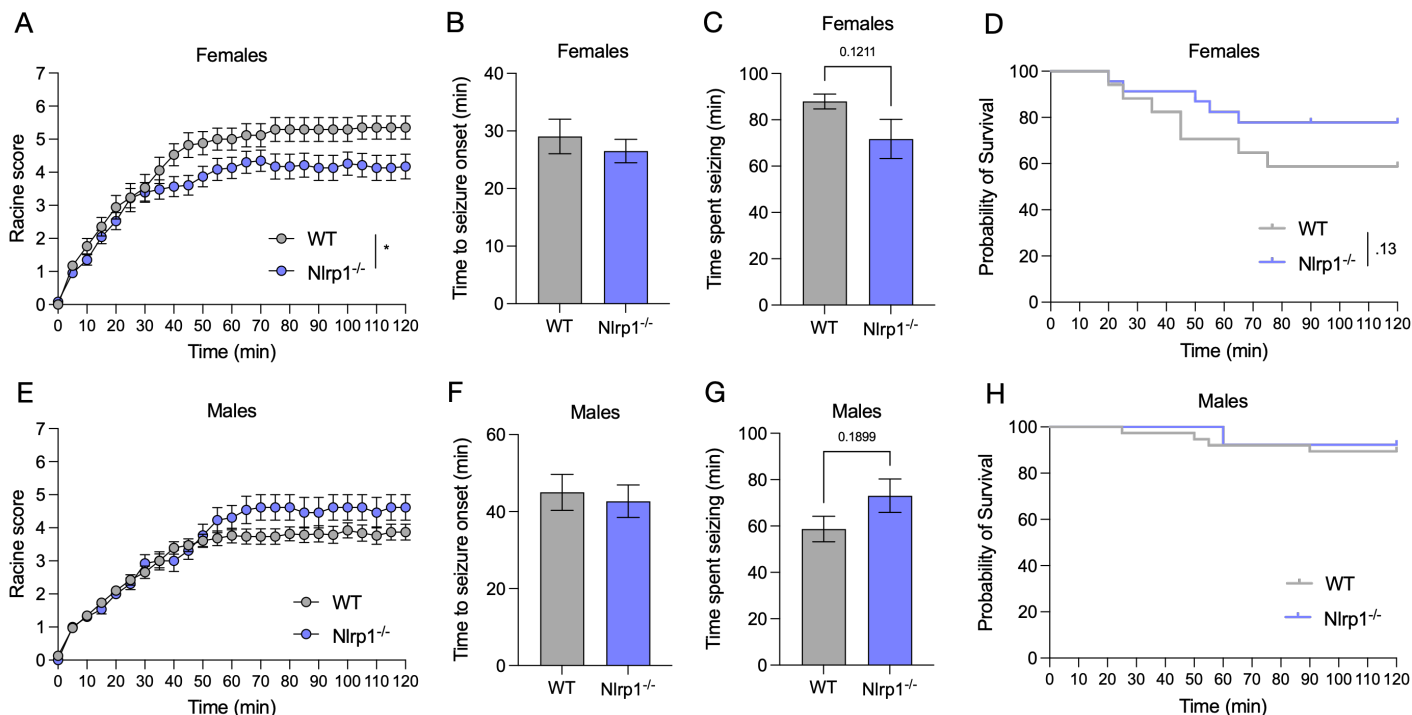


Figure 4.9. NLRP1 contributes to seizure severity in a sex-specific manner.

Six-week-old WT mice and Nlrp1^{-/-} mice were injected i.p. with 24 mg/kg kainic acid (KA) to induce seizures and scored for seizure severity beginning immediately after KA injection. Seizure severity was scored for 2 hrs using a modified Racine scale, with a score of 0 indicating baseline activity and a score of 7 indicating death. Data was plotted separated by female (A-D; WT N = 17, Nlrp1^{-/-} N = 23) and male (E-H; WT N = 38, Nlrp1^{-/-} N = 13) sex. (A,E) Seizure activity was scored every 5 min and severity plotted over time. (B,F) Time to seizure onset (Racine score 3) for mice that actively seized during the two hour scoring time post-KA administration. (C,G) Once a Racine score of 4 was reached, mice were scored at a minimum of a score of 4 from that point forward. The sum of this time is summarized as time spent seizing. (D,H) Survival curve over two hours post-administration of KA, where Racine score 7 indicates death. Data combined from at least two independent experiments (A-H). Each data point represents the average of every mouse within the group (A,E). Statistical significance calculated by two-way ANOVA (A,E), unpaired Student's t-test (B,C,F,G) or Gehan-Breslow-Wilcoxon test (D,H). Error bars indicate mean +/- s.e.m. **P* < 0.05.

Males are generally more susceptible to epilepsy episodes compared to females, moreover, menstrual cycle phases are known to affect seizure timing in females⁶³⁰⁻⁶³². The field is just beginning to unravel the underlying causes of sex differences in epilepsy, not to mention potential differences in treatment strategies. Our preliminary data exemplifying sex differences in NLRP1 involvement in seizure propagation highlights the importance of investigating seizures stratified by sex. In this case, blocking NLRP1 could be a potential anti-seizure target for females, but may have no effect or even detrimental effects in males.

Future studies may further probe other inflammasome sensors in the context of seizure onset and progression. NLRP1 is known to sense anthrax lethal toxin, but not many other definitive ligands, especially endogenous triggers, have been identified. As such, it remains a question as to what stimuli could be triggering NLRP1 inflammasome assembly in the context of seizures. A diverse array of DAMPs has been well characterized to trigger the NLRP3 inflammasome. Of these potential NLRP3 stimuli, many of which are endogenous and could very well be released upon seizure induction, such as ATP, ion fluxes, reactive oxygen species, and more. Therefore, NLRP3 remains a viable target to investigate in terms of propagating seizures.

Given our preliminary studies in conjunction with published literature concerning inflammasome activation in the context of seizures, it will be worthwhile to investigate inflammasome components as anti-seizure therapeutic targets. Yet, some inflammasome components have homeostatic functions in the CNS, as well, inflammasomes within certain cell types may protect against neuronal hyperexcitability. As such, it is of importance to better define the specific triggers, sensors, and outputs of inflammasomes as well as the relevant cell type of interest in the context of seizures. This knowledge will allow for more targeted routes of intervention to maximize treatment success and limit unnecessary side effects in the management of epilepsy.

4.2.5. Inflammasomes in Alzheimer's Disease

Alzheimer's disease (AD) is a devastating neurodegenerative disease affecting more than 6 million Americans making it the sixth leading causing of death in the United States⁶³³. The disease begins with short-term memory loss which worsens over time and progresses into more severe cognitive impairments and dementia in about 70% of cases⁶³⁴. The annual cost of care allocated to AD and other dementias was over \$300 billion and there is not yet an effective treatment to reliably curb disease symptoms⁶³³. Nearly every drug that has gone to clinical trial for AD has failed to date⁶³⁵. Thus, there is an urgent need for novel drug targets and strategies to treat AD patients.

AD is characterized by two main pathologies: the accumulation of amyloid beta (A β) and seeding of tau into neurofibrillary tangles (NFTs) in the brain⁶³⁴. Accompanying these disease markers is neuroinflammation and the decline of neuronal health, ultimately leading to the cell death that underlies memory and cognitive impairments in AD patients⁶³⁴. While the field of AD research has largely focused on targeting A β to limit disease progression, this route of treatment has yet to prove efficacious⁶³⁵. Meanwhile, the growing field of neuroimmunology has found that limiting the neuroinflammatory response to A β and tau pathologies may be an earlier and more robust method to slow AD progression⁵⁹⁷. Attention in recent years has focused in particular on targeting innate immune pathways and microglia, the resident immune cells of the CNS, for novel AD treatment strategies⁵⁹⁷.

An array of DAMPs constitutes AD pathology that could trigger inflammasome activation, including A β and NFTs themselves and spanning to reactive oxygen species, changes in ion fluxes, phagosome/lysosome disruption, ATP, extracellular debris, nucleic acids, and more. Studies have highlighted NLRP3 inflammasome activation in microglia and NLRP1 inflammasome activation in neurons as propagators of neurodegeneration in AD mouse models^{551,636}.

A β fibrils can activate the NLRP3 inflammasome in microglia and cause the release of active IL-1 β , further potentiating neuroinflammation in AD³⁷⁰. High levels of inflammatory stimuli and cytokines can lead to unintended death of bystander cells^{551,597}. Worsening the case is the finding that microglia-derived ASC specks can cross-seed A β accumulation, propagating disease³⁷¹. ASC specks have been shown to be released from cells which may further potentiate a cascade of A β accumulation and other neuroinflammatory cascades³⁷¹. Evidence of neuronal NLRP1 inflammasome activation AD patient brains has also been reported^{637,638}. *In vitro* studies have shown that NLRP1 inflammasome assembly in neurons can trigger pyroptosis⁶³⁹; as such, the inflammasome may directly cause neuron death in neurodegenerative disease.

Other receptors beyond NLRP1 and NLRP3 have not yet been investigated in depth in the context of AD. Of particular interest is a potential role for the AIM2 inflammasome⁶⁴⁰. The AIM2 sensor is activated by cytosolic DNA³⁵⁹. The ensuing loss of cellular health in AD can be accompanied by DNA damage⁶⁴¹, which could theoretically trigger AIM2 activation. Moreover, A β plaques often contain nucleic acids which could potentially trigger AIM2 activation if taken up by phagocytic plaque-associated cells such as microglia. One study indeed reports that germline loss of AIM2 can limit A β accumulation and microglial activation in an AD mouse model⁶⁴². Yet, inflammatory cytokine production was augmented and cognitive decline was not impacted by the loss of AIM2 in this study⁶⁴². Given the importance of AIM2 for proper neurodevelopment⁵⁶, as well as its function in controlling neuronal morphology³⁸¹, it is possible that complete ablation of AIM2 function is not wholly beneficial. Nevertheless, probing AIM2 in a time-sensitive and cell-specific manner could be beneficial to uncover its role in neurodegenerative disease progression.

Our studies of homeostatic inflammasome signaling in the CNS (Chapter 3) show that astrocytes harbor assembled inflammasomes. Meanwhile, the majority of pathogenic inflammasome activation in AD, and other neurodegenerative disorders, is primarily attributed to microglia and to a smaller degree neurons. Importantly, we found that inflammasome activation in astrocytes was particularly robust in the hippocampus, which is a central region of A β accumulation and neurodegeneration in AD. Collectively, these findings point towards a shift in the duty of hippocampal inflammasome signaling from protective to pathogenic in the neurodegenerative cascade. In particular, astrocyte inflammasomes may function to maintain a homeostatic state of neuronal health

and plasticity, while microglia and neuron inflammasomes may contribute to maladaptive cytokine production and/or pyroptosis. Indeed, we noted a shift in ASC speck localization from astrocytes to microglia with hippocampal aging (Chapter 3; Figure 3.4K).

A few studies have begun to target the inflammasome as a route to limit neuroinflammation-associated neurodegeneration in murine AD models^{573,574,643}. One such study found that non-steroidal anti-inflammatory drugs (NSAIDs) of the fenamate class can block NLRP3 inflammasome activation in macrophages and can effectively limit gliosis and cognitive decline in an AD mouse model⁶⁴³. Another study duo investigated the Caspase-1 inhibitor VX-765 as a method to limit cognitive decline in an AD mouse model^{573,574}. These studies collectively found that pre-symptomatic VX-765 treatment was effective in limiting disease onset⁵⁷³, while post-symptomatic VX-765 treatment was effective in reversing cognitive decline⁵⁷⁴. These reports point toward the therapeutic potential of inflammasome inhibitors as a novel class of drugs to help treat AD⁶⁴⁴.

Neuroinflammation is a hallmark of other neurodegenerative diseases including Parkinson's disease, Huntington's disease, amyotrophic lateral sclerosis, multiple sclerosis, and more⁵⁵¹. Indeed, inflammasome activation has been reported to influence the progression of many of these neurodegenerative diseases⁵⁵¹. As such, targeting the inflammasome may remain a potential therapeutic route for neurodegenerative disease beyond Alzheimer's disease. Narrowing down the relevant inflammasome components and cell types involved within each disease context will aid in the development of targeted drugs to together lessen disease progression and limit side effects.

4.3 Concluding remarks

This dissertation has presented and discussed research findings concerning the contribution of innate immune signaling to proper brain development and lifelong function. Studies in the burgeoning field of neuroimmunology have emphasized the beneficial and detrimental roles of immune system activation as responders and drivers of neuropathology. Chapter 2 of this dissertation highlights the potential consequences of aberrant immune signaling in the placenta, which can lead to perturbed fetal brain development (including immune-based signal cascades) that ultimately impact offspring behavior. Neuroimmunologic studies are increasingly uncovering the use of molecules originally characterized in the immune system that are used by brain-resident cells in homeostatic contexts. The study presented in Chapter 3 of this dissertation reports a novel role for the innate-immune based inflammasome complex in mediating astrocyte-neuron communication that underlies memory function. Thus, the body of work presented in this dissertation emphasizes a delicate balance in immune signaling that is required for brain development and function. The complexity of the brain lends to similarly complex systems that wire this organ, allowing for its intricate composition and marvelous capacity to control organism function.

Literature cited

1. Morimoto, K. & Nakajima, K. Role of the immune system in the development of the central nervous system. *Front. Neurosci.* **13**, (2019).
2. Kioussis, D. & Pachnis, V. Immune and nervous systems: More than just a superficial similarity? *Immunity* **31**, 705–710 (2009).
3. Ribeiro, M. *et al.* Meningeal $\gamma\delta$ T cell-derived IL-17 controls synaptic plasticity and short-term memory. *Science Immunology* **4**, (2019).
4. Wake, H., Moorhouse, A. J., Miyamoto, A. & Nabekura, J. Microglia: Actively surveying and shaping neuronal circuit structure and function. *Trends in Neurosciences* **36**, 209–217 (2013).
5. Ueno, M. & Yamashita, T. Bidirectional tuning of microglia in the developing brain: From neurogenesis to neural circuit formation. *Current Opinion in Neurobiology* **27**, 8–15 (2014).
6. Boulanger, L. M. Immune proteins in brain development and synaptic plasticity. *Neuron* **64**, 93–109 (2009).
7. Eroglu, C. & Barres, B. A. Regulation of synaptic connectivity by glia. *Nature* **468**, 223–231 (2010).
8. Schafer, D. P., Lehrman, E. K. & Stevens, B. The “quad-partite” synapse: Microglia-synapse interactions in the developing and mature CNS. *Glia* **61**, 24–36 (2013).
9. Knuesel, I. *et al.* Maternal immune activation and abnormal brain development across CNS disorders. *Nature Reviews Neurology* **10**, 643–660 (2014).
10. Estes, M. L. & McAllister, A. K. Maternal immune activation: Implications for neuropsychiatric disorders. *Science* **353**, 772–777 (2016).
11. Azevedo, F. A. C. *et al.* Equal numbers of neuronal and nonneuronal cells make the human brain an isometrically scaled-up primate brain. *Journal of Comparative Neurology* **513**, 532–541 (2009).
12. von Bartheld, C. S., Bahney, J. & Herculano-Houzel, S. The search for true numbers of neurons and glial cells in the human brain: A review of 150 years of cell counting. *J Comp Neurol* **524**, 3865–3895 (2016).
13. Stiles, J. & Jernigan, T. L. The basics of brain development. *Neuropsychol Rev* **20**, 327–348 (2010).
14. Hemmati-Brivanlou, A. & Melton, D. Vertebrate embryonic cells will become nerve cells unless told otherwise. *Cell* **88**, 13–17 (1997).
15. Chalasani, S. H. *et al.* Stromal Cell-Derived Factor-1 antagonizes Slit/Robo signaling in vivo. *J. Neurosci.* **27**, 973–980 (2007).
16. Arakawa, Y. *et al.* Control of axon elongation via an SDF-1 α /Rho/mDia pathway in cultured cerebellar granule neurons. *J Cell Biol* **161**, 381–391 (2003).
17. Dréau, G. L. & Martí, E. Dorsal–ventral patterning of the neural tube: A tale of three signals. *Developmental Neurobiology* **72**, 1471–1481 (2012).
18. Kessar, N., Pringle, N. & Richardson, W. D. Ventral neurogenesis and the neuron–glial switch. *Neuron* **31**, 677–680 (2001).
19. Rowitch, D. H. Glial specification in the vertebrate neural tube. *Nature Reviews Neuroscience* **5**, 409–419 (2004).
20. Kiecker, C. & Lumsden, A. Compartments and their boundaries in vertebrate brain development. *Nature Reviews Neuroscience* **6**, 553–564 (2005).
21. Lewis, J. Neurogenic genes and vertebrate neurogenesis. *Current Opinion in Neurobiology* **6**, 3–10 (1996).
22. Ransohoff, R. M. & Cardona, A. E. The myeloid cells of the central nervous system parenchyma. *Nature* **468**, 253–262 (2010).
23. Ginhoux, F. & Williams, M. Tissue-resident macrophage ontogeny and homeostasis. *Immunity* **44**, 439–449 (2016).
24. Ginhoux, F., Lim, S., Hoeffel, G., Low, D. & Huber, T. Origin and differentiation of microglia. *Front. Cell. Neurosci.* **7**, (2013).
25. Li, Q. & Barres, B. A. Microglia and macrophages in brain homeostasis and disease. *Nature Reviews Immunology* **18**, 225–242 (2018).
26. Kierdorf, K. *et al.* Microglia emerge from erythromyeloid precursors via Pu.1- and Irf8-dependent pathways. *Nature Neuroscience* **16**, 273–280 (2013).
27. Ginhoux, F. *et al.* Fate mapping analysis reveals that adult microglia derive from primitive macrophages. *Science* **330**, 841–845 (2010).

28. De, S. *et al.* Two distinct ontogenies confer heterogeneity to mouse brain microglia. *Development* **145**, (2018).
29. Swinnen, N. *et al.* Complex invasion pattern of the cerebral cortex by microglial cells during development of the mouse embryo. *Glia* **61**, 150–163 (2013).
30. Ajami, B., Bennett, J. L., Krieger, C., Tetzlaff, W. & Rossi, F. M. V. Local self-renewal can sustain CNS microglia maintenance and function throughout adult life. *Nature Neuroscience* **10**, 1538–1543 (2007).
31. Jin, N., Gao, L., Fan, X. & Xu, H. Friend or foe? Resident microglia vs bone marrow-derived microglia and their roles in the retinal degeneration. *Mol Neurobiol* **54**, 4094–4112 (2017).
32. Butovsky, O. *et al.* Identification of a unique TGF- β -dependent molecular and functional signature in microglia. *Nature Neuroscience* **17**, 131–143 (2014).
33. Matcovitch-Natan, O. *et al.* Microglia development follows a stepwise program to regulate brain homeostasis. *Science* **353**, (2016).
34. Bennett, M. L. *et al.* New tools for studying microglia in the mouse and human CNS. *Proc Natl Acad Sci* **113**, 1738–1746 (2016).
35. Hanamsagar, R. *et al.* Generation of a microglial developmental index in mice and in humans reveals a sex difference in maturation and immune reactivity. *Glia* **65**, 1504–1520 (2017).
36. Tan, Y.-L., Yuan, Y. & Tian, L. Microglial regional heterogeneity and its role in the brain. *Molecular Psychiatry* **25**, 351–367 (2020).
37. Thion, M. S., Ginhoux, F. & Garel, S. Microglia and early brain development: An intimate journey. *Science* **362**, 185–189 (2018).
38. Erny, D. *et al.* Host microbiota constantly control maturation and function of microglia in the CNS. *Nature Neuroscience* **18**, 965–977 (2015).
39. Thion, M. S. *et al.* Microbiome influences prenatal and adult microglia in a sex-specific manner. *Cell* **172**, 500–516 (2018).
40. Nadarajah, B. & Parnavelas, J. G. Modes of neuronal migration in the developing cerebral cortex. *Nature Reviews Neuroscience* **3**, 423–432 (2002).
41. Tamariz, E. & Varela-Echavarría, A. The discovery of the growth cone and its influence on the study of axon guidance. *Front. Neuroanat.* **9**, (2015).
42. Reemst, K., Noctor, S. C., Lucassen, P. J. & Hol, E. M. The indispensable roles of microglia and astrocytes during brain development. *Front. Hum. Neurosci.* **10**, (2016).
43. Allen, N. J. & Lyons, D. A. Glia as architects of central nervous system formation and function. *Science* **362**, 181–185 (2018).
44. Allen, N. J. & Eroglu, C. Cell biology of astrocyte-synapse interactions. *Neuron* **96**, 697–708 (2017).
45. Werneburg, S., Feinberg, P. A., Johnson, K. M. & Schafer, D. P. A microglia-cytokine axis to modulate synaptic connectivity and function. *Current Opinion in Neurobiology* **47**, 138–145 (2017).
46. Waites, C. L., Craig, A. M. & Garner, C. C. Mechanisms of vertebrate synaptogenesis. *Annual Review of Neuroscience* **28**, 251–274 (2005).
47. Yamaguchi, Y. & Miura, M. Programmed cell death in neurodevelopment. *Developmental Cell* **32**, 478–490 (2015).
48. Stoner, R. *et al.* Patches of disorganization in the neocortex of children with autism. *New England Journal of Medicine* **370**, 1209–1219 (2014).
49. Fang, W.-Q. *et al.* Overproduction of upper-layer neurons in the neocortex leads to autism-like features in mice. *Cell Reports* **9**, 1635–1643 (2014).
50. Davies, A. M. Trophic support. *Encyclopedia of Life Sciences* (2001).
51. Yeo, W. & Gautier, J. Early neural cell death: Dying to become neurons. *Developmental Biology* **274**, 233–244 (2004).
52. Casano, A. M., Albert, M. & Peri, F. Developmental apoptosis mediates entry and positioning of microglia in the zebrafish brain. *Cell Reports* **16**, 897–906 (2016).
53. Kuan, C.-Y. *et al.* The Jnk1 and Jnk2 protein kinases are required for regional specific apoptosis during early brain development. *Neuron* **22**, 667–676 (1999).
54. Cecconi, F., Alvarez-Bolado, G., Meyer, B. I., Roth, K. A. & Gruss, P. Apaf1 (CED-4 homolog) regulates programmed cell death in mammalian development. *Cell* **94**, 727–737 (1998).
55. Yoshida, H. *et al.* Apaf1 is required for mitochondrial pathways of apoptosis and brain development. *Cell* **94**, 739–750 (1998).

56. Lammert, C. R. *et al.* AIM2 inflammasome surveillance of DNA damage shapes neurodevelopment. *Nature* 1–6 (2020).
57. Hong, Y. K. & Chen, C. Wiring and rewiring of the retinogeniculate synapse. *Current Opinion in Neurobiology* **21**, 228–237 (2011).
58. Stephan, A. H., Barres, B. A. & Stevens, B. The complement system: An unexpected role in synaptic pruning during development and disease. *Annual Review of Neuroscience* **35**, 369–389 (2012).
59. McAllister, A. K. Major histocompatibility complex I in brain development and schizophrenia. *Biological Psychiatry* **75**, 262–268 (2014).
60. Moriyama, M. *et al.* Complement Receptor 2 is expressed in neural progenitor cells and regulates adult hippocampal neurogenesis. *J. Neurosci.* **31**, 3981–3989 (2011).
61. Wu, M. D., Montgomery, S. L., Rivera-Escalera, F., Olschowka, J. A. & O'Banion, M. K. Sustained IL-1 β expression impairs adult hippocampal neurogenesis independent of IL-1 signaling in nestin⁺ neural precursor cells. *Brain, Behavior, and Immunity* **32**, 9–18 (2013).
62. Chen, Z. & Palmer, T. D. Differential roles of TNFR1 and TNFR2 signaling in adult hippocampal neurogenesis. *Brain Behav. Immun.* **30**, 45–53 (2013).
63. Vallières, L., Campbell, I. L., Gage, F. H. & Sawchenko, P. E. Reduced hippocampal neurogenesis in adult transgenic mice with chronic astrocytic production of interleukin-6. *J. Neurosci.* **22**, 486–492 (2002).
64. Korin, B. *et al.* High-dimensional, single-cell characterization of the brain's immune compartment. *Nature Neuroscience* **20**, 1300–1309 (2017).
65. Bulloch, K. *et al.* CD11c/EYFP transgene illuminates a discrete network of dendritic cells within the embryonic, neonatal, adult, and injured mouse brain. *Journal of Comparative Neurology* **508**, 687–710 (2008).
66. Tanabe, S. & Yamashita, T. B-1a lymphocytes promote oligodendrogenesis during brain development. *Nature Neuroscience* **21**, 506–516 (2018).
67. Silver, R. & Curley, J. P. Mast cells on the mind: New insights and opportunities. *Trends in Neurosciences* **36**, 513–521 (2013).
68. Lenz, K. M. *et al.* Mast cells in the developing brain determine adult sexual behavior. *J. Neurosci.* **38**, 8044–8059 (2018).
69. Lenz, K. M. & Nelson, L. H. Microglia and beyond: Innate immune cells as regulators of brain development and behavioral function. *Front. Immunol.* **9**, (2018).
70. Salter, M. W. & Beggs, S. Sublime microglia: Expanding roles for the guardians of the CNS. *Cell* **158**, 15–24 (2014).
71. Hammond, T. R., Robinton, D. & Stevens, B. Microglia and the brain: Complementary partners in development and disease. *Annual Review of Cell and Developmental Biology* **34**, 523–544 (2018).
72. Wu, Y., Dissing-Olesen, L., MacVicar, B. A. & Stevens, B. Microglia: Dynamic mediators of synapse development and plasticity. *Trends in Immunology* **36**, 605–613 (2015).
73. Hammond, T. R. *et al.* Single-cell RNA sequencing of microglia throughout the mouse lifespan and in the injured brain reveals complex cell-state changes. *Immunity* **50**, 253–271 (2019).
74. Fantin, A. *et al.* Tissue macrophages act as cellular chaperones for vascular anastomosis downstream of VEGF-mediated endothelial tip cell induction. *Blood* **116**, 829–840 (2010).
75. Rymo, S. F. *et al.* A two-way communication between microglial cells and angiogenic sprouts regulates angiogenesis in aortic ring cultures. *PLOS One* **6**, (2011).
76. Peri, F. & Nüsslein-Volhard, C. Live imaging of neuronal degradation by microglia reveals a role for v0-ATPase a1 in phagosomal fusion in vivo. *Cell* **133**, 916–927 (2008).
77. Cunningham, C. L., Martínez-Cerdeño, V. & Noctor, S. C. Microglia regulate the number of neural precursor cells in the developing cerebral cortex. *J. Neurosci.* **33**, 4216–4233 (2013).
78. Marín-Teva, J. L. *et al.* Microglia promote the death of developing Purkinje cells. *Neuron* **41**, 535–547 (2004).
79. Wakselman, S. *et al.* Developmental neuronal death in hippocampus requires the microglial CD11b integrin and DAP12 immunoreceptor. *J. Neurosci.* **28**, 8138–8143 (2008).
80. Shigemoto-Mogami, Y., Hoshikawa, K., Goldman, J. E., Sekino, Y. & Sato, K. Microglia enhance neurogenesis and oligodendrogenesis in the early postnatal subventricular zone. *J. Neurosci.* **34**, 2231–2243 (2014).
81. Ueno, M. *et al.* Layer V cortical neurons require microglial support for survival during postnatal development. *Nature Neuroscience* **16**, 543–551 (2013).

82. Pang, Y. *et al.* Differential roles of astrocyte and microglia in supporting oligodendrocyte development and myelination in vitro. *Brain and Behavior* **3**, 503–514 (2013).
83. Wlodarczyk, A. *et al.* A novel microglial subset plays a key role in myelinogenesis in developing brain. *The EMBO Journal* **36**, 3292–3308 (2017).
84. Squarzoni, P. *et al.* Microglia modulate wiring of the embryonic forebrain. *Cell Reports* **8**, 1271–1279 (2014).
85. Pont-Lezica, L. *et al.* Microglia shape corpus callosum axon tract fasciculation: Functional impact of prenatal inflammation. *European Journal of Neuroscience* **39**, 1551–1557 (2014).
86. Lim, S.-H. *et al.* Neuronal synapse formation induced by microglia and interleukin 10. *PLOS One* **8**, (2013).
87. Miyamoto, A. *et al.* Microglia contact induces synapse formation in developing somatosensory cortex. *Nature Communications* **7**, (2016).
88. Roumier, A. *et al.* Prenatal activation of microglia induces delayed impairment of glutamatergic synaptic function. *PLOS One* **3**, (2008).
89. Basilico, B. *et al.* Microglia shape presynaptic properties at developing glutamatergic synapses. *Glia* **67**, 53–67 (2019).
90. Weinhard, L. *et al.* Microglia remodel synapses by presynaptic trogocytosis and spine head filopodia induction. *Nature Communications* **9**, (2018).
91. Schafer, D. P. *et al.* Microglia sculpt postnatal neural circuits in an activity and complement-dependent manner. *Neuron* **74**, 691–705 (2012).
92. Paolicelli, R. C. *et al.* Synaptic pruning by microglia is necessary for normal brain development. *Science* **333**, 1456–1458 (2011).
93. Filipello, F. *et al.* The microglial innate immune receptor TREM2 is required for synapse elimination and normal brain connectivity. *Immunity* **48**, 979–991 (2018).
94. Bialas, A. R. & Stevens, B. TGF- β signaling regulates neuronal C1q expression and developmental synaptic refinement. *Nature Neuroscience* **16**, 1773–1782 (2013).
95. Scott-Hewitt, N. J. *et al.* Local externalization of phosphatidylserine mediates developmental synaptic pruning by microglia. *bioRxiv* (2020).
96. Li, T. *et al.* A splicing isoform of GPR56 mediates microglial synaptic refinement via phosphatidylserine binding. *bioRxiv* 2020.04.24.059840 (2020) doi:10.1101/2020.04.24.059840.
97. Park, J., Jung, E., Lee, S.-H. & Chung, W.-S. CDC50A dependent phosphatidylserine exposure induces inhibitory post-synapse elimination by microglia. *bioRxiv* (2020).
98. Kettenmann, H., Kirchhoff, F. & Verkhratsky, A. Microglia: New roles for the synaptic stripper. *Neuron* **77**, 10–18 (2013).
99. Petrelli, F., Pucci, L. & Bezzi, P. Astrocytes and microglia and their potential link with Autism Spectrum Disorders. *Front. Cell. Neurosci.* **10**, (2016).
100. Gandal, M. J. *et al.* Shared molecular neuropathology across major psychiatric disorders parallels polygenic overlap. *Science* **359**, 693–697 (2018).
101. Vargas, D. L., Nascimbene, C., Krishnan, C., Zimmerman, A. W. & Pardo, C. A. Neuroglial activation and neuroinflammation in the brain of patients with autism. *Annals of Neurology* **57**, 67–81 (2005).
102. Suzuki, K. *et al.* Microglial activation in young adults with autism spectrum disorder. *JAMA Psychiatry* **70**, 49–58 (2013).
103. Morgan, J. T. *et al.* Abnormal microglial–neuronal spatial organization in the dorsolateral prefrontal cortex in autism. *Brain Research* **1456**, 72–81 (2012).
104. Edmonson, C., Ziats, M. N. & Rennert, O. M. Altered glial marker expression in autistic post-mortem prefrontal cortex and cerebellum. *Molecular Autism* **5**, 3 (2014).
105. Morgan, J. T. *et al.* Microglial activation and increased microglial density observed in the dorsolateral prefrontal cortex in autism. *Biological Psychiatry* **68**, 368–376 (2010).
106. Radewicz, K., Garey, L. J., Gentleman, S. M. & Reynolds, R. Increase in HLA-DR immunoreactive microglia in frontal and temporal cortex of chronic schizophrenics. *J Neuropathol Exp Neurol* **59**, 137–150 (2000).
107. Bayer, T. A., Buslei, R., Havas, L. & Falkai, P. Evidence for activation of microglia in patients with psychiatric illnesses. *Neurosci. Lett.* **271**, 126–128 (1999).
108. Zhan, Y. *et al.* Deficient neuron-microglia signaling results in impaired functional brain connectivity and social behavior. *Nature Neuroscience* **17**, 400–406 (2014).

109. Chen, S.-K. *et al.* Hematopoietic origin of pathological grooming in Hoxb8 mutant mice. *Cell* **141**, 775–785 (2010).
110. VanRyzin, J. W., Yu, S. J., Perez-Pouchoulen, M. & McCarthy, M. M. Temporary depletion of microglia during the early postnatal period induces lasting sex-dependent and sex-independent effects on behavior in rats. *eNeuro* **3**, (2016).
111. Xu, Z.-X. *et al.* Elevated protein synthesis in microglia causes autism-like synaptic and behavioral aberrations. *Nature Communications* **11**, (2020).
112. Ben-Yehuda, H. *et al.* Maternal Type-I interferon signaling adversely affects the microglia and the behavior of the offspring accompanied by increased sensitivity to stress. *Molecular Psychiatry* **25**, 1050–1067 (2020).
113. Ikezu, S. *et al.* Inhibition of colony stimulating factor 1 receptor corrects maternal inflammation-induced microglial and synaptic dysfunction and behavioral abnormalities. *Molecular Psychiatry* (2020).
114. Delpech, J.-C. *et al.* Early life stress perturbs the maturation of microglia in the developing hippocampus. *Brain Behav. Immun.* **57**, 79–93 (2016).
115. Bolton, J. L. *et al.* Gestational exposure to air pollution alters cortical volume, microglial morphology, and microglia-neuron interactions in a sex-specific manner. *Front. Synaptic Neurosci.* **9**, (2017).
116. Sanagi, T. *et al.* Segmented Iba1-positive processes of microglia in autism model marmosets. *Front. Cell. Neurosci.* **13**, (2019).
117. Sellgren, C. M. *et al.* Increased synapse elimination by microglia in schizophrenia patient-derived models of synaptic pruning. *Nature Neuroscience* **22**, 374–385 (2019).
118. Klein, S. L. & Flanagan, K. L. Sex differences in immune responses. *Nature Reviews Immunology* **16**, 626–638 (2016).
119. McCarthy, M. M., Nugent, B. M. & Lenz, K. M. Neuroimmunology and neuroepigenetics in the establishment of sex differences in the brain. *Nature Reviews Neuroscience* **18**, 471–484 (2017).
120. Hanamsagar, R. & Bilbo, S. D. Sex differences in neurodevelopmental and neurodegenerative disorders: Focus on microglial function and neuroinflammation during development. *The Journal of Steroid Biochemistry and Molecular Biology* **160**, 127–133 (2016).
121. Bordt, E. A., Ceasrine, A. M. & Bilbo, S. D. Microglia and sexual differentiation of the developing brain: A focus on ontogeny and intrinsic factors. *Glia* **68**, 1085–1099 (2020).
122. VanRyzin, J. W., Marquardt, A. E., Pickett, L. A. & McCarthy, M. M. Microglia and sexual differentiation of the developing brain: A focus on extrinsic factors. *Glia* **68**, 1100–1113 (2020).
123. Schwarz, J. M., Sholar, P. W. & Bilbo, S. D. Sex differences in microglial colonization of the developing rat brain. *Journal of Neurochemistry* **120**, 948–963 (2012).
124. Villa, A. *et al.* Sex-specific features of microglia from adult mice. *Cell Reports* **23**, 3501–3511 (2018).
125. Nelson, L. H., Warden, S. & Lenz, K. M. Sex differences in microglial phagocytosis in the neonatal hippocampus. *Brain, Behavior, and Immunity* **64**, 11–22 (2017).
126. Nelson, L. H. & Lenz, K. M. The immune system as a novel regulator of sex differences in brain and behavioral development. *Journal of Neuroscience Research* **95**, 447–461 (2017).
127. Lenz, K. M., Nugent, B. M., Haliyur, R. & McCarthy, M. M. Microglia are essential to masculinization of brain and behavior. *J. Neurosci.* **33**, 2761–2772 (2013).
128. Nelson, L. H. & Lenz, K. M. Microglia depletion in early life programs persistent changes in social, mood-related, and locomotor behavior in male and female rats. *Behavioural Brain Research* **316**, 279–293 (2017).
129. Kopec, A. M., Smith, C. J., Ayre, N. R., Sweat, S. C. & Bilbo, S. D. Microglial dopamine receptor elimination defines sex-specific nucleus accumbens development and social behavior in adolescent rats. *Nature Communications* **9**, (2018).
130. Werling, D. M. & Geschwind, D. H. Sex differences in autism spectrum disorders. *Curr Opin Neurol* **26**, 146–153 (2013).
131. Werling, D. M., Parikshak, N. N. & Geschwind, D. H. Gene expression in human brain implicates sexually dimorphic pathways in autism spectrum disorders. *Nature Communications* **7**, (2016).
132. Bilbo, S. D. Early-life infection is a vulnerability factor for aging-related glial alterations and cognitive decline. *Neurobiol Learn Mem* **94**, 57–64 (2010).
133. Bilbo, S. D., Block, C. L., Bolton, J. L., Hanamsagar, R. & Tran, P. K. Beyond infection - Maternal immune activation by environmental factors, microglial development, and relevance for autism spectrum disorders. *Exp. Neurol.* **299**, 241–251 (2018).

134. Bolton, J. L. *et al.* Maternal stress and effects of prenatal air pollution on offspring mental health outcomes in mice. *Environ. Health Perspect.* **121**, 1075–1082 (2013).
135. Bolton, J. L. *et al.* Prenatal air pollution exposure induces neuroinflammation and predisposes offspring to weight gain in adulthood in a sex-specific manner. *The FASEB Journal* **26**, 4743–4754 (2012).
136. Ricklin, D., Hajishengallis, G., Yang, K. & Lambris, J. D. Complement: A key system for immune surveillance and homeostasis. *Nature Immunology* **11**, 785–797 (2010).
137. Mastellos, D. C., DeAngelis, R. A. & Lambris, J. D. Complement-triggered pathways orchestrate regenerative responses throughout phylogenesis. *Seminars in Immunology* **25**, 29–38 (2013).
138. Noris, M. & Remuzzi, G. Overview of complement activation and regulation. *Seminars in Nephrology* **33**, 479–492 (2013).
139. Veerhuis, R., Nielsen, H. M. & Tenner, A. J. Complement in the brain. *Molecular Immunology* **48**, 1592–1603 (2011).
140. Rutkowski, M. J. *et al.* Complement and the central nervous system: Emerging roles in development, protection and regeneration. *Immunology & Cell Biology* **88**, 781–786 (2010).
141. Lubbers, R., Essen, M. F. van, Kooten, C. van & Trouw, L. A. Production of complement components by cells of the immune system. *Clinical & Experimental Immunology* **188**, 183–194 (2017).
142. Abbott, N. J., Patabendige, A. A. K., Dolman, D. E. M., Yusof, S. R. & Begley, D. J. Structure and function of the blood–brain barrier. *Neurobiology of Disease* **37**, 13–25 (2010).
143. Gasque, P., Fontaine, M. & Morgan, B. P. Complement expression in human brain. Biosynthesis of terminal pathway components and regulators in human glial cells and cell lines. *The Journal of Immunology* **154**, 4726–4733 (1995).
144. Walker, D. G. & McGeer, P. L. Complement gene expression in human brain: Comparison between normal and Alzheimer disease cases. *Molecular Brain Research* **14**, 109–116 (1992).
145. Lévi-Strauss, M. & Mallat, M. Primary cultures of murine astrocytes produce C3 and factor B, two components of the alternative pathway of complement activation. *The Journal of Immunology* **139**, 2361–2366 (1987).
146. Morgan, B. P. & Gasque, P. Extrahepatic complement biosynthesis: Where, when and why? *Clinical & Experimental Immunology* **107**, (1997).
147. Barnum, S. R. Complement biosynthesis in the central nervous system. *Critical Reviews in Oral Biology & Medicine* **6**, 132–146 (1995).
148. Druart, M. & Le Magueresse, C. Emerging roles of complement in psychiatric disorders. *Front. Psychiatry* **10**, (2019).
149. Cahoy, J. D. *et al.* A transcriptome database for astrocytes, neurons, and oligodendrocytes: A new resource for understanding brain development and function. *J. Neurosci.* **28**, 264–278 (2008).
150. Singhrao, S. K., Neal, J. W., Rushmere, N. K., Morgan, B. P. & Gasque, P. Spontaneous classical pathway activation and deficiency of membrane regulators render human neurons susceptible to complement lysis. *Am J Pathol* **157**, 905–918 (2000).
151. Rahpeymai, Y. *et al.* Complement: A novel factor in basal and ischemia-induced neurogenesis. *EMBO J* **25**, 1364–1374 (2006).
152. Bogestål, Y. R. *et al.* Signaling through C5aR is not involved in basal neurogenesis. *Journal of Neuroscience Research* **85**, 2892–2897 (2007).
153. Bénard, M. *et al.* Role of complement anaphylatoxin receptors (C3aR, C5aR) in the development of the rat cerebellum. *Molecular Immunology* **45**, 3767–3774 (2008).
154. Oomman, S., Strahlendorf, H., Dertien, J. & Strahlendorf, J. Bergmann glia utilize active caspase-3 for differentiation. *Brain Research* **1078**, 19–34 (2006).
155. Benoit, M. E. & Tenner, A. J. Complement protein C1q-mediated neuroprotection is correlated with regulation of neuronal gene and microRNA expression. *J. Neurosci.* **31**, 3459–3469 (2011).
156. Bénard, M. *et al.* Characterization of C3a and C5a receptors in rat cerebellar granule neurons during maturation: Neuroprotective effect of C5a against apoptotic cell death. *J. Biol. Chem.* **279**, 43487–43496 (2004).
157. Gorelik, A. *et al.* Developmental activities of the complement pathway in migrating neurons. *Nature Communications* **8**, (2017).
158. Carmona-Fontaine, C. *et al.* Complement fragment C3a controls mutual cell attraction during collective cell migration. *Developmental Cell* **21**, 1026–1037 (2011).

159. Shinjyo, N., Ståhlberg, A., Dragunow, M., Pekny, M. & Pekna, M. Complement-derived anaphylatoxin C3a regulates in vitro differentiation and migration of neural progenitor cells. *Stem Cells* **27**, 2824–2832 (2009).
160. Stevens, B. *et al.* The Classical Complement Cascade Mediates CNS Synapse Elimination. *Cell* **131**, 1164–1178 (2007).
161. Vainchtein, I. D. *et al.* Astrocyte-derived interleukin-33 promotes microglial synapse engulfment and neural circuit development. *Science* **359**, 1269–1273 (2018).
162. Chung, W.-S. *et al.* Astrocytes mediate synapse elimination through MEGF10 and MERTK pathways. *Nature* **504**, 394–400 (2013).
163. Iram, T. *et al.* Megf10 is a receptor for C1q that mediates clearance of apoptotic cells by astrocytes. *J. Neurosci.* **36**, 5185–5192 (2016).
164. Györfy, B. A. *et al.* Local apoptotic-like mechanisms underlie complement-mediated synaptic pruning. *PNAS* **115**, 6303–6308 (2018).
165. Martin, S. J. *et al.* Early redistribution of plasma membrane phosphatidylserine is a general feature of apoptosis regardless of the initiating stimulus: Inhibition by overexpression of Bcl-2 and Abl. *J Exp Med* **182**, 1545–1556 (1995).
166. Segawa, K. & Nagata, S. An apoptotic ‘eat me’ signal: Phosphatidylserine exposure. *Trends in Cell Biology* **25**, 639–650 (2015).
167. Li, T. *et al.* A splicing isoform of GPR56 mediates microglial synaptic refinement via phosphatidylserine binding. *The EMBO Journal* (2020).
168. Chu, Y. *et al.* Enhanced synaptic connectivity and epilepsy in C1q knockout mice. *PNAS* **107**, 7975–7980 (2010).
169. Wang, C. *et al.* Microglia mediate forgetting via complement-dependent synaptic elimination. *Science* **367**, 688–694 (2020).
170. Zhang, J. *et al.* Microglial CR3 activation triggers long-term synaptic depression in the hippocampus via NADPH oxidase. *Neuron* **82**, 195–207 (2014).
171. Lehrman, E. K. *et al.* CD47 protects synapses from excess microglia-mediated pruning during development. *Neuron* **100**, 120–134 (2018).
172. Chung, W.-S. & Barres, B. A. The role of glial cells in synapse elimination. *Current Opinion in Neurobiology* **22**, 438–445 (2012).
173. Um, J. W. Roles of glial cells in sculpting inhibitory synapses and neural circuits. *Front. Mol. Neurosci.* **10**, (2017).
174. Sekar, A. *et al.* Schizophrenia risk from complex variation of complement component 4. *Nature* **530**, 177–183 (2016).
175. Håvik, B. *et al.* The complement control-related genes CSMD1 and CSMD2 associate to schizophrenia. *Biological Psychiatry* **70**, 35–42 (2011).
176. Jun Tan, C. F. C1q as a regulator of brain development: Implications for Autism Spectrum Disorders. *Brain Disord Ther* **4**, (2015).
177. Corbett, B. A. *et al.* A proteomic study of serum from children with autism showing differential expression of apolipoproteins and complement proteins. *Molecular Psychiatry* **12**, 292–306 (2007).
178. Warren, R. P., Yonk, J., Burger, R. W., Odell, D. & Warren, W. L. DR-Positive T Cells in autism: Association with decreased plasma levels of the complement C4B protein. *NPS* **31**, 53–57 (1995).
179. Odell, D. *et al.* Confirmation of the association of the C4B null allele in autism. *Human Immunology* **66**, 140–145 (2005).
180. Warren, R. P., Burger, R. A., Odell, D., Torres, A. R. & Warren, W. L. Decreased plasma concentrations of the C4B complement protein in autism. *Arch Pediatr Adolesc Med* **148**, 180–183 (1994).
181. Kawai, T. & Akira, S. TLR signaling. *Cell Death & Differentiation* **13**, 816–825 (2006).
182. Kawasaki, T. & Kawai, T. Toll-like receptor signaling pathways. *Front. Immunol.* **5**, (2014).
183. Miyake, K. Innate immune sensing of pathogens and danger signals by cell surface Toll-like receptors. *Seminars in Immunology* **19**, 3–10 (2007).
184. Okun, E., Griffioen, K. J. & Mattson, M. P. Toll-like receptor signaling in neural plasticity and disease. *Trends in Neurosciences* **34**, 269–281 (2011).
185. Barak, B., Feldman, N. & Okun, E. Toll-like receptors as developmental tools that regulate neurogenesis during development: an update. *Front. Neurosci.* **8**, (2014).

186. Chen, C.-Y., Shih, Y.-C., Hung, Y.-F. & Hsueh, Y.-P. Beyond defense: Regulation of neuronal morphogenesis and brain functions via Toll-like receptors. *Journal of Biomedical Science* **26**, (2019).
187. Hanke, M. L. & Kielian, T. Toll-like receptors in health and disease in the brain: Mechanisms and therapeutic potential. *Clin Sci (Lond)* **121**, 367–387 (2011).
188. Liu, H.-Y., Chen, C.-Y. & Hsueh, Y.-P. Innate immune responses regulate morphogenesis and degeneration: Roles of Toll-like receptors and Sarm1 in neurons. *Neurosci. Bull.* **30**, 645–654 (2014).
189. Kaul, D. *et al.* Expression of Toll-like receptors in the developing brain. *PLOS One* **7**, (2012).
190. Zhang, Y. *et al.* An RNA-sequencing transcriptome and splicing database of glia, neurons, and vascular cells of the cerebral cortex. *J. Neurosci.* **34**, 11929–11947 (2014).
191. Bsibsi, M., Ravid, R., Gveric, D. & van Noort, J. M. Broad expression of Toll-Like Receptors in the human central nervous system. *J Neuropathol Exp Neurol* **61**, 1013–1021 (2002).
192. Olson, J. K. & Miller, S. D. Microglia initiate central nervous system innate and adaptive immune responses through multiple TLRs. *The Journal of Immunology* **173**, 3916–3924 (2004).
193. Préhaud, C., Mégrét, F., Lafage, M. & Lafon, M. Virus infection switches TLR-3-positive human neurons to become strong producers of beta interferon. *Journal of Virology* **79**, 12893–12904 (2005).
194. Jackson, A. C., Rossiter, J. P. & Lafon, M. Expression of Toll-like receptor 3 in the human cerebellar cortex in rabies, herpes simplex encephalitis, and other neurological diseases. *Journal of NeuroVirology* **12**, 229–234 (2006).
195. Lafon, M., Megret, F., Lafage, M. & Prehaud, C. The innate immune facet of brain. *J Mol Neurosci* **29**, 185–194 (2006).
196. Tang, S.-C. *et al.* Pivotal role for neuronal Toll-like receptors in ischemic brain injury and functional deficits. *PNAS* **104**, 13798–13803 (2007).
197. Kim, D. *et al.* A critical role of Toll-like Receptor 2 in nerve injury-induced spinal cord glial cell activation and pain hypersensitivity. *J. Biol. Chem.* **282**, 14975–14983 (2007).
198. Acosta, C. & Davies, A. Bacterial lipopolysaccharide regulates nociceptin expression in sensory neurons. *Journal of Neuroscience Research* **86**, 1077–1086 (2008).
199. Prinz, M. *et al.* Innate immunity mediated by TLR9 modulates pathogenicity in an animal model of multiple sclerosis. *J Clin Invest* **116**, 456–464 (2006).
200. Tahara, K. *et al.* Role of toll-like receptor signalling in A β uptake and clearance. *Brain* **129**, 3006–3019 (2006).
201. van Noort, J. M. & Bsibsi, M. Toll-like receptors in the CNS: Implications for neurodegeneration and repair. *Progress in Brain Research* **175**, 139–148 (2009).
202. Fiebich, B. L., Batista, C. R. A., Saliba, S. W., Yousif, N. M. & de Oliveira, A. C. P. Role of microglia TLRs in neurodegeneration. *Front. Cell. Neurosci.* **12**, (2018).
203. Kielian, T. Toll-like receptors in central nervous system glial inflammation and homeostasis. *Journal of Neuroscience Research* **83**, 711–730 (2006).
204. Trudler, D., Farfara, D. & Frenkel, D. Toll-like receptors expression and signaling in glia cells in neuro-amyloidogenic diseases: Towards future therapeutic application. *Mediators of Inflammation* **2010**, (2010).
205. Okun, E. *et al.* Toll-like receptors in neurodegeneration. *Brain Research Reviews* **59**, 278–292 (2009).
206. Yu, L., Wang, L. & Chen, S. Endogenous toll-like receptor ligands and their biological significance. *Journal of Cellular and Molecular Medicine* **14**, 2592–2603 (2010).
207. Xagorari, A. & Chlichlia, K. Toll-like receptors and viruses: Induction of innate antiviral immune responses. *The Open Microbiology Journal* **2**, (2008).
208. Okun, E. *et al.* TLR2 activation inhibits embryonic neural progenitor cell proliferation. *Journal of Neurochemistry* **114**, 462–474 (2010).
209. Lathia, J. D. *et al.* Toll-Like Receptor 3 is a negative regulator of embryonic neural progenitor cell proliferation. *J. Neurosci.* **28**, 13978–13984 (2008).
210. Rallabhandi, P. *et al.* Analysis of TLR4 polymorphic variants: New insights into TLR4/MD-2/CD14 stoichiometry, structure, and signaling. *The Journal of Immunology* **177**, 322–332 (2006).
211. Bsibsi, M. *et al.* Identification of soluble CD14 as an endogenous agonist for Toll-like receptor 2 on human astrocytes by genome-scale functional screening of glial cell derived proteins. *Glia* **55**, 473–482 (2007).
212. Shechter, R. *et al.* Toll-like receptor 4 restricts retinal progenitor cell proliferation. *Journal of Cell Biology* **183**, 393–400 (2008).

213. Lehnardt, S. *et al.* A vicious cycle involving release of Heat Shock Protein 60 from injured cells and activation of Toll-Like Receptor 4 mediates neurodegeneration in the CNS. *J. Neurosci.* **28**, 2320–2331 (2008).
214. Jou, I. *et al.* Gangliosides trigger inflammatory responses via TLR4 in brain glia. *The American Journal of Pathology* **168**, 1619–1630 (2006).
215. Rolls, A. *et al.* Toll-like receptors modulate adult hippocampal neurogenesis. *Nature Cell Biology* **9**, 1081–1088 (2007).
216. Ma, Y. *et al.* Toll-like receptor 8 functions as a negative regulator of neurite outgrowth and inducer of neuronal apoptosis. *J Cell Biol* **175**, 209–215 (2006).
217. Cameron, J. S. *et al.* Toll-Like Receptor 3 is a potent negative regulator of axonal growth in mammals. *J. Neurosci.* **27**, 13033–13041 (2007).
218. Butchi, N. B., Du, M. & Peterson, K. E. Interactions between TLR7 and TLR9 agonists and receptors regulate innate immune responses by astrocytes and microglia. *Glia* **58**, 650–664 (2010).
219. Lehmann, S. M. *et al.* Extracellularly delivered single-stranded viral RNA causes neurodegeneration dependent on TLR7. *The Journal of Immunology* **189**, 1448–1458 (2012).
220. Mukherjee, P. *et al.* SARM1, not MyD88, mediates TLR7/TLR9-induced apoptosis in neurons. *J Immunol* **195**, 4913–4921 (2015).
221. Lehmann, S. M. *et al.* An unconventional role for miRNA: Let-7 activates Toll-like receptor 7 and causes neurodegeneration. *Nature Neuroscience* **15**, 827–835 (2012).
222. Kim, Y. *et al.* MyD88-5 links mitochondria, microtubules, and JNK3 in neurons and regulates neuronal survival. *J Exp Med* **204**, 2063–2074 (2007).
223. Kuan, C.-Y. *et al.* A critical role of neural-specific JNK3 for ischemic apoptosis. *PNAS* **100**, 15184–15189 (2003).
224. Okuno, S., Saito, A., Hayashi, T. & Chan, P. H. The c-Jun N-terminal protein kinase signaling pathway mediates Bax activation and subsequent neuronal apoptosis through interaction with Bim after transient focal cerebral ischemia. *J. Neurosci.* **24**, 7879–7887 (2004).
225. Carboni, S. *et al.* Control of death receptor and mitochondrial-dependent apoptosis by c-Jun N-terminal kinase in hippocampal CA1 neurones following global transient ischaemia. *Journal of Neurochemistry* **92**, 1054–1060 (2005).
226. Dłużniewska, J., Beręsewicz, M., Wojewódzka, U., Gajkowska, B. & Zabłocka, B. Transient cerebral ischemia induces delayed proapoptotic Bad translocation to mitochondria in CA1 sector of hippocampus. *Molecular Brain Research* **133**, 274–280 (2005).
227. Harding, T. C. *et al.* Inhibition of JNK by overexpression of the JNK binding domain of JIP-1 prevents apoptosis in sympathetic neurons. *J. Biol. Chem.* **276**, 4531–4534 (2001).
228. Hung, Y.-F. *et al.* Endosomal TLR3, TLR7, and TLR8 control neuronal morphology through different transcriptional programs. *J Cell Biol* **217**, 2727–2742 (2018).
229. Liu, H.-Y., Huang, C.-M., Hung, Y.-F. & Hsueh, Y.-P. The microRNAs Let7c and miR21 are recognized by neuronal Toll-like receptor 7 to restrict dendritic growth of neurons. *Experimental Neurology* **269**, 202–212 (2015).
230. Fabbri, M. *et al.* MicroRNAs bind to Toll-like receptors to induce prometastatic inflammatory response. *PNAS* **109**, 2110–2116 (2012).
231. Park, C.-K. *et al.* Extracellular microRNAs activate nociceptor neurons to elicit pain via TLR7 and TRPA1. *Neuron* **82**, 47–54 (2014).
232. Liu, T., Xu, Z.-Z., Park, C.-K., Berta, T. & Ji, R.-R. Toll-like receptor 7 mediates pruritus. *Nature Neuroscience* **13**, 1460–1462 (2010).
233. Bartel, D. P. MicroRNAs: Target recognition and regulatory functions. *Cell* **136**, 215–233 (2009).
234. Valadi, H. *et al.* Exosome-mediated transfer of mRNAs and microRNAs is a novel mechanism of genetic exchange between cells. *Nature Cell Biology* **9**, 654–659 (2007).
235. Liu, H.-Y. *et al.* TLR7 negatively regulates dendrite outgrowth through the Myd88–c-Fos–IL-6 pathway. *J. Neurosci.* **33**, 11479–11493 (2013).
236. Takeuchi, O. & Akira, S. Pattern recognition receptors and inflammation. *Cell* **140**, 805–820 (2010).
237. Chen, C.-Y., Liu, H.-Y. & Hsueh, Y.-P. TLR3 downregulates expression of schizophrenia gene Disc1 via MYD88 to control neuronal morphology. *EMBO reports* **18**, 169–183 (2017).
238. Chen, C.-Y., Lin, C.-W., Chang, C.-Y., Jiang, S.-T. & Hsueh, Y.-P. Sarm1, a negative regulator of innate immunity, interacts with syndecan-2 and regulates neuronal morphology. *J Cell Biol* **193**, 769–784 (2011).

239. Osterloh, J. M. *et al.* dSarm/Sarm1 is required for activation of an injury-induced axon death pathway. *Science* **337**, 481–484 (2012).
240. Conforti, L., Gilley, J. & Coleman, M. P. Wallerian degeneration: An emerging axon death pathway linking injury and disease. *Nature Reviews Neuroscience* **15**, 394–409 (2014).
241. Park, S. J. *et al.* Toll-like receptor-2 deficiency induces schizophrenia-like behaviors in mice. *Scientific Reports* **5**, (2015).
242. Shechter, R. *et al.* Hypothalamic neuronal toll-like receptor 2 protects against age-induced obesity. *Scientific Reports* **3**, (2013).
243. Okun, E. *et al.* Toll-like receptor 3 inhibits memory retention and constrains adult hippocampal neurogenesis. *PNAS* **107**, 15625–15630 (2010).
244. Ritchie, L. *et al.* Toll-like receptor 3 activation impairs excitability and synaptic activity via TRIF signalling in immature rat and human neurons. *Neuropharmacology* **135**, (2018).
245. Okun, E. *et al.* Evidence for a developmental role for TLR4 in learning and memory. *PLOS One* **7**, (2012).
246. Kashima, D. T. & Grueter, B. A. Toll-like receptor 4 deficiency alters nucleus accumbens synaptic physiology and drug reward behavior. *PNAS* **114**, 8865–8870 (2017).
247. Hung, Y.-F., Chen, C.-Y., Li, W.-C., Wang, T.-F. & Hsueh, Y.-P. Tlr7 deletion alters expression profiles of genes related to neural function and regulates mouse behaviors and contextual memory. *Brain, Behavior, and Immunity* **72**, 101–113 (2018).
248. Khariv, V. *et al.* Toll-like receptor 9 deficiency impacts sensory and motor behaviors. *Brain, Behavior, and Immunity* **32**, 164–172 (2013).
249. Lin, C.-W. & Hsueh, Y.-P. Sarm1, a neuronal inflammatory regulator, controls social interaction, associative memory and cognitive flexibility in mice. *Brain, Behavior, and Immunity* **37**, 142–151 (2014).
250. Missig, G. *et al.* Sex-dependent neurobiological features of prenatal immune activation via TLR7. *Molecular Psychiatry* (2019).
251. Patterson, P. H. Immune involvement in schizophrenia and autism: Etiology, pathology and animal models. *Behavioural Brain Research* **204**, 313–321 (2009).
252. Malkova, N. V., Yu, C. Z., Hsiao, E. Y., Moore, M. J. & Patterson, P. H. Maternal immune activation yields offspring displaying mouse versions of the three core symptoms of autism. *Brain, Behavior, and Immunity* **26**, 607–616 (2012).
253. Becher, B., Spath, S. & Goverman, J. Cytokine networks in neuroinflammation. *Nature Reviews Immunology* **17**, 49–59 (2017).
254. Kennedy, R. H. & Silver, R. Neuroimmune signaling: Cytokines and the CNS. in *Neuroscience in the 21st Century* (eds Pfaff, D. W. & Volkow, N. D.) 1–41 (Springer, 2016).
255. Borsini, A., Zunszain, P. A., Thuret, S. & Pariante, C. M. The role of inflammatory cytokines as key modulators of neurogenesis. *Trends in Neurosciences* **38**, 145–157 (2015).
256. Filiano, A. J., Gadani, S. P. & Kipnis, J. How and why do T cells and their derived cytokines affect the injured and healthy brain? *Nature Reviews Neuroscience* **18**, 375–384 (2017).
257. Zheng, C., Zhou, X.-W. & Wang, J.-Z. The dual roles of cytokines in Alzheimer’s disease: Update on interleukins, TNF- α , TGF- β and IFN- γ . *Translational Neurodegeneration* **5**, 7 (2016).
258. Allan, S. M. & Rothwell, N. J. Cytokines and acute neurodegeneration. *Nature Reviews Neuroscience* **2**, 734–744 (2001).
259. Arvin, B., Neville, L. F., Barone, F. C. & Feuerstein, G. Z. The role of inflammation and cytokines in brain injury. *Neuroscience & Biobehavioral Reviews* **20**, 445–452 (1996).
260. Carpentier, P. A. & Palmer, T. D. Immune influence on adult neural stem cell regulation and function. *Neuron* **64**, 79–92 (2009).
261. Deverman, B. E. & Patterson, P. H. Cytokines and CNS Development. *Neuron* **64**, 61–78 (2009).
262. Bauer, S., Kerr, B. J. & Patterson, P. H. The neuropoietic cytokine family in development, plasticity, disease and injury. *Nature Reviews Neuroscience* **8**, 221–232 (2007).
263. Stolp, H. B. Neuropoietic cytokines in normal brain development and neurodevelopmental disorders. *Molecular and Cellular Neuroscience* **53**, 63–68 (2013).
264. Tanaka, T., Narazaki, M. & Kishimoto, T. IL-6 in inflammation, immunity, and disease. *Cold Spring Harb Perspect Biol* **6**, (2014).
265. Muñoz-Fernández, M. A. & Fresno, M. The role of tumour necrosis factor, interleukin 6, interferon- γ and inducible nitric oxide synthase in the development and pathology of the nervous system. *Progress in Neurobiology* **56**, 307–340 (1998).

266. Pousset, F. Developmental expression of cytokine genes in the cortex and hippocampus of the rat central nervous system. *Developmental Brain Research* **81**, 143–146 (1994).
267. Burns, T. M., Clough, J. A., Klein, R. M., Wood, G. W. & Berman, N. E. J. Developmental regulation of cytokine expression in the mouse brain. *Growth Factors* (2009).
268. Gadiant, R. A., Lachmund, A., Unsicker, K. & Ottena, U. Expression of interleukin-6 (IL-6) and IL-6 receptor mRNAs in rat adrenal medulla. *Neuroscience Letters* **194**, 17–20 (1995).
269. Johansson, S., Price, J. & Mado, M. Effect of inflammatory cytokines on Major Histocompatibility Complex expression and differentiation of human neural stem/progenitor cells. *Stem Cells* **26**, 2444–2454 (2008).
270. Oh, Y. J. & O'Malley, K. L. IL-6 increases choline acetyltransferase but not neuropeptide transcripts in sympathetic neurons. *Neuroreport* **5**, 937–940 (1994).
271. Mizuno, T., Sawada, M., Suzumura, A. & Marunouchi, T. Expression of cytokines during glial differentiation. *Brain Research* **656**, 141–146 (1994).
272. Akaneya, Y., Takahashi, M. & Hatanaka, H. Interleukin-1 beta enhances survival and interleukin-6 protects against MPP⁺ neurotoxicity in cultures of fetal rat dopaminergic neurons. *Exp Neurol* **136**, 44–52 (1995).
273. Kushima, Y., Hama, T. & Hatanaka, H. Interleukin-6 as a neurotrophic factor for promoting the survival of cultured catecholaminergic neurons in a chemically defined medium from fetal and postnatal rat midbrains. *Neuroscience Research* **13**, 267–280 (1992).
274. Hama, T. *et al.* Interleukin-6 improves the survival of mesencephalic catecholaminergic and septal cholinergic neurons from postnatal, two-week-old rats in cultures. *Neuroscience* **40**, 445–452 (1991).
275. Islam, O., Gong, X., Rose-John, S. & Heese, K. Interleukin-6 and neural stem cells: More than gliogenesis. *Molecular Biology of the Cell* **20**, (2008).
276. Wagner, J. A. Is IL-6 both a cytokine and a neurotrophic factor? *J Exp Med* **183**, 2417–2419 (1996).
277. Gilmore, J. H., Fredrik Jarskog, L., Vadlamudi, S. & Lauder, J. M. Prenatal Infection and Risk for Schizophrenia: IL-1 β , IL-6, and TNF α Inhibit Cortical Neuron Dendrite Development. *Neuropsychopharmacology* **29**, 1221–1229 (2004).
278. Sims, J. E. & Smith, D. E. The IL-1 family: Regulators of immunity. *Nature Reviews Immunology* **10**, 89–102 (2010).
279. Park, S.-Y., Kang, M.-J. & Han, J.-S. Interleukin-1 beta promotes neuronal differentiation through the Wnt5a/RhoA/JNK pathway in cortical neural precursor cells. *Molecular Brain* **11**, 39 (2018).
280. de la Mano, A. *et al.* Role of interleukin-1 β in the control of neuroepithelial proliferation and differentiation of the spinal cord during development. *Cytokine* **37**, 128–137 (2007).
281. Gougeon, P.-Y. *et al.* The pro-inflammatory cytokines IL-1 β and TNF α are neurotrophic for enteric neurons. *J. Neurosci.* **33**, 3339–3351 (2013).
282. Garber, C. *et al.* Astrocytes decrease adult neurogenesis during virus-induced memory dysfunction via IL-1. *Nature Immunology* **19**, 151–161 (2018).
283. Wang, X. *et al.* Interleukin-1beta mediates proliferation and differentiation of multipotent neural precursor cells through the activation of SAPK/JNK pathway. *Mol Cell Neurosci* **36**, 343–354 (2007).
284. McPherson, C. A., Aoyama, M. & Harry, G. J. Interleukin (IL)-1 and IL-6 regulation of neural progenitor cell proliferation with hippocampal injury: Differential regulatory pathways in the subgranular zone (SGZ) of the adolescent and mature mouse brain. *Brain, Behavior, and Immunity* **25**, 850–862 (2011).
285. Zunszain, P. A. *et al.* Interleukin-1 β : A new regulator of the kynurenine pathway affecting human hippocampal neurogenesis. *Neuropsychopharmacology : official publication of the American College of Neuropsychopharmacology* **37**, 939–949 (2012).
286. Zhang, K., Xu, H., Cao, L., Li, K. & Huang, Q. Interleukin-1 β inhibits the differentiation of hippocampal neural precursor cells into serotonergic neurons. *Brain Research* **1490**, 193–201 (2013).
287. Crampton, S. J., Collins, L. M., Toulouse, A., Nolan, Y. M. & O'Keefe, G. W. Exposure of foetal neural progenitor cells to IL-1 β impairs their proliferation and alters their differentiation – a role for maternal inflammation? *Journal of Neurochemistry* **120**, 964–973 (2012).
288. Ling, Z. D., Potter, E. D., Lipton, J. W. & Carvey, P. M. Differentiation of mesencephalic progenitor cells into dopaminergic neurons by cytokines. *Experimental Neurology* **149**, 411–423 (1998).
289. Greco, S. J. & Rameshwar, P. Enhancing Effect of IL-1 α on Neurogenesis from Adult Human Mesenchymal Stem Cells: Implication for Inflammatory Mediators in Regenerative Medicine. *The Journal of Immunology* **179**, 3342–3350 (2007).

290. Ajmone-Cat, M. A., Cacci, E., Ragazzoni, Y., Minghetti, L. & Biagioni, S. Pro-gliogenic effect of IL-1 α in the differentiation of embryonic neural precursor cells in vitro. *Journal of Neurochemistry* **113**, 1060–1072 (2010).
291. Giulian, D., Young, D. G., Woodward, J., Brown, D. C. & Lachman, L. B. Interleukin-1 is an astroglial growth factor in the developing brain. *J. Neurosci.* **8**, 709–714 (1988).
292. Nolan, A. M., Nolan, Y. M. & O’Keeffe, G. W. IL-1 β inhibits axonal growth of developing sympathetic neurons. *Molecular and Cellular Neuroscience* **48**, 142–150 (2011).
293. Boato, F. *et al.* Interleukin-1 beta and neurotrophin-3 synergistically promote neurite growth in vitro. *Journal of Neuroinflammation* **8**, 183 (2011).
294. Ma, L. *et al.* Interleukin-1 beta guides the migration of cortical neurons. *Journal of Neuroinflammation* **11**, 114 (2014).
295. Gilmore, J. H., Fredrik Jarskog, L., Vadlamudi, S. & Lauder, J. M. Prenatal infection and risk for schizophrenia: IL-1 β , IL-6, and TNF α inhibit cortical neuron dendrite development. *Neuropsychopharmacology* **29**, 1221–1229 (2004).
296. Yoshida, T. *et al.* IL-1 Receptor Accessory Protein-Like 1 associated with mental retardation and Autism mediates synapse formation by trans-synaptic interaction with Protein Tyrosine Phosphatase δ . *J. Neurosci.* **31**, 13485–13499 (2011).
297. Yoshida, T. *et al.* Interleukin-1 receptor accessory protein organizes neuronal synaptogenesis as a cell adhesion molecule. *J. Neurosci.* **32**, 2588–2600 (2012).
298. Pavlowsky, A. *et al.* A postsynaptic signaling pathway that may account for the cognitive defect due to IL1RAPL1 mutation. *Current Biology* **20**, 103–115 (2010).
299. Piton, A. *et al.* Mutations in the calcium-related gene IL1RAPL1 are associated with autism. *Hum Mol Genet* **17**, 3965–3974 (2008).
300. Carrié, A. *et al.* A new member of the IL-1 receptor family highly expressed in hippocampus and involved in X-linked mental retardation. *Nature Genetics* **23**, 25–31 (1999).
301. Gambino, F. *et al.* IL1RAPL1 controls inhibitory networks during cerebellar development in mice. *European Journal of Neuroscience* **30**, 1476–1486 (2009).
302. Houbaert, X. *et al.* Target-specific vulnerability of excitatory synapses leads to deficits in associative memory in a model of intellectual disorder. *J. Neurosci.* **33**, 13805–13819 (2013).
303. Molofsky, A. B., Savage, A. K. & Locksley, R. M. Interleukin-33 in tissue homeostasis, injury, and inflammation. *Immunity* **42**, 1005–1019 (2015).
304. Gadani, S. P., Walsh, J. T., Smirnov, I., Zheng, J. & Kipnis, J. The glia-derived alarmin IL-33 orchestrates the immune response and promotes recovery following CNS injury. *Neuron* **85**, 703–709 (2015).
305. Pomeshchik, Y. *et al.* Interleukin-33 treatment reduces secondary injury and improves functional recovery after contusion spinal cord injury. *Brain, Behavior, and Immunity* **44**, 68–81 (2015).
306. Dohi, E. *et al.* Behavioral changes in mice lacking Interleukin-33. *eNeuro* **4**, (2017).
307. Wiktor-Jedrzejczak, W. *et al.* Total absence of colony-stimulating factor 1 in the macrophage-deficient osteopetrotic (op/op) mouse. *PNAS* **87**, 4828–4832 (1990).
308. Dai, X.-M. *et al.* Targeted disruption of the mouse colony-stimulating factor 1 receptor gene results in osteopetrosis, mononuclear phagocyte deficiency, increased primitive progenitor cell frequencies, and reproductive defects. *Blood* **99**, 111–120 (2002).
309. Wang, Y. *et al.* IL-34 is a tissue-restricted ligand of CSF1R required for the development of Langerhans cells and microglia. *Nature Immunology* **13**, 753–760 (2012).
310. Greter, M. *et al.* Stroma-derived Interleukin-34 controls the development and maintenance of Langerhans cells and the maintenance of microglia. *Immunity* **37**, 1050–1060 (2012).
311. Luzina, I. G. *et al.* Regulation of inflammation by interleukin-4: A review of “alternatives”. *J Leukoc Biol* **92**, 753–764 (2012).
312. Gadani, S. P., Cronk, J. C., Norris, G. T. & Kipnis, J. IL-4 in the brain: A cytokine to remember. *The Journal of Immunology* **189**, 4213–4219 (2012).
313. Zhang, J. *et al.* IL4-driven microglia modulate stress resilience through BDNF-dependent neurogenesis. *bioRxiv* 2020.02.01.929646 (2020) doi:10.1101/2020.02.01.929646.
314. Bhattarai, P. *et al.* IL4/STAT6 signaling activates neural stem cell proliferation and neurogenesis upon amyloid- β 42 aggregation in adult zebrafish brain. *Cell Reports* **17**, 941–948 (2016).
315. Wolf, S. A. *et al.* Adaptive peripheral immune response increases proliferation of neural precursor cells in the adult hippocampus. *The FASEB Journal* **23**, 3121–3128 (2009).

316. Wolf, S. A. *et al.* CD4-positive T lymphocytes provide a neuroimmunological link in the control of adult hippocampal neurogenesis. *The Journal of Immunology* **182**, 3979–3984 (2009).
317. Ziv, Y. *et al.* Immune cells contribute to the maintenance of neurogenesis and spatial learning abilities in adulthood. *Nature Neuroscience* **9**, 268–275 (2006).
318. Derecki, N. C. *et al.* Regulation of learning and memory by meningeal immunity: A key role for IL-4. *J Exp Med* **207**, 1067–1080 (2010).
319. Li, J. *et al.* IL-9 and Th9 cells in health and diseases—from tolerance to immunopathology. *Cytokine Growth Factor Rev* **37**, 47–55 (2017).
320. Fontaine, R. H. *et al.* IL-9/IL-9 receptor signaling selectively protects cortical neurons against developmental apoptosis. *Cell Death Differ* **15**, 1542–1552 (2008).
321. Mehler, M. F., Rozental, R., Dougherty, M., Spray, D. C. & Kessler, J. A. Cytokine regulation of neuronal differentiation of hippocampal progenitor cells. *Nature* **362**, 62–65 (1993).
322. Mesples, B., Fontaine, R. H., Lelievre, V., Launay, J.-M. & Gressens, P. Neuronal TGF- β 1 mediates IL-9/mast cell interaction and exacerbates excitotoxicity in newborn mice. *Neurobiology of Disease* **18**, 193–205 (2005).
323. Ransohoff, R. M. Chemokines and chemokine receptors: Standing at the crossroads of immunobiology and neurobiology. *Immunity* **31**, 711–721 (2009).
324. Moser, B., Wolf, M., Walz, A. & Loetscher, P. Chemokines: multiple levels of leukocyte migration control. *Trends in Immunology* **25**, 75–84 (2004).
325. Li, M. & Ransohoff, R. M. Multiple roles of chemokine CXCL12 in the central nervous system: A migration from immunology to neurobiology. *Progress in Neurobiology* **84**, 116–131 (2008).
326. Zhu, Y. & Murakami, F. Chemokine CXCL12 and its receptors in the developing central nervous system: Emerging themes and future perspectives. *Developmental Neurobiology* **72**, 1349–1362 (2012).
327. Guyon, A. CXCL12 chemokine and its receptors as major players in the interactions between immune and nervous systems. *Front. Cell. Neurosci.* **8**, (2014).
328. Tissir, F., Wang, C.-E. & Goffinet, A. M. Expression of the chemokine receptor Cxcr4 mRNA during mouse brain development. *Developmental Brain Research* **149**, 63–71 (2004).
329. Reiss, K., Mentlein, R., Sievers, J. & Hartmann, D. Stromal cell-derived factor 1 is secreted by meningeal cells and acts as chemotactic factor on neuronal stem cells of the cerebellar external granular layer. *Neuroscience* **115**, 295–305 (2002).
330. Zhu, Y. *et al.* Role of the chemokine SDF-1 as the meningeal attractant for embryonic cerebellar neurons. *Nature Neuroscience* **5**, 719–720 (2002).
331. Klein, R. S. *et al.* SDF-1 α induces chemotaxis and enhances Sonic hedgehog-induced proliferation of cerebellar granule cells. *Development* **128**, 1971–1981 (2001).
332. Zou, Y.-R., Kottmann, A. H., Kuroda, M., Taniuchi, I. & Littman, D. R. Function of the chemokine receptor CXCR4 in haematopoiesis and in cerebellar development. *Nature* **393**, 595–599 (1998).
333. Ma, Q. *et al.* Impaired B-lymphopoiesis, myelopoiesis, and derailed cerebellar neuron migration in CXCR4- and SDF-1-deficient mice. *PNAS* **95**, 9448–9453 (1998).
334. Lu, M., Grove, E. A. & Miller, R. J. Abnormal development of the hippocampal dentate gyrus in mice lacking the CXCR4 chemokine receptor. *PNAS* **99**, 7090–7095 (2002).
335. Stumm, R. K. *et al.* CXCR4 regulates interneuron migration in the developing neocortex. *J. Neurosci.* **23**, 5123–5130 (2003).
336. López-Bendito, G. *et al.* Chemokine signaling controls intracortical migration and final distribution of GABAergic interneurons. *J. Neurosci.* **28**, 1613–1624 (2008).
337. Lysko, D. E., Putt, M. & Golden, J. A. SDF1 regulates leading process branching and speed of migrating interneurons. *J. Neurosci.* **31**, 1739–1745 (2011).
338. Yang, S. *et al.* Cxcl12/Cxcr4 signaling controls the migration and process orientation of A9-A10 dopaminergic neurons. *Development* **140**, 4554–4564 (2013).
339. Casoni, F. *et al.* SDF and GABA interact to regulate axophilic migration of GnRH neurons. *J Cell Sci* **125**, 5015–5025 (2012).
340. Memi, F. *et al.* CXC Chemokine Receptor 7 (CXCR7) affects the migration of GnRH neurons by regulating CXCL12 availability. *J. Neurosci.* **33**, 17527–17537 (2013).
341. Gilmour, D., Knaut, H., Maischein, H.-M. & Nüsslein-Volhard, C. Towing of sensory axons by their migrating target cells in vivo. *Nature Neuroscience* **7**, 491–492 (2004).

342. Lieberam, I., Agalliu, D., Nagasawa, T., Ericson, J. & Jessell, T. M. A Cxcl12-Cxcr4 chemokine signaling pathway defines the initial trajectory of mammalian motor axons. *Neuron* **47**, 667–679 (2005).
343. Li, Q. *et al.* Chemokine signaling guides axons within the retina in zebrafish. *J. Neurosci.* **25**, 1711–1717 (2005).
344. Chalasani, S. H., Sabelko, K. A., Sunshine, M. J., Littman, D. R. & Raper, J. A. A chemokine, SDF-1, reduces the effectiveness of multiple axonal repellents and is required for normal axon pathfinding. *J. Neurosci.* **23**, 1360–1371 (2003).
345. Tsai, H.-H. *et al.* The chemokine receptor CXCR2 controls positioning of oligodendrocyte precursors in developing spinal cord by arresting their migration. *Cell* **110**, 373–383 (2002).
346. Dziembowska, M. *et al.* A role for CXCR4 signaling in survival and migration of neural and oligodendrocyte precursors. *Glia* **50**, 258–269 (2005).
347. Lee, M., Lee, Y., Song, J., Lee, J. & Chang, S.-Y. Tissue-specific role of CX3CR1 expressing immune cells and their relationships with human disease. *Immune Netw* **18**, (2018).
348. Arnoux, I. & Audinat, E. Fractalkine signaling and microglia functions in the developing brain. *Neural Plast* **2015**, (2015).
349. Hatori, K., Nagai, A., Heisel, R., Ryu, J. K. & Kim, S. U. Fractalkine and fractalkine receptors in human neurons and glial cells. *Journal of Neuroscience Research* **69**, 418–426 (2002).
350. Harrison, J. K. *et al.* Role for neuronally derived fractalkine in mediating interactions between neurons and CX3CR1-expressing microglia. *PNAS* **95**, 10896–10901 (1998).
351. Cardona, A. E. *et al.* Scavenging roles of chemokine receptors: Chemokine receptor deficiency is associated with increased levels of ligand in circulation and tissues. *Blood* **112**, 256–263 (2008).
352. Cardona, A. E. *et al.* Control of microglial neurotoxicity by the fractalkine receptor. *Nature Neuroscience* **9**, 917–924 (2006).
353. Arnoux, I. *et al.* Adaptive phenotype of microglial cells during the normal postnatal development of the somatosensory “Barrel” cortex. *Glia* **61**, 1582–1594 (2013).
354. Hoshiko, M., Arnoux, I., Avignone, E., Yamamoto, N. & Audinat, E. Deficiency of the microglial receptor CX3CR1 impairs postnatal functional development of thalamocortical synapses in the barrel cortex. *J. Neurosci.* **32**, 15106–15111 (2012).
355. Broz, P. & Dixit, V. M. Inflammasomes: Mechanism of assembly, regulation and signalling. *Nature Reviews Immunology* **16**, 407–420 (2016).
356. Shi, J. *et al.* Cleavage of GSDMD by inflammatory caspases determines pyroptotic cell death. *Nature* **526**, 660–665 (2015).
357. Martinon, F., Burns, K. & Tschopp, J. The inflammasome: A molecular platform triggering activation of inflammatory caspases and processing of proIL- β . *Molecular Cell* **10**, 417–426 (2002).
358. Rühl, S. *et al.* ESCRT-dependent membrane repair negatively regulates pyroptosis downstream of GSDMD activation. *Science* **362**, 956–960 (2018).
359. Walsh, J. G., Muruve, D. A. & Power, C. Inflammasomes in the CNS. *Nature Reviews Neuroscience* **15**, 84–97 (2014).
360. Ramos, H. J. *et al.* IL-1 β signaling promotes CNS-intrinsic immune control of West Nile virus infection. *PLoS Pathog.* **8**, (2012).
361. Hoegen, T. *et al.* The NLRP3 inflammasome contributes to brain injury in pneumococcal meningitis and is activated through ATP-dependent lysosomal cathepsin B release. *J. Immunol.* **187**, 5440–5451 (2011).
362. Kaushik, D. K., Gupta, M., Kumawat, K. L. & Basu, A. NLRP3 inflammasome: Key mediator of neuroinflammation in murine Japanese encephalitis. *PLoS One* **7**, (2012).
363. Kumar, M. *et al.* Inflammasome adaptor protein Apoptosis-associated speck-like protein containing CARD (ASC) is critical for the immune response and survival in west Nile virus encephalitis. *J. Virol.* **87**, 3655–3667 (2013).
364. Mitchell, A. J. *et al.* Inflammasome-dependent IFN- γ drives pathogenesis in *Streptococcus pneumoniae* meningitis. *J. Immunol.* **189**, 4970–4980 (2012).
365. de Rivero Vaccari, J. P. *et al.* Therapeutic neutralization of the NLRP1 inflammasome reduces the innate immune response and improves histopathology after traumatic brain injury. *J. Cereb. Blood Flow Metab.* **29**, 1251–1261 (2009).
366. Abulafia, D. P. *et al.* Inhibition of the inflammasome complex reduces the inflammatory response after thromboembolic stroke in mice. *J. Cereb. Blood Flow Metab.* **29**, 534–544 (2009).

367. Shi, F. *et al.* The NALP3 inflammasome is involved in neurotoxic prion peptide-induced microglial activation. *J Neuroinflammation* **9**, 73 (2012).
368. Halle, A. *et al.* The NALP3 inflammasome is involved in the innate immune response to amyloid-beta. *Nat. Immunol.* **9**, 857–865 (2008).
369. Codolo, G. *et al.* Triggering of inflammasome by aggregated α -synuclein, an inflammatory response in synucleinopathies. *PLOS One* **8**, (2013).
370. Heneka, M. T. *et al.* NLRP3 is activated in Alzheimer's disease and contributes to pathology in APP/PS1 mice. *Nature* **493**, 674–678 (2013).
371. Venegas, C. *et al.* Microglia-derived ASC specks cross-seed amyloid- β in Alzheimer's disease. *Nature* **552**, 355–361 (2017).
372. McKinnon, P. J. Maintaining genome stability in the nervous system. *Nature Neuroscience* **16**, 1523–1529 (2013).
373. McKinnon, P. J. Genome integrity and disease prevention in the nervous system. *Genes Dev.* **31**, 1180–1194 (2017).
374. Sagulenko, V. *et al.* AIM2 and NLRP3 inflammasomes activate both apoptotic and pyroptotic death pathways via ASC. *Cell Death & Differentiation* **20**, 1149–1160 (2013).
375. Adamczak, S. E. *et al.* Pyroptotic neuronal cell death mediated by the AIM2 inflammasome. *J Cereb Blood Flow Metab* **34**, 621–629 (2014).
376. Fernandes-Alnemri, T., Yu, J.-W., Datta, P., Wu, J. & Alnemri, E. S. AIM2 activates the inflammasome and cell death in response to cytoplasmic DNA. *Nature* **458**, 509–513 (2009).
377. Hornung, V. *et al.* AIM2 recognizes cytosolic dsDNA and forms a caspase-1-activating inflammasome with ASC. *Nature* **458**, 514–518 (2009).
378. Hu, B. *et al.* The DNA-sensing AIM2 inflammasome controls radiation-induced cell death and tissue injury. *Science* **354**, 765–768 (2016).
379. Lugin, J. & Martinon, F. The AIM2 inflammasome: Sensor of pathogens and cellular perturbations. *Immunological Reviews* **281**, 99–114 (2018).
380. Micco, A. D. *et al.* AIM2 inflammasome is activated by pharmacological disruption of nuclear envelope integrity. *PNAS* **113**, 4671–4680 (2016).
381. Wu, P.-J., Liu, H.-Y., Huang, T.-N. & Hsueh, Y.-P. AIM 2 inflammasomes regulate neuronal morphology and influence anxiety and memory in mice. *Scientific Reports* **6**, (2016).
382. Mednick, S. A., Machon, R. A., Huttunen, M. O. & Bonett, D. Adult schizophrenia following prenatal exposure to an influenza epidemic. *Arch. Gen. Psychiatry* **45**, 189–192 (1988).
383. Brown, A. S. *et al.* Serologic evidence of prenatal influenza in the etiology of schizophrenia. *Arch. Gen. Psychiatry* **61**, 774–780 (2004).
384. Chess, S. Autism in children with congenital rubella. *J Autism Child Schizophr* **1**, 33–47 (1971).
385. Boksa, P. Effects of prenatal infection on brain development and behavior: A review of findings from animal models. *Brain, Behavior, and Immunity* **24**, 881–897 (2010).
386. Solek, C. M., Farooqi, N., Verly, M., Lim, T. K. & Ruthazer, E. S. Maternal immune activation in neurodevelopmental disorders. *Developmental Dynamics* **247**, 588–619 (2018).
387. Estes, M. L. & McAllister, A. K. Immune mediators in the brain and peripheral tissues in autism spectrum disorder. *Nature Reviews Neuroscience* **16**, 469–486 (2015).
388. Hyman, S. L., Arndt, T. L. & Rodier, P. M. Environmental agents and autism: Once and future associations. in *International Review of Research in Mental Retardation* vol. 30 171–194 (Academic Press, 2005).
389. Atladóttir, H. O. *et al.* Maternal infection requiring hospitalization during pregnancy and autism spectrum disorders. *J Autism Dev Disord* **40**, 1423–1430 (2010).
390. Zerbo, O. *et al.* Maternal infection during pregnancy and autism spectrum disorders. *J Autism Dev Disord* **45**, 4015–4025 (2015).
391. Brown, A. S. *et al.* Elevated maternal C-reactive protein and autism in a national birth cohort. *Molecular Psychiatry* **19**, 259–264 (2014).
392. Penner, J. D. & Brown, A. S. Prenatal infectious and nutritional factors and risk of adult schizophrenia. *Expert Rev Neurother* **7**, 797–805 (2007).
393. Patterson, P. H. Maternal effects on schizophrenia risk. *Science* **318**, 576–577 (2007).
394. Brown, A. S. Prenatal infection as a risk factor for schizophrenia. *Schizophr Bull* **32**, 200–202 (2006).

395. Buka, S. L. *et al.* Maternal cytokine levels during pregnancy and adult psychosis. *Brain, Behavior, and Immunity* **15**, 411–420 (2001).
396. Wu, Y. W. Systematic review of chorioamnionitis and cerebral palsy. *Ment Retard Dev Disabil Res Rev* **8**, 25–29 (2002).
397. Sun, Y., Vestergaard, M., Christensen, J., Nahmias, A. J. & Olsen, J. Prenatal exposure to maternal infections and epilepsy in childhood: A population-based cohort study. *Pediatrics* **121**, 1100–1107 (2008).
398. Hao, L. Y., Hao, X. Q., Li, S. H. & Li, X. H. Prenatal exposure to lipopolysaccharide results in cognitive deficits in age-increasing offspring rats. *Neuroscience* **166**, 763–770 (2010).
399. Krstic, D. *et al.* Systemic immune challenges trigger and drive Alzheimer-like neuropathology in mice. *J Neuroinflammation* **9**, 151 (2012).
400. Khandaker, G. M. *et al.* Inflammation and immunity in schizophrenia: Implications for pathophysiology and treatment. *Lancet Psychiatry* **2**, 258–270 (2015).
401. Careaga, M., Van de Water, J. & Ashwood, P. Immune dysfunction in autism: A pathway to treatment. *Neurotherapeutics* **7**, 283–292 (2010).
402. Pardo, C. A., Vargas, D. L. & Zimmerman, A. W. Immunity, neuroglia and neuroinflammation in autism. *Int Rev Psychiatry* **17**, 485–495 (2005).
403. Meyer, U. Prenatal poly(I:C) exposure and other developmental immune activation models in rodent systems. *Biological Psychiatry* **75**, 307–315 (2014).
404. Afroz, K. F. & Alviña, K. Maternal elevated salt consumption and the development of autism spectrum disorder in the offspring. *Journal of Neuroinflammation* **16**, 265 (2019).
405. McCullough, L. E. *et al.* Maternal inflammatory diet and adverse pregnancy outcomes: Circulating cytokines and genomic imprinting as potential regulators? *Epigenetics* **12**, 688–697 (2017).
406. Giovanoli, S. *et al.* Stress in puberty unmasks latent neuropathological consequences of prenatal immune activation in mice. *Science* **339**, 1095–1099 (2013).
407. Lauritsen, M. B. Autism spectrum disorders. *Eur Child Adolesc Psychiatry* **22**, 37–42 (2013).
408. American Psychiatric Association. *Diagnostic and statistical manual of mental disorders*. (American Psychiatric Association, 2013).
409. Garbett, K. *et al.* Immune transcriptome alterations in the temporal cortex of subjects with autism. *Neurobiol. Dis.* **30**, 303–311 (2008).
410. Jyonouchi, H., Geng, L., Streck, D. L. & Toruner, G. A. Children with autism spectrum disorders (ASD) who exhibit chronic gastrointestinal (GI) symptoms and marked fluctuation of behavioral symptoms exhibit distinct innate immune abnormalities and transcriptional profiles of peripheral blood (PB) monocytes. *Journal of Neuroimmunology* **238**, 73–80 (2011).
411. Chez, M. G., Dowling, T., Patel, P. B., Khanna, P. & Kominsky, M. Elevation of tumor necrosis factor- α in cerebrospinal fluid of autistic children. *Pediatr. Neurol.* **36**, 361–365 (2007).
412. Estes, M. L. *et al.* Baseline immunoreactivity before pregnancy and poly(I:C) dose combine to dictate susceptibility and resilience of offspring to maternal immune activation. *Brain, Behavior, and Immunity* (2020).
413. Gaboriau-Routhiau, V. *et al.* The key role of segmented filamentous bacteria in the coordinated maturation of gut helper T cell responses. *Immunity* **31**, 677–689 (2009).
414. Mazmanian, S. K., Liu, C. H., Tzianabos, A. O. & Kasper, D. L. An immunomodulatory molecule of symbiotic bacteria directs maturation of the host immune system. *Cell* **122**, 107–118 (2005).
415. Parracho, H. M., Bingham, M. O., Gibson, G. R. & McCartney, A. L. Differences between the gut microflora of children with autistic spectrum disorders and that of healthy children. *Journal of Medical Microbiology*, **54**, 987–991 (2005).
416. Finegold, S. M. Desulfovibrio species are potentially important in regressive autism. *Medical Hypotheses* **77**, 270–274 (2011).
417. Coury, D. L. *et al.* Gastrointestinal conditions in children with Autism Spectrum Disorder: Developing a research agenda. *Pediatrics* **130**, 160–168 (2012).
418. Hsiao, E. Y. *et al.* Microbiota modulate behavioral and physiological abnormalities associated with neurodevelopmental disorders. *Cell* **155**, 1451–1463 (2013).
419. Kim, S. *et al.* Maternal gut bacteria promote neurodevelopmental abnormalities in mouse offspring. *Nature* **549**, 528–532 (2017).
420. Smith, S. E. P., Li, J., Garbett, K., Mirnics, K. & Patterson, P. H. Maternal immune activation alters fetal brain development through Interleukin-6. *J. Neurosci.* **27**, 10695–10702 (2007).

421. Wu, W.-L., Hsiao, E. Y., Yan, Z., Mazmanian, S. K. & Patterson, P. H. The placental interleukin-6 signaling controls fetal brain development and behavior. *Brain Behav. Immun.* **62**, 11–23 (2017).
422. Rudolph, M. D. *et al.* Maternal IL-6 during pregnancy can be estimated from newborn brain connectivity and predicts future working memory in offspring. *Nature Neuroscience* **21**, 765–772 (2018).
423. Choi, G. B. *et al.* The maternal interleukin-17a pathway in mice promotes autism-like phenotypes in offspring. *Science* **351**, 933–939 (2016).
424. Lammert, C. R. *et al.* Cutting Edge: critical roles for microbiota-mediated regulation of the immune system in a prenatal immune activation model of autism. *The Journal of Immunology* (2018).
425. Estes, M. L., Elmer, B. M., Carter, C. C. & McAllister, A. K. Maternal immune activation causes age-specific changes in cytokine receptor expression in offspring throughout development. *bioRxiv* (2018).
426. Garay, P. A., Hsiao, E. Y., Patterson, P. H. & McAllister, A. K. Maternal immune activation causes age- and region-specific changes in brain cytokines in offspring throughout development. *Brain, Behavior, and Immunity* **31**, 54–68 (2013).
427. Smith, S. E. P., Elliott, R. M. & Anderson, M. P. Maternal immune activation increases neonatal mouse cortex thickness and cell density. *J Neuroimmune Pharmacol* **7**, 529–532 (2012).
428. Ben-Reuven, L. & Reiner, O. Dynamics of cortical progenitors and production of subcerebral neurons are altered in embryos of a maternal inflammation model for autism. *Molecular Psychiatry* (2019).
429. Shin Yim, Y. *et al.* Reversing behavioural abnormalities in mice exposed to maternal inflammation. *Nature* **549**, 482–487 (2017).
430. Grzadzinski, R., Lord, C., Sanders, S. J., Werling, D. & Bal, V. H. Children with autism spectrum disorder who improve with fever: Insights from the Simons Simplex Collection. *Autism Res* **11**, 175–184 (2018).
431. Reed, M. D. *et al.* IL-17a promotes sociability in mouse models of neurodevelopmental disorders. *Nature* **577**, 249–253 (2020).
432. Su, Z. *et al.* tRNA-derived fragments and microRNAs in the maternal-fetal interface of a mouse maternal-immune-activation autism model. *RNA Biology* (2020).
433. Tandon, R. *et al.* Definition and description of schizophrenia in the DSM-5. *Schizophr. Res.* **150**, 3–10 (2013).
434. Moran, P. *et al.* Gene × Environment interactions in schizophrenia: Evidence from genetic mouse models. *Neural Plast* (2016).
435. Brown, A. S. *et al.* Elevated maternal Interleukin-8 levels and risk of schizophrenia in adult offspring. *AJP* **161**, 889–895 (2004).
436. Samuelsson, A.-M., Jennische, E., Hansson, H.-A. & Holmäng, A. Prenatal exposure to interleukin-6 results in inflammatory neurodegeneration in hippocampus with NMDA/GABAA dysregulation and impaired spatial learning. *American Journal of Physiology-Regulatory, Integrative and Comparative Physiology* **290**, 1345–1356 (2006).
437. Allswede, D. M., Yolken, R. H., Buka, S. L. & Cannon, T. D. Cytokine concentrations throughout pregnancy and risk for psychosis in adult offspring: a longitudinal case-control study. *The Lancet Psychiatry* **7**, 254–261 (2020).
438. Boozalis, T., Teixeira, A. L., Cho, R. Y.-J. & Okusaga, O. C-Reactive Protein correlates with negative symptoms in patients with Schizophrenia. *Front. Public Health* **5**, (2018).
439. Kang, W. S., Kim, S. K. & Park, H. J. Association of the promoter haplotype of IFN- γ -Inducible Protein 16 gene with schizophrenia in a Korean population. *Psychiatry Investig* **17**, 140–146 (2020).
440. Prata, J., Santos, S. G., Almeida, M. I., Coelho, R. & Barbosa, M. A. Bridging Autism Spectrum Disorders and Schizophrenia through inflammation and biomarkers - pre-clinical and clinical investigations. *Journal of Neuroinflammation* **14**, 179 (2017).
441. Stefansson, H. *et al.* Common variants conferring risk of schizophrenia. *Nature* **460**, 744–747 (2009).
442. Ripke, S. *et al.* Biological insights from 108 schizophrenia-associated genetic loci. *Nature* **511**, 421–427 (2014).
443. Shi, L., Fatemi, S. H., Sidwell, R. W. & Patterson, P. H. Maternal influenza infection causes marked behavioral and pharmacological changes in the offspring. *J. Neurosci.* **23**, 297–302 (2003).
444. Zuckerman, L., Rehavi, M., Nachman, R. & Weiner, I. Immune activation during pregnancy in rats leads to a post-pubertal emergence of disrupted latent inhibition, dopaminergic hyperfunction, and altered limbic morphology in the offspring: A novel neurodevelopmental model of schizophrenia. *Neuropsychopharmacology* **28**, 1778–1789 (2003).

445. Meyer, U. *et al.* Adult behavioral and pharmacological dysfunctions following disruption of the fetal brain balance between pro-inflammatory and IL-10-mediated anti-inflammatory signaling. *Molecular Psychiatry* **13**, 208–221 (2008).
446. Upthegrove, R., Manzanares-Teson, N. & Barnes, N. M. Cytokine function in medication-naive first episode psychosis: A systematic review and meta-analysis. *Schizophrenia Research* **155**, 101–108 (2014).
447. Elmer, B. M., Estes, M. L., Barrow, S. L. & McAllister, A. K. MHC1 requires MEF2 transcription factors to negatively regulate synapse density during development and in disease. *J. Neurosci.* **33**, 13791–13804 (2013).
448. Dogan, Y. *et al.* Intracranial ultrasound abnormalities and fetal cytomegalovirus infection: Report of 8 cases and review of the literature. *FDT* **30**, 141–149 (2011).
449. Ellman, L. M. *et al.* Structural brain alterations in schizophrenia following fetal exposure to the inflammatory cytokine interleukin-8. *Schizophrenia Research* **121**, 46–54 (2010).
450. Brown, A. S. *et al.* Prenatal infection and cavum septum pellucidum in adult schizophrenia. *Schizophrenia Research* **108**, 285–287 (2009).
451. Ozawa, K. *et al.* Immune activation during pregnancy in mice leads to dopaminergic hyperfunction and cognitive impairment in the offspring: A neurodevelopmental animal model of schizophrenia. *Biological Psychiatry* **59**, 546–554 (2006).
452. Dalton, V. S., Verdurand, M., Walker, A., Hodgson, D. M. & Zavitsanou, K. Synergistic effect between maternal infection and adolescent cannabinoid exposure on serotonin 5HT1A receptor binding in the hippocampus: Testing the “two hit” hypothesis for the development of schizophrenia. *ISRN Psychiatry* (2012).
453. Richetto, J., Calabrese, F., Riva, M. A. & Meyer, U. Prenatal immune activation induces maturation-dependent alterations in the prefrontal GABAergic transcriptome. *Schizophr Bull* **40**, 351–361 (2014).
454. Rodriguez, J. I. & Kern, J. K. Evidence of microglial activation in autism and its possible role in brain underconnectivity. *Neuron Glia Biol* **7**, 205–213 (2011).
455. Munn, N. A. Microglia dysfunction in schizophrenia: An integrative theory. *Medical Hypotheses* **54**, 198–202 (2000).
456. De Picker, L. J., Morrens, M., Chance, S. A. & Boche, D. Microglia and brain plasticity in acute psychosis and schizophrenia illness course: A meta-review. *Front Psychiatry* **8**, (2017).
457. Voineagu, I. *et al.* Transcriptomic analysis of autistic brain reveals convergent molecular pathology. *Nature* **474**, 380–384 (2011).
458. Doorduyn, J. *et al.* Neuroinflammation in schizophrenia-related psychosis: A PET study. *J Nucl Med* **50**, 1801–1807 (2009).
459. Busse, S. *et al.* Different distribution patterns of lymphocytes and microglia in the hippocampus of patients with residual versus paranoid schizophrenia: Further evidence for disease course-related immune alterations? *Brain, Behavior, and Immunity* **26**, 1273–1279 (2012).
460. Zürcher, N. R. *et al.* [11 C]PBR28 MR–PET imaging reveals lower regional brain expression of translocator protein (TSPO) in young adult males with autism spectrum disorder. *Molecular Psychiatry* (2020).
461. Schafer, D. P. & Stevens, B. Microglia function in central nervous system development and plasticity. *Cold Spring Harb Perspect Biol* **7**, (2015).
462. Smolders, S. *et al.* Maternal immune activation evoked by polyinosinic:polycytidylic acid does not evoke microglial cell activation in the embryo. *Front. Cell. Neurosci.* **9**, (2015).
463. Giovanoli, S., Weber-Stadlbauer, U., Schedlowski, M., Meyer, U. & Engler, H. Prenatal immune activation causes hippocampal synaptic deficits in the absence of overt microglia anomalies. *Brain Behav. Immun.* **55**, 25–38 (2016).
464. Mattei, D. *et al.* Maternal immune activation results in complex microglial transcriptome signature in the adult offspring that is reversed by minocycline treatment. *Translational Psychiatry* **7**, 1120–1120 (2017).
465. Manitz, M. P. *et al.* Flow cytometric characterization of microglia in the offspring of PolyI:C treated mice. *Brain Research* **1636**, 172–182 (2016).
466. Eßlinger, M. *et al.* Schizophrenia associated sensory gating deficits develop after adolescent microglia activation. *Brain, Behavior, and Immunity* **58**, 99–106 (2016).
467. Manitz, M. P. *et al.* The role of microglia during life span in neuropsychiatric disease — an animal study. *Schizophrenia Research* **143**, 221–222 (2013).

468. Juckel, G. *et al.* Microglial activation in a neuroinflammatory animal model of schizophrenia — a pilot study. *Schizophrenia Research* **131**, 96–100 (2011).
469. Almond, D. & Currie, J. Killing Me Softly: The Fetal Origins Hypothesis. *J Econ Perspect* **25**, 153–172 (2011).
470. Bordeleau, M., Fernández de Cossío, L., Chakravarty, M. M. & Tremblay, M.-È. From Maternal Diet to Neurodevelopmental Disorders: A Story of Neuroinflammation. *Frontiers in Cellular Neuroscience* **14**, (2021).
471. Cortés-Albornoz, M. C., García-Guáqueta, D. P., Velez-van-Meerbeke, A. & Talero-Gutiérrez, C. Maternal Nutrition and Neurodevelopment: A Scoping Review. *Nutrients* **13**, 3530 (2021).
472. Fitzgerald, E., Parent, C., Kee, M. Z. L. & Meaney, M. J. Maternal Distress and Offspring Neurodevelopment: Challenges and Opportunities for Pre-clinical Research Models. *Front Hum Neurosci* **15**, 635304 (2021).
473. Susser, E. S. & Lin, S. P. Schizophrenia After Prenatal Exposure to the Dutch Hunger Winter of 1944–1945. *Archives of General Psychiatry* **49**, 983–988 (1992).
474. Zengeler, K. E. & Lukens, J. R. Innate immunity at the crossroads of healthy brain maturation and neurodevelopmental disorders. *Nature Reviews Immunology* 1–15 (2021) doi:10.1038/s41577-020-00487-7.
475. Kinsella, M. T. & Monk, C. Impact of Maternal Stress, Depression & Anxiety on Fetal Neurobehavioral Development. *Clin Obstet Gynecol* **52**, 425–440 (2009).
476. Talge, N. M., Neal, C., Glover, V., & the Early Stress, Translational Research and Prevention Science Network: Fetal and Neonatal Experience on Child and Adolescent Mental Health. Antenatal maternal stress and long-term effects on child neurodevelopment: how and why? *Journal of Child Psychology and Psychiatry* **48**, 245–261 (2007).
477. Brown, A. S. & Derkits, E. J. Prenatal infection and schizophrenia: a review of epidemiologic and translational studies. *Am J Psychiatry* **167**, 261–280 (2010).
478. Han, V. X., Patel, S., Jones, H. F. & Dale, R. C. Maternal immune activation and neuroinflammation in human neurodevelopmental disorders. *Nat Rev Neurol* **17**, 564–579 (2021).
479. Patterson, P. H. Immune involvement in schizophrenia and autism: Etiology, pathology and animal models. *Behavioural Brain Research* **204**, 313–321 (2009).
480. Ellul, P. *et al.* Parental autoimmune and autoinflammatory disorders as multiple risk factors for common neurodevelopmental disorders in offspring: a systematic review and meta-analysis. *Transl Psychiatry* **12**, 1–8 (2022).
481. Deverman, B. E. & Patterson, P. H. Cytokines and CNS Development. *Neuron* **64**, 61–78 (2009).
482. Millard, S. J., Weston-Green, K. & Newell, K. A. The effects of maternal antidepressant use on offspring behaviour and brain development: Implications for risk of neurodevelopmental disorders. *Neuroscience & Biobehavioral Reviews* **80**, 743–765 (2017).
483. Homberg, J. R., Schubert, D. & Gaspar, P. New perspectives on the neurodevelopmental effects of SSRIs. *Trends in Pharmacological Sciences* **31**, 60–65 (2010).
484. Marchocki, Z., Russell, N. E. & Donoghue, K. O. Selective serotonin reuptake inhibitors and pregnancy: A review of maternal, fetal and neonatal risks and benefits. *Obstet Med* **6**, 155–158 (2013).
485. Ansorge, M. S., Morelli, E. & Gingrich, J. A. Inhibition of Serotonin But Not Norepinephrine Transport during Development Produces Delayed, Persistent Perturbations of Emotional Behaviors in Mice. *J. Neurosci.* **28**, 199–207 (2008).
486. Ansorge, M. S., Zhou, M., Lira, A., Hen, R. & Gingrich, J. A. Early-Life Blockade of the 5-HT Transporter Alters Emotional Behavior in Adult Mice. *Science* **306**, 879–881 (2004).
487. Araujo, J. S. A. de, Delgado, I. F. & Paumgarten, F. J. R. Antenatal exposure to antidepressant drugs and the risk of neurodevelopmental and psychiatric disorders: a systematic review. *Cad. Saúde Pública* **36**, (2020).
488. Bonnin, A. *et al.* A transient placental source of serotonin for the fetal forebrain. *Nature* **472**, 347–350 (2011).
489. Bonnin, A. & Levitt, P. Fetal, maternal, and placental sources of serotonin and new implications for developmental programming of the brain. *Neuroscience* **197**, 1–7 (2011).
490. Malm, H. *et al.* Gestational Exposure to Selective Serotonin Reuptake Inhibitors and Offspring Psychiatric Disorders: A National Register-Based Study. *J Am Acad Child Adolesc Psychiatry* **55**, 359–366 (2016).

491. Oberlander, T. F., Gingrich, J. A. & Ansorge, M. S. Sustained Neurobehavioral Effects of Exposure to SSRI Antidepressants During Development: Molecular to Clinical Evidence. *Clinical Pharmacology & Therapeutics* **86**, 672–677 (2009).
492. Sujan, A. C., Öberg, A. S., Quinn, P. D. & D’Onofrio, B. M. Maternal antidepressant use during pregnancy and offspring neurodevelopmental problems – a critical review and recommendations for future research. *J Child Psychol Psychiatry* **60**, 356–376 (2019).
493. Maltepe, E. & Fisher, S. J. Placenta: the forgotten organ. *Annu Rev Cell Dev Biol* **31**, 523–552 (2015).
494. Ander, S. E., Diamond, M. S. & Coyne, C. B. Immune responses at the maternal-fetal interface. *Science Immunology* **4**, eaat6114 (2019).
495. Sun, J.-Y. *et al.* Placental Immune Tolerance and Organ Transplantation: Underlying Interconnections and Clinical Implications. *Frontiers in Immunology* **12**, (2021).
496. Lammert, C. R. & Lukens, J. R. Modeling Autism-Related Disorders in Mice with Maternal Immune Activation (MIA). *Methods Mol Biol* **1960**, 227–236 (2019).
497. Kim, S. *et al.* Maternal gut bacteria promote neurodevelopmental abnormalities in mouse offspring. *Nature* **549**, 528–532 (2017).
498. Reed, M. D. *et al.* IL-17a promotes sociability in mouse models of neurodevelopmental disorders. *Nature* **577**, 249–253 (2020).
499. Carlezon, W. A. *et al.* Maternal and early postnatal immune activation produce sex-specific effects on autism-like behaviors and neuroimmune function in mice. *Sci Rep* **9**, 16928 (2019).
500. Gogos, A., Sbisa, A., Witkamp, D. & van den Buuse, M. Sex differences in the effect of maternal immune activation on cognitive and psychosis-like behaviour in Long Evans rats. *Eur J Neurosci* **52**, 2614–2626 (2020).
501. Kalish, B. T. *et al.* Maternal immune activation in mice disrupts proteostasis in the fetal brain. *Nat Neurosci* **24**, 204–213 (2021).
502. Keever, M. R. *et al.* Lasting and Sex-Dependent Impact of Maternal Immune Activation on Molecular Pathways of the Amygdala. *Frontiers in Neuroscience* **14**, (2020).
503. Smith, C. J. *et al.* Neonatal immune challenge induces female-specific changes in social behavior and somatostatin cell number. *Brain Behav Immun* **90**, 332–345 (2020).
504. Yan, R. *et al.* Structural basis for the recognition of SARS-CoV-2 by full-length human ACE2. *Science* **367**, 1444–1448 (2020).
505. Argueta, L. B. *et al.* SARS-CoV-2 Infects Syncytiotrophoblast and Activates Inflammatory Responses in the Placenta. *bioRxiv* 2021.06.01.446676 (2021) doi:10.1101/2021.06.01.446676.
506. Bordt, E. A. *et al.* Maternal SARS-CoV-2 infection elicits sexually dimorphic placental immune responses. *Science Translational Medicine* **13**, eabi7428 (2021).
507. Gabory, A., Roseboom, T. J., Moore, T., Moore, L. G. & Junien, C. Placental contribution to the origins of sexual dimorphism in health and diseases: sex chromosomes and epigenetics. *Biology of Sex Differences* **4**, 5 (2013).
508. Meakin, A. S., Cuffe, J. S. M., Darby, J. R. T., Morrison, J. L. & Clifton, V. L. Let’s Talk about Placental Sex, Baby: Understanding Mechanisms That Drive Female- and Male-Specific Fetal Growth and Developmental Outcomes. *International Journal of Molecular Sciences* **22**, (2021).
509. Rosenfeld, C. S. Sex-Specific Placental Responses in Fetal Development. *Endocrinology* **156**, 3422–3434 (2015).
510. Cowan, M. & Petri, W. A. Microglia: Immune Regulators of Neurodevelopment. *Frontiers in Immunology* **9**, (2018).
511. Lukens, J. R. & Eyo, U. B. Microglia and Neurodevelopmental Disorders. *Annual Review of Neuroscience* **45**, null (2022).
512. Schafer, D. P. *et al.* Microglia sculpt postnatal neural circuits in an activity and complement-dependent manner. *Neuron* **74**, 691–705 (2012).
513. Ceasrine, A. M. *et al.* Maternal diet disrupts the placenta-brain axis in a sex-specific manner. 2021.11.12.468408 Preprint at <https://doi.org/10.1101/2021.11.12.468408> (2021).
514. Sohel, A. J., Shutter, M. C. & Molla, M. Fluoxetine. in *StatPearls* (StatPearls Publishing, 2022).
515. Mitchell, A. A. *et al.* Medication use during pregnancy, with particular focus on prescription drugs: 1976–2008. *American Journal of Obstetrics and Gynecology* **205**, 51.e1–51.e8 (2011).
516. Herr, N., Bode, C. & Duerschmied, D. The Effects of Serotonin in Immune Cells. *Front Cardiovasc Med* **4**, 48 (2017).

517. Campbell, B. M., Charych, E., Lee, A. W. & Möller, T. Kynurenines in CNS disease: regulation by inflammatory cytokines. *Front Neurosci* **8**, 12 (2014).
518. Velasquez, J., Goeden, N. & Bonnin, A. Placental serotonin: implications for the developmental effects of SSRIs and maternal depression. *Frontiers in Cellular Neuroscience* **7**, (2013).
519. Rampono, J., Proud, S., Hackett, L. P., Kristensen, J. H. & Ilett, K. F. A pilot study of newer antidepressant concentrations in cord and maternal serum and possible effects in the neonate. *Int J Neuropsychopharmacol* **7**, 329–334 (2004).
520. Hoo, R., Nakimuli, A. & Vento-Tormo, R. Innate Immune Mechanisms to Protect Against Infection at the Human Decidual-Placental Interface. *Front Immunol* **11**, 2070 (2020).
521. Yockey, L. J. & Iwasaki, A. Interferons and Proinflammatory Cytokines in Pregnancy and Fetal Development. *Immunity* **49**, 397–412 (2018).
522. Buchrieser, J. *et al.* IFITM proteins inhibit placental syncytiotrophoblast formation and promote fetal demise. *Science* **365**, 176–180 (2019).
523. Hsiao, E. Y. & Patterson, P. H. Activation of the maternal immune system induces endocrine changes in the placenta via IL-6. *Brain Behav Immun* **25**, 604–615 (2011).
524. Hsiao, E. Y. & Patterson, P. H. Placental regulation of maternal-fetal interactions and brain development. *Dev Neurobiol* **72**, 1317–1326 (2012).
525. Faas, M. M. & De Vos, P. Innate immune cells in the placental bed in healthy pregnancy and preeclampsia. *Placenta* **69**, 125–133 (2018).
526. Vazirinejad, R., Ahmadi, Z., Arababadi, M. K., Hassanshahi, G. & Kennedy, D. The Biological Functions, Structure and Sources of CXCL10 and Its Outstanding Part in the Pathophysiology of Multiple Sclerosis. *NIM* **21**, 322–330 (2014).
527. Weckman, A. M., Ngai, M., Wright, J., McDonald, C. R. & Kain, K. C. The Impact of Infection in Pregnancy on Placental Vascular Development and Adverse Birth Outcomes. *Front in Microbiology* **10**, (2019).
528. Braun, A. E. *et al.* Examining Sex Differences in the Human Placental Transcriptome During the First Fetal Androgen Peak. *Reprod. Sci.* **28**, 801–818 (2021).
529. Hui, C. W. *et al.* Sex Differences of Microglia and Synapses in the Hippocampal Dentate Gyrus of Adult Mouse Offspring Exposed to Maternal Immune Activation. *Frontiers in Cellular Neuroscience* **14**, (2020).
530. Ozaki, K. *et al.* Maternal immune activation induces sustained changes in fetal microglia motility. *Sci Rep* **10**, 21378 (2020).
531. Hayes, L. N. *et al.* Prenatal immune stress blunts microglia reactivity, impairing neurocircuitry. *Nature* 1–8 (2022) doi:10.1038/s41586-022-05274-z.
532. Giovanoli, S. *et al.* Late prenatal immune activation causes hippocampal deficits in the absence of persistent inflammation across aging. *Journal of Neuroinflammation* **12**, 221 (2015).
533. Smolders, S., Notter, T., Smolders, S. M. T., Rigo, J.-M. & Brône, B. Controversies and prospects about microglia in maternal immune activation models for neurodevelopmental disorders. *Brain, Behavior, and Immunity* **73**, 51–65 (2018).
534. Kliman, H. J. *et al.* Pathway of Maternal Serotonin to the Human Embryo and Fetus. *Endocrinology* **159**, 1609–1629 (2018).
535. Filiano, A. J., Gadani, S. P. & Kipnis, J. Interactions of innate and adaptive immunity in brain development and function. *Brain Research* **1617**, 18–27 (2015).
536. Tanabe, S. & Yamashita, T. The role of immune cells in brain development and neurodevelopmental diseases. *International Immunology* **30**, 437–444 (2018).
537. Gobin, V., Van Steendam, K., Denys, D. & Deforce, D. Selective serotonin reuptake inhibitors as a novel class of immunosuppressants. *International Immunopharmacology* **20**, 148–156 (2014).
538. Szałach, Ł. P., Lisowska, K. A. & Cudała, W. J. The Influence of Antidepressants on the Immune System. *Arch Immunol Ther Exp (Warsz)* **67**, 143–151 (2019).
539. Chen, H. J. *et al.* Prenatal stress causes intrauterine inflammation and serotonergic dysfunction, and long-term behavioral deficits through microbe- and CCL2-dependent mechanisms. *Translational Psychiatry* **10**, (2020).
540. Lee, L.-J. Neonatal Fluoxetine Exposure Affects the Neuronal Structure in the Somatosensory Cortex and Somatosensory-Related Behaviors in Adolescent Rats. *Neurotox Res* **15**, 212–223 (2009).
541. Bairy, K. L., Madhyastha, S., Ashok, K. P., Bairy, I. & Malini, S. Developmental and behavioral consequences of prenatal fluoxetine. *Pharmacology* **79**, 1–11 (2007).

542. Forcelli, P. A. & Heinrichs, S. C. Teratogenic effects of maternal antidepressant exposure on neural substrates of drug-seeking behavior in offspring. *Addict Biol* **13**, 52–62 (2008).
543. Lisboa, S. F. S., Oliveira, P. E., Costa, L. C., Venâncio, E. J. & Moreira, E. G. Behavioral evaluation of male and female mice pups exposed to fluoxetine during pregnancy and lactation. *Pharmacology* **80**, 49–56 (2007).
544. Bleker, L. S., De Rooij, S. R. & Roseboom, T. J. Programming Effects of Prenatal Stress on Neurodevelopment—The Pitfall of Introducing a Self-Fulfilling Prophecy. *Int J Environ Res Public Health* **16**, 2301 (2019).
545. Colonna, M. & Butovsky, O. Microglia Function in the Central Nervous System During Health and Neurodegeneration. *Annu Rev Immunol* **35**, 441–468 (2017).
546. Zheng, D., Liwinski, T. & Elinav, E. Inflammasome activation and regulation: toward a better understanding of complex mechanisms. *Cell Discov* **6**, 1–22 (2020).
547. Broz, P. & Dixit, V. M. Inflammasomes: Mechanism of assembly, regulation and signalling. *Nature Reviews Immunology* **16**, 407–420 (2016).
548. Sharma, D. & Kanneganti, T.-D. The cell biology of inflammasomes: Mechanisms of inflammasome activation and regulation. *Journal of Cell Biology* **213**, 617–629 (2016).
549. Bergsbaken, T., Fink, S. L. & Cookson, B. T. Pyroptosis: host cell death and inflammation. *Nature Reviews Microbiology* **7**, 99–109 (2009).
550. Yu, P. *et al.* Pyroptosis: mechanisms and diseases. *Sig Transduct Target Ther* **6**, 1–21 (2021).
551. Albornoz, E. A., Woodruff, T. M. & Gordon, R. Inflammasomes in CNS Diseases. in *Inflammasomes: Clinical and Therapeutic Implications* (eds. Cordero, M. D. & Alcocer-Gómez, E.) 41–60 (Springer International Publishing, 2018). doi:10.1007/978-3-319-89390-7_3.
552. Voet, S., Srinivasan, S., Lamkanfi, M. & van Loo, G. Inflammasomes in neuroinflammatory and neurodegenerative diseases. *EMBO Molecular Medicine* **11**, e10248 (2019).
553. Heneka, M. T., McManus, R. M. & Latz, E. Inflammasome signalling in brain function and neurodegenerative disease. *Nat Rev Neurosci* **19**, 610–621 (2018).
554. Miller, A. H. & Raison, C. L. The role of inflammation in depression: from evolutionary imperative to modern treatment target. *Nat Rev Immunol* **16**, 22–34 (2016).
555. Guzman-Martinez, L. *et al.* Neuroinflammation as a Common Feature of Neurodegenerative Disorders. *Frontiers in Pharmacology* **10**, (2019).
556. Jayaraj, R. L., Azimullah, S., Beiram, R., Jalal, F. Y. & Rosenberg, G. A. Neuroinflammation: friend and foe for ischemic stroke. *Journal of Neuroinflammation* **16**, 142 (2019).
557. Heneka, M. T., Kummer, M. P. & Latz, E. Innate immune activation in neurodegenerative disease. *Nat Rev Immunol* **14**, 463–477 (2014).
558. Lammert, C. R. *et al.* AIM2 inflammasome surveillance of DNA damage shapes neurodevelopment. *Nature* **580**, 647–652 (2020).
559. Zielinski, M. R. *et al.* The NLRP3 inflammasome modulates sleep and NREM sleep delta power induced by spontaneous wakefulness, sleep deprivation and lipopolysaccharide. *Brain, Behavior, and Immunity* **62**, 137–150 (2017).
560. Liu, X. & Quan, N. Microglia and CNS Interleukin-1: Beyond Immunological Concepts. *Frontiers in Neurology* **9**, (2018).
561. Tzeng, T.-C. J. *et al.* A fluorescent reporter mouse for inflammasome assembly demonstrates an important role for cell bound and free ASC specks during in vivo infection. *Cell Rep* **16**, 571–582 (2016).
562. Eckert, M. J. & Abraham, W. C. Effects of Environmental Enrichment Exposure on Synaptic Transmission and Plasticity in the Hippocampus. in *Neurogenesis and Neural Plasticity* (eds. Belzung, C. & Wigmore, P.) 165–187 (Springer, 2013).
563. Hüttenrauch, M., Salinas, G. & Wirths, O. Effects of Long-Term Environmental Enrichment on Anxiety, Memory, Hippocampal Plasticity and Overall Brain Gene Expression in C57BL6 Mice. *Front. Mol. Neurosci.* **9**, (2016).
564. Jung, C. K. E. & Herms, J. Structural Dynamics of Dendritic Spines are Influenced by an Environmental Enrichment: An In Vivo Imaging Study. *Cerebral Cortex* **24**, 377–384 (2014).
565. Leggio, M. G. *et al.* Environmental enrichment promotes improved spatial abilities and enhanced dendritic growth in the rat. *Behavioural Brain Research* **163**, 78–90 (2005).
566. Manahan-Vaughan, D. & Buschler, A. Brief environmental enrichment elicits metaplasticity of hippocampal synaptic potentiation in vivo. *Front. Behav. Neurosci.* **6**, (2012).

567. Ohline, S. M. & Abraham, W. C. Environmental enrichment effects on synaptic and cellular physiology of hippocampal neurons. *Neuropharmacology* **145**, 3–12 (2019).
568. Medendorp, W. E. *et al.* Altered Behavior in Mice Socially Isolated During Adolescence Corresponds With Immature Dendritic Spine Morphology and Impaired Plasticity in the Prefrontal Cortex. *Frontiers in Behavioral Neuroscience* **12**, (2018).
569. Silva-Gómez, A. B., Rojas, D., Juárez, I. & Flores, G. Decreased dendritic spine density on prefrontal cortical and hippocampal pyramidal neurons in postweaning social isolation rats. *Brain Research* **983**, 128–136 (2003).
570. Bettio, L. E. B., Rajendran, L. & Gil-Mohapel, J. The effects of aging in the hippocampus and cognitive decline. *Neuroscience & Biobehavioral Reviews* **79**, 66–86 (2017).
571. Driscoll, I. *et al.* The Aging Hippocampus: Cognitive, Biochemical and Structural Findings. *Cerebral Cortex* **13**, 1344–1351 (2003).
572. Hou, Y. *et al.* Ageing as a risk factor for neurodegenerative disease. *Nat Rev Neurol* **15**, 565–581 (2019).
573. Flores, J., Noël, A., Foveau, B., Beauchet, O. & LeBlanc, A. C. Pre-symptomatic Caspase-1 inhibitor delays cognitive decline in a mouse model of Alzheimer disease and aging. *Nature Communications* **11**, 4571 (2020).
574. Flores, J. *et al.* Caspase-1 inhibition alleviates cognitive impairment and neuropathology in an Alzheimer's disease mouse model. *Nat Commun* **9**, 3916 (2018).
575. Magee, J. C. & Grienberger, C. Synaptic Plasticity Forms and Functions. *Annual Review of Neuroscience* **43**, 95–117 (2020).
576. Martin, S. J., Grimwood, P. D. & Morris, R. G. M. Synaptic Plasticity and Memory: An Evaluation of the Hypothesis. *Annual Review of Neuroscience* **23**, 649–711 (2000).
577. Runge, K., Cardoso, C. & de Chevigny, A. Dendritic Spine Plasticity: Function and Mechanisms. *Frontiers in Synaptic Neuroscience* **12**, (2020).
578. Pchitskaya, E. & Bezprozvanny, I. Dendritic Spines Shape Analysis—Classification or Clusterization? Perspective. *Frontiers in Synaptic Neuroscience* **12**, (2020).
579. Hering, H. & Sheng, M. Dendritic spines : structure, dynamics and regulation. *Nat Rev Neurosci* **2**, 880–888 (2001).
580. Martinon, F., Burns, K. & Tschopp, J. The inflammasome: A molecular platform triggering activation of inflammatory caspases and processing of proIL- β . *Molecular Cell* **10**, 417–426 (2002).
581. Nguyen, P. T. *et al.* Microglial Remodeling of the Extracellular Matrix Promotes Synapse Plasticity. *Cell* **182**, 388-403.e15 (2020).
582. Wang, Y. *et al.* Astrocyte-secreted IL-33 mediates homeostatic synaptic plasticity in the adult hippocampus. *Proc Natl Acad Sci U S A* **118**, e2020810118 (2021).
583. Dankovich, T. M. & Rizzoli, S. O. The Synaptic Extracellular Matrix: Long-Lived, Stable, and Still Remarkably Dynamic. *Frontiers in Synaptic Neuroscience* **14**, (2022).
584. Dityatev, A. & Schachner, M. Extracellular matrix molecules and synaptic plasticity. *Nat Rev Neurosci* **4**, 456–468 (2003).
585. Jakovljević, A. *et al.* Structural and Functional Modulation of Perineuronal Nets: In Search of Important Players with Highlight on Tenascins. *Cells* **10**, 1345 (2021).
586. Araque, A., Parpura, V., Sanzgiri, R. P. & Haydon, P. G. Tripartite synapses: glia, the unacknowledged partner. *Trends Neurosci* **22**, 208–215 (1999).
587. Chung, W.-S., Allen, N. J. & Eroglu, C. Astrocytes Control Synapse Formation, Function, and Elimination. *Cold Spring Harb Perspect Biol* **7**, a020370 (2015).
588. Halassa, M. M., Fellin, T., Takano, H., Dong, J.-H. & Haydon, P. G. Synaptic Islands Defined by the Territory of a Single Astrocyte. *J Neurosci* **27**, 6473–6477 (2007).
589. Cayrol, C. & Girard, J.-P. Interleukin-33 (IL-33): A nuclear cytokine from the IL-1 family. *Immunological Reviews* **281**, 154–168 (2018).
590. Cayrol, C. & Girard, J.-P. The IL-1-like cytokine IL-33 is inactivated after maturation by caspase-1. *Proceedings of the National Academy of Sciences* **106**, 9021–9026 (2009).
591. Talabot-Ayer, D., Lamacchia, C., Gabay, C. & Palmer, G. Interleukin-33 is biologically active independently of caspase-1 cleavage. *J Biol Chem* **284**, 19420–19426 (2009).
592. Bellinger, F. P., Madamba, S. & Siggins, G. R. Interleukin 1 beta inhibits synaptic strength and long-term potentiation in the rat CA1 hippocampus. *Brain Res* **628**, 227–234 (1993).

593. Goshen, I. *et al.* A dual role for interleukin-1 in hippocampal-dependent memory processes. *Psychoneuroendocrinology* **32**, 1106–1115 (2007).
594. Ross, F. M., Allan, S. M., Rothwell, N. J. & Verkhratsky, A. A dual role for interleukin-1 in LTP in mouse hippocampal slices. *J Neuroimmunol* **144**, 61–67 (2003).
595. Case, C. L. *et al.* Caspase-11 stimulates rapid flagellin-independent pyroptosis in response to *Legionella pneumophila*. *PNAS* **110**, 1851–1856 (2013).
596. Bonnin, A. & Levitt, P. Fetal, Maternal and Placental Sources of Serotonin and New Implications for Developmental Programming of the Brain. *Neuroscience* **197**, 1–7 (2011).
597. Ennerfelt, H. E. & Lukens, J. R. The role of innate immunity in Alzheimer's disease. *Immunological Reviews* **297**, 225–246 (2020).
598. Lee, J.-H. *et al.* Astrocytes phagocytose adult hippocampal synapses for circuit homeostasis. *Nature* **590**, 612–617 (2021).
599. Agard, N. J., Maltby, D. & Wells, J. A. Inflammatory Stimuli Regulate Caspase Substrate Profiles. *Mol Cell Proteomics* **9**, 880–893 (2010).
600. Sakers, K. *et al.* Astrocytes locally translate transcripts in their peripheral processes. *Proceedings of the National Academy of Sciences* **114**, E3830–E3838 (2017).
601. Boulay, A.-C. *et al.* Translation in astrocyte distal processes sets molecular heterogeneity at the gliovascular interface. *Cell Discov* **3**, 1–20 (2017).
602. Mazaré, N. *et al.* Local Translation in Perisynaptic Astrocytic Processes Is Specific and Changes after Fear Conditioning. *Cell Rep* **32**, 108076 (2020).
603. O'Leary, L. A. *et al.* Characterization of Vimentin-Immunoreactive Astrocytes in the Human Brain. *Frontiers in Neuroanatomy* **14**, (2020).
604. Wilhelmsson, U. *et al.* The role of GFAP and vimentin in learning and memory. *Biological Chemistry* **400**, 1147–1156 (2019).
605. Potokar, M., Morita, M., Wiche, G. & Jorgačevski, J. The Diversity of Intermediate Filaments in Astrocytes. *Cells* **9**, 1604 (2020).
606. Schiweck, J., Eickholt, B. J. & Murk, K. Important Shapeshifter: Mechanisms Allowing Astrocytes to Respond to the Changing Nervous System During Development, Injury and Disease. *Frontiers in Cellular Neuroscience* **12**, (2018).
607. Ducza, L. *et al.* NLRP2 Is Overexpressed in Spinal Astrocytes at the Peak of Mechanical Pain Sensitivity during Complete Freund Adjuvant-Induced Persistent Pain. *International Journal of Molecular Sciences* **22**, 11408 (2021).
608. Minkiewicz, J., de Rivero Vaccari, J. P. & Keane, R. W. Human astrocytes express a novel NLRP2 inflammasome. *Glia* **61**, 1113–1121 (2013).
609. Zhang, Q. *et al.* Kynurenine regulates NLRP2 inflammasome in astrocytes and its implications in depression. *Brain, Behavior, and Immunity* **88**, 471–481 (2020).
610. Kelley, N., Jeltema, D., Duan, Y. & He, Y. The NLRP3 Inflammasome: An Overview of Mechanisms of Activation and Regulation. *Int J Mol Sci* **20**, 3328 (2019).
611. Kepp, O., Galluzzi, L. & Kroemer, G. Mitochondrial control of the NLRP3 inflammasome. *Nat Immunol* **12**, 199–200 (2011).
612. Yu, J.-W., Fariás, A., Hwang, I., Fernandes-Alnemri, T. & Alnemri, E. S. Ribotoxic Stress through p38 Mitogen-activated Protein Kinase Activates in Vitro the Human Pyrin Inflammasome. *J Biol Chem* **288**, 11378–11383 (2013).
613. Vyleta, M. L., Wong, J. & Magun, B. E. Suppression of ribosomal function triggers innate immune signaling through activation of the NLRP3 inflammasome. *PLoS One* **7**, e36044 (2012).
614. Epilepsy. <https://www.who.int/news-room/fact-sheets/detail/epilepsy>.
615. Mohseni-Moghaddam, P., Roghani, M., Khaleghzadeh-Ahangar, H., Sadr, S. S. & Sala, C. A literature overview on epilepsy and inflammasome activation. *Brain Research Bulletin* **172**, 229–235 (2021).
616. Laxer, K. D. *et al.* The consequences of refractory epilepsy and its treatment. *Epilepsy & Behavior* **37**, 59–70 (2014).
617. Rijkers, K. *et al.* The role of interleukin-1 in seizures and epilepsy: A critical review. *Experimental Neurology* **216**, 258–271 (2009).
618. Vezzani, A. *et al.* Powerful anticonvulsant action of IL-1 receptor antagonist on intracerebral injection and astrocytic overexpression in mice. *Proceedings of the National Academy of Sciences* **97**, 11534–11539 (2000).

619. Noe, F. M. *et al.* Pharmacological blockade of IL-1 β /IL-1 receptor type 1 axis during epileptogenesis provides neuroprotection in two rat models of temporal lobe epilepsy. *Neurobiol Dis* **59**, 183–193 (2013).
620. Vertex Pharmaceuticals Incorporated. *A Phase 2b, Randomized, Double-Blind, Placebo-Controlled, Parallel-Group, Dose-Ranging Study to Evaluate the Efficacy and Safety of VX-765 in Subjects With Treatment-Resistant Partial Epilepsy With a 24-Week Open-Label Extension.* <https://clinicaltrials.gov/ct2/show/NCT01501383> (2020).
621. Dawson, R. & Wallace, D. R. Kainic acid-induced seizures in aged rats: neurochemical correlates. *Brain Res Bull* **29**, 459–468 (1992).
622. Lévesque, M. & Avoli, M. The kainic acid model of temporal lobe epilepsy. *Neurosci Biobehav Rev* **37**, 2887–2899 (2013).
623. Sharma, S., Puttachary, S., Thippeswamy, A., Kanthasamy, A. G. & Thippeswamy, T. Status Epilepticus: Behavioral and Electroencephalography Seizure Correlates in Kainate Experimental Models. *Front Neurol* **9**, 7 (2018).
624. Almeida, C. I. C. Relevance of astrocytes/microglia communication for NLRP3 signalling in the CNS - proof of concept in an ex vivo epilepsy model. in *Relevance of astrocytes/microglia communication for NLRP3 signalling in the CNS - proof of concept in an ex vivo epilepsy model* (2018).
625. Rosa, N. M. da S. Exploring the effect of NLRP3 inflammasome inhibition in the ex vivo model of epileptogenesis. (2017).
626. Siracusa, R., Fusco, R. & Cuzzocrea, S. Astrocytes: Role and Functions in Brain Pathologies. *Frontiers in Pharmacology* **10**, (2019).
627. McNeill, J., Rudyk, C., Hildebrand, M. E. & Salmaso, N. Ion Channels and Electrophysiological Properties of Astrocytes: Implications for Emergent Stimulation Technologies. *Frontiers in Cellular Neuroscience* **15**, (2021).
628. Tan, C.-C. *et al.* NLRP1 inflammasome is activated in patients with medial temporal lobe epilepsy and contributes to neuronal pyroptosis in amygdala kindling-induced rat model. *Journal of Neuroinflammation* **12**, 18 (2015).
629. Meng, X.-F. *et al.* Inhibition of the NLRP3 inflammasome provides neuroprotection in rats following amygdala kindling-induced status epilepticus. *Journal of Neuroinflammation* **11**, 212 (2014).
630. Reddy, D. S. The neuroendocrine basis of sex differences in epilepsy. *Pharmacology Biochemistry and Behavior* **152**, 97–104 (2017).
631. Samba Reddy, D., Thompson, W. & Calderara, G. Molecular mechanisms of sex differences in epilepsy and seizure susceptibility in chemical, genetic and acquired epileptogenesis. *Neurosci Lett* **750**, 135753 (2021).
632. Scharfman, H. E. & MacLusky, N. J. Sex differences in the neurobiology of epilepsy: a preclinical perspective. *Neurobiol Dis* **72PB**, 180–192 (2014).
633. Alzheimer's Disease Facts and Figures. *Alzheimer's Disease and Dementia* <https://www.alz.org/alzheimers-dementia/facts-figures>.
634. Tarawneh, R. & Holtzman, D. M. The Clinical Problem of Symptomatic Alzheimer Disease and Mild Cognitive Impairment. *Cold Spring Harb Perspect Med* **2**, a006148 (2012).
635. Cummings, J., Lee, G., Ritter, A., Sabbagh, M. & Zhong, K. Alzheimer's disease drug development pipeline: 2020. *Alzheimer's & Dementia: Translational Research & Clinical Interventions* **6**, e12050 (2020).
636. Heneka, M. T. Inflammasome activation and innate immunity in Alzheimer's disease. *Brain Pathol* **27**, 220–222 (2017).
637. Kaushal, V. *et al.* Neuronal NLRP1 inflammasome activation of Caspase-1 coordinately regulates inflammatory interleukin-1-beta production and axonal degeneration-associated Caspase-6 activation. *Cell Death Differ* **22**, 1676–1686 (2015).
638. Saresella, M. *et al.* The NLRP3 and NLRP1 inflammasomes are activated in Alzheimer's disease. *Mol Neurodegener* **11**, 23 (2016).
639. Tan, M.-S. *et al.* Amyloid- β induces NLRP1-dependent neuronal pyroptosis in models of Alzheimer's disease. *Cell Death Dis* **5**, e1382 (2014).
640. Choubey, D. Type I interferon (IFN)-inducible Absent in Melanoma 2 proteins in neuroinflammation: implications for Alzheimer's disease. *J Neuroinflammation* **16**, 236 (2019).
641. Lin, X. *et al.* Contributions of DNA Damage to Alzheimer's Disease. *Int J Mol Sci* **21**, 1666 (2020).

642. Wu, P.-J., Hung, Y.-F., Liu, H.-Y. & Hsueh, Y.-P. Deletion of the Inflammasome Sensor Aim2 Mitigates A β Deposition and Microglial Activation but Increases Inflammatory Cytokine Expression in an Alzheimer Disease Mouse Model. *Neuroimmunomodulation* **24**, 29–39 (2017).
643. Daniels, M. J. D. *et al.* Fenamate NSAIDs inhibit the NLRP3 inflammasome and protect against Alzheimer's disease in rodent models. *Nat Commun* **7**, 12504 (2016).
644. White, C. S., Lawrence, C. B., Brough, D. & Rivers-Auty, J. Inflammasomes as therapeutic targets for Alzheimer's disease. *Brain Pathol* **27**, 223–234 (2017).